Self-assembly of

cross-linked polymer micelles into

complex higher-order aggregates

Niels ten Brummelhuis

Self-assembly of

cross-linked polymer micelles into

complex higher-order aggregates

Dissertation

zur Erlangung des akademischen Grades
Doktor der Naturwissenschaften
(Dr. rer. nat.)
in der Wissenschaftsdisziplin „Polymer- und Kolloidchemie"

eingereicht an der
Mathematisch-Naturwissenschaftlichen Fakultät
der Universität Potsdam

von

Niels ten Brummelhuis

geboren am 14.10.1985 in Heerenveen, die Niederlande

Potsdam, Januar 2011

Table of contents

Chapter 1: Introduction

Nature achieves great complexity with only a minor number of key components. Nearly all proteins e.g. are built up of the 21 natural amino acids, which together can be used to perform almost all tasks necessary for the catalysis of a large number of reactions, selective binding, signal transduction and everything else needed to maintain life. A second group of building blocks, the ribonucleic acids (DNA and RNA) are built up of only four different units each, which is enough to encode for all proteins present in nature and, together with a range of proteins, control the production of all components in a living cell.

Though the basic components are simple enough, their interaction culminates in very complex behavior, with the complexity having steadily increased during evolution. The fact that from basic building blocks complex structures can be formed can be traced back to the ability of the single components to specifically build structures over multiple length scales. The 21 natural amino acids are linked to a linear amino acid chain in a specific order, encoded in the DNA. The expression of genes in the DNA takes place by transcription into mRNA by RNA-polymerases and subsequent translation into the corresponding peptide sequence in the ribosomes. The primary structure of the amino acid sequence folds into secondary structures, such as a-helices, β-sheets and turns. These structures then order into tertiary structures which are the final soma of the proteins. The tertiary structures can assemble into quaternary structures by specific interaction with other proteins.

In DNA and RNA a similar kind of ordering takes place. DNA forms the well-known double helix from complementary strands of DNA, due to the specific hydrogen bonding between two nucleotide residues (Adenine with Thymine and Cytosine with Guanine). This secondary structure can obtain a super-ordering when certain specifically binding proteins, such as histones and proteins associated with signal transduction, are present, or can e.g. form supercoiled structures. RNA (only different from DNA because of an extra hydroxyl group in the backbone and the use of Uracil instead of Thymine) does not normally form such stable structures, but a secondary structure is often obtained through hydrogen bonding interaction

between short stretches of nucleotides, in some cases leading to shapes that are used for the catalysis of reactions. The most famous example of this is perhaps the way in which transfer RNA (tRNA) is used in the recognition of triplets on the messenger RNA (mRNA) for the translation of the RNA sequence into the amino acid chain.

Through the interaction of proteins, nucleic acids, lipid bilayers and other components organelles are formed which together build up cells. In higher organisms these are ordered in such a way that they form organs which are specialized in performing one or a few basic functions. The organs in turn build up the entire organism.

Going from the basic building blocks, it becomes clear that complexity starts with only a minor number of building blocks which act together in complex ways.

Chemistry has not even begun to approach the kind of complexity that nature achieves. Drawing inspiration from nature, the building of complex structures by self-assembly has been one of the major topics in chemistry in general and especially in polymer chemistry.

In polymer chemistry often only two levels of organization are achieved, namely the primary structure of the polymer chain and the aggregates built from the single polymer chains, such as micelles, etc. (also see Chapter 2). This work focuses on increasing the complexity of the aggregates formed from polymer chains, firstly by trying to introduce asymmetry in the aggregates and secondly by inducing super-organization of the primary aggregates. Asymmetric aggregates, e.g. Janus type micelles, or vesicles with an asymmetric membrane, are formed using aggregation motives which incorporate two different polymer chains in one aggregate. Here either the spontaneous demixing of the polymer chains is used to obtain phase separation, or phase separation is induced by an external stimulus. Two approaches are chosen to induce phase separation, namely selectively influencing the solvent quality of one of the components making up the polymer structure, or by using a template.

The materials that are obtained are strongly responsive to external stimuli, whether that is pH, ionic strength, temperature, the presence of small molecules and ions, etc.. The influence of these stimuli is also investigated in more detail.

Chapter 2: Background

2.1 Introduction

To be able to understand the context in which this work was performed, some background knowledge on polymer chemistry is required. Some general principles are explained in this chapter. Also some background on more specific themes relevant to this work is given.

2.2 Morphologies

Polymers, from ancient Greek, meaning, loosely translated, "many parts", are widely used and applied to perform many different tasks. For all applications which can be conceived, different properties are needed to fulfill the intended requirements. Some materials need to be flexible, others hard. Some need to be light, others can be heavy. Some should have a low melting point or glass transition temperature, whereas others should be resistant to high temperatures. Some materials should be biodegradable, whereas others should be able to stand the tusk of time, and so on.

In polymer chemistry there are numerous parameters which govern the behavior of materials. First and foremost the nature of the monomers can be changed. Also molecular weight and dispersity strongly influence the performance of the final material. Increasing the number of variables further, different topologies of the polymers can be used, such as linear chains, stars, brushes and other branched structures[1,2]. Beyond this, the stereochemistry of the polymer chains (the backbone of many synthetic polymers contains stereoactive centers) can, under certain conditions, also be influenced. These differences can lead to strong differences in e.g. the crystallinity of the material[3]. Combinations of different monomers open up even more possibilities. Some architectures which are often used are statistical copolymers, where the monomers are mixed randomly, gradient copolymers, where the concentration of the different monomers varies throughout the polymer chain and block copolymers of different types.

For statistical copolymers mostly an averaging of the properties of the single components is observed, whereas for block copolymers the properties of both blocks are maintained. Obviously, also the ratio of the different monomers can be varied, as well as the degree to which gradients are formed. Beyond properties of the monomers also end-groups need to be considered.

All these parameters can be used in combination, which offers an uncountable number of different polymer structures that can be accessed, yielding an unending number of different properties that can be obtained, even without considering the processing of the polymers, which can also strongly impact the behavior of the final material.

2.2.1 Block copolymer morphologies

The morphologies that are formed from block copolymers have been widely studied[4]. A very general overview is given for diblock copolymers.

Depending on the composition of the block copolymer they will form different morphologies in bulk. This can be explained by the fact that most polymers will phase separate at sufficiently high concentration and at sufficiently high molecular weight. Using block copolymers, no macroscopic phase separation can take place, since the blocks are covalently linked. Microphase separation does take place though.
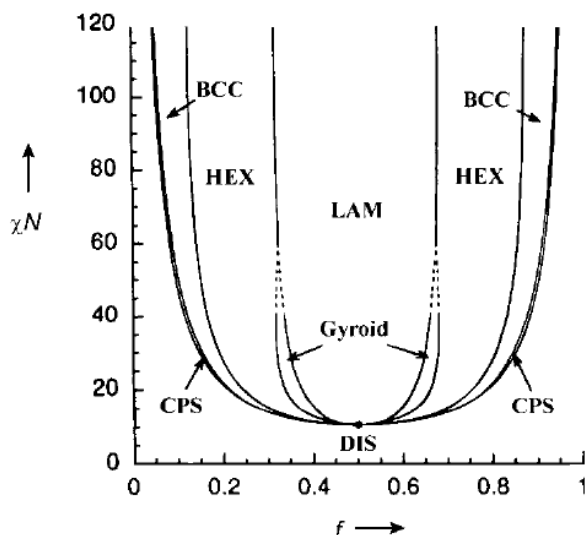
Figure 1: Mean-field phase diagram of bulk morphologies formed by diblock copolymers[5] (LAM: lamellar, HEX: hexagonal cylinders, BCC: spherical micelles with cubic packing, CPS: close-packed spheres, DIS: disordered). f is the fraction of one of the polymers. χ_N is the chi-parameter from the Flory-Huggins theory, which describes the penalty for mixing of two components.

The morphology that is formed can to some degree be predicted using the molecular weight fraction of the different blocks as shown in Figure 1 for a mean-field calculation of diblock copolymers.
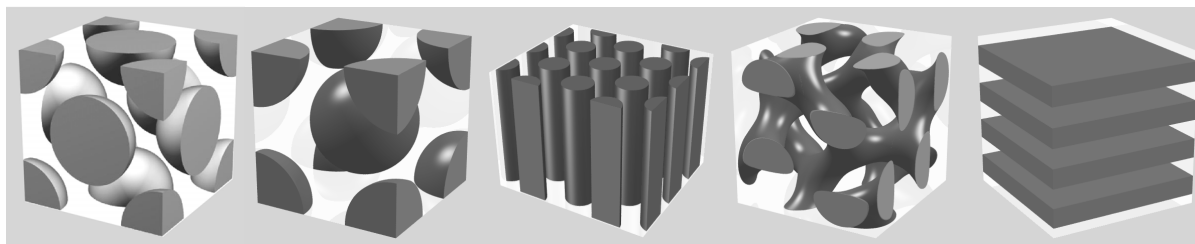
Figure 2: Different phases observed for increasingly symmetric molecular weights of the different blocks of diblock copolymers[6] (from left to right: FCC and BCC (different spherical micelles with cubic packing), hexagonally packed cylinders, gyroid (Ia3d), lamellae). The dark objects represent one of the two blocks, the empty space the other.

For very asymmetric ratios of the blocks packed spheres are formed. When the blocks become more and more symmetric the morphologies go from a hexagonal packing of cylinders, over different bicontinuous structures to lamellar structures.

That different morphologies are formed is caused by an interplay between the minimization of the interface surface and entropic penalties due to the stretching of the polymer chains.

In principle similar trends apply to the morphologies that are formed in solution, except that in solution the interaction of the polymer with the solvent should be taken into account. The solution equivalent structures to spheres, cylinders and lamellae are micelles, worm-like micelles and vesicles (Figure 3).
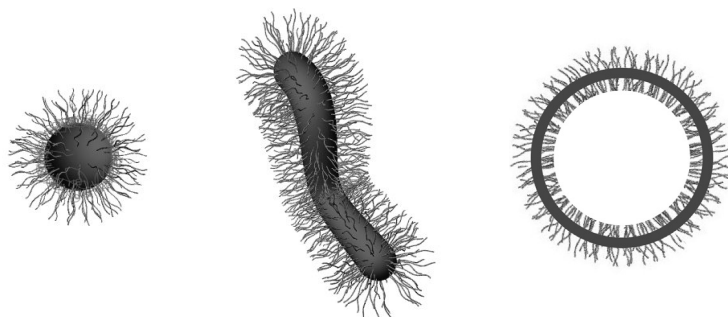

Figure 3: Different morphologies block copolymers can adopt in solution[6]. Left to right: micelles, worm-like micelles, vesicles.

2.3 Stimuli responsive polymers

In solution, several external factors influence the behavior of polymers, e.g. their solubility. Whether a polymer is soluble is influenced by the solvent quality, which can be either good, Theta (meaning the random coil acts as an ideal chain) or bad. The transition from a good to a bad solvent is hardly ever a sharp one; mostly it is a gradual transition. Some of the major influences on polymer solubility that can easily be influenced are discussed here. These are pH, ionic strength, temperature and light. The behavior of different groups of polymers to these stimuli is discussed.

2.3.1 Polyions

The group of polyions can be divided into polycations, polyanions and polyampholyte polymers. In all cases, a distinction can be made between polymers bearing strongly and weakly acidic or basic groups. Examples of weak acids and bases are monomers with carboxylic acids or primary, secondary and tertiary amines, respectively. Examples of strong polyions are monomers with sulfonate or phosphate groups, or with quaternized amines. Polyampholytes can be subdivided into two classes, which exhibit similar behavior, namely polymers where the monomer contains both cationic and anionic species (Zwitterionic polymers, e.g. polybetaines) and copolymers containing a mixture of monomers bearing positive and negative charges.

The solubility of weak polyions is strongly dependent on pH, since charges can be introduced into the polymer. In water, polymer solubility typically improves with charging of the polymer. Polyampholytic species have no net charge at their isoelectric point and thus are less soluble around this pH, whereas at higher and lower pH the polymers are soluble. Around the isoelectric point a complex coacervate phase is formed.

For polymers, the pK_a and pK_b values are often shifted to higher values compared to their low molecular weight counterparts, because the high charge density inhibits the charging of neighboring groups through entropic penalties paid for the stretching of the polymer chains. With increasing ionic strength this becomes less important due to the shielding of the charges. Though the solubility of strongly ionic groups is not dependent on pH, the same influence of salt is observed.

One group of (pseudo) polymers which should be mentioned here are coordination polymers, built up of "monomers" with multiple groups capable of binding multivalent cations. These monomers assemble into polymeric structures upon addition of such cations. The average length of the polymer chains is determined by the amount of end-groups with only one coordinating moiety. The effective charge of these polymers can be either positive or negative, depending on what kind of coordinating groups are used. If coordinating groups are used with multiple carboxylic acid groups, the negative charge of the carboxylic acid groups overcompensates the charge of the cation. When non-ionic coordinating groups, e.g. terpyridine moieties, are used, no charge is carried by the monomer unit itself, which leaves the polymer with a positive charge originating from the bound cations.

2.3.2 Thermoresponsive polymers

All polymers in principle display thermoresponsive behavior since in any given system the interaction between solvent and polymer, and with that the solvent quality, changes. Besides

gradual changes in solubility also sharp transitions can be observed. Two such effects are often found, namely Upper Critical Solution Temperature (UCST, highest temperature in the phase diagram where two phases are still formed) and Lower Critical Solution Temperature (LCST, lowest temperature in the phase diagram where two phases are still formed). The first of these is the temperature above which the polymer becomes soluble at any concentration. The second is the temperature below which the polymer is soluble at any mixing ratio. All polymers show this kind of behavior in any solvent, though the experimental window is not always wide enough to observe the transitions. The UCST or LCST is not to be confused with the cloud point temperature, which is the temperature at which the polymer precipitates from a certain solution. This temperature can vary strongly with e.g. polymer concentration. Phase diagrams for both UCST and LCST behavior are shown in Figure 4.
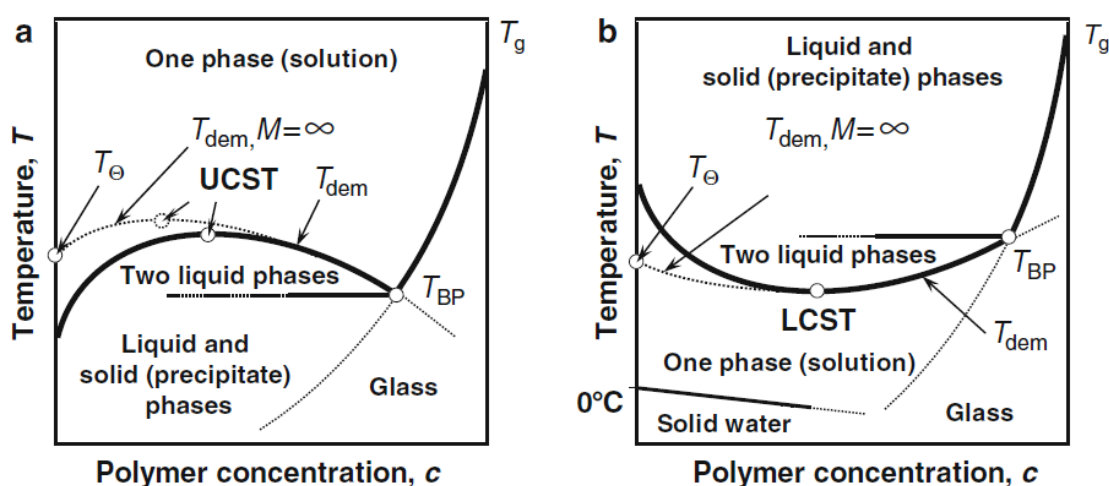
Figure 4: Phase diagrams of A) UCST and B) LCST behavior[7] (T_{dem}: temperature of demixing; T_g: glass transition temperature; T_{BP}: temperature corresponding to the Berghmans point; T_θ: theta temperature; M: molecular weight).

That the UCST and LCST transitions are often sharp is due to a cooperativity effect. The dissolution or precipitation of some monomer units triggers the same to happen to the rest of the polymer. Generally the transitions are reversible, though in many cases a hysteresis between the heating and cooling cycle is observed.

LCST polymers have been classified into three classes, named Type I through III[7]. Type I polymers show a shift of the LCST towards lower polymer concentrations and lower temperatures with increasing molecular weight. A phase diagram for poly(2-isopropyl-2-oxazoline) with different molecular weights is shown in Figure 5. This data shows that the LCST of this polymer, a Type I thermoresponsive polymer, shows exactly that behavior. Type II, to which the most well-known thermoresponsive polymer, poly(*N*-isopropyl acrylamide) belongs, does not show a dependence of the LCST with molecular weight. Type III polymers (e.g. poly(methylvinylether)) show both types of behavior.

Figure 5: Phase diagram for the LCST behavior of poly(2-isopropyl-2-oxazoline) (here abbreviated as PIPOZ) of different molecular weights as reported by Van Mele *et a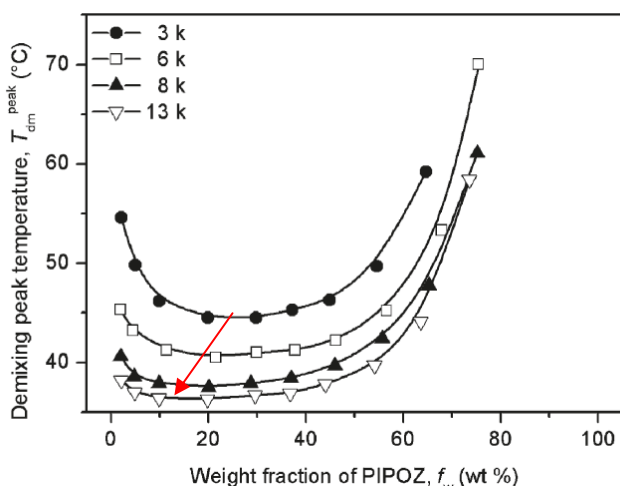l.*[8] (T_{dem}^{peak}: temperature at which a peak in the DSC measurements was observed, corresponding to the cloud point temperature. 3 k, 6 k, etc. indicate the number average molecular weights of the polymers).

Since it is the interaction between the solvent and the polymer which leads to thermoresponsive behavior, the solvent quality also strongly influences the thermoresponsive behavior. One can think of e.g. co-solvents and ionic strength. For co-solvents it is clear that a good solvent will shift the LCST to higher temperatures, whereas a poor solvent will lower the critical temperature. The same is true for the use of different salts though. The influence of ionic strength is strongly dependent on the nature of the salt. Hofmeister[9] was the first to describe this phenomenon for the precipitation of proteins isolated from egg-white. He noticed that certain salts induce the precipitation of protein (kosmotropic salts, order inducing) and others prevent it (chaotropic salts, disorder inducing), and that certain ions do so more strongly than others. Figure 6 shows for some often used ions whether they are kosmotropes or chaotropes. Though the mechanism is not fully clear yet, it seems likely that both the interaction of the salts with water (through binding of water molecules) and with the protein or polymer play a significant role in determining whether a salt is chaotropic or kosmotropic[10]. Generally the nature of the anion has a much stronger effect than the nature of the cation.

$$ Citrate^{3-} > SO_4^{2-} > PO_4H^{2-} > F^- > CH_3COO^- > Cl^- > Br^- > I^- > NO_3^- > ClO_4^- > SCN^- $$

$$ N(CH_3)_4^+ > NH_4^+ > Cs^+ > Rb^+ > K^+ > Na^+ > H^+ > Ca^{2+} > Mg^{2+} $$

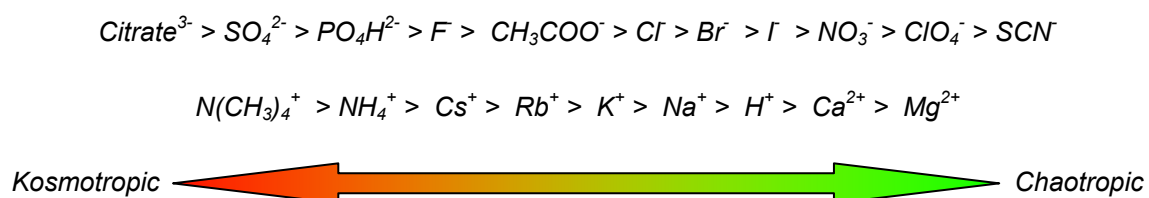Kosmotropic   Chaotropic

Figure 6: Hofmeister series, describing, for a selection of ions, which anionic and cationic ions influence the nature of the salt (being either kosmotropic or chaotropic) to what extent.

In some cases alternative behavior can be observed, which can e.g. be related to the charge of the surface of the particles[11].

2.3.3 Light responsive polymers

Though most polymers do not show light responsive behavior there are a number of classes of monomers that are either degraded or undergo a conformational transformation upon irradiation with light. A good example of a group of monomers which undergo a conformational transition upon irradiation, are monomers containing diazene groups. Using light with a short wavelength, these groups undergo a transition from the *trans-* to a *cis-*conformation. The reverse transformation follows either with time, an increase in temperature or by irradiation with longer wavelength light. When these monomers are used in combination with monomers which are close to undergoing a transition, e.g. thermoresponsive polymers, the irradiation with light can lead to a lowering of the cloud point temperature and thereby to the precipitation of the polymer from solution. This effect can be traced back to a stronger hydrophobic interaction between the diazene moieties. The percentage of light-responsive groups is critical in steering the effectiveness of this switch. Often the addition of cyclodextrins is used to enhance the effect. Cyclodextrin binds to the light responsive monomer in its *trans-*conformation but not in its *cis-*conformation. The binding of the strongly hydrophilic cyclodextrin enhances the solubility of the monomer in water, making the influence of the transformation from *trans* to *cis* more pronounced[12].

Another example of light responsive comonomers are monomers with spyrobenzopyran groups. In a polar surrounding these groups are normally charged, but they become uncharged upon irradiation. This feature can be used much in the same way as the previously mentioned system[13].

Besides conformational transitions, light responsiveness can also be expressed as the irreversible cleavage of the responsive group, which can change the solubility of the polymer.

2.4 C3Ms

Complex Coacervate Core Micelles[14] (abbreviated C3Ms, also known as PolyIon Complex (PIC) micelles, Block Ionomer Complex (BIC) micelles or Inter PolyEleCtrolyte (IPEC) micelles) were first described by Harada and Kataoka[15]. C3Ms are micelles formed by the interaction of two oppositely charged polymer blocks. That is, by the interaction of a polyanion block with a polycation block. Using at least one block copolymer, the precipitation of the complex as a complex coacervate can be prevented. This leads to the formation of micelles with a complex coacervate core, which are stabilized by a soluble, non-ionic polymer block[16]. The driving force for the formation of complex coacervates is not only enthalpic in nature, through the attraction between oppositely charged ions, but also entropic since counter ions and (hydration) water molecules are released, which is entropically favorable.

For C3Ms to be formed, both polyelectrolytes need to be charged to some degree, yielding a strong pH dependence when weak polyions are used. Shielding of the charges using high ionic strength can also lead to a dissociation of the complex.

Since C3Ms offer the possibility of introducing two different non-ionic polymer blocks in one micelle through the use of two diblock copolymers, it is possible to obtain micelles with two different types of polymer in the corona. The relatively high concentration of polymer in the corona can lead to phase separation, which can yield e.g. patchy or Janus micelles, the latter having two distinct hemispheres. This was first shown by the group of CohenStuart[17].
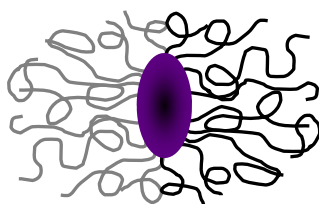

Figure 7: Schematic structure of a complex coacervate core Janus micelle.

The Janus micelles (C3JMs) which were described had, due to the repulsion between the two coronal blocks and a minimization of the interfacial area between the two coronal blocks, an oblate ellipsoidal (sphere that has been compressed in one direction) core and a prolate ellipsoidal (sphere that is elongated in one direction) corona, as schematically shown in Figure 7.

C3Ms have been proposed as vehicles to be used in drug delivery[18]. A special example is the use of C3Ms for the delivery of nucleic acids[19]. In that case, DNA or RNA is not only incorporated in the micelles, it is an integral part of them since the negatively charged nucleic acids are typically complexed with block copolymers bearing positive charge.

Besides micelles, also vesicles can be prepared[20]. Whether micelles or vesicles are formed is dependent on the relative amounts of complex coacervate (core material) and neutral, soluble material, as was mentioned in paragraph 2.2.

Another category of polymer assemblies based on the same type of interactions are vesicles and layers prepared by Layer-by-Layer assembly of polyanions and polycations[21]. The assemblies are prepared through the complexation of a polyion with an oppositely charged surface, followed by the addition of the other polyion. By application of several layers of polyions, applied alternatingly, a relatively thick and stable layer can be obtained. By dissolution of the substrate e.g. vesicles can be obtained, which have been proposed as drug-delivery vehicles, microreactors, etc..

2.5 Janus structures

In the last decades, several kinds of Janus type structures, deriving their name from the Greek deity Janus, the two faced god, have been created with sizes ranging over multiple length scales, from some nanometers to several micrometers. Janus structures are structures which exhibit two different 'faces', with different properties. The creation of these particles has received a lot of interest since the end of the 20th century, both out of academic interest and driven by industrial needs. It offers a new way to introduce super-ordering in a system on a nanometer scale, distinctly different from normal block copolymers or other asymmetric structures. Janus particles might be interesting as e.g. surfactants or as drug-delivery vehicles. In addition they display some similarity with numerous proteins in that they are not centrosymmetric but display different properties at different positions. They can therefore be suggested as model systems for the study of the aggregation behavior of certain proteins.

Several methods have been used to prepare Janus particles, ranging from the synthesis of complex, asymmetric polymeric or dendritic structures[22], the cross-linking of bulk morphologies[23,24], electrospraying or electrospinning[25] or the coating of particles on surfaces (either solid/liquid, liquid/liquid or liquid/gas)[26].

Most of these methods yield rather unresponsive particles due to their cross-linked nature. One of the few methods that, by self-assembly, yields thermodynamically stable and highly responsive (to ionic strength, pH, etc.) has been described by Voets *et al.*[17], who used C3Ms with two different neutral water soluble blocks which yield a corona in which phase separation takes place. In theory this phase separation can yield either patched, onion-type or Janus type micelles (Complex Coacervate Core Janus Micelles, C3JMs) (Figure 22).

This thesis works towards increasing the number of different methods by which this type of micelles can be prepared, and studies the aggregation behavior of C3JMs in comparison to C3Ms without a phase separated corona.

Not only micelles exhibiting a phase separated structure are of interest. Also for vesicles phase separation is an interesting theme, e.g. for the production of vesicles with asymmetric membranes. One approach that has been used to obtain such structures is the use of triblock copolymers[27]. One general problem of preparing such vesicles is that vesicles are normally obtained for systems with high amounts of the membrane forming block. Therefore the solubilizing blocks are mostly relatively short, which makes it harder to obtain a phase separated system.

2.6 The biotin streptavidin binding motive

Proteins are well known for their ability to very specifically bind all types of groups, whether small molecules, other proteins, surfaces, etc.. One of the strongest, non-covalent, specific binding motives known is the binding of biotin (vitamin B7) by avidin or streptavidin. The binding has a dissociation constant in the order of 10^{-13} M. Biotin is a coenzyme in the metabolism of e.g. fatty acids and leucine as well as in the generation of glucose. As a coenzyme it is covalently bound to the enzyme. Streptavidin is a 52.8 kDa tetrameric protein which is obtained from the bacterium *Streptomyces avidinii*. As far as function is concerned streptavidin is closely related to the glycoprotein avidin which can be isolated from egg-white. Both proteins are thought to work as antibiotics, binding any available biotin to prevent other organisms from growing.

2.7 Polymerization techniques

Over the last century a number of methods have been developed to, in a controlled fashion, prepare polymers. Among these are the so-called living polymerizations, which are polymerization techniques where no termination and chain transfer can take place. Additionally, the initiation step should be considerably faster than the chain propagation, in order to obtain a good control over the degree of polymerization. Living polymerizations show a predictable relationship between monomer conversion and average molecular weight and are often, but not necessarily, characterized by narrow molecular weight distributions. The fact that ideally no termination reactions take place, also makes it possible to control the end-groups. The only true living polymerization techniques are living anionic- and cationic-polymerizations, since in these cases side reactions can be fully circumvented by working under extremely pure conditions (preventing the presence of moisture and other terminating agents). Though extremely useful and much more widely used over the last decade, controlled radical polymerization techniques can technically not be considered living since some termination always takes place through the recombination or disproportionation of radicals. The effective concentration of radicals is usually so low that only a very minor amount of termination takes place.

2.7.1 Anionic polymerization

Anionic polymerization relies on the use of carbanion or other anionic species, such as oxyanions for propagation. Here a distinction between the polymerization of vinyl monomers and the anionic ring opening polymerization of heterocyclic monomers is made. For a more detailed overview the reviews by Baskaran and Müller as well as by Penczek *et al.* and Bywater *et al.*[28, 29,30] are recommended.

Living anionic polymerization of vinyl monomers

Though anionic polymerization was already known at that point, Szwarc *et al.* were the first to show the living nature of this polymerization technique in 1956 for the polymerization of styrene. This was the starting point of many investigations into living anionic polymerization.

The anionic polymerization of vinyl monomers is typically initiated using alkali metal containing substances, e.g. sodium naphthalenide or butyl lithium. After the initial nucleophilic attack of the anionic species onto the monomer, the alkali metal ion is present as a counterion. The ion pair can have the character of a contact ion-pair, solvent separated ion-pair or be present as free ions.
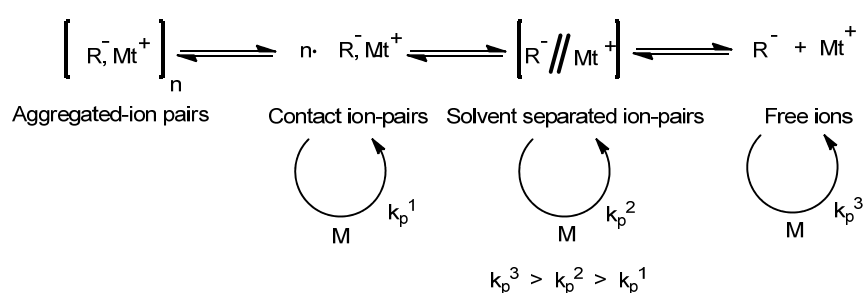

Figure 8: Mechanism of anionic polymerization (Mt: alkali metal, k_p: polymerization rate, M: monomer addition).

In anionic polymerization, the aggregation of ions, their solvation and ion-pair dissociation play the major role in determining whether the polymerization is controlled or not, since these factors strongly influence the rate of monomer addition. Though a detailed explanation of the influence of all these factors is beyond the scope of this section, it suffices to say that by adjusting the experimental conditions, e.g. using different counter ions (a bigger counter ion normally leads to faster polymerization), changing solvent polarity (more polar solvent yields faster polymerization due to easier ion-pair dissociation), the addition of salt or coordinating species (changing the solvation and ion-pair dissociation), etc., many monomers have successfully been polymerized in a controlled manner. At first, especially the polymerization of acrylic monomers was a challenge since the nucleophilic attack of the initiator or growing chain-end onto ester groups was a serious side reaction, limiting the usefulness of anionic polymerization for the polymerization of this group of monomers. Through the use of different initiator systems and coordinating groups these side reactions can be circumvented.

The polymerization of numerous monomers through anionic polymerization is impossible because many functional groups terminate the polymerization. This problem can to some degree be circumvented by the use of appropriate protecting groups.

In anionic polymerization the order in which monomers are added is very important, because the initiating group should be nucleophilic enough to initiate the polymerization of the following block. This seriously limits the types of block copolymers that can be synthesized. The order of reactivity for some often used monomers:

Styrene > butadiene > isoprene > vinyl pyridines > methacrylates > epoxides

Other than with radical polymerization techniques, it is relatively easy to control the tacticity of the polymer prepared through anionic polymerization. This is mostly done using coordinating groups which favor the addition of monomers in a particular orientation.

Living anionic ring-opening polymerization of heterocyclic monomers

Poly(ethylene oxide) (PEO) is one of the most widely used water soluble polymers. This polymer can only be prepared using ionic polymerization, unlike most vinyl monomers, which are also readily polymerized through radical polymerization. Numerous other heterocyclic monomers can also be polymerized anionically. As with the polymerization of vinyl monomers, the key process of polymerization consists of the nucleophilic attack of an anion onto the monomer. In case of cyclic monomers this leads to a ring opening. Besides PEO, many polymers are prepared by anionic ring-opening polymerization, for instance polypeptides via amino acid *N*-carboxyanhydride (NCA) polymerization and cyclic ethers and esters via lactones.

2.7.2 Living cationic (ring-opening) polymerization

Cationic polymerization relies on cationic species to propagate the polymerization. Cationic polymerizations are started using strong (Lewis) acids which yield large anions upon dissociation, such as hydrogen iodide (with extra iodide present) or perchloric acid. The resulting carbenium-ion which is formed for vinyl monomers, can be nucleophilically attacked by other monomers (propagation). As with anionic polymerization the kinetics can be strongly influenced by varying the reaction conditions, especially by the addition of coordinating groups which influence the nature of the ion-pair. Polyvinyl ethers, polyisobutylene and copolymers of isobutylene and dienes ("butyl rubber") are e.g. produced using cationic polymerization[31].

Heterocyclic monomers are also frequently polymerized using living cationic polymerization, e.g. the polymerization of THF, ethylene oxide and oxazolines. Here e.g. triflic acid is used to initiate the polymerization, forming an oxonium ion in the case of THF and ethylene oxide and a delocalized cation for oxazolines. Nucleophilic attack of another monomer and ring opening forms the propagating step[32]. The general mechanism of living cationic polymerization and the polymerization of oxazolines through living ring opening polymerization are shown in Figure 9.

General mechanism of cationic polymerization
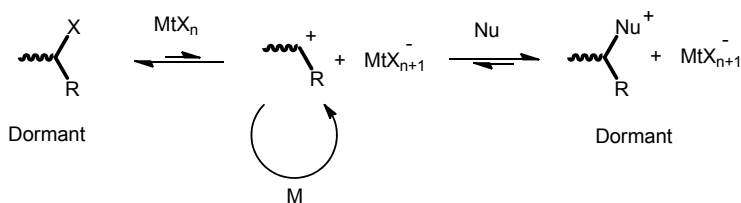
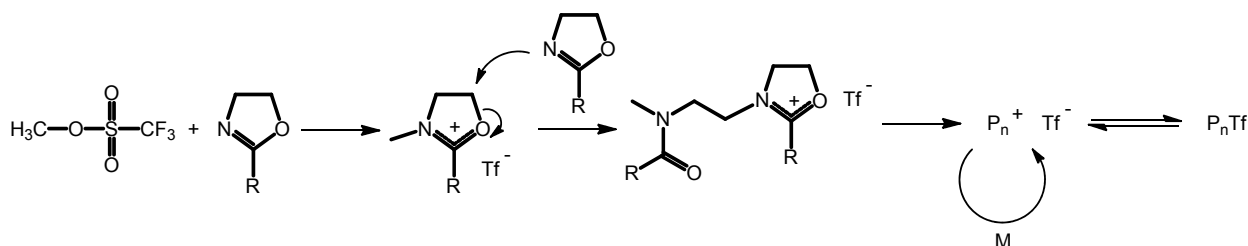Polymerization of oxazolines using methyl triflate

Figure 9: The general mechanism of cationic polymerization, as well as the polymerization of oxazolines by living cationic polymerization.

2.7.3 Controlled radical polymerizations

The group of controlled radical polymerization techniques offers a wide range of possibilities for the production of numerous different polymer morphologies and which can be adapted for the controlled polymerization of an extremely large number of different monomers. It is worthwhile mentioning that these techniques are significantly more tolerant towards functional groups and solvents than the abovementioned ionic polymerization techniques.

In general, the methods rely on the reversible stabilization of the growing polymer chain, using either a reversibly activated and deactivated end-group (ATRP, NMP) or the degenerative transfer of an end-group (RAFT). Numerous such groups have been used over the last decades, some of the most widely used are described here.

RAFT

Reversible Addition Fragmentation chain Transfer (RAFT) polymerization is probably the most widely applicable polymerization technique known, since it is compatible with numerous functional groups and solvents. That RAFT polymerizations can display a "*quasi-living*" character was first observed in 1998[33]. Generally thiocarbonylthio compounds are used to control the polymerization. The initiation of the polymerization involves the generation of radicals, mostly using azo-compounds such as AIBN, but also other radical sources can be used. The mechanism of the polymerization is shown in Scheme 1.

After the initiation, the propagating radical can add to the thiocarbonylthio compound (Chain Transfer Agent, CTA) which is followed by the fragmentation of the CTA, releasing a radical R⋅. This radical can form a new propagating species, polymerizing until in turn adding to a CTA, thereby activating other R groups, or at a later stage, polymer chains. This method allows the total concentration of radicals in solution to be kept relatively low, which is the main reason for the small degree of termination reactions and the narrow molecular weight distributions. The molecular weight of the polymer is, in an ideal case, determined by the concentration of CTA in relationship with the conversion of monomer. To obtain controlled polymerizations the proper CTA should be chosen, meaning the Z and R groups should be chosen correctly. A guideline for the choice of CTA for several classes of monomers is shown in Figure 10.

Scheme 1: Mechanism of RAFT polymerization.
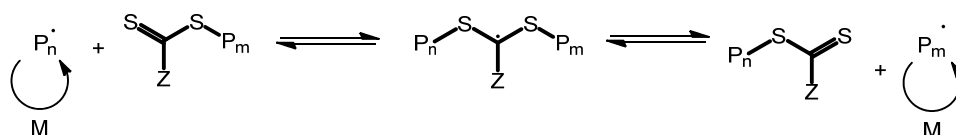
(1) Radical generation
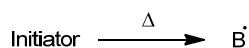
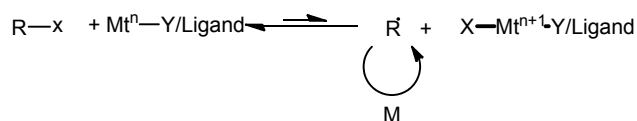(2) CTA activation/initialization
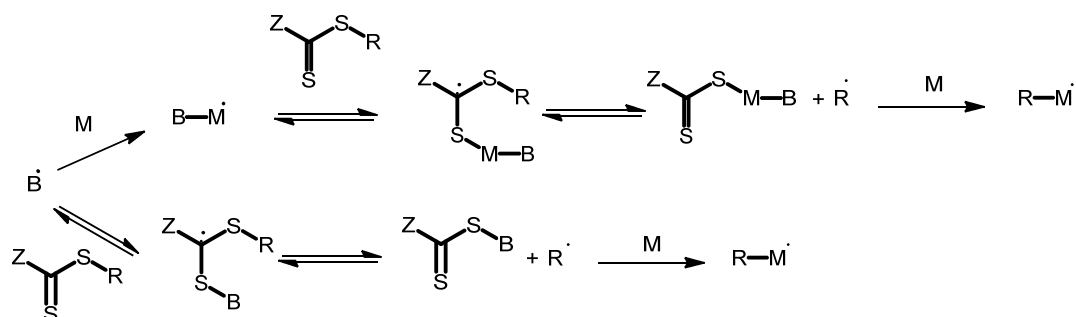
(3) Chain equilibrium

(4) Termination

Radical combination

The Z-group, which activates or inactivates the thiocarbonyl double bond, should allow for fast interchange of polymer chains. The R-leaving groups should be able to quickly and efficiently initiate the polymerization of the monomer (or monomers, in case of copolymers), and therefore should be a better leaving group than the dormant polymer chain. Inherent to the RAFT mechanism is also, though often ignored, a small amount of end-groups which arise from the direct initiation by the radical source[34].

Figure 10: Some general guidelines for the choice of a RAFT-agent[35].

ATRP

Atom Transfer Radical Polymerization (ATRP) is, besides RAFT, one of the most generally applicable controlled radical polymerization techniques. ATRP uses an initiator with a transferable halogen atom (mostly chlorine or bromine) together with a catalyst, normally a transition metal species (typically Cu(I)), often together with some ligand. In contrast to RAFT polymerization no radical initiator is used in normal ATRP. Reverse ATRP requires a radical initiator to generate the catalytically active transition metal species by reduction. The general mechanism of ATRP is shown in Scheme 2.

The reversible transfer of the halogen atom ensures the control over the polymerization. As in RAFT, the initiating system should be chosen properly, to ensure control over the polymerization. Therefore the proper initiators, transition metals and ligands for the transition metals should be taken. The purpose of choosing the latter wisely is to control the availability of the transition metal.

In comparison to RAFT, less different monomers can be polymerized with ATRP since the use of transition metals is required to obtain controlled polymerization. This limits the use of many monomers which form complexes with the transition metal, though such problems can be handled to some degree.

Scheme 2: Mechanism of normal and reverse ATRP.

Normal ATRP

$$R\text{—}x \quad + Mt^n\text{—}Y/Ligand \rightleftharpoons \quad R^\bullet \quad + \quad X\text{—}Mt^{n+1}\text{-}Y/Ligand$$

$$M$$

Reverse ATRP

$$Initiator \xrightarrow{\Delta} B^\bullet$$

$$B^\bullet \; + \; Y\,Mt^{n+1} \rightleftharpoons \quad B\text{—}Y \quad + \quad Mt^n$$

$$P_n\text{—}x \quad + Mt^n\text{—}Y/Ligand \rightleftharpoons \quad P_n^\bullet \; + \; X\text{—}Mt^{n+1}$$

$$M$$

For biological and medical applications ATRP has for a long time not been considered a viable method of polymerization since it has proven difficult to fully remove all transition metal, which is often toxic. In the last couple of years this problem has been to some degree circumvented by developing conditions where only minute amounts of transition metal is present, or by using non-ionic transition metal (e.g. Cu(0)) which show the same behavior, at their surface, as the ions which are normally used, but which do so without leaving traces of metal in the product[36].

NMP

Nitroxide Mediated Polymerization[37] is the third relatively widely used controlled radical polymerization technique. As the name says, the polymerization is mediated by nitroxide species, that is $(R)_2$-N-O$^\bullet$ stable free radical groups. As in ATRP, this technique relies on the reversible addition of a group to the end of the propagating chain.

In NMP, there are two main methods, namely bimolecular and unimolecular. The bimolecular mechanism uses normal radical initiation and an excess of nitroxide groups which, after initiation, reversibly combine with the radical of the propagating chain. The unimolecular method uses alkoxyamine initiators. This allows for a better control of the molecular weight of the polymer since the number of growing chains is independent on the formation of radicals by e.g. the thermal degradation of AIBN, which is often hard to control.

Scheme 3: Mechanism of bimolecular and unimolecular NMP.

Bimolecular NMP
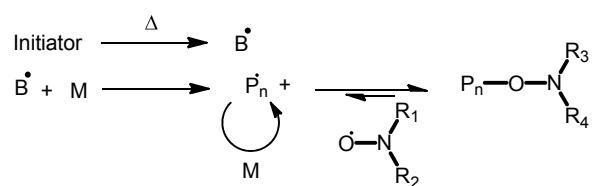
Unimolecular NMP
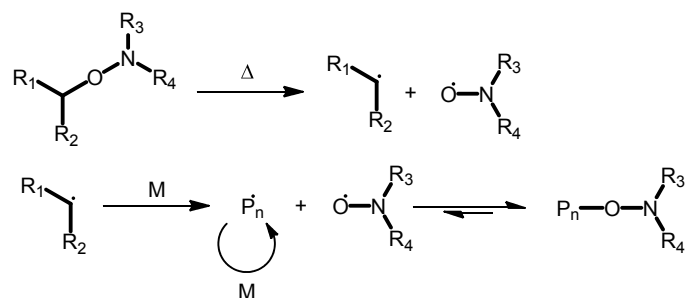
Chapter 3: Polyoxazoline-based core cross-linked micelles

3.1 Simultaneous functionalization and core cross-linking

3.1.1 Introduction

The cross-linking of polymer micelles has become an important research topic over the last years. The cross-linking of self-assembled structures has the advantage that the structures are significantly more stable towards external influences, such as dilution. For applications in e.g. drug-delivery, where normally only very small amounts of the drug is administered, this prevents the drug-delivery-vehicle from disintegrating in the blood-stream[38]. Also for catalytical applications, as e.g. described by Fréchet *et al.*[39], the cross-linking of the micelles allows for a one-pot multistep catalysis procedure, since the active species stay spatially separated.

Here, thiol-yne chemistry, the radical addition of thiols to triple bonds, is used in such a way that a simultaneous functionalization and cross-linking of the micelles takes place. The cross-linking is a side-reaction of the thiol-yne chemistry at high (local) concentration of alkyne groups.

Thiol-yne chemistry has lately attracted more and more attention as a tool in the creation and functionalization of macromolecules[40,41], e.g. for the creation of highly branched structures. Thiol-yne chemistry can be, like thiol-ene chemistry[42], a "click" reaction when the reaction conditions are chosen properly. Using thiol-yne chemistry, not only one but two functional groups can be attached to one unit (the second addition technically being a thiol-ene addition). Whereas thiol-ene addition onto polymers has been extensively studied[42,43], thiol-yne chemistry has, to the best of our knowledge, never been performed on the side chains of polymers, even though several suitable polymers have been described in literature[44].

3.1.2 Results and discussion

Monomer synthesis

The oxazoline monomer used in this work, 2-(3-butinyl)-2-oxazoline (ButinOx), was synthesized analogous to 2-(3-butenyl)-2-oxazoline as described by Greß *et al.*[42]. The three step process is shown in Scheme 4. More details are given in the appendix to this chapter.

Scheme 4: The synthesis of 2-(3-butinyl)-2-oxazoline ((1) *N*-Hydroxysuccinimide, EDAC, dichloromethane, rt, 12 h; (2) 2-chloroethylamine hydrochloride, 0.94 N aqueous NaOH, dichloromethane, rt, 12 h; (3) KOH, methanol, 70 °C, 12 h).
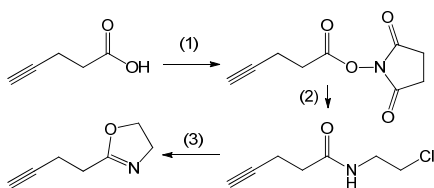
The overall yield of this three-step procedure was 28 %. The melting point of the monomer was determined to be 55 °C.

Polymer synthesis

A block copolymer of PButinOx and poly(2-ethyl-2-oxazoline) (PEtOx) was synthesized in acetonitrile using methyl triflate as an initiator for the sequential cationic ring opening polymerization of the two monomers. The conversion of the first monomer should be complete at the moment the second monomer is added. PButinOx$_{21}$-*b*-PEtOx$_{390}$ (as determined by ^{1}H-NMR, Figure 11) with an apparent PDI of 1.27 (SEC in NMP, PS standards, M_n^{App} 67 kg/mol) was obtained. A monomodal distribution is observed, indicating that no (detectible) PButinOx homopolymer is formed.
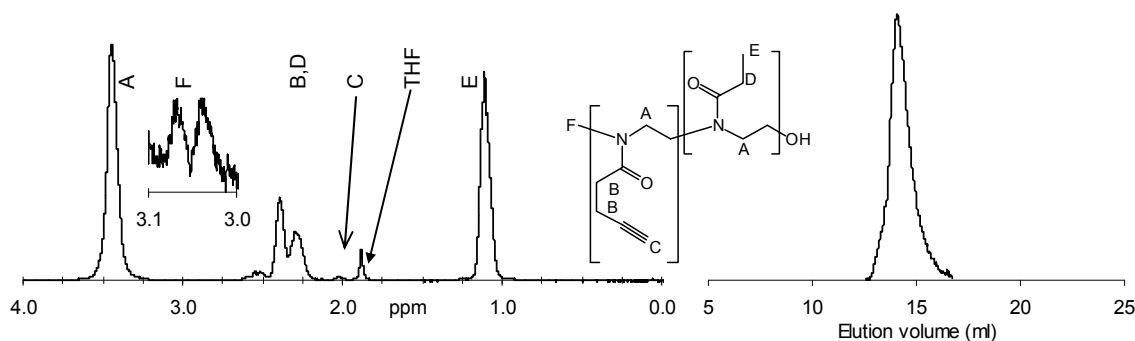
Figure 11: ^{1}H-NMR (CDCl$_3$) and SEC (in NMP) elugram of PButinOx$_{21}$-*b*-PEtOx$_{390}$ (integral peak F relative to A: 0.0018; C relative to A: 0.0132).

Cross-linking and functionalization of PButinOx-*b*-PEtOx micelles

In attempts to modify a homopolymer of PButinOx under conditions typically used for thiol-ene modifications, the production of large amounts of insoluble material is observed, indicating that a cross-linking reaction takes place upon modification of PButinOx with thiyl radicals. Though this cross-linking can be circumvented by using lower concentrations of polymer and higher excesses of thiol, a significant difference in the reactivity of the ButinOx and ButenOx is nevertheless observed.

The simultaneous functionalization and cross-linking of PButinOx is used to produce, in a single step, core cross-linked and functionalized micelles, using a block copolymer of PButinOx and PEtOx in aqueous solution. The first block forms the core of the micelles and is cross-linked as well as functionalized during the reaction. The second block is water soluble at room temperature and stabilizes the micelles. The synthetic procedure is shown in Scheme 5. The cross-linking is performed using one equivalent (to triple bonds) of the respective thiol. After irradiation with UV-light for approximately 18 hours an excess of the thiol is added to functionalize any leftover double or triple bonds.

The micelles formed in aqueous solution are characterized by dynamic and static light scattering. All light scattering samples were prepared at a concentration of 1 g/l, unless mentioned otherwise. They were shortly subjected to centrifugation prior to the filling of the light scattering tubes, in order to remove any dust.

At a concentration of 10 g/l (this concentration was used for the cross-linking reaction) aggregates are formed with a hydrodynamic radius of ~ 50 nm. Static light scattering revealed a radius of gyration of 44/38 nm respectively (as determined using partial Zimm and Guinier analyses respectively), with an aggregation number of approximately 22 polymer chains. The R_g/R_h ratio (~ 0.8) indicates that the aggregates are indeed micelles (0.775 is expected for hard-spheres).

The micelles maintain their size upon cross-linking, as could be shown by dynamic and static light scattering. With both techniques nearly identical sizes were found for the cross-linked micelles compared to the non-cross-linked micelles.

Scheme 5: Polymer synthesis (top) and cross-linking of micelles (bottom).

(1) methyl triflate, acetonitrile, 70 °C
(2) 2-ethyl-2-oxazoline
(3) Aq KOH, MeOH, 70 °C, 5h.
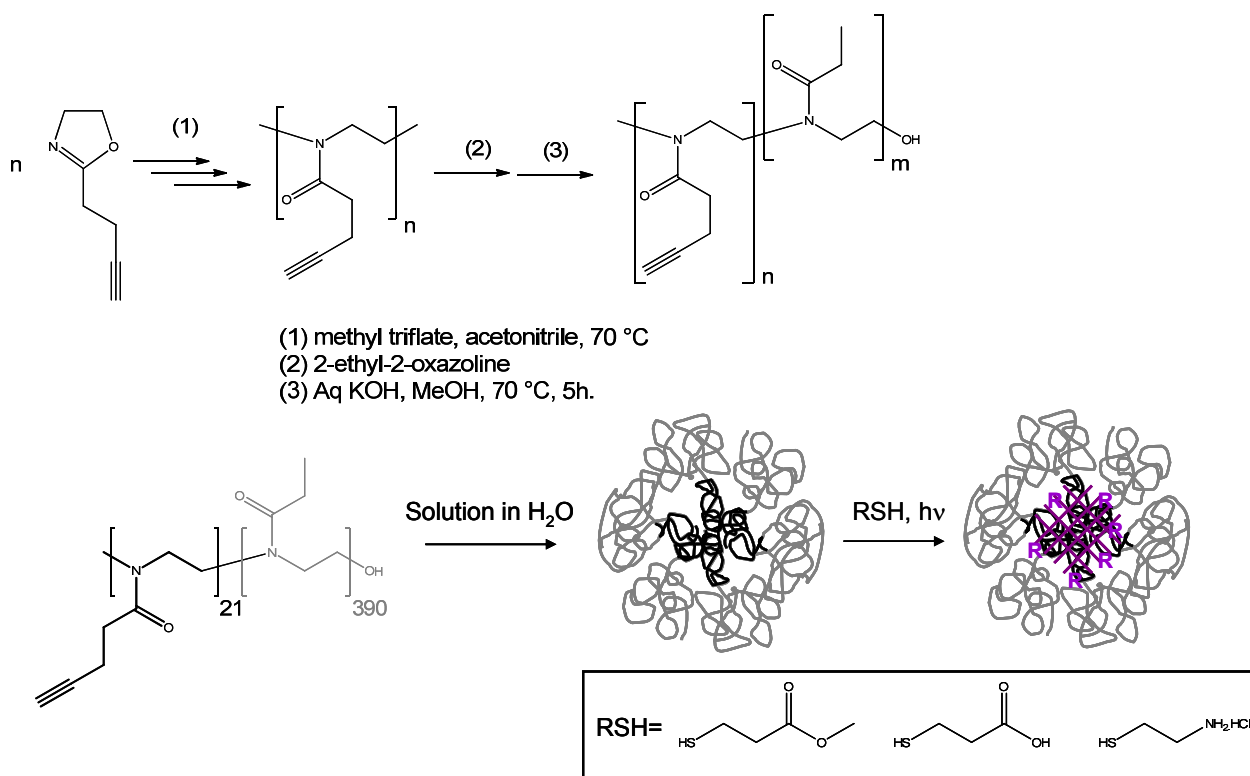
Dynamic light scattering is performed in THF to confirm that cross-linking takes place. In a non-selective solvent like THF, no larger aggregates are expected when no cross-linking takes place. For the precursor block copolymer only small objects, likely molecularly dissolved polymer chains, with a R_h of 7 nm are observed, and the scattering intensity is extremely low. For all cross-linked micelles (cross-linked either with an ester (methyl 3-mercaptopropionate), acid (3-mercaptopropionic acid) or base (2-aminoethanethiol hydrochloric acid) larger aggregates (R_h 25 - 30 nm) and far stronger scattering intensities are observed, so that it can be concluded that cross-linking took place.

Numerous analytical methods were performed to quantify the number of 3-mercaptopropionic acid and 2-aminoethanethiol groups incorporated into the micelles upon cross-linking. Unfortunately, it showed impossible to do so (FT-IR, elemental analysis, ^{1}H-NMR and acid/base titrations did not yield viable ways to quantify the number of functional groups). The presence of these groups could be shown using zeta-potential measurements though. Table 1 shows that the zeta-potential for the acid cross-linked is negative at pH 11 (far more so than for the non-cross-linked micelles at the same pH), showing the presence of acidic groups. The same is true for base cross-linked micelles, which show a strong positive charge at pH 3.

Table 1: Results from zeta-potential measurements.

	ζ-potential (mV)	Peak width (mV)
Polymer, pH 3	1.28	6.72
Polymer, pH 11	-0.37	3.97
Acid CL micelles	-3.43	3.73
Base CL micelles	7.59	3.54

For the ester cross-linked micelles the number of ester groups incorporated into the micelles could be estimated to be ~ 0.37 groups/triple bond using Raman spectroscopy, by comparing the relative integrals of the C=O stretch peak of the ester (at ~ 1740 cm^{-1}) and the C=O stretch of the amide backbone (at ~ 1630 cm^{-1}). As a reference a poly[2-(3-butenyl)-2-oxazoline] fully functionalized with methyl 3-mercaptopropionate (as prepared in ref 42) was used.

To get some insight into the mechanism of the cross-linking reaction, micelles were modified with methyl 3-mercaptopropionate in different ratios (with 2, 5 and 10 equivalences of thiol to triple bonds respectively). Besides the fact that the number of ester groups is relatively easily determined, the use of the ester is also advantageous since it is likely concentrated in the core of the micelles (which is not necessarily the case for the other thiols due to their solubility in water). No excess thiol is added after the initial cross-linking as was done in the earlier experiments. The Raman spectra of the products are shown in Figure 12. The number of ester groups per triple bond and the size of the micelles as determined by DLS are summarized in Figure 13.
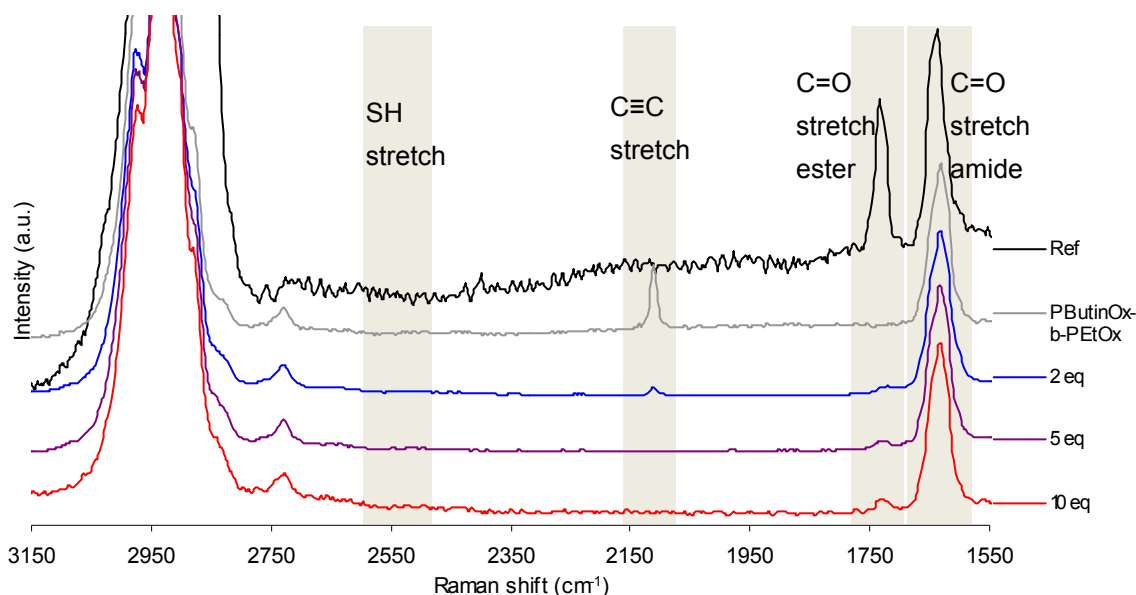
Figure 12: Raman spectra for PButinOx-*b*-PEtOx and micelles cross-linked with 2, 5 and 10 equivalences of methyl 3-mercaptopropionate respectively and the reference substance (PButenOx fully modified with methyl 3-mercaptopropionate). Spectra are normalized to the area under the amide C=O stretch peak.

The Raman spectra can also be used to visualize triple bonds and eventual thiol groups. Any peaks arising from C=C stretch that might occur, overlap with the C=O stretch of the amide

groups and are therefore not observed. The comparison of the relative integrals of the amide and ester C=O stretching peaks gives increasing degrees of functionalization with increasing amounts of thiol, the degree of functionalization increasing to up to 1.97. Though the presence of minor amounts of disulfide enclosed in the core cannot be excluded, the presence of thiols can be. With 10 equivalents of thiol, the highest amount of thiol used, cross-linking still takes place, as is shown by light scattering in THF.
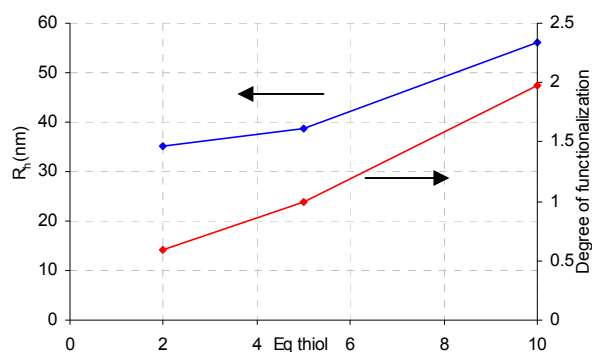
Figure 13: R_h of the micelles in THF (1 g/l) and degree of functionalization for micelles cross-linked with different equivalences of methyl 3-mercaptopropionate, determined using Raman spectroscopy.

Furthermore, the spectra indicate that indeed some triple bonds remain when low amounts of thiol (2 equivalent) are used. At five equivalent of thiol all triple bonds are consumed. The degree of functionalization is approximately 1 at these reaction conditions, which indicates that primarily triple bonds have been consumed. This shows the opposite trend of what was reported by Bowman *et al.*[41], who reported that the addition to the vinyl group is much quicker than the addition to the alkyne group. This difference might be due to a strong steric hindrance in the core of the micelle.

The size of the micelles cross-linked using 10 equivalents is significantly larger than the size of those at lower amounts of thiol, which is likely due to the incorporation of thiol in the micelles and a change in the effective packing parameter, as is schematically depicted in Figure 14. A crude calculation will tell that the radius of the core can easily double upon addition of ten equivalent of methyl 3-mercaptopropionate. Though all of the thiol is removed after the reaction the cross-linking stabilizes the swollen micelles.
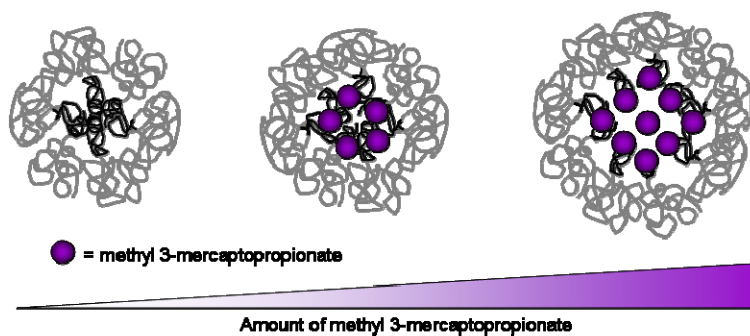
⬤ = methyl 3-mercaptopropionate

Amount of methyl 3-mercaptopropionate

Figure 14: Schematic representation of the swelling of micelles by added methyl 3-mercaptopropionate.

Two different cross-linking mechanisms can be envisioned, between which we cannot distinguish with the data at hand. Firstly the combination of two carbon radicals would lead to cross-linking, and secondly the addition of a carbon radical to a double or triple bond. Both mechanisms are shown in Figure 15. Since the concentration of radicals is rather low, the second pathway seems more likely.
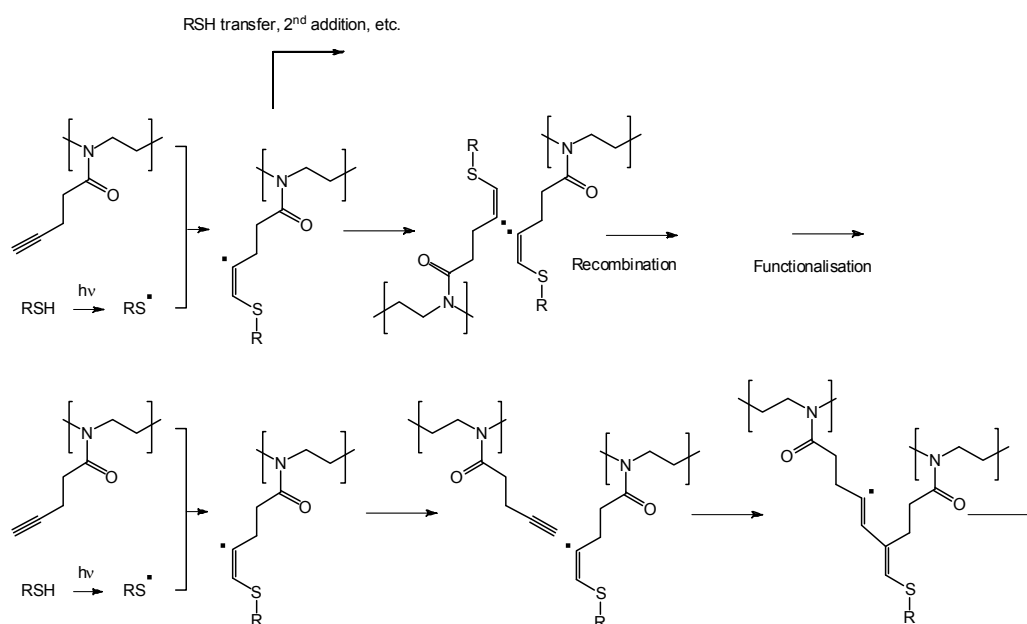
Figure 15: Examples of the suggested mechanism of cross-linking.

Why this cross-linking takes place is not fully clear, but since the cross-linking can, for the homopolymer, be prohibited by performing the reaction at more dilute conditions, the confinement in the micelle system is likely beneficial to the cross-linking. The influence of the local concentration is investigated by performing the cross-linking reaction of the block copolymer in THF, in which no micelles are formed. In this case no cross-linking is observed either, which supports the theory that the local concentration plays a major role in the cross-linking.

The cross-linking side reaction is only observed for the oxazoline monomer bearing triple bonds, not for its double bond counterpart, as could be shown by performing the same reaction (with one equivalent of methyl 3-mercaptopropionate) using a block copolymer of poly[2-(3-butenyl)-2-oxazoline] and poly(2-ethyl-2-oxazoline). The synthesis and characterization of this polymer are described in the appendix to this chapter. The reaction did not yield cross-linked micelles, which confirms that the reactivity of the triple bonds or any of its reaction products is needed to achieve cross-linking. Irradiation of PButinOx-*b*-PEtOx micelles with UV-light in the absence of thiol groups did not lead to cross-linking either. Likely the double bond formed after the first addition, which has a thioether neighboring group that makes it more reactive than its PButenOx counterpart, is involved in the cross-linking[45].

Lately thiol-yne chemistry has been used to produce numerous different functional materials[40,41], but in none of these any cross-linking was reported. One of the most obvious differences between those systems and the one at hand is the fact that the reported systems mostly concern (relatively) small and often stiff molecules. One theory is that some cross-linking might also occur for the systems described in literature, but that it is not directly observed because of insufficient possibilities for characterization and because of purification steps, though this cannot be easily proven. Also the local concentration is lower for these systems.

The fact that functional groups can readily be introduced in the micelles (e.g. pH responsive groups) makes it an ideal system to study the influence of charged groups on the aggregation behavior of cross-linked micelles, which is discussed in the following section.

3.1.3 Conclusion

A new method to simultaneously cross-link and functionalize polyoxazoline-based micelles is presented. This is achieved through the addition of thiyl radicals to the triple bonds in the core of poly[2-(3-butinyl)-2-oxazoline]-*b*-poly(2-ethyl-2-oxazoline) micelles. While cross-linking, nearly full functionalization can be achieved when a sufficiently high excess of thiol is used. The cross-linking of poly[2-(3-butinyl)-2-oxazoline] can be prohibited when its (local) concentration is low enough.

3.2 pH and thermoresponsive behavior of core cross-linked micelles

3.2.1 Introduction

In the last paragraph it was shown that micelles could, using thiol-yne chemistry, be easily cross-linked and functionalized simultaneously. Different types of functional groups could be introduced, some of which introduce a pH-responsive moiety. Generally, the cross-linking of structures renders them inert to some degree. This paragraph shows that using a Type I thermoresponsive polymer, the low degree of flexibility in the core of the core cross-linked micelles can still influence the behavior of the micelles as a whole.

The influence of the introduced charges in the core of the core-cross-linked micelles on the thermoresponsive behavior of the coronal block is investigated.

3.2.2 Results and discussion

The LCST behavior of the micelles is evaluated considering a number of parameters, such as pH, ionic strength and the nature of the salt. The cloud point temperatures (T_{cp}) of the micelles (the non-cross-linked micelles and the micelles cross-linked with either ester groups, acidic or basic moieties) are measured at three different pH values, namely at pH 3, 7 and 11, covering the range of fully charged to non-charged for the acid and base cross-linked micelles. The cloud point determinations were performed using 1 g/l solutions unless noted otherwise. The pH of the aqueous solutions was set using small amounts of 0.1 or 1 M HCl or NaOH solution. The results of these experiments are shown in Figure 16.

For the non-cross-linked micelles a slight, unexpected pH dependence of the cloud point temperature is observed (a slightly higher cloud point of 57.4 °C instead of 56.5 °C is found at pH 3)). This seems to be an intrinsic property of PEtOx, since commercially available homopolymer and block copolymers of poly(2-(3-butenyl)-2-oxazoline) and PEtOx (see appendix to this chapter) show the same trend. The fact that the cloud point temperature is highest at pH 3 suggests the presence of a small number of basic groups. The most likely explanation for the presence of basic groups would be a partial hydrolysis of the amide groups in the backbone, yielding secondary amine groups (as found in polyethylene imine). These groups were not observed in ^{13}C-NMR though, suggesting that if they are present, the degree of hydrolysis is very low. The fact that this behavior has not been reported before is likely due to the fact that slight amounts (e.g. 0.1 M) of salt are sufficient to shield these electrostatic interactions. Another explanation might be an effect of the Hofmeister series, which would suggest that

hydrochloric acid is chaotropic (though hydrochloric acid is not technically a salt). Since the concentration of HCl in solution is only 1 mM at pH 3, this would make the chaotropic effect of HCl extremely strong, which is unlikely.
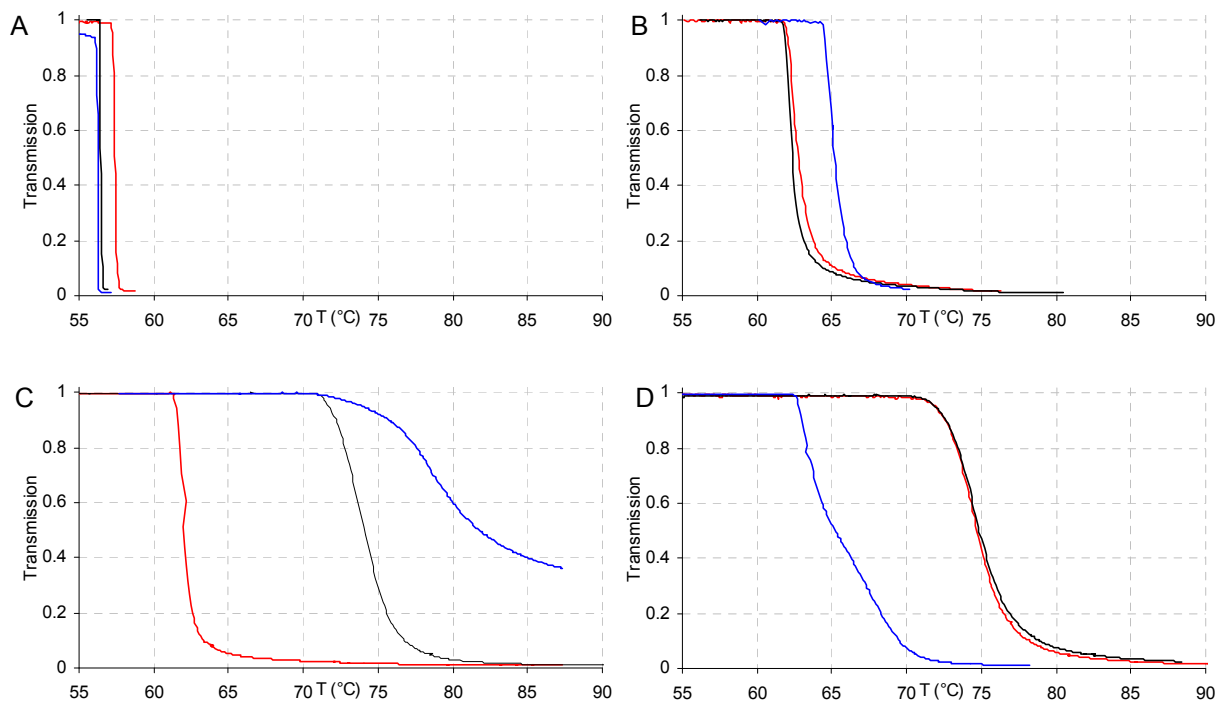

Figure 16: Cloud point determination of PButinOx-*b*-PEtOx A) micelles at 10 g/l (the data for 10 g/l are shown since this is the concentration at which the cross-linking is performed), B) methyl 3-mercaptopropionate cross-linked micelles (1 g/l), C) 3-mercaptopropionic acid cross-linked micelles (1 g/l), D) 2-aminoethanethiol HCl cross-linked micelles (1 g/l), at different pH values (red: pH 3, black: pH 7, blue: pH 11).

When comparing the cloud point temperatures of non-cross-linked micelles at 1 g/l (data presented in the appendix to this chapter, a comparison should be made between identical concentrations since the cloud point temperature is strongly dependent on the concentration of the solution for a Type I thermoresponsive polymer) to ester cross-linked micelles, only a minor difference between the respective T_{cp}s is observed (at pH 7 60.4 and 62.0 °C respectively). This indicates that the cross-linking itself only influences the cloud point temperature to a minor degree.

A far more dramatic effect is observed for the acid and base cross-linked micelles, which show a lower cloud point temperature in an uncharged state than in the charged state. The uncharged micelles show very similar T_{cp}s (61.7 and 63.2 °C for the acid and base cross-linked micelles respectively) as the non-cross-linked or the ester cross-linked micelles. The change in T_{cp} with pH is not trivial for block copolymer structures. The T_{cp} of block copolymers of PNIPAAm with acrylic acid e.g. are only reported to shift slightly[46], in contrast to the behavior of statistical copolymers[47]. The behavior could be explained by the swelling of the core upon charging of the

micelles[48], which decreases the concentration of the polymer chains near the core, which in turn leads to a higher cloud point (since the cloud point of a Type I thermoresponsive polymer such as PEtOx is strongly dependent on concentration). Another explanation is the introduction of electrostatic repulsion between micelles, so that collapsed micelles do not immediately aggregate upon the collapse of the PEtOx corona. DLS did not show significant difference in size with pH though. Also upon heating to temperatures above the T_{cp} of the non-cross-linked or ester cross-linked micelles, but below the observed cloud point temperature of the micelles at hand, no change in size is observed, indicating that there is no collapse of the corona at this temperature. This shows that it is not the repulsion between collapsed micelles that stabilizes them in solution. It rather indicates that the influence on the polymer density near the core is likely the major cause of the shift in cloud point temperature with pH. This would only cause a very minor increase in the overall size of the micelles and is therefore unlikely to be observed using DLS.

Note that though the T_{cp} of the micelles is shifted to higher temperatures, it is still within the temperature range available at normal pressure. This is not the case upon mere functionalization of a PButenOx-*b*-PEtOx block copolymer, as was shown by the functionalization of this block copolymer with acidic or basic moieties (Figure 17, the synthesis of these polymers is described in the appendix to this chapter). Light scattering on these fully functionalized, non-cross-linked polymers at a pH where the functional groups are fully charged, shows that though a very small number (as indicated by the low scattering intensity) of large aggregates is present in solution, this is the case both above and below the temperature where a cloud point is to be expected for the equivalent non-charged polymers, showing that there is no formation of micelles (the core of which would be formed by collapsed PEtOx, stabilized by the charged block) at higher temperatures[49]. This suggests that the cross-linking limits the influence of the charged block by limiting the variation in concentration.
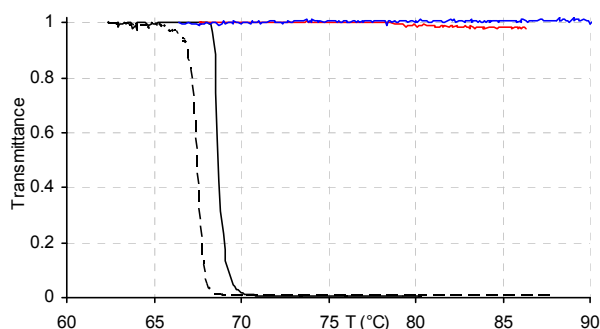
Figure 17: The effect of functionalization on the cloud point temperature of PButenOx-*b*-PEtOx. Black solid line: normal micelles, black dashed line: micelles cross-linked with 1,3-dithiolpropane, blue: 2-aminoethanethiol HCl modified polymer (pH 7), red: 3-mercaptopropionic acid modified polymer (pH 7, 1 g/l).

Since charge plays such a significant role in these systems it is to be expected that salt, which shields the charges and thereby might prevent the swelling of the core of the micelles, also has a significant influence on the pH- and thermoresponsiveness of the micelles. Using three different salts (sodium thiocyanate, sodium nitrate and sodium sulfate, a chaotropic, relatively neutral and kosmotropic salt respectively) the influence of different Hofmeister salts (see paragraph 2.3.2) is explored.

The acid cross-linked micelles were used in these experiments, in which the pH, salt and ionic strength were varied. The results are shown in Figure 18 through Figure 20 and are summarized in Figure 21.
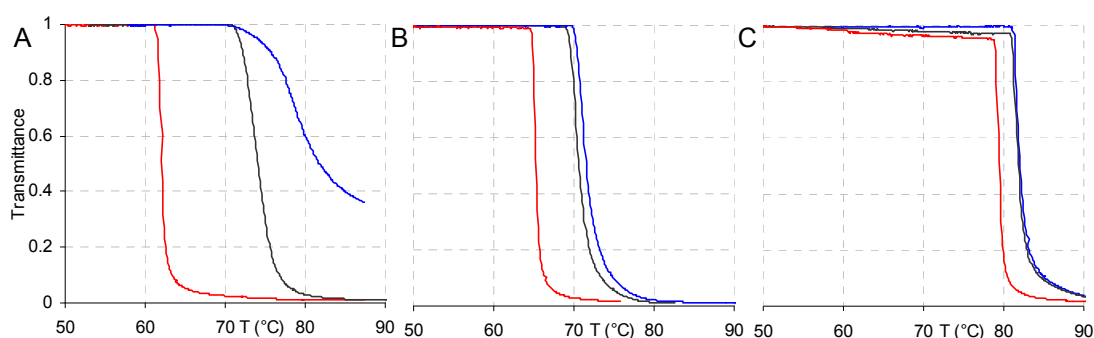
Figure 18: Cloud point determination of 3-mercaptopropionic acid cross-linked PButinOx-*b*-PEtOx micelles at pH 3 (red), 7 (black) or 11 (blue) at NaSCN concentrations of A) 0 M, B) 0.01 M and C) 0.1 M.
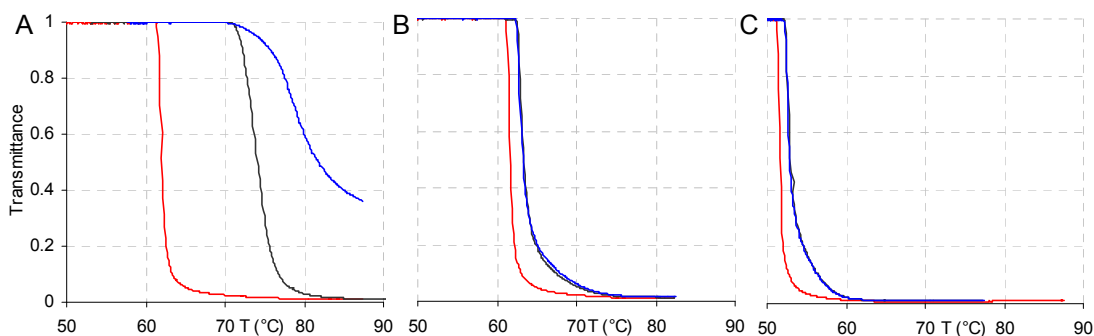
Figure 19: Cloud point determination of 3-mercaptopropionic acid cross-linked PButinOx-*b*-PEtOx micelles at pH 3 (red), 7 (black) or 11 (blue) at NaNO₃ concentrations of A) 0 M, B) 0.1 M and C) 1 M.
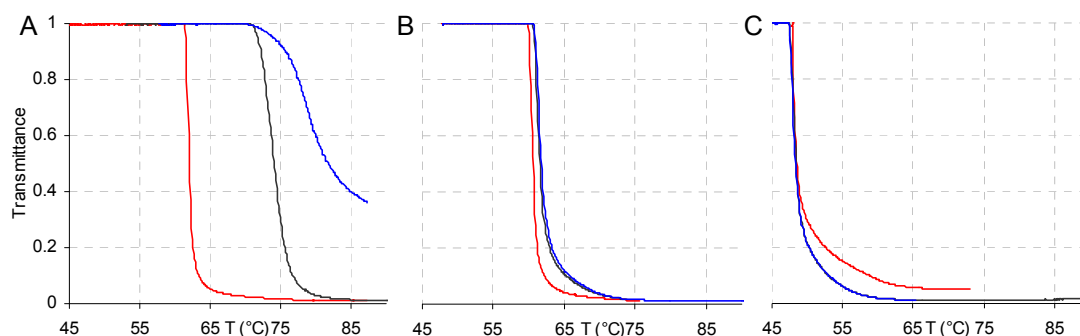
Figure 20: Cloud point determination of 3-mercaptopropionic acid cross-linked PButinOx-*b*-PEtOx micelles at pH 3 (red), 7 (black) or 11 (blue) at Na$_2$SO$_4$ concentrations of A) 0 M, B) 0.01 M and C) 0.1 M.
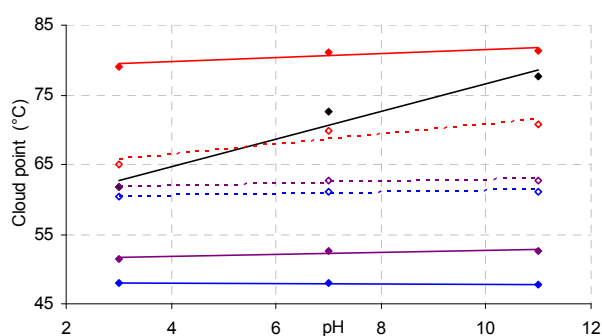
Figure 21: Cloud point temperatures of 3-mercaptopropionic acid cross-linked PButinOx-*b*-PEtOx micelles at different pH values with different salts and ionic strengths (black: no salt, dashed red: 0.01 M NaSCN, solid red: 0.1 M NaSCN, 0.1 M NaNO$_3$, dashed purple: 0.1 M NaNO$_3$, solid purple: 1 M NaNO$_3$, dashed blue: 0.01 M Na$_2$SO$_4$, solid blue: 0.1 M Na$_2$SO$_4$) (also see Appendix).

These experiments show that, upon increasing the salt concentration to 0.1 M, the dependence of the T$_{cp}$ on pH is practically lost (for NaNO$_3$ e.g. the initial difference in T$_{cp}$ between pH 3 and 11 of 16.1 °C is reduced to only 1.3 °C). Indeed, already at even lower ionic strength (e.g. 0.01 M) the effect is strongly weakened. An additional effect is observed which varies from salt to salt. The Hofmeister series predicts that some salts work as chaotropes, inhibiting self-assembly, and others as kosmotropes, inducing structure in a system. They do so because of their different influences on the structure of water and the interaction of the polymer with water. Here, the same effect is observed through the cloud point temperature of the micelles. As expected, the cloud point of the micelles increases when going from kosmotropic to chaotropic, that is, from Na$_2$SO$_4$ (47.8 °C at 0.1 M, pH 7) over NaNO$_3$ (62.7 °C at 0.1 M, pH 7) to NaSCN (81.3 °C at 0.1 M, pH 7).

3.2.3 Conclusion

The pH- and thermoresponsive behavior of core cross-linked polymer micelles, synthesized using a simultaneous cross-linking and functionalization by thiol-yne chemistry, is studied. Through the use of 3-mercaptopropionic acid and 2-aminoethanethiol in the cross-linking and

functionalization, pH-responsive groups are introduced. At low ionic strength the charging of the cores leads to higher cloud point temperatures, due to a swelling of the core and therefore a decrease in the local concentration of poly(2-ethyl-2-oxazoline). Since PEtOx is a Type I thermoresponsive polymer, its cloud point temperature strongly depends on the local concentration. Shielding of the charges using increasing amounts of salt weakens this effect. The use of different Hofmeister salts leads to a salting-in or salting-out of the micelles.

In principle the range of temperatures available using this type of systems is not limited to the range shown in this study (60 - 85 °C). To get closer to body temperature one only need change from PEtOx to poly(2-isopropyl-2-oxazoline), which has a far lower LCST (~ 36 °C) that is even tunable over a certain range because the cloud point temperature of the polymer is dependent on the molecular weight of the polymer[50] (Figure 5) and the concentration[51,52,53]. Alternatively also copolymers can be used.

Chapter 4: Core cross-linked complex coacervate core micelles and their aggregation behavior

4.1 Introduction

Complex Coacervate Core Micelles (C3Ms) are micelles formed by the complexation of a polyanion and a polycation, stabilized by at least one non-ionic, soluble polymer block, which is introduced using a block copolymer of a polyionic block and a non-ionic block. C3Ms are considered promising vehicles for drug-delivery, can be used for the preservation of proteins, etc.[14,15,16]. C3Ms are stimuli-responsive and are especially sensitive to changes in pH and ionic strength.

For numerous applications, this responsiveness can be both a blessing and a curse, since it can e.g. be useful for the release of drugs. At the same time it can lead to unwanted release through the disintegration of the aggregates before they can reach their destination. This can lead to side effects which should be circumvented as much as possible. For that reason it is of high importance that the vehicles used in e.g. drug delivery show some stability within the blood stream. One of the approaches to increase the stability is to cross-link the complexes, either reversibly or irreversibly (e.g. see Chapter 3).

Reversible cross-linking, especially a triggered disintegration of the cross-linking groups, would be the ideal approach since in this way the release of the active compound can be controlled[54]. The behavior of such systems can be complicated though, and cross-linked C3Ms have hardly been studied so far[48,55,56]. Especially the influence of external stimuli on the solution behavior of cross-linked structures is still relatively unknown.

The fact that two different polymers, one containing a polyanion block and the other a polycation block, can be used to form C3Ms, means that two different non-ionic polymer blocks can be introduced in the C3Ms. If two polymers are chosen which strongly phase segregate, a

microscopic phase separation can be achieved, leading to either onion-like, patchy or Janus micelles (see Figure 22).
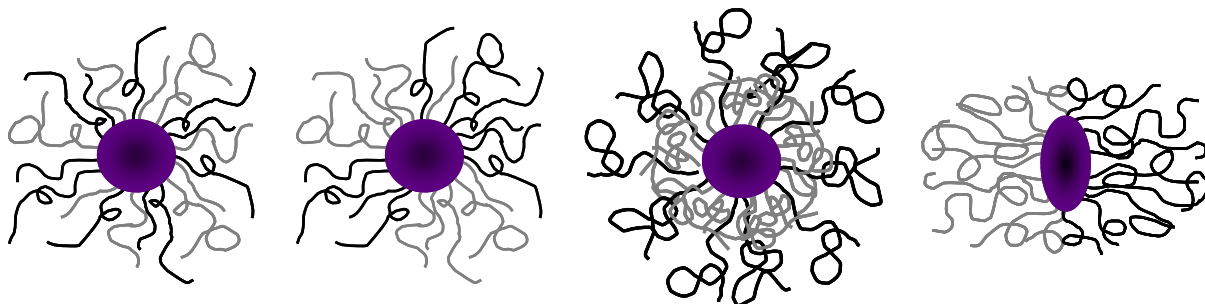
Figure 22: Schematic representations of (from left to right) mixed, patchy, onion-like and Janus micelles.

This chapter focuses firstly on the creation of Janus micelles (Complex Coacervate Core Janus Micelles, C3JMs) and their use for the creation of higher-order aggregates. Higher-order aggregates are obtained either directly from the Janus micelles, or by their interaction with other nanoparticles.

The creation of Janus micelles has received significant attention over the last decades (paragraph 2.5) since they might offer new and more complex properties. The two distinct phases in the corona of the particles display different properties and the micelles can therefore function as giant amphiphiles.

In this context both the properties of some novel non-cross-linked C3Ms and the properties of core cross-linked C3Ms (C5Ms) are studied. Besides determining the influence of cross-linking, also the interaction of the cross-linked structures with surfaces and their ability to build higher-order aggregates is investigated[57].

Secondly, this chapter deals with the behavior of micelles with a mixed corona, for which, using an external stimulus, phase separation can be induced. The structures that are formed upon introduction of this stimulus are studied. One way to do so is the cross-linking of the complex coacervate phase of these aggregates, thereby stabilizing the morphologies to some degree. It is also shown that this approach offers an easy way to obtain structures which were previously unattainable.

These two different approaches are separately discussed in paragraph 4.3 and 4.4 respectively.

4.2 Polymer synthesis

The polymers which were used have been chosen such that the C3Ms can be cross-linked easily. This is achieved by using carboxylic acid groups to create polyanions and primary amines for the polycations. These two moieties can easily and under mild conditions (also in aqueous solution) be cross-linked. The polyion blocks are typically either polymethacrylic acid (PMAA) or polyacrylic acid (PAA) (polyanions) and polyvinyl amine (PVA), 2-aminoethanethiol modified poly[2-(3-butenyl)-2-oxazoline] (PButenOx) (weak polybases), or poly(2-methyl vinylpyridine) (P2MVP, strong polybase) in one case. A variety of different non-ionic polymers is used, such as poly(ethylene oxide) (PEO), poly(dimethylacrylamide) (PDMAAm), poly(*N*-isopropylacrylamide) (PNIPAAm), polyvinylalcohol (PVOH) and poly(2-ethyl-2-oxazoline) (PEtOx).

It is expected that at least when using PEO with some other non-ionic polymer, phase separation might occur, since the polyamides are chemically very different from PEO and phase separation is known to occur for PEO/PAAm systems[17]. For other combinations phase separation is less likely to take place. Unfortunately the χ-parameters, describing the interaction between the different polymers, are unknown, so that this expectation cannot be substantiated.

The synthetic procedure by which the polymers have been synthesized is described in detail in the appendix. Polymethacrylic acid-*block*-poly(ethylene oxide) (PMAA-*b*-PEO) is synthesized by anionic polymerization in THF, of *tert*-butyl methacrylate and ethylene oxide, using diphenyl methyl potassium as an initiator[58]. The poly(*tert*-butyl methacrylate) block is deprotected by hydrolysis, yielding PMAA-*b*-PEO (Figure 23).

Using living cationic ring opening polymerization a poly[2-(3-butenyl)-2-oxazoline]-*block*-poly(2-ethyl-2-oxazoline) (PButenOx-*b*-PEtOx) polymer was synthesized. This was done in acetonitrile using methyl triflate as an initiator (Figure 24).
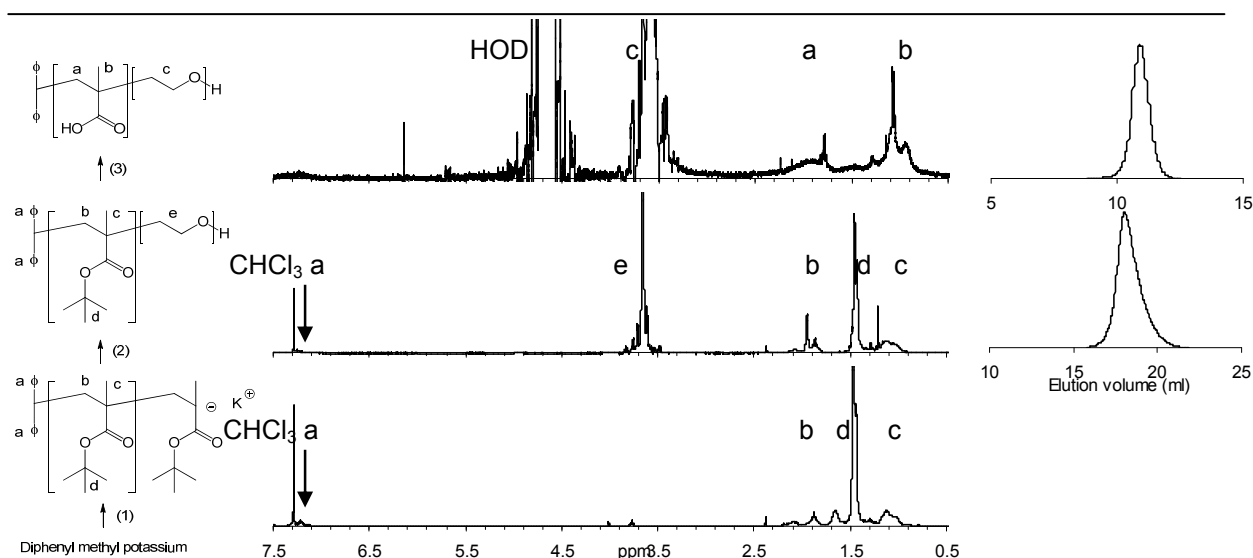
Figure 23: Synthesis pathway of PMAA-*b*-PEO, SEC elugram (THF) of PtBuMA-*b*-PEO and of PMAA-*b*-PEO (H₂O) and ¹H-NMR of PtBuMA (first block, CDCl₃), PtBuMA-*b*-PEO (CDCl₃) and PMAA-*b*-PEO (D₂O) before and after deprotection. (Reaction conditions: (1): Dry THF, *tert*-butyl methacrylate, diphenyl methyl potassium, - 80 °C, 2 h, (2): ethylene oxide, 45 °C, 3 days , (3): CHCl₃, TFA, 8 h.)
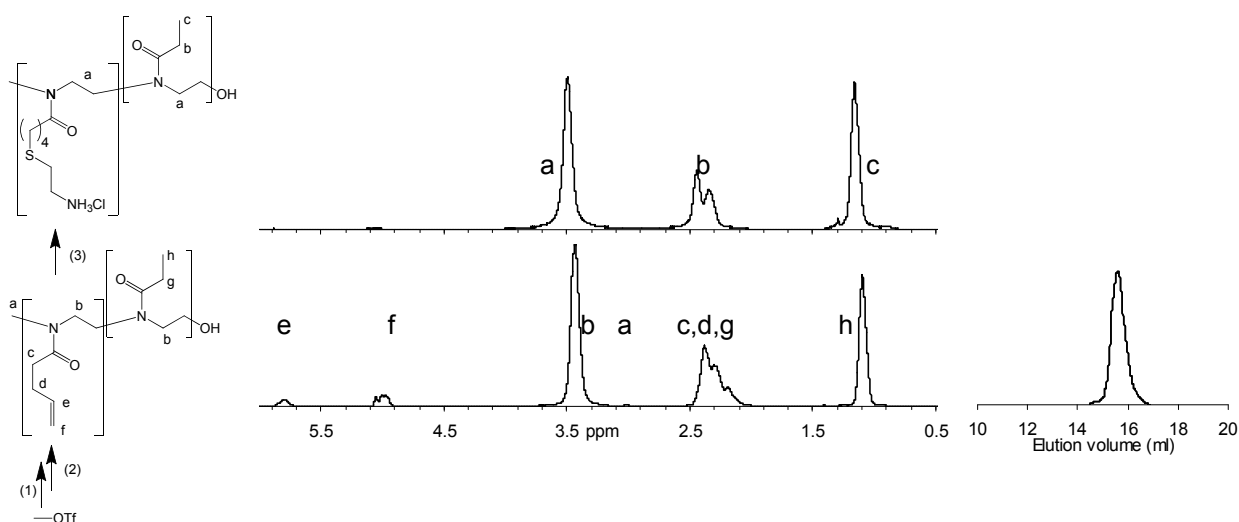
Figure 24: Synthesis of amine functionalized PButenOx-*b*-PEtOx, SEC elugram of PButenOx-*b*-PEtOx (NMP) and ¹H-NMR spectra of PButenOx-*b*-PEtOx (CDCl₃) and 2-aminoethanethiol HCl functionalized PButenOx-*b*-PEtOx (CDCl₃). (Reaction conditions: (1): 2-(3-butenyl)-2-oxazoline, methyl triflate, acetonitrile, 70 °C, 3 days, (2): 2-ethyl-2-oxazoline, 70 °C, 21 days, (3): 2-aminoethanethiol HCl, H₂O, UV.)

The PButenOx-*b*-PEtOx block copolymer was further modified with 2-aminoethanethiol HCl in a "thiol-click" reaction, as shown in Figure 24. Only very few double bonds were observed after this modification, which indicates that the functionalization was nearly quantitative (degree of functionalization > 95 %).

For the polymerization of all other polymers RAFT/MADIX was used, using a number of different chain transfer agents (CTAs). MADIX[59] is the name generally used for RAFT polymerizations using xanthate CTAs.

Except PVA, PVOH and P2MVP, all polymer blocks could be polymerized without further modification or deprotection. PVA was synthesized by the polymerization of *N*-vinyl phthalimide (VPh). After the polymerization of the second block the PVPh block was deprotected by hydrolysis[60]. PVOH was synthesized by the polymerization of vinyl acetate (VAc), followed by its hydrolysis to polyvinyl alcohol. P2MVP was synthesized by the polymerization of 2-vinyl pyridine (2VP), followed by quaternization with iodomethane.

The synthetic pathways for all polymers are summarized in Figure 25 through Figure 30. Table 2 summarizes the block lengths (as determined by a combination of ^{1}H-NMR (end-group analysis and monomer conversion) and SEC) and PDIs that were determined for the final polymers and their precursors.
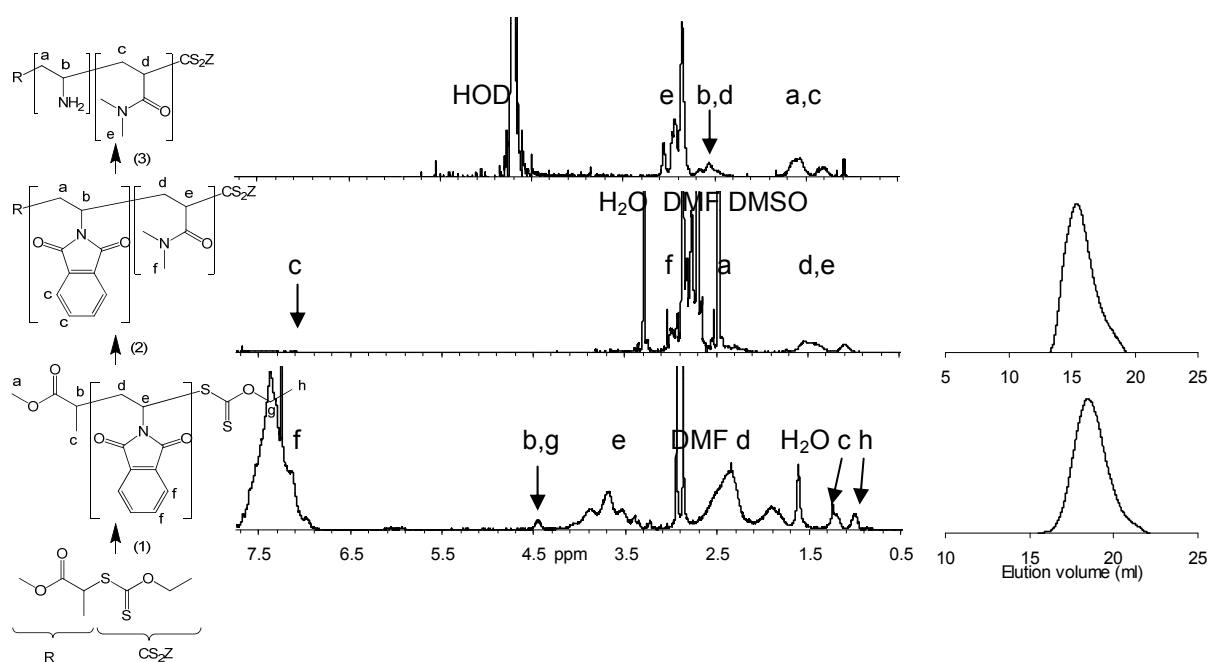
Figure 25: Synthesis of PVA-*b*-PDMAAm, SEC elugram of PVPh (THF) and PVPh-*b*-PDMAAm (NMP) and ^{1}H-NMR spectra of PVPh (CDCl₃) and PVPh-*b*-PDMAAm (DMSO-d₆) and PVA-*b*-PDMAAm (D₂O). (Reaction conditions: (1): *O*-ethyl-*S*-(1-methoxycarbonyl) ethyldithiocarbonate (1 eq), *N*-vinylphthalimide (40 eq), 0.1 eq AIBN, DMF, 70 °C, 16 hours, (2): 1eq PVPh, 400 eq DMAAm, 0.1 eq AIBN, DMF, 65 °C, 6 days, (3): dioxane, methanol, hydrazine, 65 °C, 16 h.)
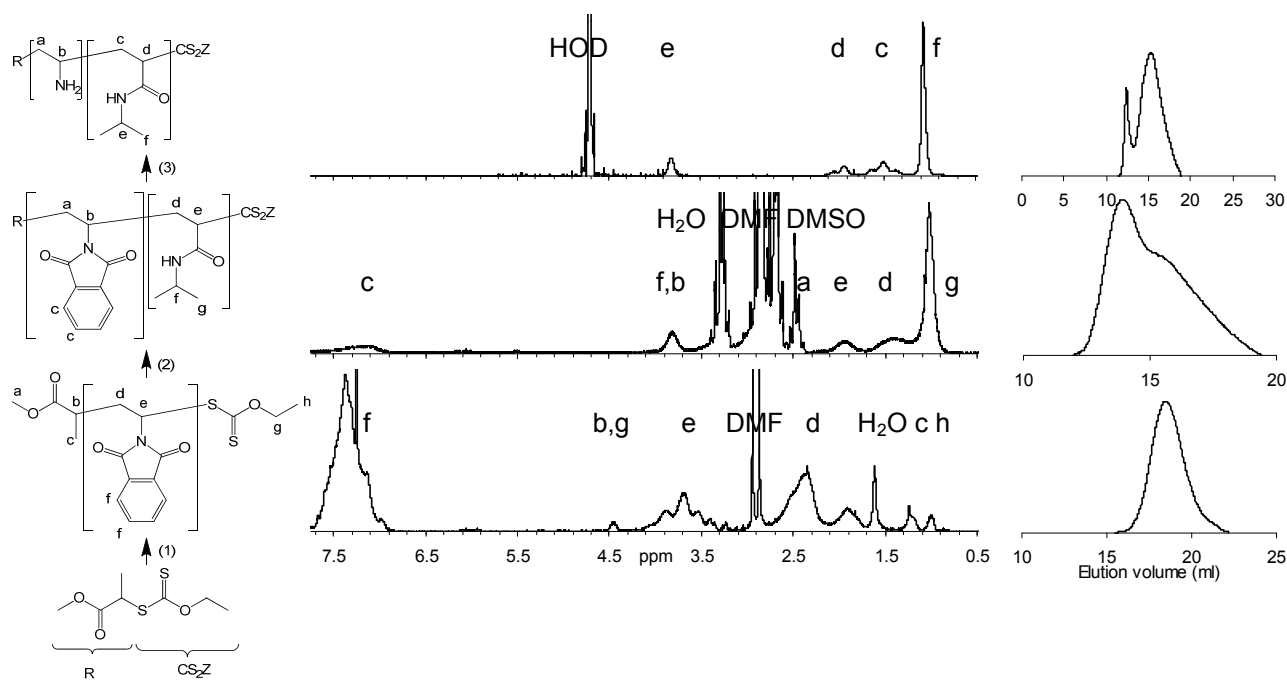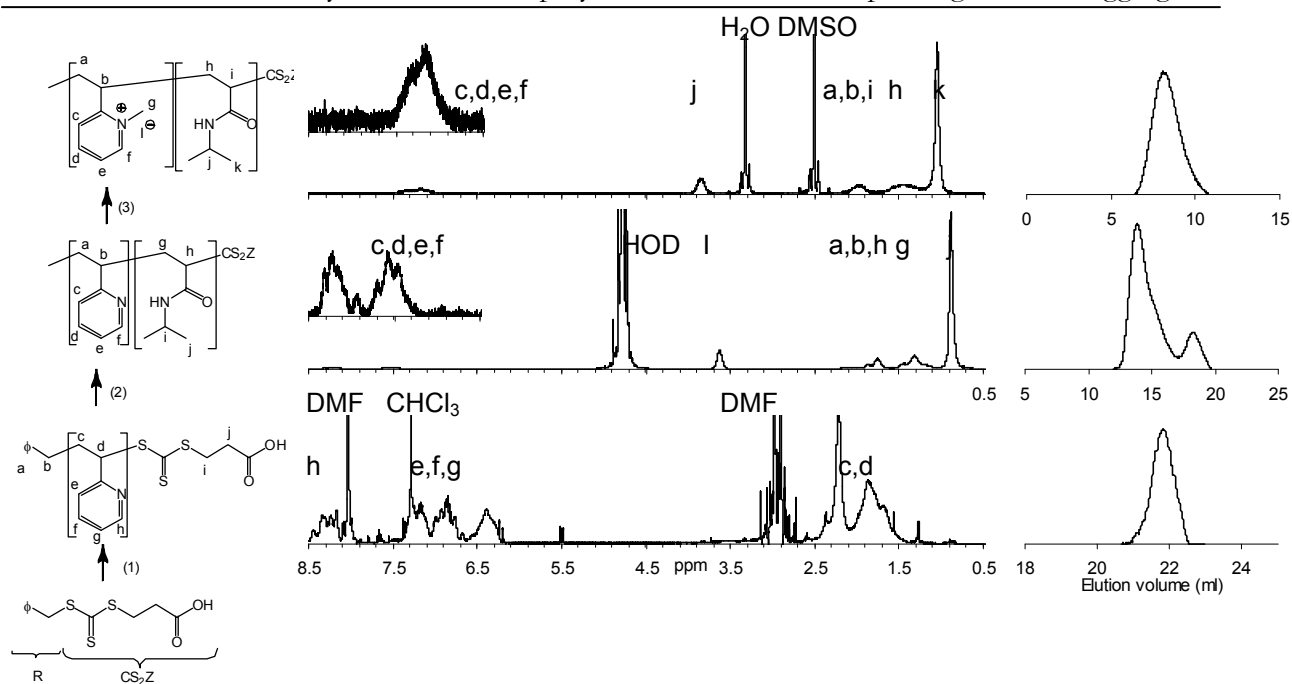
Figure 26: Synthesis of PVA-*b*-PNIPAAm. SEC elugrams of PVPh (THF), PVPh-*b*-PNIPAAm (NMP) and PVA-*b*-PNIPAAm (H$_2$O). ^{1}H-NMR spectra of PVPh (CDCl$_3$) and PVPh-*b*-PNIPAAm (DMSO-d$_6$) and PVA-*b*-PNIPAAm (D$_2$O). (Reaction conditions: (1): *O*-ethyl-*S*-(1-methoxycarbonyl) ethyldithiocarbonate (1 eq), *N*-vinylphthalimide (40 eq), 0.1 eq AIBN, DMF, 70 °C, 16 hours, (2): 1eq PVPh, 400 eq NIPAAm, 0.1 eq AIBN, DMF, 65 °C, 6 days, (3): dioxane, methanol, hydrazine, 65 °C, 16 h.)

In the SEC elugram of PVA-*b*-PNIPAAm a bimodal distribution is found. The main peak in this case is likely the polymer. The smaller peak at lower elution times (higher molecular weight) is attributed to the presence of some larger aggregates of the polymer, possibly formed through hydrogen bonding interaction.

The precursor to this polymer, PVPh-*b*-PNIPAAm, similarly shows a bimodal distribution but indicating the presence of some of the precursor PVPh homopolymer moreover. This is not observed in the final product, which might indicate that the significant change in molecular weight of this homopolymer upon hydrazinolysis allows for the removal of the homopolymer by dialysis.
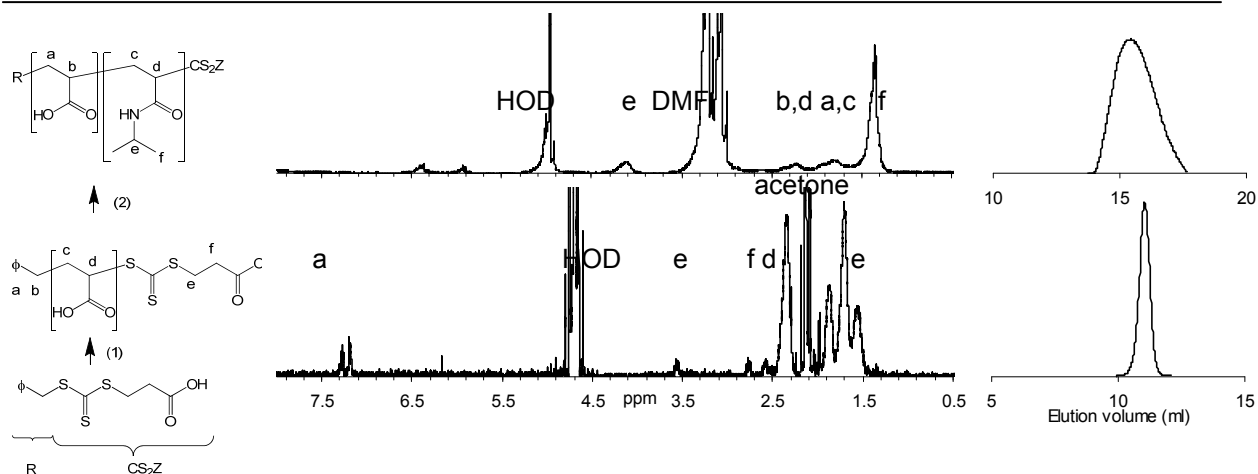
Figure 27: Synthesis of PAA-*b*-PNIPAAm, SEC elugrams of PAA (H_2O) and PAA-*b*-PNIPAAm (NMP) and the corresponding ¹H-NMR spectra in D_2O. (Reaction conditions: (1): 1 eq BPATT, 40 eq acrylic acid, 0.1 eq ACVA, 1:1 H_2O/acetone, 65 °C, 5 days, (2): 1 eq PAA, 400 eq NIPAAm, 0.1 eq AIBN, DMF, 65 °C, 4 days.)
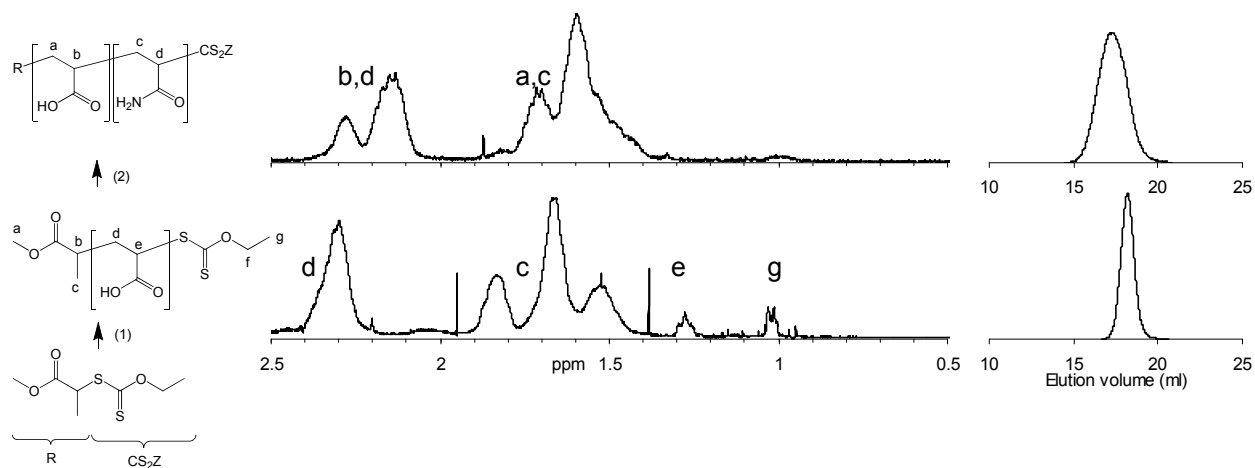
Figure 28: Synthesis of PAA-*b*-PAAm, SEC elugrams of PAA and PAA-*b*-PAAm in water, as well as the corresponding ¹H-NMR spectra (D_2O). (Reaction conditions: (1): *O*-ethyl-*S*-(1-methoxycarbonyl) ethyldithiocarbonate (1 eq), acrylic acid (40 eq), 0.1 eq AIBN, 1:1 methanol H_2O, 65 °C, 6 days, (2): 1 eq PAA, 400 eq acrylamide, 0.1 eq AIBN, 4:1 isopropanol H_2O, 65 °C, 7 days.)
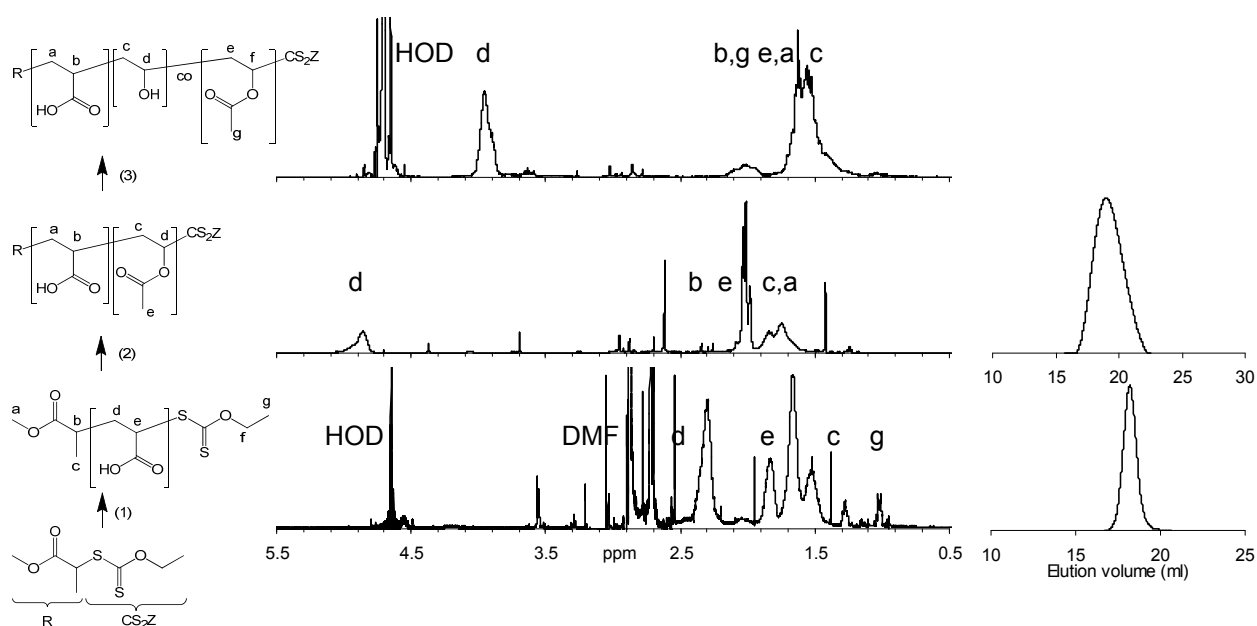
Figure 29: Synthesis of PAA-*b*-PVOH, SEC elugrams of PAA (H_2O) and PAA-*b*-PVAc (THF) and the ^{1}H-NMR spectra of PAA, PAA-*b*-PVAc and PAA-*b*-PVOH (in D_2O, $CDCl_3$ and D_2O respectively). (Reaction conditions: (1): *O*-ethyl-*S*-(1-methoxycarbonyl) ethyldithiocarbonate (1 eq), acrylic acid (40 eq), 0.1 eq AIBN, 1:1 methanol H_2O, 65 °C, 6 days, (2): 1eq PAA, 400 eq vinyl acetate, 0.1 eq AIBN, DMF, 65 °C, 7 days, (3): MeOH, KOH, 24 h.)

The degree of hydrolysis of the PVOH block is approximately 92 %, as determined by ^{1}H-NMR (Figure 29). This is close to the ideal degree of hydrolysis described in literature[61,62]. The solubility of the PVOH block in water increases with higher degrees of hydrolysis up to a certain point (~ 85 %), due to a decrease in the strength of the hydrophobic interactions. Beyond this point, strong hydrogen bonding interaction between polymer chains diminishes the solubility.

Figure 30: Synthesis of P2MVP-*b*-PNIPAAm, SEC elugram of P2VP (THF), P2VP-*b*-PNIPAAm (NMP) and P2MVP-*b*-PNIPAAm (H₂O), as well as ¹H-NMR spectra of P2VP (in CDCl₃), P2VP-*b*-PNIPAAm (D₂O) and P2MVP-*b*-PNIPAAm (DMSO-d₆). (Reaction conditions: (1): 1 eq BPATT, 40 eq 2-vinylpyridine, 0.1 eq AIBN, DMF, 65 °C, 5 days, (2): 1 eq P2VP, 400 eq NIPAAm, 0.1 eq AIBN, DMF, 65 °C, 5 days, (3): DMF, iodomethane, 60 °C, 48 h.)

The degree of quaternization was checked by determining the number of charged groups (at pH 11, to not take into account non-quaternized pyridine groups) by titration with a polyvinyl sulfonate while measuring the conductance of the solution. The degree of quaternization was determined to be quantitative.

Table 2: Summary of block lengths and polydispersity indices for the polymers used in this chapter.

1ˢᵗ block	2ⁿᵈ block	1ˢᵗ block M_n^{App}	App PDI	Eluent, standard	Block copolymer M_n^{App}	App PDI	Eluent, standard
PMAA₆₃	PEO₅₅₁	8840	1.5	THF, PtBuMA	9010	1.31	THF, PtBuMA
PButenOx₃₃	PEtOx₁₈₄	-	-	-	21520	1.03	NMP, PS
PVA₃₆	PDMAAm₄₀₀	920	1.32	THF, PS	23930	1.49	NMP, PS
PVA₃₆	PNIPAAm₃₆₈	920	1.32	THF, PS	23000	1.65	NMP, PS
PAA₅₃	PNIPAAm₃₀₀	3680	1.95	H₂O, PAA Na	27840	1.21	NMP, PS
PAA₃₈	PAAm₄₀₀	2380	3.0	H₂O, PAA Na	17400	(4.2)	H₂O, PEG
PAA₃₈	PVOH₁₈₀*	2380	3.0	H₂O, PAA Na	3910	1.97	THF,PS
P2MVP₃₆	PNIPAAm₃₆₈	900	1.05	THF, PS	76000	1.77	DMSO, PMMA

*: Degree of deprotection ~92%.

The synthesis of these polymers was successful, yielding mostly polymers with relatively low PDIs. Different combinations of anion and cation containing block copolymers were used for the preparation and characterization of C3Ms.

4.3 C3JMs and C5JMs

4.3.1 Introduction

C3Ms are in most cases thermodynamically stable structures, which can easily disintegrate or reorder upon dilution, changes in pH or ionic strength, and the addition of other (e.g. ionic) compounds to the system. To stabilize the C3Ms and thereby make them more suitable for use in e.g. drug delivery the cross-linking of the micelles has been suggested[56,63].

The cross-linking of micelles in general has been performed using numerous methods, using functional groups in the core of the micelles, e.g. to build disulfide bridges (which have the additional advantage that they can easily be broken), carbon-carbon bonds (by different curing procedures) or even light responsive moieties.

In this paragraph the synthesis and behavior of C3Ms which exhibit a phase separated corona is described. From this basis, the behavior of core cross-linked C3Ms (C5Ms) is studied. Primarily the formation of amide bonds from primary amines and carboxylic acid groups is used to this end. Though they cannot disintegrate, the cross-linked micelles should still be responsive to the same stimuli as before cross-linking, making e.g. swelling of the core still plausible. By changing the pH the net charge in the cores of the micelles should be affected, the influence of which on the behavior of the micelles is investigated.

Besides cross-linking of the micelles which involves both types of functional groups, it is also possible to cross-link one of the available functional groups, that is either the carboxylic acid groups or the amine groups. This selective cross-linking yields a system from which one of the original block copolymers can freely dissociate. Since one of the blocks is permanently cross-linked the effect of dilution cannot lead to the complete dissociation of the micelles anymore. Additionally the critical aggregation concentration (CAC) might be well below the CMC of the non-cross-linked micelles due to a cooperativity effect in the binding of the free block copolymer. If these structures combine extremely low CACs with responsiveness towards pH and ionic strength that would make them ideal vehicles for drug-delivery.

4.3.2 C3JMs

Influence of pH and f⁺

The ratio of acidic and basic groups is an important variable which strongly affects the stability of C3Ms. This ratio can be described by the fraction f^+, which is defined as follows[64]:

$$f^+ = \frac{[+]}{[+]+[-]}$$

wherein [+] and [-] are the respective concentrations of groups which can be charged positive or negative. For strong acids and bases, the concentration of charged groups is identical to these values independent of the pH. This is not the case for weak acids and bases, since the degree of ionization is strongly influenced by pH, more negative charge being created at high pH and more positive charge at low pH. This leads to a strong effect of both f^+ and pH on the morphology and stability of the micelles when weakly acidic and basic groups are used. At extreme pH values only one of the blocks will be charged, so that at this pH no C3Ms will be formed. This effect is clearly observed in all the systems that have been investigated in this work.

This behavior is explored in more detail. For a system consisting of PMAA-*b*-PEO and PVA-*b*-PDMAAm, as well as for the system of PMAA-*b*-PEO and PVA-*b*-PNIPAAm, f^+ series measured at constant pH (pH = 7) and pH series at constant f^+ (f^+ = 0.5) are shown in Figure 31 and Figure 32. All investigations are performed in aqueous solution.
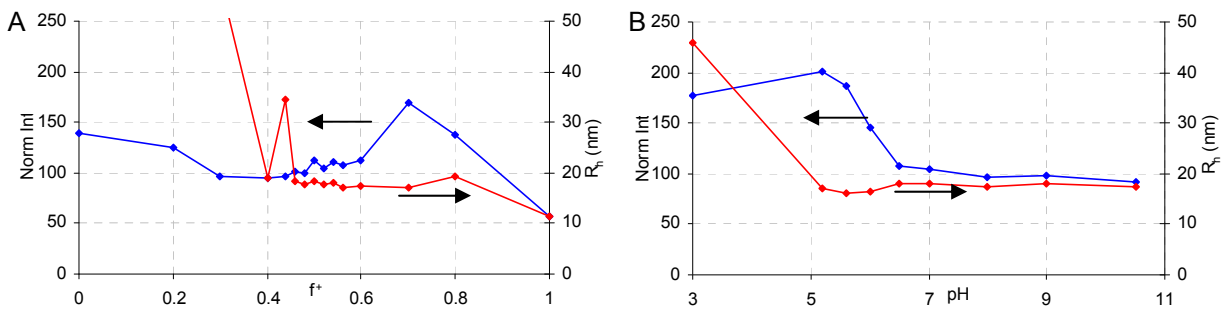
Figure 31: f^+ series at pH 7 (A) and pH series at f^+ 0.5 (B) for the PMAA-*b*-PEO/PVA-*b*-PDMAAm C3M system (1 g/l, 1 mM NaNO₃).
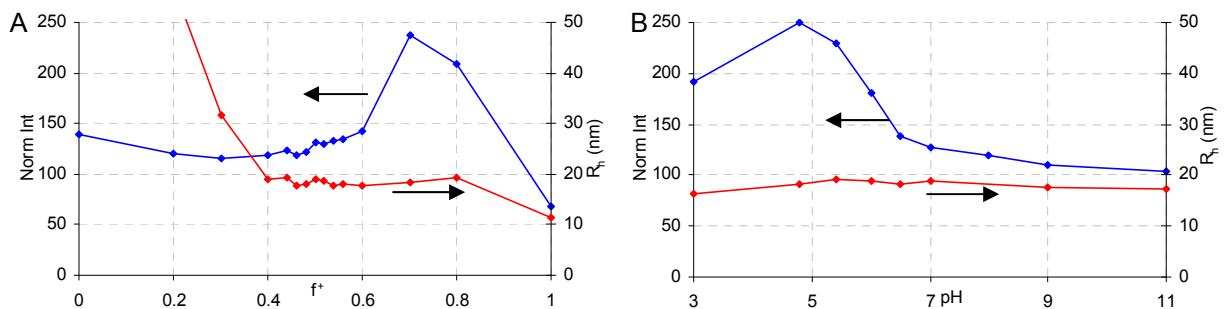
Figure 32: f^+ series at pH 7 (A) and pH series at f^+ 0.5 (B) for the PMAA-*b*-PEO/PVA-*b*-PNIPAAm C3M system (1 g/l, 1 mM NaNO₃).

In literature it has been described for many C3M systems that a peak in scattering intensity is observed at the optimal mixing conditions, due to higher concentrations of C3Ms. The increase in C3M concentration is due to a stronger driving force for complexation. Around the peak two

regions can be distinguished. One region close to the peak, where C3Ms are present at lower concentrations and coexist with some less well defined aggregates, and a region further from the optimal conditions, where only loose aggregates and molecularly dissolved chains are present[64].

This kind of behavior is also observed in the systems at hand. At a constant pH of 7, a peak at $f^+ \sim 0.7$ is observed, whereas at $f^+ = 0.5$ an optimum around pH 5 is observed. This means that at pH 7 equal amounts of positively and negatively charged groups are present at $f^+ = 0.7$. Since the degrees of charging for PVA and PMAA should be approximately equal at this pH, this indicates a slight error in the relative block lengths determined for the block copolymers (a longer PMAA block, a shorter PVA block, or a combination of the two). The fact that a peak is found at $\sim$ pH 5 (lower pH) when f^+ is fixed at 0.5 (the original values will be used for consistency, though they do not necessarily represent the actual values), can be explained by the fact that relative to the optimal conditions at pH 7 ($f^+ = 0.7$) less basic groups are present, meaning that the degree of ionization for these groups needs to be higher to obtain equal amounts of positively and negatively charged groups. Of course the degree of ionization of the PMAA block decreases at the same time.

The scattering intensities at the peaks are very similar, so that it can be concluded that the stability of the micelles is approximately equal for both optimal conditions.

This is also shown for a PAA-*b*-PVOH/PVA-*b*-PNIPAAm system (Figure 33). Here it is also clear that the optimal f^+ found for a certain pH (optimal $f^+ = 0.8$ at pH 7), yields the same pH when the f^+ is kept constant at that optimal value (f^+ kept at 0.8 → optimum at pH $\sim$ 7).

For both the PMAA-*b*-PEO/PVA-*b*-PDMAAm and the PMAA-*b*-PEO/PVA-*b*-PNIPAAm system, a strong increase in the size of the aggregates is observed at low pH. This can be attributed to hydrogen bonding interactions between PEO and PMAA[65] or between PMAA and PDMAAm or PNIPAAm[66], leading to the formation of large aggregates. The same would be true for PAA instead of PMAA. This was also shown for the block copolymers used in this work (PMAA-*b*-PEO, PAA-*b*-PDMAAm (PAA_{35}-*b*-$PDMAAm_{400}$, PDI^{App} 1.20, SEC in NMP, PS-standards, synthesis by RAFT polymerization using 2-dodecylsulfanylthiocarbonylsulfanyl-2-methyl propionic acid (DMP) as a CTA, the exact synthesis is not described) and PAA-*b*-PNIPAAm). The DLS data is shown in the appendix. In all cases a significantly stronger scattering intensity is observed at pH 3. This effect is strongest for PMAA-*b*-PEO and weakest for PAA-*b*-PDMAAm.
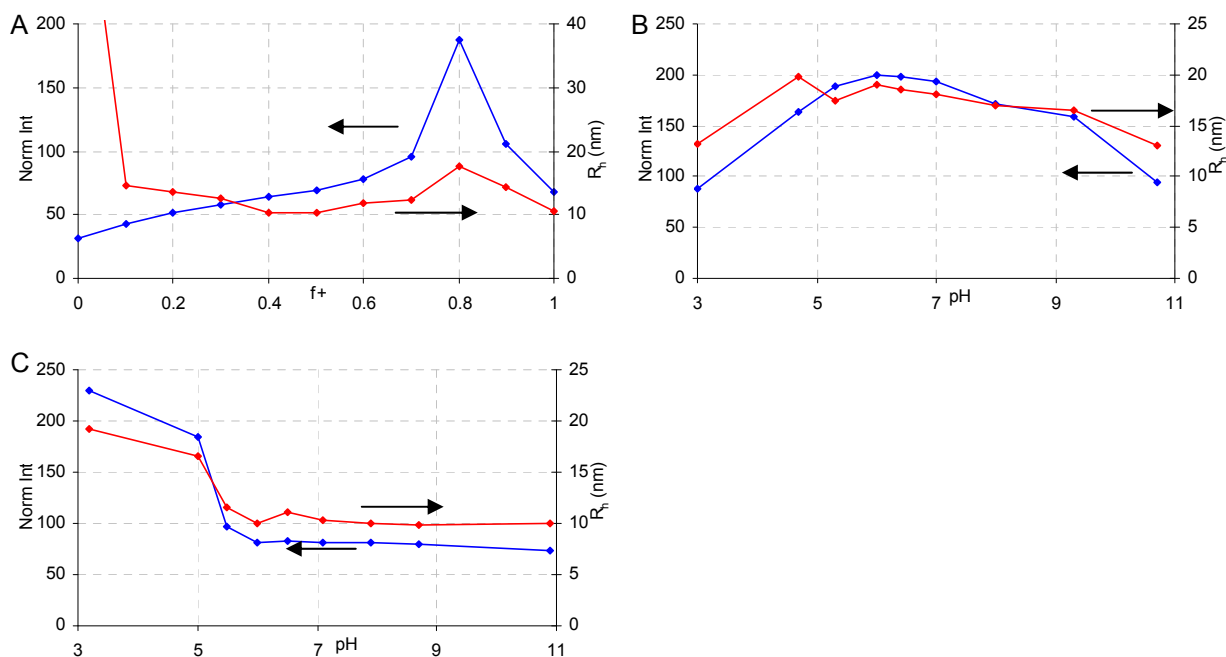
Figure 33: f^+ series at pH 7 (A) and pH series at $f^+ = 0.8$ (B) or 0.5 (C) for the PAA-*b*-PVOH/PVA-*b*-PNIPAAm C3M system (1 g/l, 1 mM NaNO$_3$).

SLS

For a set of optimal parameters of the PMAA-*b*-PEO/PVA-*b*-PDMAAm and PMAA-*b*-PEO/PVA-*b*-PNIPAAm systems a more thorough characterization is useful. Angle-dependent DLS experiments were performed at f^+ 0.5, pH 5, the data being analyzed with partial Guinier and Zimm analyses.

These experiments yielded $R_g = 25$ nm and an aggregation number (defined as the number of chains of the anion containing block copolymer with enough cation containing block copolymer chains to match the charge) $N_{agg} = 12$ for the PMAA-*b*-PEO/PVA-*b*-PDMAAm system, and $R_g = 26$ and $N_{agg} = 20.5$ for the PMAA-*b*-PEO/PVA-*b*-PNIPAAm. For the PAA-*b*-PVOH/PVA-*b*-PNIPAAm system $R_g = 16$ nm and $N_{agg} = 10$ were found.

The R_g/R_h ratios are significantly larger than unity for the first two systems (~ 1.3 and ~ 1.5 respectively), and somewhat smaller than unity for the last mentioned system (~ 0.95). Though this cannot be used as hard proof, a R_g/R_h ratio of 1 is normally taken as an indication for hollow spheres, R_g/R_h values around 0.775 as an indication for solid spheres, whereas values higher than 1 are indicative of elongated structures. This would imply that the first two types of micelles are elongated, which would fit the expected ellipsoidal shape for this type of micelles (paragraph 2.4).

Influence of salt

When salt is added to the solutions this is known to shield the charges and thereby weaken the driving force for complexation. Sufficiently high concentrations of salt thereby prohibit the formation of C3Ms. The concentration of C3Ms is decreased with increasing ionic strength. For the PMAA-*b*-PEO/PVA-*b*-PDMAAm and PMAA-*b*-PEO/PVA-*b*-PNIPAAm systems, this is shown using increasing amounts of sodium nitrate. These experiments are also performed at f^+ 0.5, pH 5. For both systems, an initial drop in the corrected scattering intensity (the scattering intensity is corrected for the dilution of the C3Ms upon addition of the 2 M NaNO$_3$ solution, pH 5) is observed, indicating that the concentration or size of the micelles decreases. Since the size of the micelles is relatively stable, the concentration of C3Ms must yield the biggest effect, as was expected.
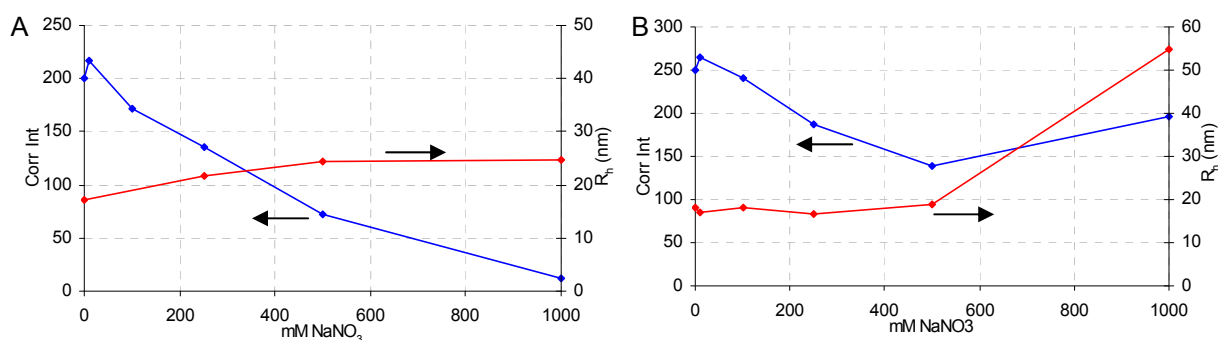
Figure 34: Influence of ionic strength (sodium nitrate) on the stability of the C3Ms made of A) PMAA-*b*-PEO/PVA-*b*-PDMAAm and B) PMAA-*b*-PEO/PVA-*b*-PNIPAAm (1 g/l diluted with appropriate amount of 2 M NaNO₃, pH 5).

For the PMAA-*b*-PEO/PVA-*b*-PNIPAAm system an initial decrease is observed, followed by an increase in scattering intensity and size of the aggregates. This effect is due to the salting out of the PNIPAAm block, the LCST (which in the absence of salt is approximately 32 °C) of which is shifted to a temperature below room temperature. Therefore aggregates are formed with a core of collapsed PNIPAAm, which might be stabilized by the charged PVA block. Please note that no or very little complex coacervate material will be formed.

4.3.3 Corona structure

Voets *et al.* described that when two different non-ionic blocks which tend to phase separate are used to stabilize the C3Ms, this can lead to the formation of Janus micelles[17]. The polymers used to prepare C3JMs in that work were PAA-*b*-PAAm and P2MVP-*b*-PEO block copolymers. The synthesis of the equivalent system with carboxylic acid groups and primary amines (instead of a quaternized amine) was tried (in order to reproduce these results), in the form of PMAA-*b*-PEO and PVA-*b*-PAAm block copolymers. The synthesis of the PVA-*b*-PAAm, though the

synthesis of PVPh-*b*-PAAm was successful, did not yield a water soluble polymer, the reason for which is still unknown. Instead, the PMAA-*b*-PEO/PVA-*b*-PDMAAm and PMAA-*b*-PEO/PVA-*b*-PNIPAAm systems introduced before were studied to determine whether phase separation takes place in the corona of these micelles. If yes, the question is posed whether Janus type micelles or other types of micelles are formed.

The mixing of the non-ionic blocks is most easily studied using NOESY (Nuclear Overhauser Effect SpectroscopY), which gives information about the proximity of two nuclei, in the form of cross-correlation peaks when the two nuclei are within approximately 5 Å of each other. The NOESY spectra for the two systems are shown in Figure 35 and Figure 36. In both cases no NOE cross-correlation is observed between the peak corresponding to PEO and those attributed to PDMAAm or PNIPAAm respectively, which indicates a phase separation of PEO and PDMAAm, respectively PEO and PNIPAAm.
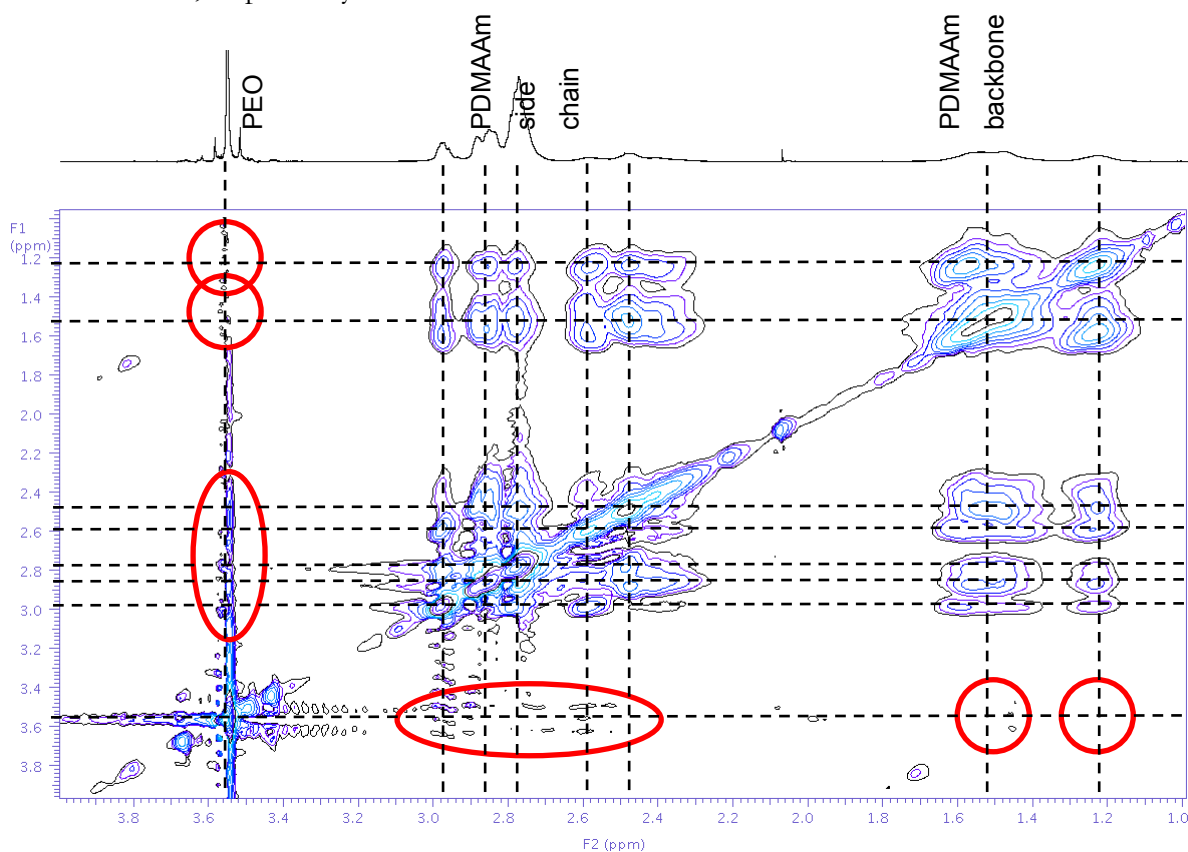
Figure 35: 2D-NOESY spectra of PMAA-*b*-PEO/PVA-*b*-PDMAAm C3Ms (600 MHz, negative signals, 10 g/l in D₂O). Red circles are used to indicate where peaks were to be expected in case of NOE signal (measurements by Olaf Niemeyer).
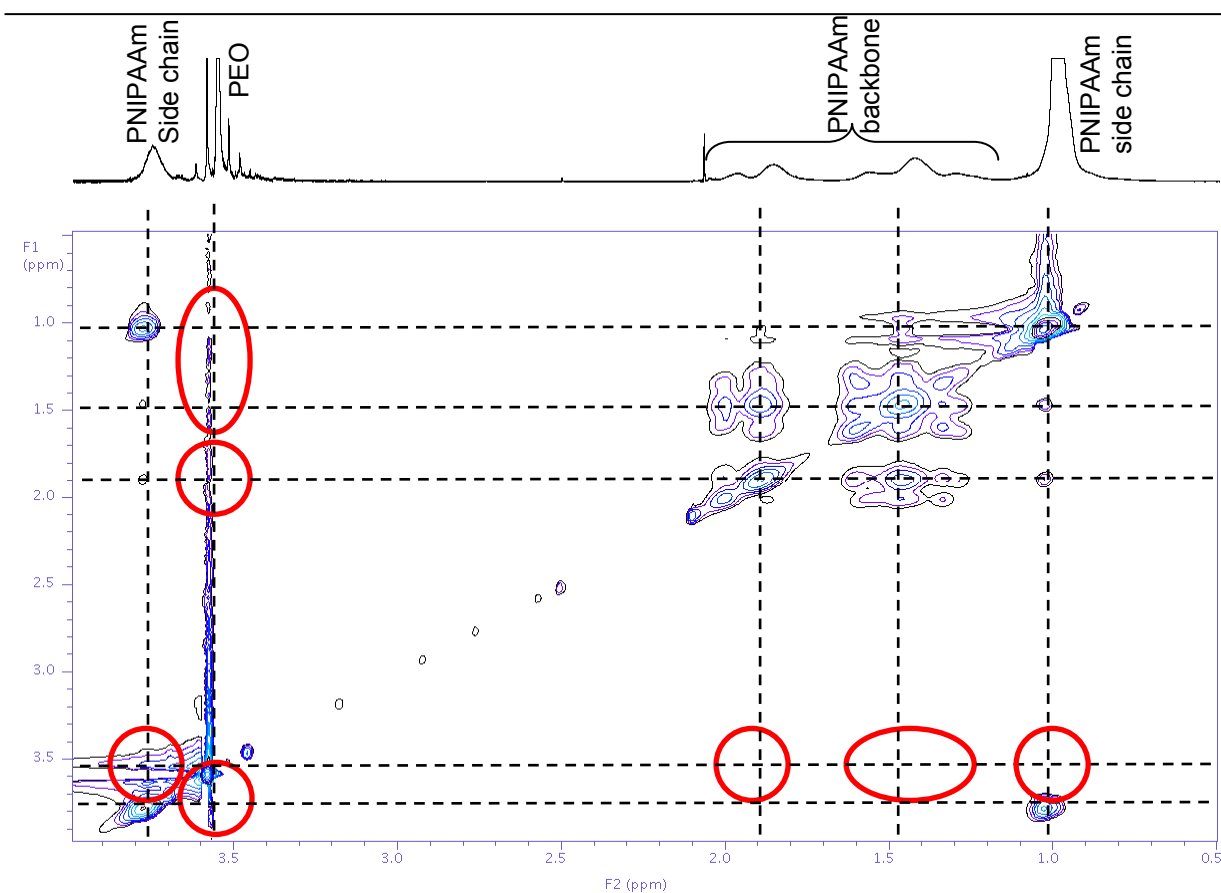
Figure 36: 2D-NOESY spectrum of PMAA-*b*-PEO/PVA-*b*-PNIPAAm C3Ms (600 MHz, room temperature, negative signals, 10 g/l in D$_2$O). Red circles are used to indicate where peaks were to be expected in case of NOE signal (measurements by Olaf Niemeyer).

Besides NOESY, SERS (Surface Enhanced Raman Spectroscopy) is used to show the phase separation. This is done by selectively adsorbing one of the two coronal blocks onto gold nanoparticles, using thiol or disulfide (end-)groups (thiol and disulfide groups readily react with gold surfaces, forming stable bonds through chemisorption). The adsorption should lead to a strong change in the intensity of the peaks in the Raman spectrum corresponding to the adsorbed polymer. Since for Janus particles only one of the hemispheres will be able to bind to the gold nanoparticle, only the Raman peaks of this polymer block should be affected.

CTA end-groups can readily be reduced to thiol end-groups, e.g. by reduction[67], but also by e.g. aminolysis. Thiol or disulfide end-groups are introduced into the C3Ms by reducing the CTA end-group of the PVA-*b*-PDMAAm or PVA-*b*-PNIPAAm block copolymers with sodium borohydride. Any oxidation of the resulting thiol end-groups, e.g. during purification (which is done by dialysis in water) leads to the formation of disulfide bonds. This is not a problem since, in dilute solution, the resulting triblock copolymer would only yield flower like micelles, where the outer blocks of the triblock copolymer are incorporated into the same micelle. Additionally, the adsorption of the disulfide bonds onto the gold surface should be just as effective as the adsorption of free thiols[68]. That adsorption takes place is shown in paragraph 4.3.6. The Raman

spectra of PMAA-*b*-PEO/PVA-*b*-PNIPAAm[i] C3Ms with and without gold nanoparticles (R_h ~ 20 nm) are shown in Figure 37.
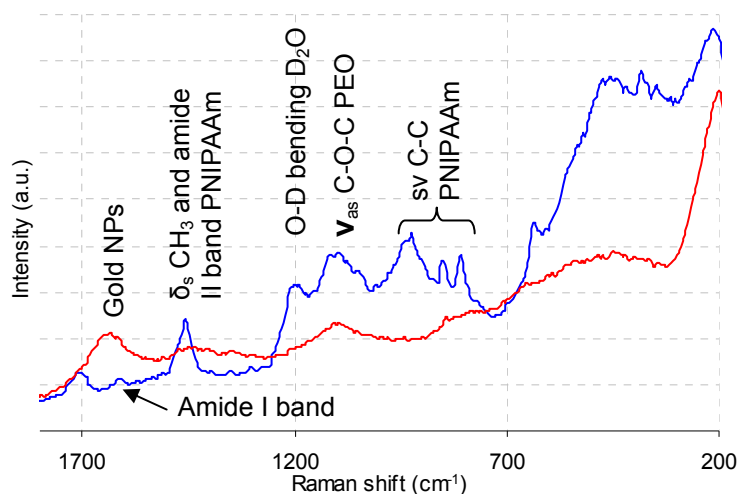
Figure 37: Raman spectra of C3Ms of PMAA-*b*-PEO/PVA-*b*-PNIPAAm (10 g/l in D₂O, blue) of which the PNIPAAm has a thiol end-group, and these C3Ms with gold nanoparticles (red, 1:1 mixture of C3M solution and gold nanoparticle solution; 0.1 g/l, R_h ~ 20 nm) (sv: skeletal vibration, δ_s: symmetric deformation, ν_{as}: asymmetric stretching).

The peaks between 840 - 950 cm⁻¹ (C-C skeletal vibrations), at approximately 1440 - 1490 cm⁻¹ (CH₃ symmetric deformation at ~ 1460 and amide II band at ~ 1480 cm⁻¹) and at 1636 cm⁻¹ (amide I band) could be attributed to PNIPAAm[69]. The peak at ~ 1120 cm⁻¹ (C-O-C asymmetric stretch) could be attributed to PEO[70]. After addition of gold nanoparticles only the single peak attributed to PEO is still visible. Ideally SERS enhances the signals of adsorbed moieties but can, depending on the orientation of the molecules to the gold surface, also lead to the disappearance of peaks, as is the case here. The fact that all PNIPAAm peaks disappear indicates that the gold nanoparticles are only in contact with this block, not the PEO block. In case of a mixed corona the gold nanoparticles would be in contact with both blocks, therefore it can be concluded that the corona of the micelles has a phase separated morphology. The size of the gold nanoparticles (approximately equal to the size of the micelles) also eliminates the possibility that patchy micelles are formed, since particles of that size should also be in contact with any eventual patches of PEO.

The possibility that no phase separated corona is formed *ab initio*, but is induced by the binding of the thiol end-groups to the gold surface moreover, can be discarded since in that case

---

[i] The CTA of the PVA-*b*-PNIPAAm block copolymer was reduced to a thiol as described in the appendix to this chapter.

a cross-linking between the gold nanoparticles is to be expected in the presence of low amounts of micelles, which is not observed (paragraph 4.3.6), not for C3Ms nor for C5Ms.

CryoTEM is performed to gain insight into the structure of the core of the micelles; due to the high amounts of solvent in the corona of the micelles, the contrast is not high enough to see the corona. This a problem which cannot easily be solved by staining since the presence of salt would strongly influence the behavior and stability of the micelles. Phase separation in the corona of the micelles can also influence the core of the micelles, as was described by Voets *et al.*[14]. They explained this by a minimization of the surface area between the coronal blocks, which translates into an oblate-ellipsoidal core morphology for Janus micelles.
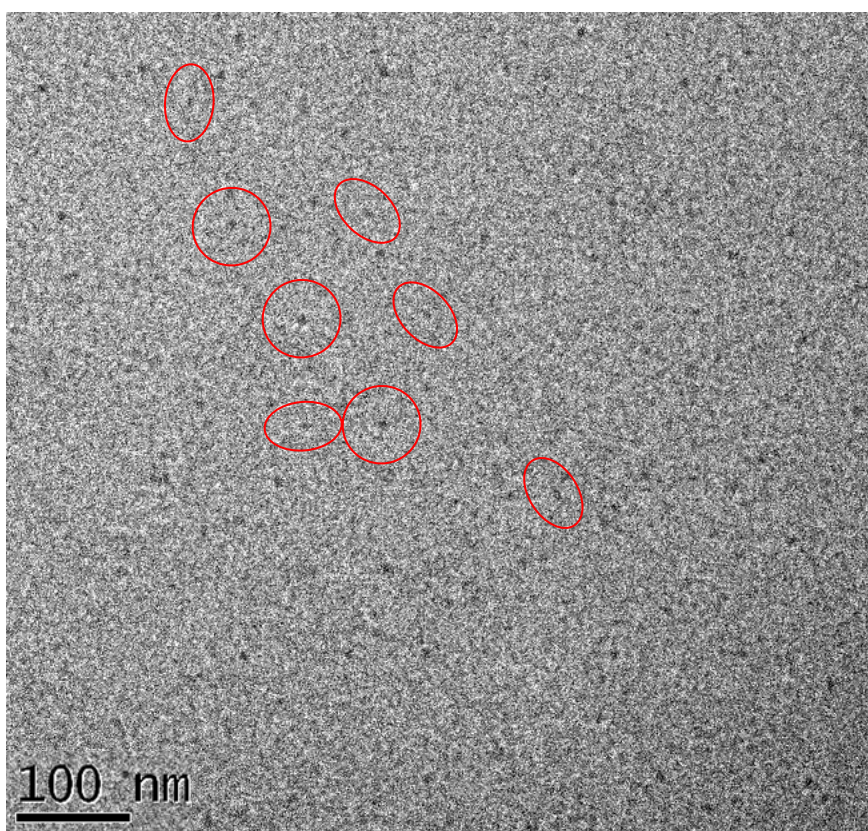
Figure 38: CryoTEM image of PMAA-*b*-PEO/PVA-*b*-PDMAAm C3Ms at pH 5, f^+ 0.5 (10 g/l in D_2O). Due to the low contrast only the cores of the micelles are visible. Red circles function as a guide to the eyes, showing some of the ellipsoidal and spherical objects (images courtesy of Prof. Dr. Janne Ruokolainen).

CryoTEM images for the PMAA-*b*-PEO/PVA-*b*-PDMAAm and the PMAA-*b*-PEO/PVA-*b*-PNIPAAm systems are shown in Figure 38 and Figure 39. For both systems micelles are observed. Though for such small objects it is difficult to distinguish between spherical and elliptical objects, both do seem to be present (primary axes of ~ 8 nm in diameter and a secondary axis (thickness) of ~ 4 nm) which would be consistent with an oblate ellipsoidal form (the orientation of the micelles relative to the plane of the image can vary). The presence of elliptical cores would be another indication that Janus micelles are indeed formed. Nevertheless

this is not a definite proof since thermal fluctuations in the form of the micelles could also yield similar results.
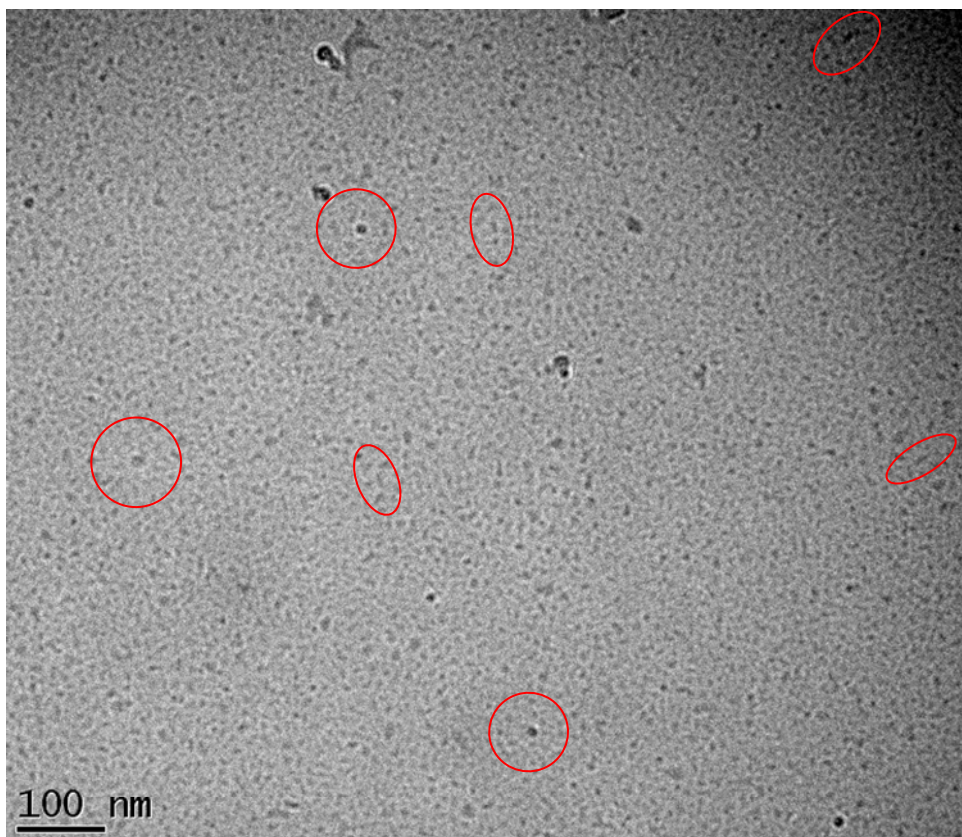
Figure 39: CryoTEM image of PMAA-*b*-PEO/PVA-*b*-PNIPAAm C3Ms at pH 5, f^+ 0.5 (10 g/l in D_2O). Due to the low contrast only the cores of the micelles are visible. Red circles function as a guide to the eyes, showing some of the ellipsoidal and spherical objects (image courtesy of Prof. Dr. Janne Ruokolainen).

Also DDLS experiments were performed to show the prolate ellipsoid shape of the Janus micelles, but unfortunately the scattering intensity of the micelles, even at 10 g/l was not high enough for this method to be useful.

In the future, SANS measurements will be performed to gain more insight into the structure of the micelles, but all available data indicate that these two systems do indeed form Janus micelles. SAXS would also yield more information on the structure of the micelles, but the resolution of the generally available machines is insufficient to obtain proper scattering curves for objects with such low contrasts. For this reason stronger radiation sources are needed to properly investigate the structures at hand.

Influence of temperature on C3JMs

PMAA-*b*-PEO/PVA-*b*-PNIPAAm C3Ms contain a thermoresponsive block (PNIPAAm). Accordingly, it is likely that temperature strongly influences the structure of the aggregates, due to

the collapse of the PNIPAAm above its LCST. Since a second neutral water soluble block is present, which is unaffected by the change in temperature, stable aggregates might be formed. Figure 40 shows the size of the micelles and the according scattering intensity for different temperatures.
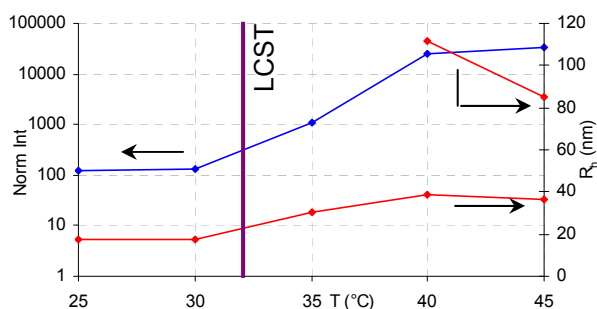
Figure 40: Temperature series for C3Ms of PMAA-*b*-PEO/PVA-*b*-PNIPAAm at pH 5, *f*⁺ 0.5 (1 g/l, 1 mM NaNO₃).

A clear increase in scattering intensity and aggregate size above the LCST of PNIPAAm (32 °C) is observed. No macroscopic precipitation takes place, but stable larger aggregates are formed. Likely, onion type micelles are formed, with a PNIPAAm core covered with a layer of complex coacervate material. The micelles are stabilized by the PEO block. Such micelles were e.g. reported by Voets *et al.*[71].

As a side note, it is of course of significance at what ratio the different components of the C3Ms are mixed, as is shown for the PAA-*b*-PVOH/PVA-*b*-PNIPAAm system. Temperature series were measured at a *f*⁺ 0.8, pH 7 and *f*⁺ 0.5, pH 5 (Figure 41), which are both optimal conditions.
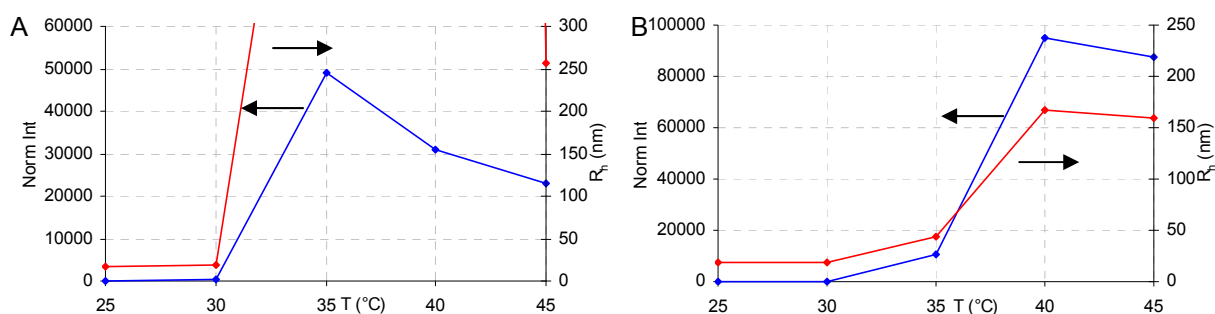
Figure 41: Temperature series for C3Ms of PAA-*b*-PVOH/PVA-*b*-PNIPAAm at *f*⁺ 0.8, pH 7 (A) and *f*⁺ 0.5, pH 5 (B) (1 g/l, 1 mM NaNO₃).

Clear differences are observed for the different conditions. When large amounts of PNIPAAm are incorporated in the micelles (*f*⁺ 0.8, pH 7) this leads to macroscopic precipitation of the micelles, whereas stable larger aggregates are found above the LCST of PNIPAAm when lower amounts of PNIPAAm are incorporated (as e.g. at *f*⁺ 0.5, pH 5). Logically the amount of

PNIPAAm that is incorporated in the micelles can also be changed by using block copolymers with shorter or longer PNIPAAm blocks.

4.3.4 C5Ms

Selective cross-linking

Though numerous different methods of cross-linking can be conceived, three different ones have been used to produce Core Cross-linked Complex Coacervate Core Micelles (C5Ms). To compare the different methods, the same C3M system was cross-linked three times, that being the PMAA-*b*-PEO/PVA-*b*-PDMAAm system. Cross-linking methods are chosen such that, at the optimum conditions for this system (f^+ 0.5, pH 5), either the carboxylic acid groups or the amine groups are cross-linked selectively. The last method yields amide bonds, thereby cross-linking both polymers selectively with each other.

To cross-link the amine groups selectively, glutaraldehyde is chosen. For the cross-linking of carboxylic acid groups 1,4-butanediol diglycidyl ether (BDDGE) is used. The formation of amide bonds is performed with NHS/EDC chemistry[72]. The selective cross-linking is schematically depicted in Figure 42.
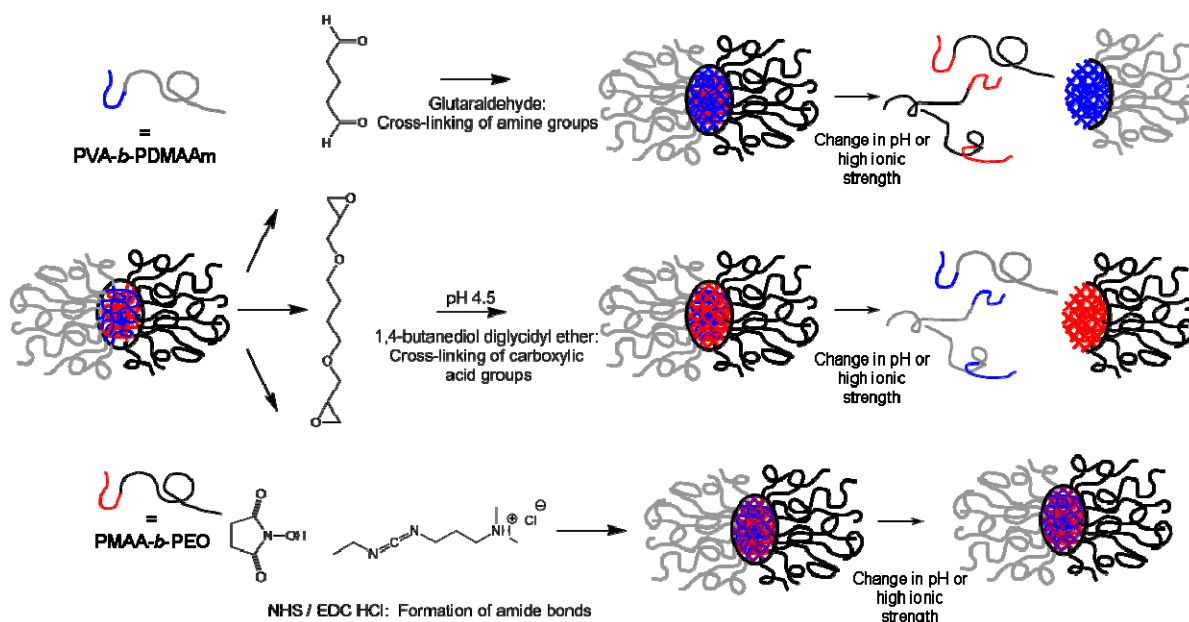
Figure 42: Selective core cross-linking of C3Ms (though the micelles from which one of the block copolymers has dissociated has been drawn as being in direct contact with the solution, a wrapping by the remaining non-ionic block can also be envisioned).[72]

The stability of the micelles in which only one of the block copolymers has been cross-linked is studied using pH and ionic strength series, which are shown in Figure 43 and Figure 44.
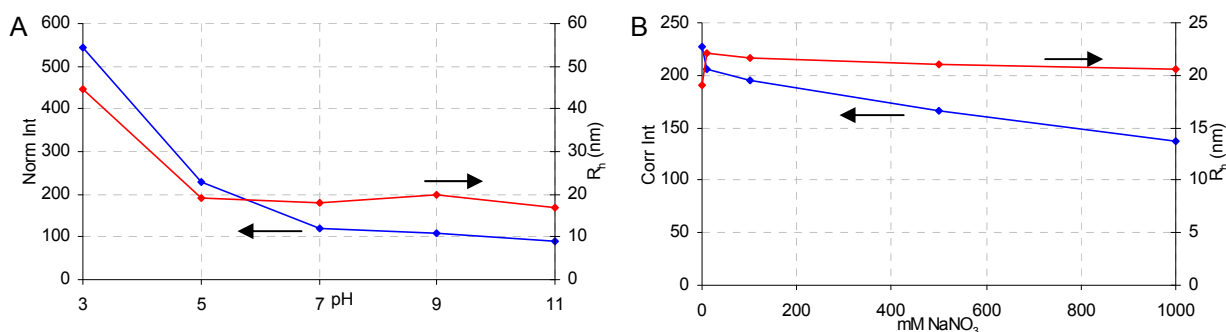
Figure 43: pH (A) and ionic strength (B) series (at pH 5) for PMAA-*b*-PEO/PVA-*b*-PDMAAm where the PVA-*b*-PDMAAm block copolymer has been cross-linked with 0.5 equivalent of glutaraldehyde (A: 1 g/l, 1 mM NaNO$_3$, B: 1 g/l diluted with 2 M NaNO$_3$ solution).
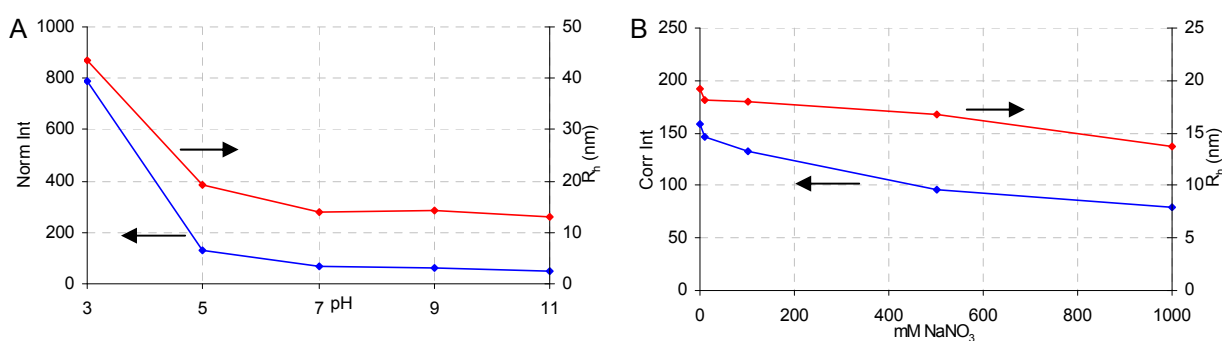
Figure 44: pH (A) and ionic strength (B) series (at pH 5) for PMAA-*b*-PEO/PVA-*b*-PDMAAm where the PMAA-*b*-PEO block copolymer has been cross-linked with 0.5 equivalent of BDDGE (A: 1 g/l, 1 mM NaNO$_3$, B: 1 g/l diluted with 2 M NaNO$_3$ solution).

The C5Ms cross-linked with glutaraldehyde show a relatively minor (compared to the non-cross-linked system, for which the data is shown in Figure 31 and Figure 34) responsiveness with pH and ionic strength. The observed strong increase in scattering intensity at lower pH is likely due to the formation of complexes of PMAA and PEO or PMAA and PDMAAm (also found for the non-cross-linked system, see appendix). Additionally, already at pH 5 an increase in the scattering intensity is observed whereas the size of the micelles does not change yet at this pH as compared to the size found at higher pH. This is likely similar to the optima found at this pH for the non-cross-linked system, meaning that the interaction between the cross-linked PVA core and PMAA-*b*-PEO is strongest at this pH. Furthermore, a small decrease in scattering intensity with increasing ionic strength is observed (at 1 M NaNO$_3$ a decrease to ~ 65 % of the scattering intensity found at 1 mM is observed), which is due to the dissociation of the C5Ms into cross-linked micelles, consisting of cross-linked PVA-*b*-PDMAAm, and molecularly dissolved PMAA-*b*-PEO chains.

The micelles cross-linked with BDDGE show very similar behavior. Here as well an increase in the scattering intensity and R$_h$ is observed at low pH. This can also be ascribed to interaction between PMAA and either PEO or PDMAAm, even though the PMAA block is cross-linked. As suggested in Figure 42 though, the dissociation of the PVA-*b*-PDMAAm block copolymer from

the micelles might lead to an enhanced accessibility of the core of the micelles (PMAA) thereby allowing for complexation. This cross-linking method leads to larger changes in the size of the aggregates (ranging from ~ 20 nm at pH 5, 1 mM NaNO$_3$, to ~ 13 nm at high pH or ionic strength) than found when cross-linking with glutaraldehyde (R$_h$ is lowered from 22 to 20 nm). This is easily explained by considering the relative weight of the two different block copolymers (corrected for the number of chargeable groups) which are 474 g/mol for PMAA-*b*-PEO and 1149 g/mol for PVA-*b*-PDMAAm. It is clear that at $f^+ = 0.5$ most of the micelle's mass can be attributed to the PVA-*b*-PDMAAm block copolymer, the release of which would therefore lead to more pronounced changes in the molecular weight and therefore size of the micelles.

A selective cross-linking of one of the block copolymer components of C3Ms can obviously be performed. More interesting though is the fact that, while cross-linking one of the polymers, the other is still free to associate with or dissociate from the cross-linked micelle, in a reversible fashion (the pH of the solutions initially is approximately 7, before the pH is set to the values plotted in the various graphs, showing reversibility). The same thing was observed by Kabanov *et al.* for systems of PMAA-*b*-PEO with P4EVP (poly(4-ethyl vinylpyridinium bromide) homopolymer, where the PMAA block was cross-linked[73].

Though this has not experimentally been shown yet, it is likely that the critical aggregation concentration (CAC) for these systems is decreased to that of C3Ms. The CAC values are normally already rather low (for the only C3JM system described thus far 27 mg/l[14] e.g.). Though purely speculative, the entropic contribution of the cross-linked block copolymer is eliminated upon selective cross-linking. Additionally cooperative binding might take place due to the high local concentration of ionic groups. This would lead to a stronger driving force for complexation, thereby decreasing the CAC. This feature would be very interesting for drug-delivery purposes since an extremely low CAC could be combined with a (partial) disintegration upon application of changes in the solvent conditions.

Cross-linking by formation of amide bonds

Using NHS/EDC (*N*-hydroxysuccinimide/1-ethyl-3-(3-dimethylaminopropyl)carbodiimide HCl) chemistry, not only one of the polymers is cross-linked, but two polymer chains of different types are selectively cross-linked, thereby cross-linking the C3Ms as a whole. This has the distinct advantage over the abovementioned cross-linking methods that their composition can be fixed, even at extreme pH or high ionic strength. The cross-linking density is very important, since it strongly influences the stability of the C5Ms on the one hand, but also determines the number of remaining functional groups. At very low cross-linking densities, some chains might still be able to dissociate from the micelles, whereas at full cross-linking no ionic groups are present anymore (all are consumed in the cross-linking procedure). The most interesting region lays between these

extremes, where the micelles are thoroughly cross-linked but still contain significant amounts of acidic and basic groups.

For the PAA-*b*-PNIPAAm/PButenOx-*b*-PEtOx system, which will be discussed in more detail later on in this chapter, the influence of the cross-linking density is investigated. The most straightforward quantification of the stability of the micelles is the relative decrease in scattering intensity upon addition of high concentrations of salt. The micelles were cross-linked with 0.5, 1 and 2.5 equivalents of NHS and EDC (at room temperature, f^+ 0.4, pH 7) compared to the number of acidic groups. For the micelles with the lowest amount of cross-linking agent present, a decrease in scattering intensity by a factor of 1.8 was observed upon increasing the ionic strength from 1 mM to 1 M NaNO$_3$. At 1 equivalent of NHS/EDC this decrease is only 1.6, whereas at 2.5 eq of cross-linking agent only a decrease by a factor of 1.4 is observed. This clearly indicates that the mobility of the chains is reduced with higher amounts of cross-linking agent (and therefore higher degrees of cross-linking).

C5JMs

The C3JM systems discussed before (PMAA-*b*-PEO/PVA-*b*-PDMAAm and PMAA-*b*-PEO/PVA-*b*-PNIPAAm) have been cross-linked using 0.5 equivalent (to acidic/basic groups) of NHS/EDC, forming amide bonds in the core of the micelles. pH and ionic strength series are shown in Figure 45 and Figure 46. When mentioning C5Ms later in this chapter, this refers to micelles cross-linked using NHS/EDC chemistry.

Both systems show a relatively constant micelle size (R$_h$ ~ 20 nm, similar to the size of non-cross-linked C3JMs), with a slight peak in scattering intensity at pH 5 as was also found for the micelles cross-linked with other methods. Besides the R$_h$, also the R$_g$ and N$_{agg}$ stay the same, indicating that the micelles composition is maintained.

Compared to the effect of salt for the non-cross-linked systems, the effect seen here is very minor (29 vs. 70 % decrease in scattering intensity for the PMAA-*b*-PEO/PVA-*b*-PDMAAm system at 0.5 M salt, drops of 20 vs. 50 % in scattering intensity for the PMAA-*b*-PEO/PVA-*b*-PNIPAAm system). This observation indicates that the cross-linking was successful. The marked increase in scattering intensity and aggregate size at 1 M NaNO$_3$ for the system containing PNIPAAm is due to the shift of the LCST of this polymer to lower temperatures.
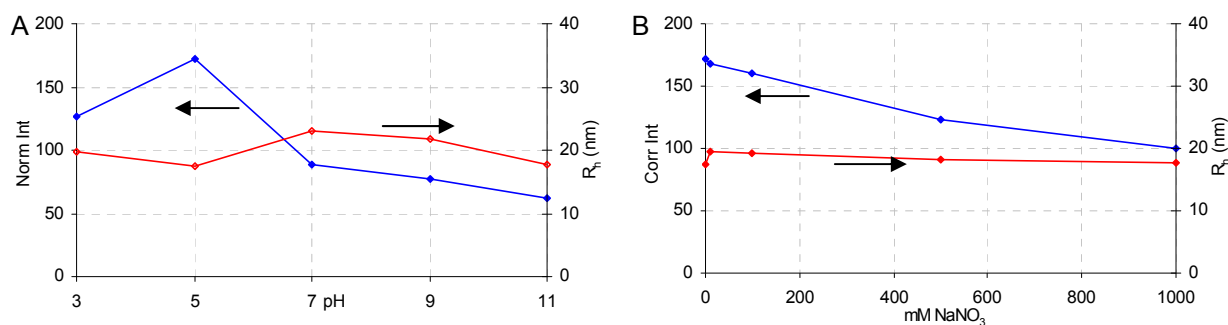
Figure 45: pH (A) and ionic strength (B) series (at pH 5) for PMAA-*b*-PEO/PVA-*b*-PDMAAm cross-linked with 0.5 equivalent of NHS/EDC (A: 1 g/l, 1 mM NaNO₃, B: 1 g/l diluted with 2 M NaNO₃ solution).
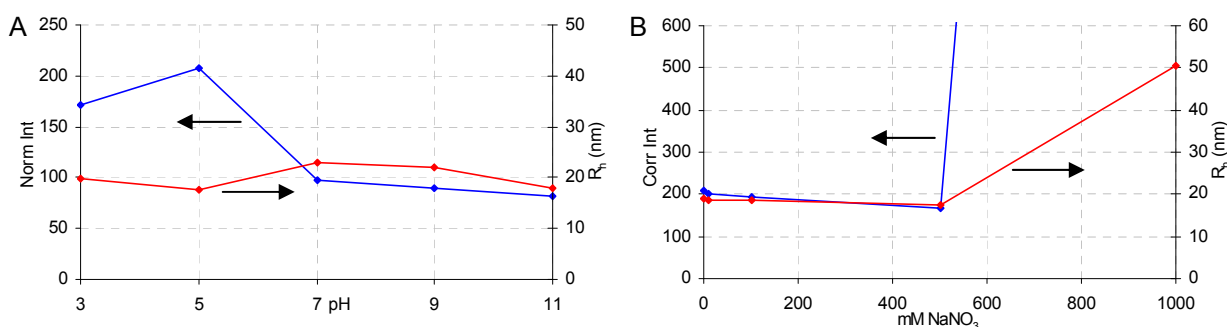
Figure 46: pH (A) and ionic strength (B) series (at pH 5) for PMAA-*b*-PEO/PVA-*b*-PNIPAAm cross-linked with 0.5 equivalent of NHS/EDC (A: 1 g/l, 1 mM NaNO₃, B: 1 g/l diluted with 2 M NaNO₃ solution).

This effect of salt was also observed for the non-cross-linked system, with the difference that, in all likelihood, no C3Ms were present anymore at that ionic strength, only leading to micelles with a core consisting of collapsed PNIPAAm, stabilized by the PVA block, coexisting with molecularly dissolved PMAA-*b*-PEO chains. For C5Ms this disintegration cannot take place, so that even at high ionic strength the micelles should be intact. The large aggregates found at 1 M salt therefore must be aggregates of C5Ms.

4.3.5 Higher-order aggregates

Higher-order aggregates induced by temperature

By changing the solvent quality selectively for one of the two coronal blocks, that block can become less soluble or insoluble in the solvent. If one hemisphere of C5JMs collapses, a amphiphile is formed, which will aggregate. This was already shown for e.g. Janus micelles prepared by the cross-linking of bulk morphologies, having a PMMA/PS corona[74]. In that case variations in the solvent mixture were used, but numerous other methods can be used to effectively do the same thing. For thermoresponsive polymers e.g. changes in temperature can be used to this affect, as well as changes in ionic strength as was already observed.

The addition of salt (not even necessarily a strongly kosmotropic one) can lower the cloud point temperature (T_{cp}) of PNIPAAm. At 1 M NaNO$_3$ the T_{cp} is already shifted to a temperature below room temperature. This is also confirmed in a temperature dependent experiment (Figure 47), where the T_{cp} is found to lay between 20 and 25 °C (in the absence of salt $T_{cp} \sim 32$ °C).
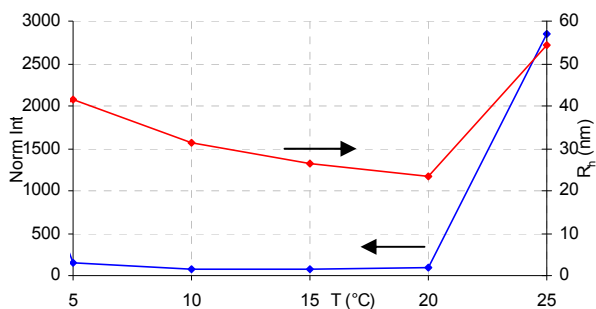
Figure 47: Temperature series (0.5 g/l, 1 M NaNO$_3$, pH 5) for PMAA-*b*-PEO/PVA-*b*-PNIPAAm cross-linked with 0.5 equivalent of NHS/EDC.

It is well known that numerous polymers exhibit LCST behavior, though not in the experimentally accessible window (0 - 100 °C for aqueous solutions). This also holds true for PEO and PDMAAm. Using kosmotropic salts, their T_{cp} can be shifted to lower temperatures. This is shown in Figure 52 for the C5Ms of PMAA-*b*-PEO/PVA-*b*-PDMAAm. A LCST is observed around 60 °C.
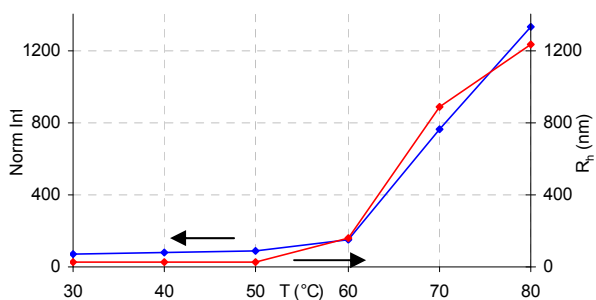
Figure 48: Temperature series (0.5 g/l, 1 M Na$_2$SO$_4$, pH 5) for PMAA-*b*-PEO/PVA-*b*-PDMAAm cross-linked with 0.5 equivalent of NHS/EDC.

For homopolymers of PDMAAm and PEO with similar degrees of polymerization to the corresponding blocks in the block copolymers which were used to prepare the C5Ms, temperature dependent DLS was measured under identical conditions. These experiments (data shown in the appendix to this chapter) showed LCST behavior for both polymers. For PDMAAm clouding started to occur around 45 °C, whereas clouding of the PEO solution started at approximately 65 °C. This suggests that initially only PDMAAm collapses, followed by PEO at slightly higher temperatures.

The thermoresponsive behavior of the micelles with pH is also studied. The pH might not be able to dictate whether micelles are formed or not, but it still strongly influences the charge in the cores of the micelles. Charge does not (strongly) influence the T_{cp} of PNIPAAm (it is always observed between 30 and 35 °C), unlike the behavior that was observed for micelles with a PEtOx corona (see Chapter 3). Since the cloud point temperature of PNIPAAm (a type II thermoresponsive polymer) is hardly dependent on concentration, whereas the T_{cp} of PEtOx (a Type I thermoresponsive polymer) is, this indicates that changes in the local concentration are indeed responsible for the changes in the T_{cp} observed in systems with a PEtOx corona.
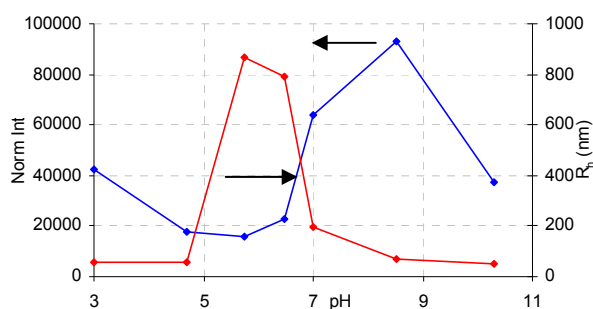
Figure 49: R_h and scattering intensity at 45 °C for PMAA-*b*-PEO/PVA-*b*-PNIPAAm C5Ms (1 g/l, 1 mM NaNO₃) at different pH values.

The aggregation products of the C5Ms at elevated temperatures obviously change with the pH of the solution (Figure 49). At pH values between ~ 4.5 and 7 the micelles precipitate (extra data shown in the appendix to this chapter). At more extreme pH values, stable aggregates are formed with a stable R_h of 50 - 70 nm. The system at pH 7 is an intermediate case, where a small amount of (or very slow) precipitation takes place, coexisting with some larger aggregates (~ 200 nm).

Angle-dependent light scattering and the evaluation of the data with partial Zimm and Guinier fits, shows exactly the same behavior. The R_g ranges from 50 - 60 nm at extreme pH values up to ~ 160 nm for the intermediate pH range. The large discrepancy between the R_g and R_h reported in Figure 49 at these intermediate pH values is due to the slower measurements and longer equilibration times taken for the angle-dependent measurements, allowing for more sedimentation.

Stable aggregates are only formed at higher temperatures when enough net charge is present in the core of the micelles. This charge might lead to electrostatic repulsion, thereby altering the effective packing parameter of the C5Ms and prohibiting further aggregation. Also the swelling of the core might affect the packing parameter.

The only system exhibiting similar behavior that, to the best of our knowledge, has been described thus far is a system where PNIPAAm chains have been grafted onto casein[75]. The casein bears both acidic and basic moieties and has an isoelectric point around pH 5. Both at higher and lower pH values a net charge is present, which was shown to prevent the PNIPAAm from macroscopic precipitation even above its LCST. The major difference of that system to the C5Ms described here is that with C5Ms another solvating block is present in addition to the charged moieties, reducing the amount of charged groups which is necessary for stabilization.

4.3.6 Higher-order aggregates through the interaction with nanoparticles

Silica nanoparticles

PEO is known to specifically bind to silica surfaces[76] through hydrogen bonding interaction between hydroxyl groups on the silica surface and the oxygen in the PEO chain. If C5Ms contain PEO it is therefore to be expected that the C5Ms will adsorb. This is not easily achieved using C3Ms, since silica also bears a negative charge with which polycations can complex (as e.g. used in the preparation of LbL-vesicles, see paragraph 2.4). This competition between silica and the polyanionic block would likely disrupt, at least to some degree, the structure of the C3Ms. With C5Ms this ionic interactions cannot lead to the disintegration of the micelles. Firstly, the C5JMs with PEO/PDMAAm coronas are used to build aggregates containing silica and C5Ms.

Colloidal silica particles (Ludox™) were used. Two different commercial products are taken, namely Ludox HS-40 and Ludox TM-50, with hydrodynamic radii of 10 and 17 nm respectively (as determined by DLS). The concentrated solutions were diluted to 1 g/l. Mixtures of Ludox and C5Ms were prepared in different ratios. The light scattering data for the mixtures of Ludox HS-40 at pH 7, 5 and 3 is shown in Figure 50.

At pH 7 and 5, a gradual increase in the average size of the aggregates with the fraction of C5Ms is found by cumulant analysis (not shown). With a Contin analysis, two populations of particles are observed at higher weight fractions of C5Ms, one with the size of the C5Ms ($R_h \sim 20$ nm) and one with a R_h of ~ 35 nm. At lower weight fractions particles bigger than the micelles are found, which indicates that also in this case micelles coexist with a population of larger particles, but it proved difficult to fit this properly, due to the relatively similar sizes. It can be concluded that besides micelles, also silica covered with C5Ms are present in solution.
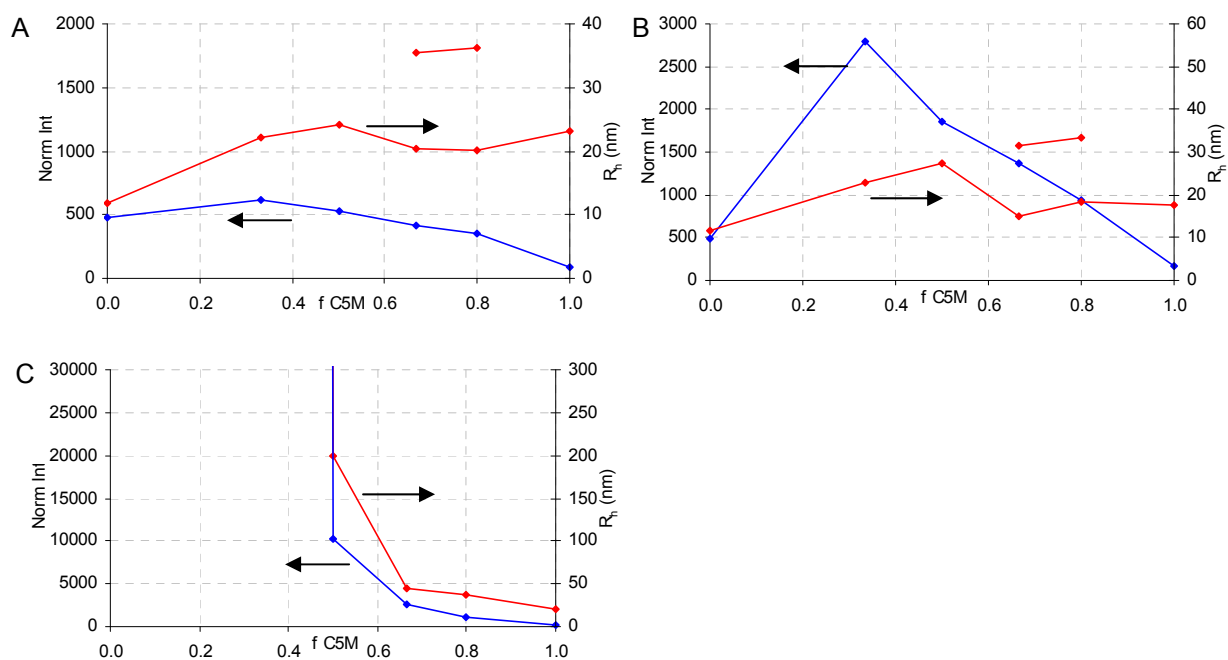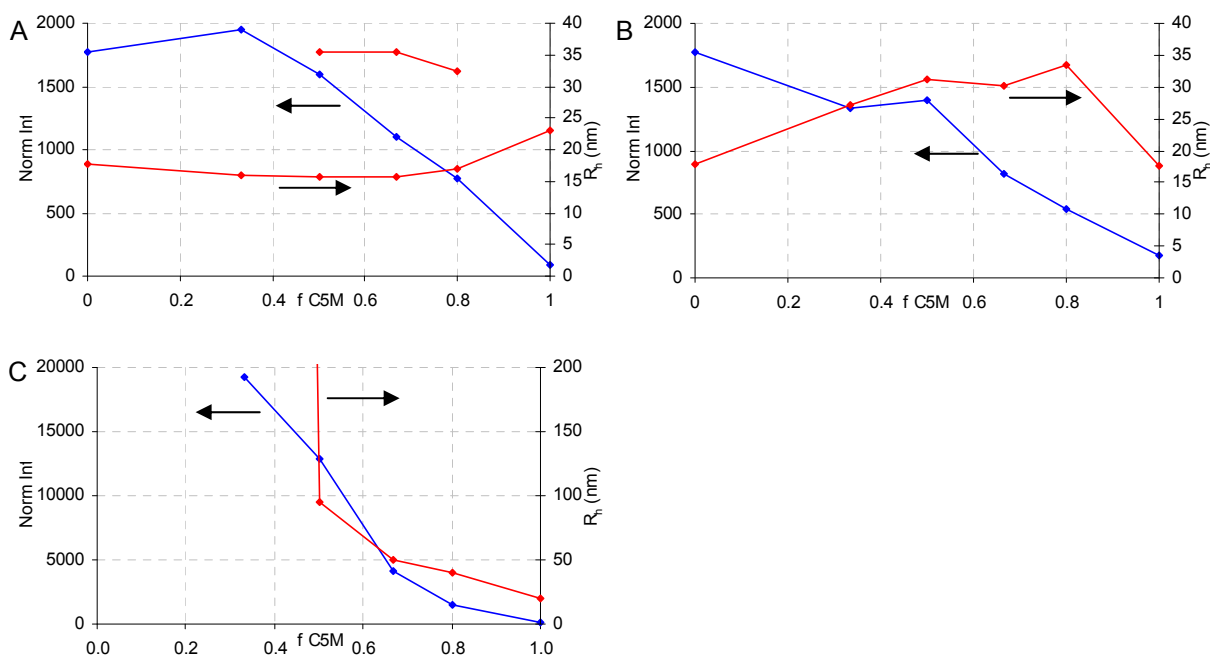
Figure 50: Mixtures of Ludox HS-40 with different amounts of PMAA-*b*-PEO/PVA-*b*-PDMAAm C5Ms at A) pH 7, B) pH 5 and C) pH 3 (1 g/l, 1 mM NaNO₃).

At pH 3, silica is unstable in solution because the charge density on the surface of the particles is decreased and becomes insufficient to maintain colloidal stability. At low amounts of C5Ms this precipitation is observed (as observed in DLS and by eye). At higher weight fractions of C5Ms, stable aggregates with sizes similar to the aggregates found at other pH values are found (R_h 35 - 40 nm). This shows that the C5Ms adsorb onto the surface of the particles and stabilize the silica particles in solution.

Since also the C5Ms bear a certain amount of charge, the nature of the interaction between the silica and the C5Ms should be discussed. At pH 7 both the C5Ms and the silica bear a negative net charge. This suggests that no (or even a slightly repulsive) electrostatic interaction is to be expected[77]. Therefore electrostatic interaction can be excluded as a driving force for the aggregation of the C5Ms with silica nanoparticles. It can therefore be concluded that indeed PEO adsorbs onto the surface of the particles.
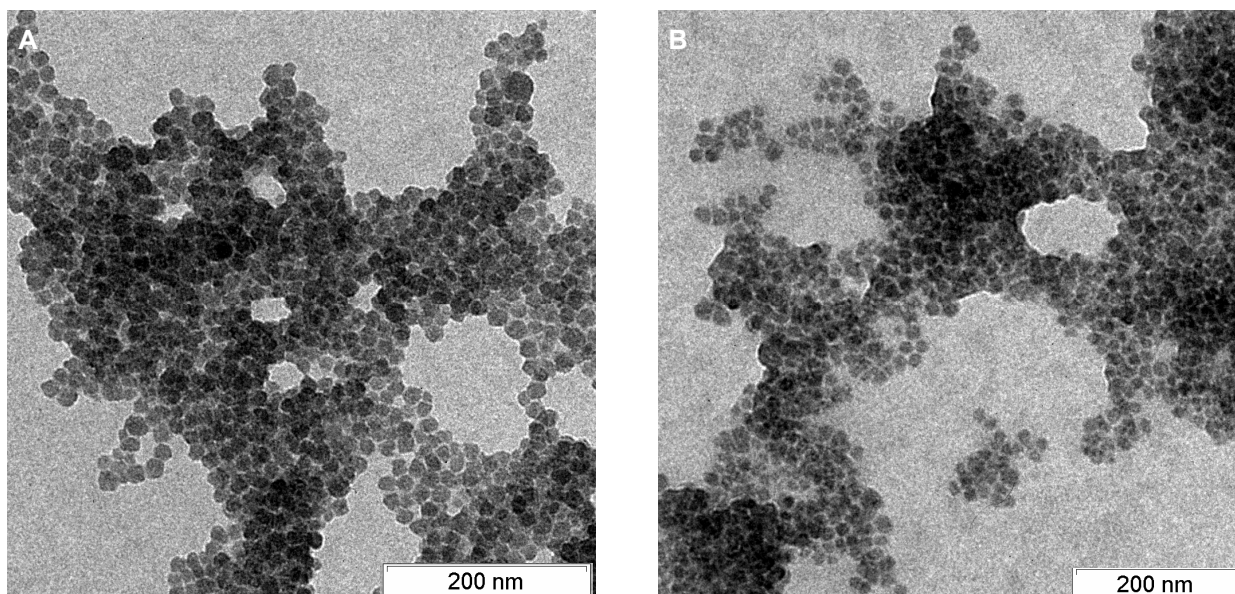
Figure 51: TEM image of silica HS-40 with 0.33 (A) respectively 0.5 (B) weight equivalence of PMAA-*b*-PEO/PVA-*b*-PDMAAm C5Ms (dried from 1 g/l, 1 mM NaNO₃ solutions) (images courtesy of Jiayin Yuan).

Using transmission electron microscopy (TEM) the precipitated and stabilized silica particles were visualized. Due to their low contrast, it is not possible to directly see the polymer without staining. Figure 51 shows TEM images of two samples where the silica precipitated. Figure 52 shows images of stabilized silica particles. For the former case, large amounts of aggregated material are observed and hardly any single silica particles. For the stabilized particles some aggregation was found, but only into relatively small clusters. Even then, in many cases, it could be seen that the particles do not actually touch each other, but are separated from each other. This is likely due to the adsorbed micelles. Such clustering is therefore likely a drying effect.
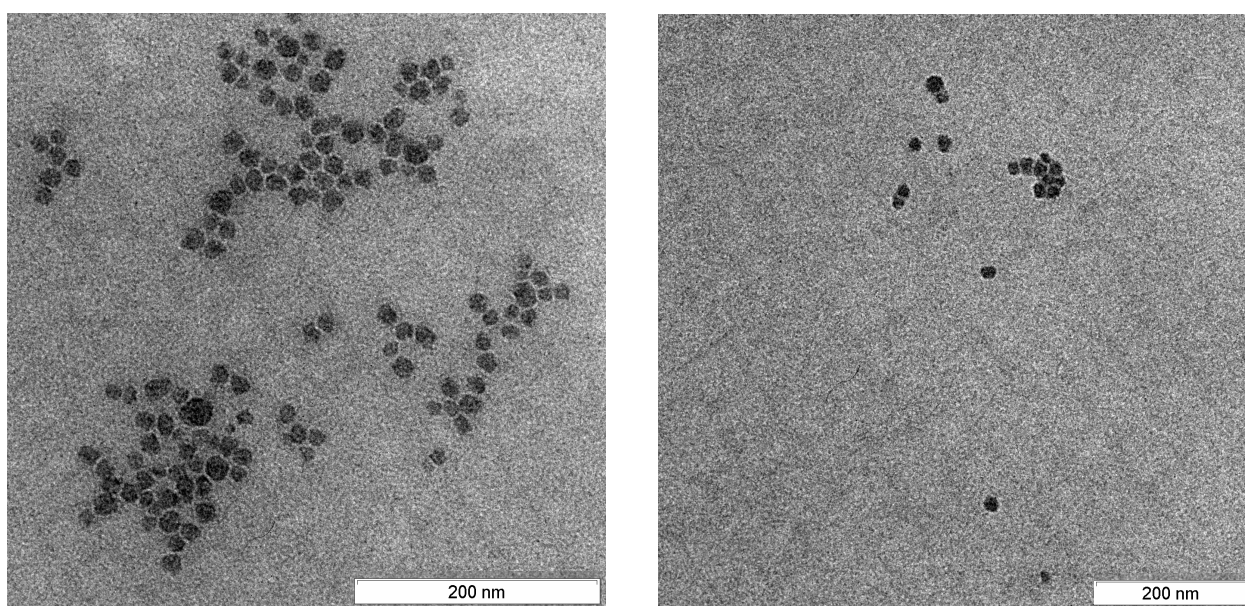
Figure 52: TEM images of silica HS-40 stabilized with 0.67 weight equivalence of PMAA-*b*-PEO/PVA-*b*-PDMAAm C5Ms (dried from 1 g/l, 1 mM NaNO₃ solutions) (images courtesy of Jiayin Yuan).

As can be seen from Figure 53, very similar behavior is observed when Ludox TM-50 instead of HS-40 is used, since also in this case aggregates with hydrodynamic radii of ~ 35 nm coexisting with micelles are observed (though because of the larger silica particles and the relatively small difference in the size of the different fractions fitting proved difficult in some cases). As in the systems with Ludox HS-40, the larger silica particles are also stabilized by the core cross-linked micelles.

Figure 53: Mixtures of Ludox TM-50 with different amounts of PMAA-*b*-PEO/PVA-*b*-PDMAAm C5Ms at A) pH 7, B) pH 5 and C) pH 3 (1 g/l, 1 mM NaNO₃).

By using different C5Ms, such as the PMAA-*b*-PEO/PVA-*b*-PNIPAAm system, a thermoresponsive switch can be introduced. In this case the behavior is only investigated at pH 7. The influence of temperature is investigated as well (Figure 54).
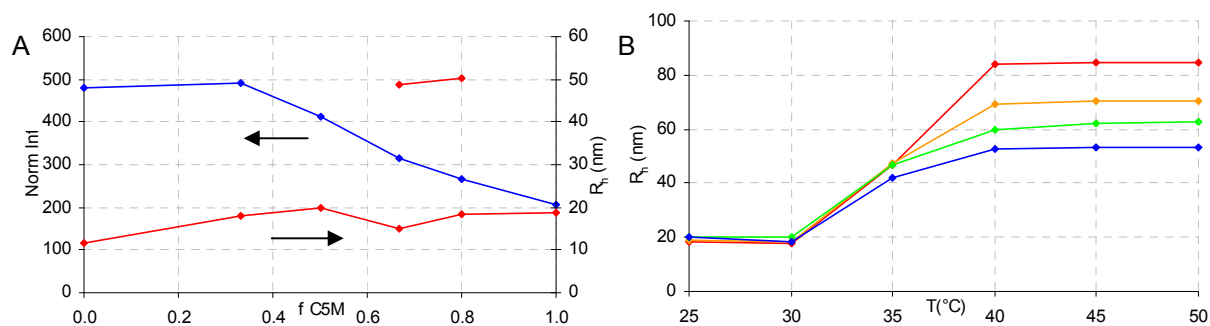
Figure 54: Mixtures of Ludox HS-40 with different amounts of PMAA-*b*-PEO/PVA-*b*-PNIPAAm C5Ms (A) at room temperature, pH 7 and (B) hydrodynamic radius (as determined by Contin analysis) as a function of temperature for different mixtures of Ludox and C5Ms (red: 0.33 wt eq C5Ms, orange: 0.5 wt eq C5Ms, green: 0.67 wt eq C5Ms, blue: 0.8 wt eq C5Ms) (1 g/l, 1 mM NaNO₃).

At room temperature a fraction of larger aggregates is observed, though these are marginally bigger than the ones observed for the PMAA-*b*-PEO/PVA-*b*-PDMAAm system ($R_h \sim 50$ instead of 35 nm). This indicates that these C5Ms also adsorb onto the silica nanoparticles. When the different samples are heated, a clear trend in the sizes of the aggregates is observed, namely that the largest aggregates are formed at low weight fractions of C5Ms ($R_h \sim 80$ nm) (at high temperatures the R_h found with a cumulant analysis and a Contin fit were nearly identical, meaning that a monodisperse mixture of aggregates is formed) and the smallest at the highest weight fraction of C5Ms ($R_h = 50$ nm) which is identical compared to the size of aggregates of C5Ms and silica particles at room temperature.

At room temperature, where PEO is adsorbed onto the silica, the PNIPAAm block is in contact with the bulk solution, thereby stabilizing the silica particles. Upon heating and collapse of the PNIPAAm, two things can happen. Firstly, the PEO can stay adsorbed on the surface of the silica particles, thereby forcing the PNIPAAm to remain facing the bulk solution, effectively forming hydrophobic patches on the aggregates. This would lead to precipitation from solution. Secondly, the hydrophobic PNIPAAm can compete with the PEO for adsorption onto the surface, not through hydrogen bonding but through hydrophobic interaction. If PNIPAAm does so to a sufficient degree this would not necessarily lead to precipitation.

No macroscopic precipitation is observed, nor are aggregates with hydrodynamic radii around 200 nm (as would be expected in the absence of silica as shown in Figure 49). Instead aggregates with nearly identical sizes as observed for the silica with C5Ms adsorbed onto its surface at room temperature ($R_h \sim 50$ nm) are observed. This strongly indicates that PNIPAAm adsorbs onto the silica at elevated temperatures. This way of aggregation is schematically shown in Figure 55. SLS can unfortunately not be used, firstly because no monomodal distribution of particles is formed, and secondly because the refractive index of the aggregates is hard to determine.
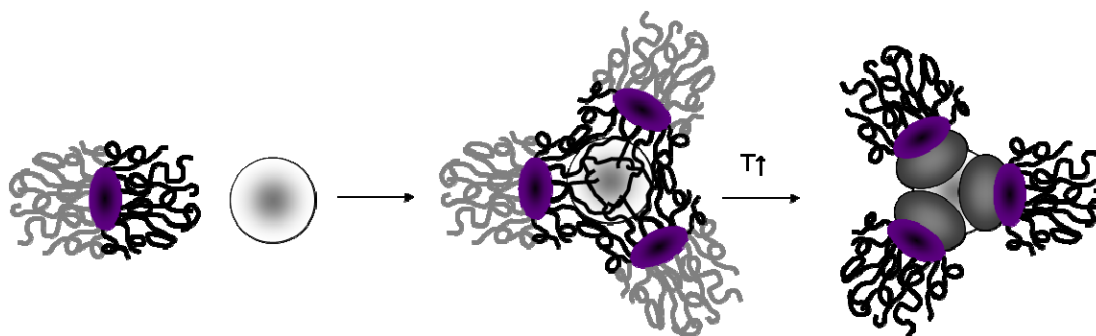
Figure 55: Schematic representation of the aggregation behavior of silica with thermoresponsive C5JMs containing a PEO block (black polymer chains: PEO, gray polymer chains: PNIPAAm).

T↑

The fact that larger aggregates are found at lower weight fractions of C5Ms can be explained by the presence of "excess" silica surface, allowing a certain amount of the PEO to absorb onto the silica anyway, thereby creating cross-links between different silica particles (Figure 56).
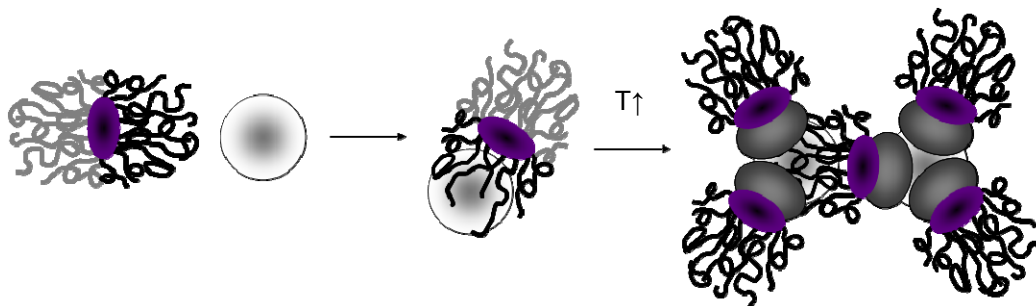
Figure 56: Cross-linking between silica nanoparticles in the presence of low amounts of C5Ms (black polymer chains: PEO, gray polymer chains: PNIPAAm).

As a comparison, a thermoresponsive C5M system without any PEO was also used, namely PAA-*b*-PNIPAAm/PButenOx-*b*-PEtOx (described in more detail in paragraph 4.4.3). For this system no second population of particles was found, only small particles. Also, upon heating (data shown in Figure 57) no significant difference in the size of the aggregates is observed between the mixtures with different composition. The size of the aggregates is also similar to that of the aggregates found in the absence of silica (Figure 66). It can therefore be concluded that in this system there is no interaction between the C5Ms and the silica, confirming that PEO is needed for adsorption. The data also suggests that the collapsed PNIPAAm does not interact (to a significant extent) with the silica, which might be due to kinetic effects; the fast collapse and aggregation of the C5Ms with other micelles does not allow time for a reordering of the PNIPAAm on the surface of the silica particles.
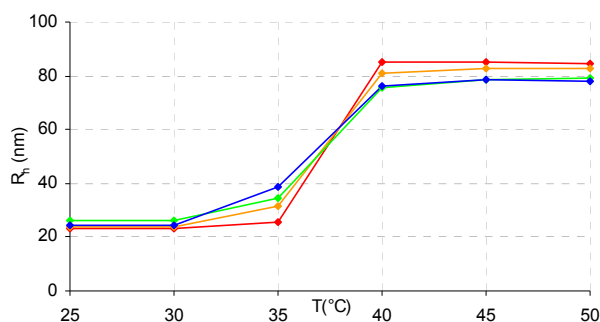
Figure 57: Hydrodynamic radius (as determined by Contin analysis) of mixtures of Ludox HS-40 with different amounts of PAA-*b*-PNIPAAm/PButenOx-*b*-PEtOx as a function of temperature (red: 0.33 wt eq C5Ms, orange: 0.5 wt eq C5Ms, green: 0.67 wt eq C5Ms, blue: 0.8 wt eq C5Ms) (1 g/l, 1 mM NaNO₃).

When the pH of the mixtures of PMAA-*b*-PEO/PVA-*b*-PNIPAAm C5Ms and Ludox-HS40 is lowered, a precipitation of the material is observed in all cases. Acidification at higher temperatures, where PNIPAAm instead of the PEO is collapsed onto the silica particles also

yields precipitation. Though the system is too complex to make any conclusions, it can be speculated that the net charge in the cores of the micelles is changed and that this triggers a change in the effective packing parameter of the micelles, like with the thermoresponsive behavior of the C5M system in the absence of silica nanoparticles. Not only the change in the surface charge of the silica would drive the precipitation, but also this change in packing parameter.

Gold nanoparticles

Thiol and disulfide groups are well known to chemisorb strongly and selectively onto gold surfaces. This has been extensively used to e.g. create self-assembled monolayers (SAMs)[78]. Since one of the block copolymers used in the creation of C5JMs is prepared by RAFT polymerization (both PVA-*b*-PDMAAm and PVA-*b*-PNIPAAm, depending on the system), CTA end-groups, containing sulfur, are present only in one of the Janus micelle's hemispheres. As described in paragraph 4.3.3 these groups can be reduced to thiol end-groups. When this is done for C5JMs, one of the hemispheres bears thiol groups which are capable of binding to gold surfaces. This is shown using gold nanoparticles with a size of approximately 20 nm ($R_h \sim 22$ nm as determined by DLS). Upon addition of PMAA-*b*-PEO/PVA-*b*-PNIPAAm C5Ms, a strong increase in the size of the particles is observed. The size of the aggregates stabilizes at a size of ~ 48 nm (Figure 58). Since the refractive index of the gold nanoparticles is far greater than that of the micelles, the scattering intensity is mainly governed by the concentration of gold nanoparticles, but nevertheless a peak is observed around f C5Ms (weight fraction of C5Ms) of approximately 0.2. The size of the aggregates of gold nanoparticles and C5Ms ($R_h = 48$ nm) is very similar to the sizes of the aggregates found upon adsorption of C5JMs onto silica nanoparticles ($R_h \sim 50$ nm).
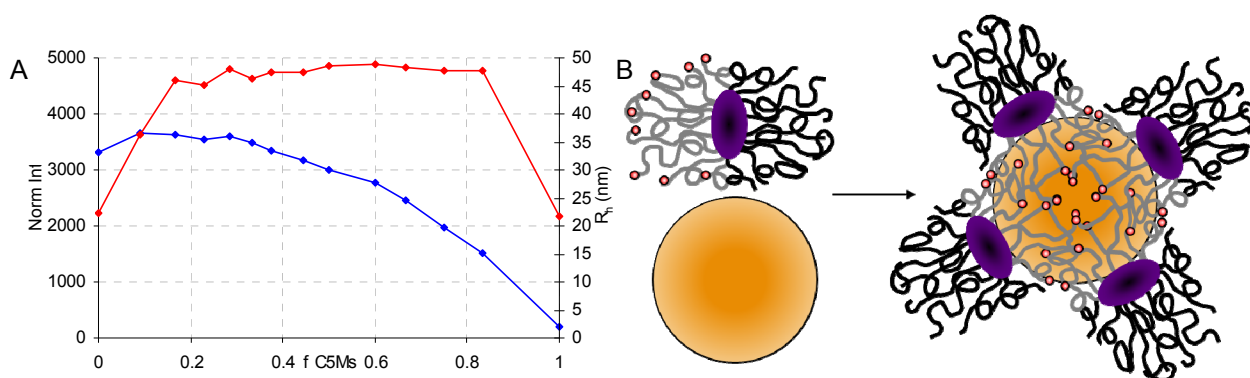
Figure 58: A: Mixtures of gold nanoparticles ($R_h \sim 20$ nm, ~ 0.1 g/l, pH 5) with different amounts of PMAA-*b*-PEO/PVA-*b*-PNIPAAm C5Ms of which the CTA end-groups were reduced (a 1 g/l, 1 mM NaNO$_3$, pH 5 solution was titrated to the gold nanoparticles), B: Schematic representation of the adsorption of C5JMs with thiol end-groups in one hemisphere onto gold nanoparticles (black chains: PEO, gray chains: PNIPAAm-SH, orange sphere: gold nanoparticle).

Whereas the complexation of micelles with silica can only take place when the micelles are cross-linked, because of ionic interactions which could otherwise disrupt the C3M structure, this

is not true for the complexation of C3Ms with gold nanoparticles, since the gold surface itself is not charged. Unfortunately the gold nanoparticles are typically stabilized by tannic acid and sodium citrate, which can both have multiple charges, and are therefore likely to interfere with the formation of C3Ms. Nevertheless the identical behavior is observed when PMAA-*b*-PEO/PVA-*b*-PNIPAAm (of which the CTA groups have been reduced to thiols) C3Ms are used as when C5Ms are used. This indicates that binding of C3Ms onto the gold nanoparticles also takes place, without any changes in the morphology of the C3JMs. Using Raman spectroscopy (paragraph 4.3.3) it could be shown that only the PNIPAAm block is in direct contact with the gold nanoparticles.

4.3.7 C5Ms as charge bearing building blocks for complex C3M structures

The fact that core cross-linked complex coacervate core micelles are stable even at extreme pH values makes it possible to introduce a third polymer in the micelles, namely a polymer bearing permanently charged groups. This is done by setting the pH of the C5M solution such that the micelles have a net charge which is opposite to the charge of the polymer which should be incorporated into the micelles, e.g. basic pH for polymers bearing quaternized amine groups, or acidic pH for polymers bearing sulfonate groups. Both pathways are implemented, once by the addition of a P2MVP-*b*-PNIPAAm block copolymer and once by the addition of polystyrene sulfonate sodium salt (PSS·Na) homopolymer (M_n = 70 kg/mol). The PMAA-*b*-PEO/PVA-*b*-PDMAAm C5JM system was used as the C5M counterpart to these two polymers.

Different fractions of the polymers with strong ions were added to the C5Ms at pH values 3, 5, and 11, which yield C5Ms with either equal, zero or opposite charge compared to the strong polyions. The data for the P2MVP-*b*-PNIPAAm is shown in Figure 59 and the data for the PSS·Na in Figure 60.
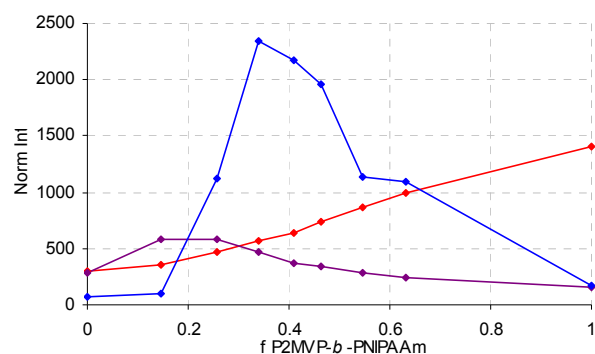
Figure 59: Normalized scattering intensity for complex coacervate core complexes formed from PMAA-*b*-PEO/PVA-*b*-PDMAAm and P2MVP-*b*-PNIPAAm at different pH values and fraction of P2MVP-*b*-PNIPAAm (red: pH 3, purple: pH 5, blue: pH 11) (1 g/l, 1 mM NaNO₃).
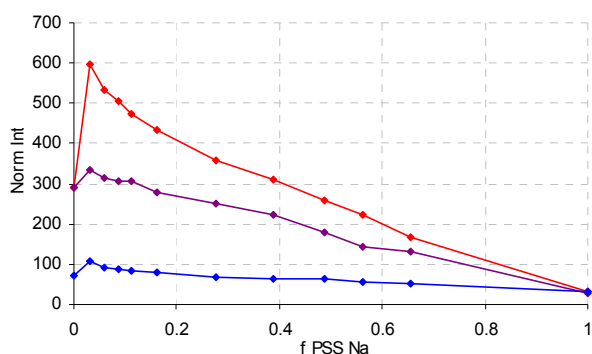
Figure 60: Normalized scattering intensity for complex coacervate core complexes formed from PMAA-*b*-PEO/PVA-*b*-PDMAAm and PSS·Na at different pH values and fraction of PSS·Na (red: pH 3, purple: pH 5, blue: pH 11) (1 g/l, 1 mM NaNO₃).

In these figures only the normalized scattering intensity is plotted for clarity. The fraction of P2MVP-*b*-PNIPAAm and PSS·Na (*f* P2MVP-*b*-PNIPAAm and *f* PSS·Na) are the respective fractions of these polymers as calculated by the number of charges. For the C5Ms the number of charges is taken that would be reached if e.g. all acidic groups would be charged, including those used for the cross-linking (the number of charged groups is overestimated).

Starting with the addition of P2MVP-*b*-PNIPAAm, it is obvious that at pH 3 no interaction takes place as is clear from the linear increase in scattering intensity, which indicates that only a superposition of two different species is observed. The fact that at this pH the scattering intensity increases with the amount of P2MVP-*b*-PNIPAAm indicates that larger aggregates of the P2MVP-*b*-PNIPAAm block copolymer are present. Why P2MVP-*b*-PNIPAAm forms aggregates at this pH is not exactly clear at this point, but it cannot be based on hydrophobic interaction between the P2MVP blocks, e.g. because of incomplete quaternization, since at pH 3 the pyridine groups should be charged even without quaternization. At pH 5 a weak maximum is observed around a P2MVP-*b*-PNIPAAm fraction of 0.2. At pH 11 this maximum shifts to ~ 0.35 and becomes much more pronounced. This shift is to be expected since at pH 5 only a very minor number of carboxylic acid groups will be charged, meaning that only little P2MVP is needed to compensate this charge. At pH 11 nearly all carboxylic acid groups are charged, therefore more P2MVP is needed for charge equilibration. At these maxima the R_h of the micelles increases from 20 to 50 nm. The fact that the scattering intensity at the maximum observed at pH 11 is much stronger than the scattering intensity at the maximum for pH 5 is related to the higher stability of the complexes since at pH 11 more charges are involved in the complexation. Therefore more and more stable aggregates are formed.

That such a strong effect is seen at all indicates that the core is still accessible, including a lot of water, especially when charged. More work should be done to show what the exact structure

of these micelles is. One can imagine that in this particular case the PNIPAAm which is incorporated into the corona of the micelles might mix with the chemically similar PDMAAm, or form a separate phase, e.g. as a ring around the neck of the Janus micelle (as schematically shown in Figure 61).
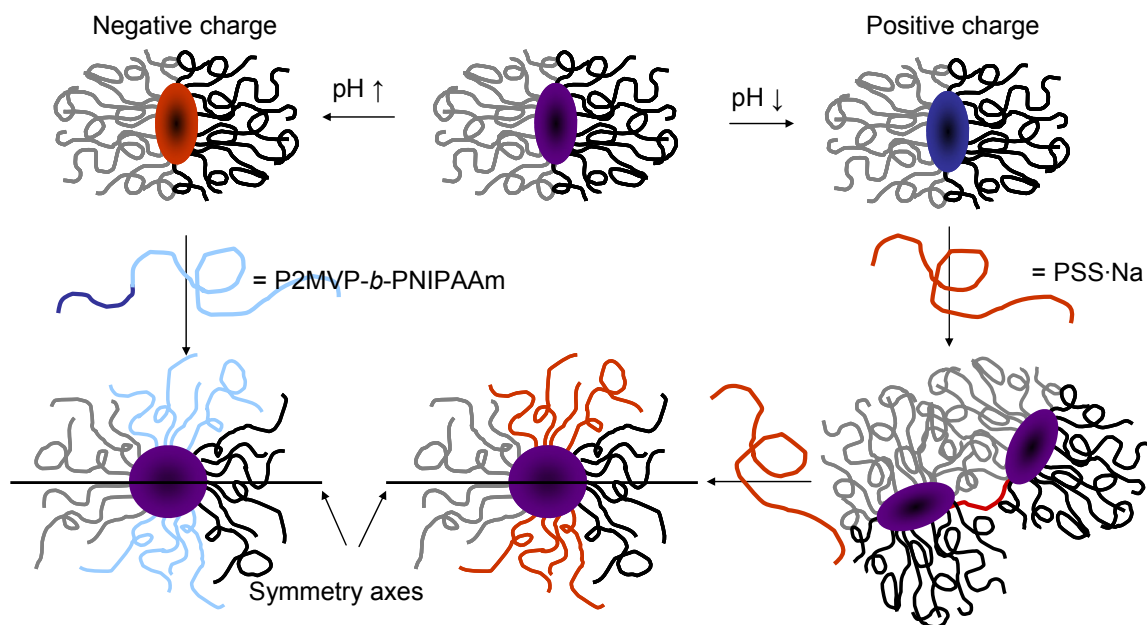
Figure 61: Schematic representation of the formation of C3M structures from C5JMs and permanently charged (block co)polymers.

Upon addition of PSS·Na a similar effect is observed. At pH 11 and 5 the data points lay, more or less, on a straight line, which indicates that no interaction between the C5Ms and PSS·Na takes place. At pH 3 though, where the C5Ms bear a net positive charge, a peak is observed at very low amounts of PSS·Na, followed by a linear decrease in scattering intensity, the scattering intensities of which are still stronger than expected in the absence of complexation (scattering intensities equal to the ones found at pH 5 would be expected). This stronger scattering intensity indicates that also in this case C3Ms are formed. The size of the micelles is stable at $R_h \sim 35$ nm at pH 3, whereas only aggregates with sizes around 18 nm are found e.g. for the mixtures at pH 11, which is the size of the C5Ms.

The peak that is observed cannot be explained by the complexation of C5Ms with the PSS·Na chains alone, since than an initial increase of the scattering intensity, directly followed by a linear decrease would be expected. This is not the case here, since after the peak first a stronger decrease is observed, gradually going over in a linear decrease. Though just speculation, this might be due to a cross-linking between different micelles in the presence of low amounts of PSS·Na, a single PSS·Na polymer chain complexing with two or more micelles simultaneously

(Figure 61). The presence of higher-order aggregates of the C5Ms is not clearly reflected in the sizes of the aggregates that are found.

When C3Ms are formed with such a high molecular weight PSS, of which one chain alone already bears as much charge as one micelle would bear when no functional groups were consumed by the cross-linking procedure, this introduces an excess negative charge in the micelles, which makes cross-linking by the PSS chains rather likely at low amounts of it. At higher amounts of PSS all micelles will be saturated with negative charge, in which case no cross-linking will take place anymore. Similar behavior was recently observed for a system where a triblock copolymer bearing positive charges in the middle block (PS-*b*-P2MVP-*b*-PEO) is complexed with single stranded DNA (ssDNA). At a 1:1 charge ratio less ssDNA chains are present than micelles, which leads to a cross-linking of the micelles into larger aggregates[79].

4.3.8 Conclusion

Upon complexation of two block copolymers with PEO and either PDMAAm or PNIPAAm blocks into Complex Coacervate Core Micelles (C3Ms), Janus micelles could be prepared, in which the two water soluble neutral polymer blocks phase separated into two distinct hemispheres. The Janus character could be shown using NOESY, CryoTEM and SERS.

The formed Complex Coacervate Core Janus Micelles (C3JMs) could be cross-linked using different methods, e.g. selectively cross-linking the acidic or basic moieties with BDDGE respectively glutaraldehyde. These procedures cross-link only one of the block copolymers, leaving the other block free to dissociate or re-associate with the cross-linked micelles. Using NHS/EDC chemistry the composition of the micelles could be stabilized through the formation of amide bonds. These micelles are referred to as C5Ms or C5JMs (Core Cross-linked Complex Coacervate Core (Janus) Micelles).

It could be shown that the stability in solution of the higher-order aggregates formed for C5JMs containing PNIPAAm varies with pH. Stable aggregates are formed at extreme pH values, whereas precipitation is found for more neutral pH. This shows that the charge in the core can strongly affect the effective packing parameter of the amphiphilic micelles.

The C5Ms could be used for the stabilization of silica nanoparticles through the physical adsorption of PEO onto the silica surface. Upon acidification of the solution, silica precipitates from solution. This could be circumvented by using sufficient amounts of micelles to cover the surface of the silica particles. The inhomogeneous layer on the silica nanoparticles could be rearranged on the surface by inducing a collapse of the PNIPAAm hemisphere, after which this hemisphere faces the nanoparticle. This shows that the adsorption of the hydrophobic

PNIPAAm is much stronger than that of PEO. For systems without PEO such structures were not found, likely because the direct vicinity of the surface (as is found when the micelles are bound to the silica particles by the binding of PEO) is needed, since a quick rearrangement is necessary to prevent the formation of higher-order aggregates of micelles.

The adsorption of C5JMs of which the CTA groups, present in one of the hemispheres, have been reduced to thiol groups, onto gold nanoparticles could also be shown.

Furthermore, the stability of the micelles towards changes in pH can be used to introduce a net charge in the micelles. This charge allows for complexation of the C5Ms with polymers containing permanently, oppositely charged groups. This was shown by complexing the C5Ms with P2MVP-*b*-PNIPAAm and PSS·Na.

4.4 Inducing a Janus character by external stimuli

4.4.1 Introduction

As was shown in the last paragraphs it is possible to make C3JMs and C5JMs using two phase separating block copolymers, cross-link them, and use them to make higher-order aggregates. Here it is shown that it is also possible to prepare C3Ms with a mixed corona, induce phase separation by applying an external stimulus and cross-linking these structures, thereby fixing the phase separated state. The removal of the stimulus yields Janus particles (Figure 62) which are fully soluble again.
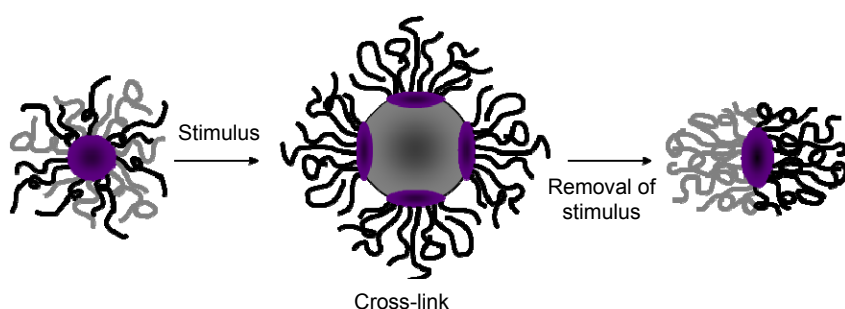
Figure 62: Schematic representation of how external stimuli and cross-linking can be used to induce phase separation in a mixed system.

This approach was applied to a PAA-*b*-PNIPAAm/PButenOx-*b*-PEtOx (the PButenOx block was functionalized with primary amine groups using thiol-ene chemistry) C3M system. This system has the advantage that PNIPAAm and PEtOx are relatively similar in nature, making a phase separation less likely than for the systems described thus far. Besides that, the PNIPAAm block provides a practical way of inducing phase separation, simply by heating of the solution and a collapse of the PNIPAAm. PEtOx is also a thermoresponsive polymer, though its cloud point temperature is far higher.

4.4.2 C3Ms

In order to better understand the system at hand, the non-cross-linked system is studied first, starting with the influence of f^+, pH, ionic strength and temperature (Figure 63).
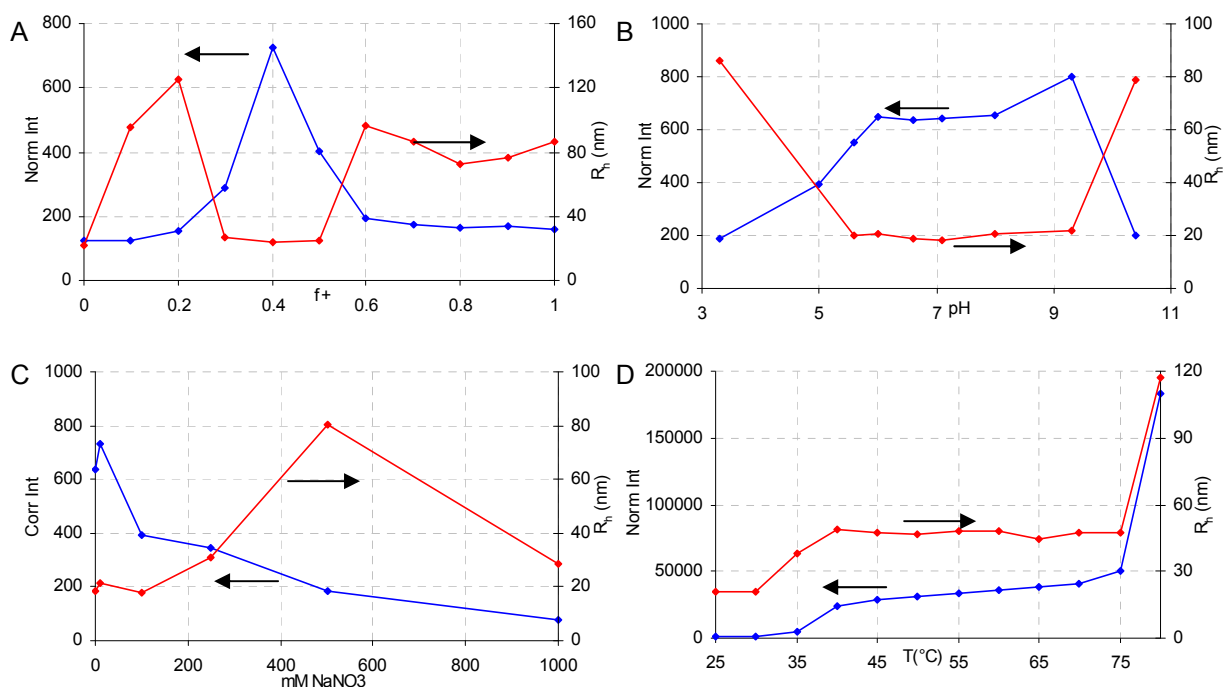
Figure 63: C3Ms of PAA-*b*-PNIPAAm/PButenOx-*b*-PEtOx A) f^+ series at pH 7, B) pH series at f^+ 0.5, C) ionic strength series at f^+ 0.4, pH 7 and D) temperature series at f^+ 0.4, pH 7 (1 g/l, 1 mM NaNO₃, except in C, where a 1 g/l solution is diluted with 2 M NaNO₃ solution).

A clear maximum in scattering intensity is observed at f^+ 0.4 (at pH 7). At this f^+ the C3Ms seem to be stable at a wide range of pH values (6 - 9), possibly due to an additional hydrophobic effect introduced by the relatively hydrophobic backbone of the PButenOx block. At these optimal conditions the micelles have an approximate R_h of 20 - 25 nm. Using angle dependent DLS, using partial Zimm and Guinier fits, radii of gyration around 16 nm and N_{agg} or ~ 18 were found. The resulting R_g/R_h ratio (~ 0.8) supports the assumption that the micelles are spherical.

As expected, the scattering intensity strongly decreases with increasing ionic strength. In the temperature series two steps are observed, one at ~ 30 °C (collapse of PNIPAAm) and one at ~ 75 °C, which can be attributed to the collapse of PEtOx. The complexes then precipitate from solution. Between the two steps the scattering intensity and size of the aggregates are rather stable (R_h ~ 50 nm), indicating that PEtOx stabilizes the aggregates. At 45 °C, where PNIPAAm is collapsed, an angle dependent DLS measurement is performed which yielded an R_g of ~ 30 nm, so that solid spheres may be assumed (R_g/R_h ~ 0.6).

Whether a mixed corona is formed or not is determined using NOESY. The NOESY spectrum is shown in Figure 64.
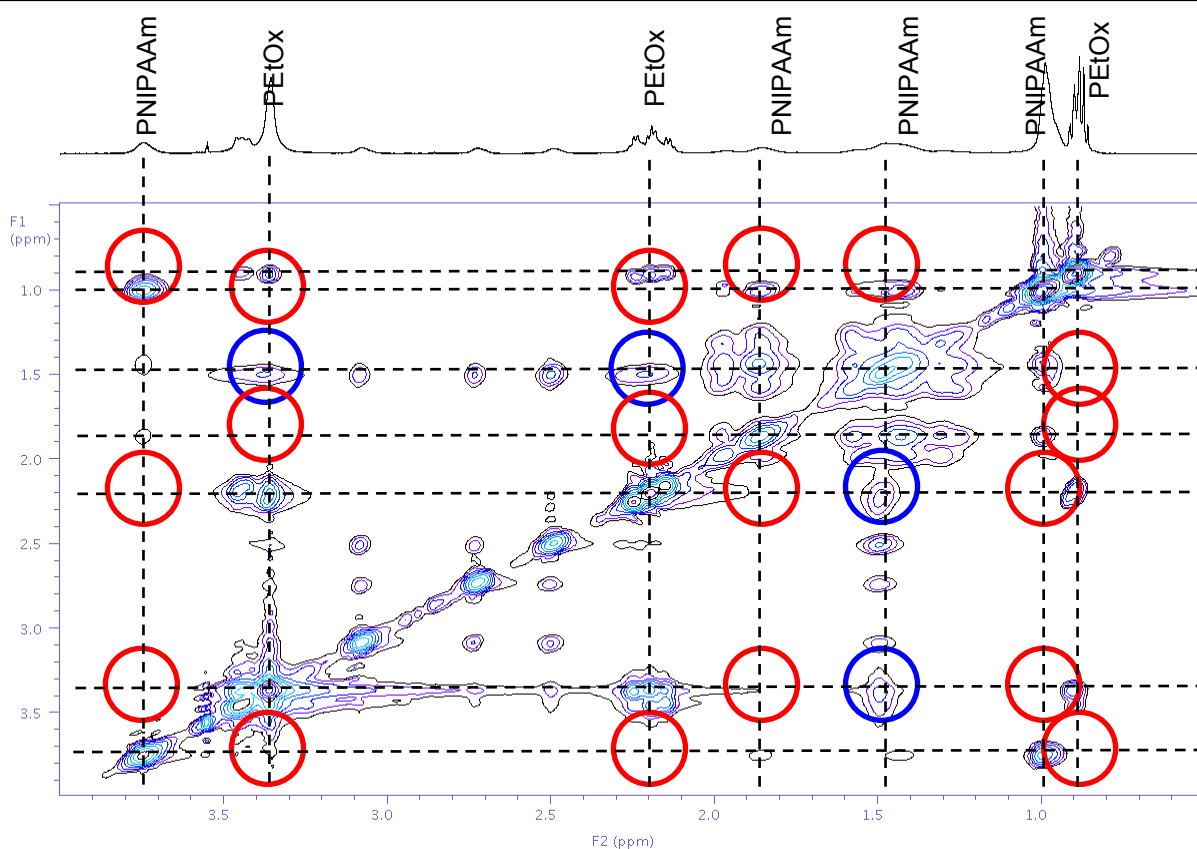
Figure 64: 2D-NOESY spectrum of PAA-*b*-PNIPAAm/PButenOx-*b*-PEtOx C3Ms, (600 MHz, negative peaks, 10 g/l in D$_2$O). Red circles indicate where NOE peaks could have been observed but are not, blue circles indicate NOE cross-correlation (measurements by Olaf Niemeyer).

In this case cross-correlation between the signals of the PNIPAAm and PEtOx is found, which indicates that the polymers in the corona are mixed. Unfortunately, a literature search did not yield any values for the χ-parameters of any of these polymer mixtures to see whether these support the fact that the combinations PNIPAAm/PEO and PDMAAm/PEO yield phase separation whereas a PNIPAAm/PEtOx combination does not. The χ-parameter describes the interaction between a given pair of components.

4.4.3 Cross-linked structures

Micelles cross-linked at room temperature

To begin with the PAA-*b*-PNIPAAm/PButenOx-*b*-PEtOx C3Ms are cross-linked at room temperature, using NHS/EDC-chemistry. The solution behavior of these C5Ms with pH and ionic strength is shown in Figure 65.
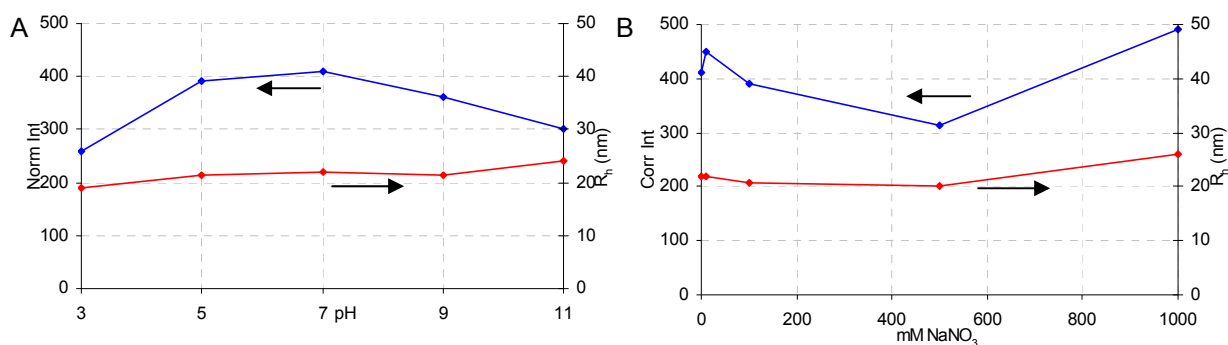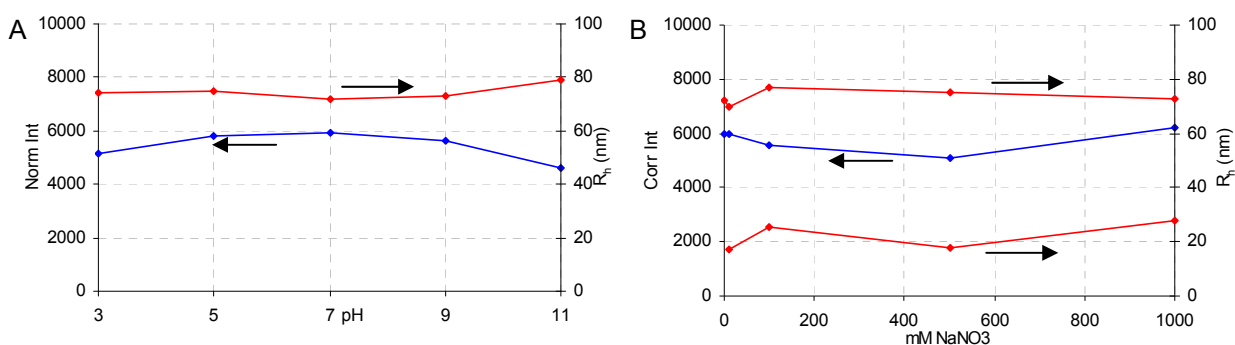
Figure 65: The behavior of C5Ms of PAA-*b*-PNIPAAm/PButenOx-*b*-PEtOx cross-linked at room temperature with pH (1 g/l, 1 mM NaNO₃) (A) and ionic strength (1 g/l diluted with 2 M NaNO₃) (B).

By cross-linking, nearly all dependence with pH and ionic strength disappears, save for a slight maximum in scattering intensity around pH 7. At 1 M sodium nitrate a strong increase in scattering intensity is observed, which, as discussed for other systems, can be attributed to a shift of the LCST of PNIPAAm to a lower temperature. The size of the micelles is maintained upon cross-linking ($R_h \sim 22$ nm, before cross-linking ~ 20 nm)
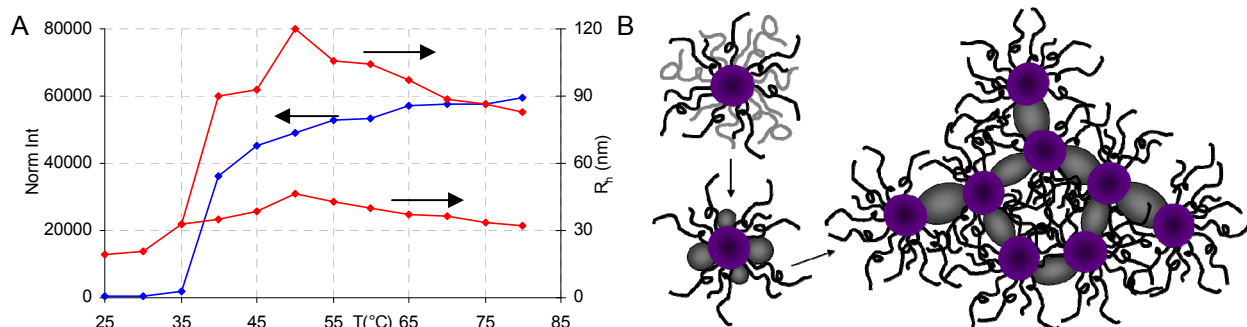
Figure 66: A: The behavior of C5Ms of PAA-*b*-PNIPAAm/PButenOx-*b*-PEtOx, cross-linked at room temperature, with temperature (1 g/l, 1 mM NaNO₃). B: Schematic representation of the thermoresponsive behavior of core cross-linked micelles with a mixed corona.

Figure 66 shows the thermoresponsive behavior of these C5Ms at pH 7. As with the corresponding C3Ms, larger, stable aggregates are formed above the LCST of PNIPAAm. The aggregates are slightly larger in this case ($R_h \sim 100$ vs. 50 nm) though. From Contin analysis, it is obvious that two fractions of aggregates are present ($R_h \sim 35$ and ~ 100 nm). The size of the smaller aggregates is consistent with the size of the aggregates formed by non-cross-linked micelles above the LCST of PNIPAAm. Above 80 °C precipitation of the micelles occurs due to the collapse of the PEtOx block. The fraction of larger aggregates arises from the cross-linking of the situation with a mixed corona, which prohibits a phase separation in the corona and reordering of the chains from taking place (Figure 66).

The thermoresponsive behavior of the micelles is also investigated as a function of the pH. Instead of reporting the scattering intensity measured with light scattering, the transmittance,

measured using a UV-Vis spectrophotometer with temperature control, is reported. The transmittance can be directly correlated with the scattering intensity. The measured transmittance curves are shown in Figure 67.

The change in transmittance/scattering intensity with temperature is altered dramatically with pH. In all cases, an initial, slight decrease in transmittance is observed around 35 °C, which corresponds to the collapse of PNIPAAm. In nearly all cases, except at pH values up to 4 and above 10, a second step, corresponding to the collapse of PEtOx, is also observed. At intermediate pH values, the T_{cp} of PEtOx is lowered. The closer the pH value gets to 7, at which pH the collapse of PNIPAAm also triggers the slow collapse of PEtOx, the lower the transition temperature. The observed behavior can, as reported in Chapter 3, be traced back to the charge that is present in the core of the micelles. At extreme pH values, a strong net charge is present in the core, thereby swelling it and decreasing the local concentration of PEtOx close to the core, leading to higher cloud point temperatures (even to T_{cp} > 90 °C). With a more neutral charge in the core, the core becomes less swollen and the local PEtOx concentration increases and therefore the cloud point temperature is lowered. This same behavior was also observed for micelles with a corona purely consisting of PEtOx (see Chapter 3).

This type of behavior is typical for Type I thermoresponsive polymers since the cloud point temperature of these polymers strongly depends on the local concentration. PNIPAAm, a Type II thermoresponsive polymer, does not show this behavior, whereas PEtOx or other poly-2-oxazolines or e.g. poly(N-vinyl caprolactam)[80] would.
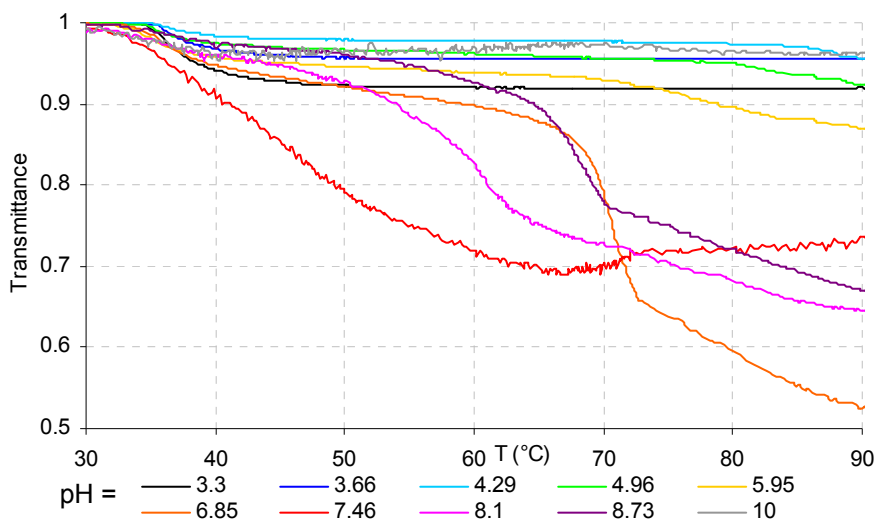
Figure 67: Transmittance of solutions of C5Ms consisting of PAA-*b*-PNIPAAm/PButenOx-*b*-PEtOx, cross-linked at room temperature at different pH values (1 g/l, 1 mM NaNO₃).

Structures cross-linked at higher temperature

Since at higher temperatures different aggregates are formed through the collapse of PNIPAAm, it is interesting to cross-link these structures, firstly because a phase separation, which might be maintained after cooling down, is induced, but also while this gives insight into the structure of the aggregates above the LCST of PNIPAAm. The cross-linking was performed at f^+ 0.4, pH 7, 50 °C, at which temperature the PNIPAAm block is collapsed and larger aggregates are formed ($R_h \sim$ 50 nm) as is shown in Figure 63. pH, ionic strength and temperature series for these cross-linked structures are shown in Figure 68 and Figure 71.
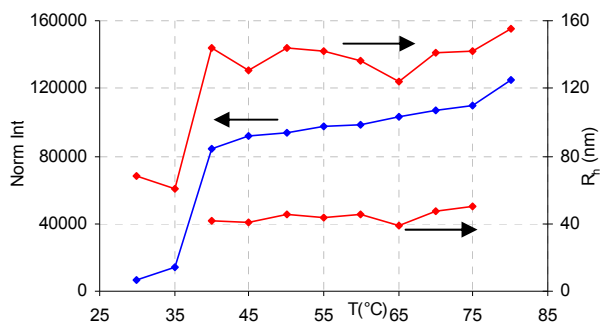

Figure 68: The behavior of C5Ms of PAA-*b*-PNIPAAm/PButenOx-*b*-PEtOx cross-linked at 50°C with pH (1 g/l, 1 mM NaNO₃) and ionic strength (1 g/l diluted with 2 M NaNO₃, pH 7).

The pH and ionic strength series indicate that stable larger aggregates ($R_h \sim$ 75 nm) are formed, which coexist with a small number of smaller particles (R_h 20 - 30 nm). These smaller particles are likely cross-linked micelles very similar to the ones found when cross-linking was performed at room temperature, though possibly with a phase separated corona. The scattering intensity of these micelles only constitutes approximately 5 % of the total scattering intensity. By static light scattering (full Zimm-analysis, performed by correcting the scattering intensity for each angle for the percentage of scattering, as determined by Contin analysis, that can be attributed to this population of particles) an R_g for the fraction of larger structures of 82 nm is found. The R_g/R_h ratio (1.1) therefore indicates slightly elongated structures.

Using CryoTEM the structure of the C5Ms is visualized (Figure 69).
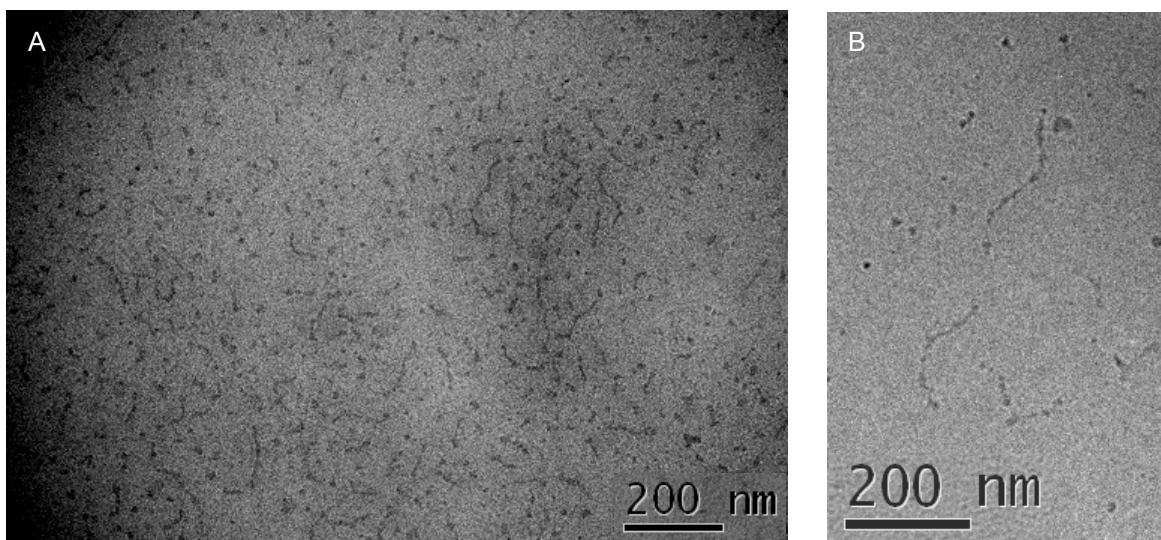
Figure 69: CryoTEM image of PAA-*b*-PNIPAAm/PButenOx-*b*-PEtOx C5Ms cross linked at 50°C (A: 10 g/l in D$_2$O, 1 mM NaNO$_3$, pH 7, B: 10 times diluted with H$_2$O) (images courtesy of Prof. Dr. Janne Ruokolainen).

Worm-like micelles are observed using CryoTEM, coexisting with small spherical micelles, as DLS already suggested. Though in one of the images it looks as if branched structures are present, this can, based on CryoTEM images taken for more dilute solutions (e.g. shown in Figure 69 B), be excluded. This observation is due to several worm-like micelles which partly lay on top of each other. When looking closely, a kind of 'pearl-necklace' structure can be recognized. The reason for the coexistence of both micelles and worm-like micelles can be found in the structures that are formed above the LCST of PNIPAAm. Generally, spherical objects are observed upon the collapse of PNIPAAm in the presence of a stabilizing block. Assuming that in the current system aggregates are formed with a core of collapsed PNIPAAm[71], the morphology of the complex coacervate phase on this core is critical. If the PNIPAAm phase is completely covered with a complex coacervate shell, the cross linking of this shell will yield vesicular structures. If patches of complex coacervate material cover the PNIPAAm core, the cross-linking of the structures will yield (Janus) micellar structures. Worm-like micelles are to be expected when there is contact between the complex coacervate patches, as is shown in Figure 70. The "pearl-necklace" structure of the worm-like micelles confirms this hypothesis; the ticker patches of complex coacervate material arise from the cores of the single micelles, whereas the more narrow complex coacervate material is formed from the bridges between the cores.

This suggests that the fraction of PNIPAAm compared to the fraction of core material, together with the interfacial tension between the different phases, governs the structure that is formed upon cross-linking at elevated temperatures. Attempts to visualize these structures using CryoTEM did not yield undisputable indications that support or weaken this theory.
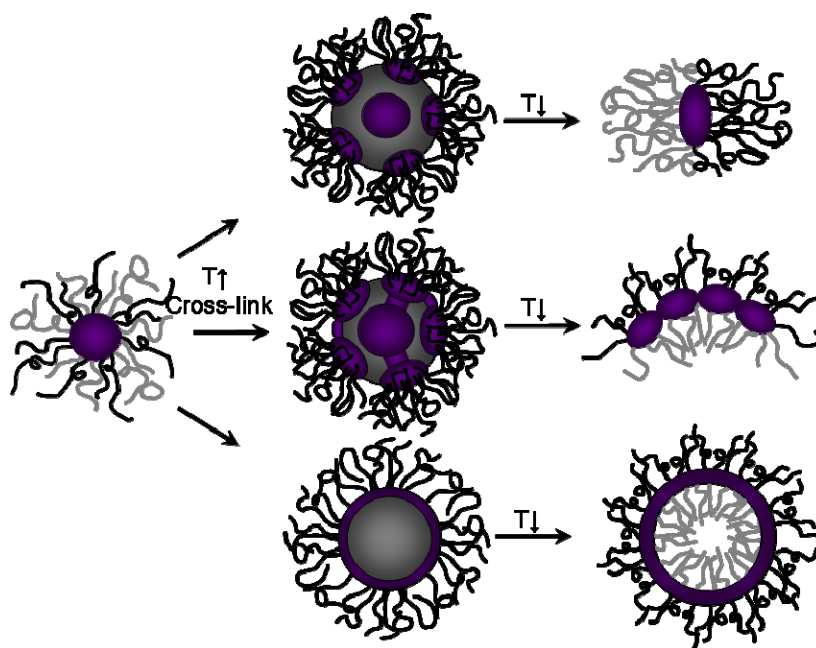
Figure 70: Schematic overview of how Janus micelles, worm-like micelles and vesicular structures might be formed after cross-linking of collapsed mixed micelles.

Such phase-separated worm-like micelles are very similar to some structures, obtained through the cross-linking of bulk-morphologies[24], which is not surprising considering the similarities in the way they were prepared. Though in this work only micelles and worm-like micelles were found, it is very likely that also vesicles are accessible using this methodology. This assumption is also supported by systems described in literature, where exactly this type of morphology is obtained[81].

Unfortunately it was impossible to obtain a proper NOESY spectrum for these worm-like micelles because of their limited solubility. Though this could not be proven, it is to be expected that upon cross-linking the phase separated morphology is maintained.

The heating of solutions of these particles yields two fractions of aggregates in the temperature range before PEtOx precipitates (at ~ 80 °C), one similar in size to the aggregates of the non-cross-linked C3Ms (~ 50 nm, accounting for ~ 15 % of the total scattering intensity) and a fraction of larger particles with radii around 135 nm (accounting for ~ 80 % of the scattering intensity). The fact that such poorly defined particles are found upon the collapse of the PNIPAAm block can be related to the difficulty in reforming exactly those structures that were originally cross-linked, leading to larger, poorly defined aggregates.

Figure 71: The behavior of C5Ms of PAA-*b*-PNIPAAm/PButenOx-*b*-PEtOx cross-linked at 50 °C with temperature (1 g/l, 1 mM NaNO$_3$, pH 7).

The ratio of core material to PNIPAAm can e.g. be influenced by the addition of extra PNIPAAm homopolymer (the synthesis of which is described in the appendix) to the solution, which also collapses and makes the PNIPAAm core of the aggregates bigger. Cross-linking of such aggregates in the presence of 0.3, 0.6, 1.2 and 2.3 weight equivalent of PNIPAAm homopolymer (to C3Ms) were performed. A short summary of the light scattering data is shown in Table 3.

Table 3: Summary of light scattering data for C5Ms of PAA-*b*-PNIPAAm/PButenOx-*b*-PEtOx in the presence of different amounts of PNIPAAm homopolymer. The scattering intensity is corrected for the weight fraction of C5Ms (at pH 7, 1 g/l, 1 mM NaNO$_3$, 25 °C).

wt eq PNIPAAm	Norm Int	Corr Int	R_h cum (nm)	R_h contin (nm)
0.00	5951	5951	73	72
0.29	3907	5056	61	62
0.59	2595	4115	52	49
1.17	1551	3368	53	53
2.34	1116	3731	50	54

In none of the samples with extra PNIPAAm a second fraction of (smaller) particles could be confirmed, though this might well be a problem in the fitting of the DLS data. It is therefore difficult to determine whether only shorter worm-like micelles are present or less of them, together with higher numbers of spherical micelles. The size of the cross-linked structures decreases to a constant R_h of approximately 50 nm, after which no further decrease is observed. This means that the size or number of the worm-like micelles to some degree depends on the size of the PNIPAAm block relative to the core material. As the C5Ms cross-linked in the absence of additional PNIPAAm, these micelles are stable towards pH and ionic strength.

The size of the aggregates formed above the LCST of PNIPAAm is stable at R_h ~ 130 nm for all systems. For the sample cross-linked in the presence of the highest amount of PNIPAAm, some precipitation is observed though, likely due to the fact that not all extra PNIPAAm, which is still present after cross-linking, can be stabilized.

4.4.4 Cross-linking of other C3M systems at higher temperature

Larger structures are not only formed for PAA-*b*-PNIPAAm/PButenOx-*b*-PEtOx C5Ms cross-linked at higher temperatures, but are also formed for systems consisting of e.g. PAA-*b*-PAAm/PVA-*b*-PNIPAAm and PMAA-*b*-PEO/PVA-*b*-PNIPAAm when cross-linked at elevated temperatures. By comparing the composition and size of the aggregates found after cross-linking of these systems, some indications can be found to answer the question what determines the size of the C5Ms when cross-linked at higher temperatures. To do so, it is presumed that only the relative weight ratio of the different components in the system determines the morphology. The fact that one system is known to form Janus micelles, should not influence the structure since phase separation will also take place for the other systems at temperatures above the LCST of PNIPAAm.

Two main factors which could influence the structure of these micelles can be imagined. Firstly, the relative amount of core material compared to PNIPAAm can influence the morphology of the cross-linked micelles. This is consistent with the way in which the mechanism has been drawn in Figure 70. Secondly, the amount of the other, stabilizing block, and the fraction of PNIPAAm in the system should be considered. A summary of the sizes and compositions of the different systems is shown in Table 4.

Table 4: Summary of the size and composition of C5Ms prepared at 50 °C (CC:PNIPAAm: amount of complex coacervate material relative to PNIPAAm by mass, PNIPAAm:PX: amount of PNIPAAm compared to the amount of the other non-ionic block by mass, PNIPAAm:total: mass fraction of PNIPAAm in the system).

Composition		CC:PNIPAAm	PNIPAAm:PX	PNIPAAm:total	R_h (nm)	% scatt int	R_h (nm)	% scatt int
PAA$_{38}$-*b*-PAAm$_{400}$	PVA$_{36}$-*b*-PNIPAAm$_{368}$	0.100	1.546	0.573	35	100	-	-
PMAA$_{63}$-*b*-PEO$_{551}$	PVA$_{36}$-*b*-PNIPAAm$_{368}$	0.112	3.002	0.692	120	75	~20	20
PButenOx$_{33}$-*b*-PEtOx$_{184}$	PAA$_{53}$-*b*-PNIPAAm$_{300}$	0.428	1.159	0.436	75	80	~20	5

In this table, the systems are ordered from high to low amounts of presumably spherical micelles. For the PAA-*b*-PAAm/PVA-*b*-PNIPAAm system only smaller aggregates were found (with $R_h \sim 35$ nm), which does not exclude the possibility that some larger aggregates coexist with micelles, but the fact that these two fractions cannot be fitted separately means that the fraction of larger aggregates is very minor. For the PMAA-*b*-PEO/PVA-*b*-PNIPAAm and PAA-*b*-PNIPAAm/PButenOx-*b*-PEtOx systems only ~ 20 and 5 % of the total scattering intensity could be attributed to normal micelles respectively. When comparing the compositions of these systems, the only factor that varies systematically with the fraction of micelles is the amount of complex coacervate material relative to the amount of PNIPAAm. This confirms that the size of the complex coacervate patches and therefore their average distance to each other governs the amount of larger aggregates. The size of the aggregates does not seem to be directly set by the ratio of core material and PNIPAAm, but is likely more dependent on a combination of this ratio

and the size of the aggregates formed above the LCST of PNIPAAm, which is more dependent on the ratio between the amount of PNIPAAm and the second stabilizing block. This parameter should be studied in more detail to determine how the size of the worm-like micelles can be influenced most effectively.

4.4.5 Conclusion

Using polymers containing PNIPAAm and PEtOx blocks, C3Ms could be prepared with a mixed corona which consists of two thermoresponsive polymers, the cloud point temperatures of which are distinctly different. The mixing of the corona could be shown by NOESY.

C3Ms cross-linked at room temperature exhibit an interesting influence of the pH on the thermoresponsive nature of the micelles is observed. As with the C5JMs containing PEO and PNIPAAm, the pH and thereby the charge in the core of the micelles strongly influences the structures that are formed, and the stability of these higher-order aggregates. The difference that is observed is that the charge of the core also influences the cloud point temperature of the PEtOx block much in the same way as described in Chapter 3, by decreasing the local concentration near the core of the micelles and thereby the cloud point temperature.

Asymmetry can be induced by applying external stimuli which induce phase separation. Thus far it could not be proven that upon cross-linking and removal of the stimulus the phase separated state is maintained. It could be shown though that the polymer chains in the corona of micelles cross-linked at room temperature are no longer able to rearrange and thereby stay mixed. Upon heating at best patchy micelles are formed. This suggests that also in the case of micelles cross-linked at higher temperatures this flexibility is lacking, thereby fixating the phase separated state. The cross-linking of complex coacervate structures at elevated temperatures can also be used to study the structure of these aggregates above the T_{cp} of PNIPAAm.

This procedure yields worm-like micelles as was clearly observed by CryoTEM. These micelles exhibit a "pearl-necklace" structure. This indicates that above the LCST of the PNIPAAm the cores of the micelles are partly intact but have some contact with each other. The fraction of these worm-like micelles can be influenced by changing the ratio of PNIPAAm relative to the amount of core material, e.g. by the mixing of the C3Ms with PNIPAAm homopolymer.

Chapter 5: Asymmetry from a symmetric protein template

5.1 Introduction

The binding of biotin by streptavidin is a widely used motive, well known for the selective and extremely strong binding. This motive has also been used in polymer chemistry, where polymers functionalized with biotin-moieties are used to make protein-polymer conjugates. Such conjugates (not only with streptavidin but also with other proteins) are attractive systems to e.g. influence the catalytic activity of enzymes or the binding of proteins to substrates, especially when stimuli responsive polymers are used. For example PNIPAAm (or copolymers of NIPAAm with other monomers, such as acrylic acid) has been grafted from or onto streptavidin, in a position near the active site of the protein[82]. This allows for a reversible blocking of the binding site, which is controlled by the application of external stimuli (e.g. temperature and pH). Also photoresponsive polymers have been used in such a way[83].

In this study the controlled aggregation of streptavidin using three-arm star polymers and the formation of Janus-type aggregates based on the biotin-streptavidin binding is reported. Janus structures are obtained through the selective blocking of three out of four binding sites by a three-arm star polymer, leaving one binding site for another (linear) biotin end-functionalized polymer.

5.2 Polymer synthesis

The biotin end-functionalized polymers used in this study (Figure 78) are prepared by RAFT polymerization (three-armed star of PAAm (s-PAAm) and PNIPAAm homopolymer) or living anionic polymerization (PEO). The allyl end-group introduced in the PEO is converted to a thiol group (Figure 74), and the CTAs used in RAFT are reduced using sodium borohydride to yield thiol end-groups. These are in turn reacted with maleimide-biotin, yielding biotin end-functionalized polymers. The synthetic pathways for the synthesis of these polymers are described in the appendix and schematically shown in Figure 72, Figure 74 and Figure 76.
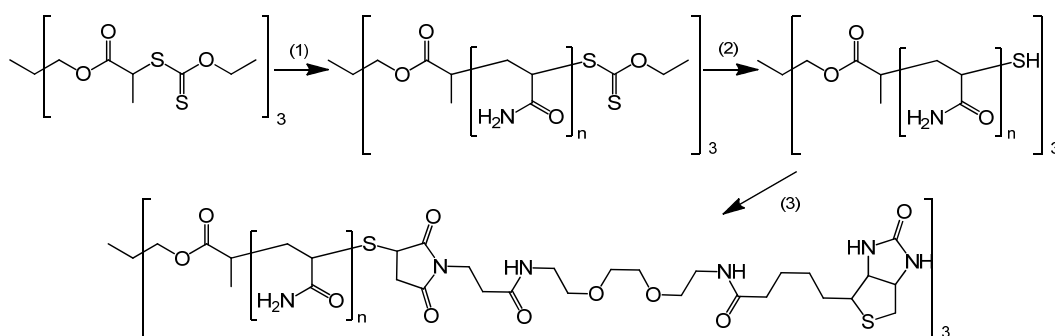
Figure 72: Synthesis pathway of three armed star PAAm end-functionalized with biotin. (Reaction conditions: (1): trifunctional CTA, acrylamide, AIBN, *N,N*-dimethylacetamide, 70 °C, 24 h, (2): H_2O, $NaBH_4$, (3): $NaBH_4$, HCl, biotin-maleimide.)

By RAFT using a trifunctional Chain Transfer Agent (CTA) a three-armed star PAAm is polymerized. The xanthate residue is reduced to a thiol[67] which is used to end-functionalize the polymer with maleimide-biotin. In this way a biotin end-functionalized three-armed star polymer was obtained (M_n^{App} = 4.7 kg/mol, n ~ 120, PDI^{App} = 2.41, as determined by SEC in H_2O with PEO standards, Figure 73).
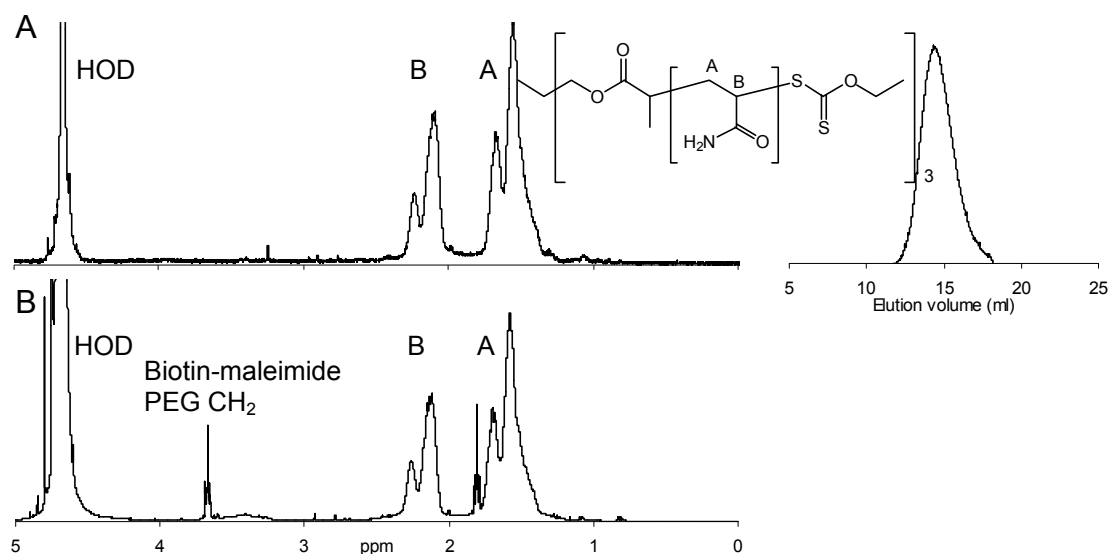
Figure 73: A) ^{1}H-NMR and SEC elugram (in water) of s-PAAm, as well as its chemical structure. B) ^{1}H-NMR of biotin end-functionalized s-PAAm.

The success of the reduction of the CTA is confirmed by elemental analysis (S/C ratio by moles before reduction = $5.58 \cdot 10^{-3}$, after reduction $2.48 \cdot 10^{-3}$). The presence of only half the number of sulfur atoms is consistent with the reduction of the CTA groups. After the functionalization with biotin-maleimide a couple of weak new peaks are observed in the ^{1}H-NMR spectrum. The clearest one is the peak which can be attributed to the PEG linker (at ~ 3.7 ppm) of the biotin-maleimide. The integral of this peak indicates full functionalization.
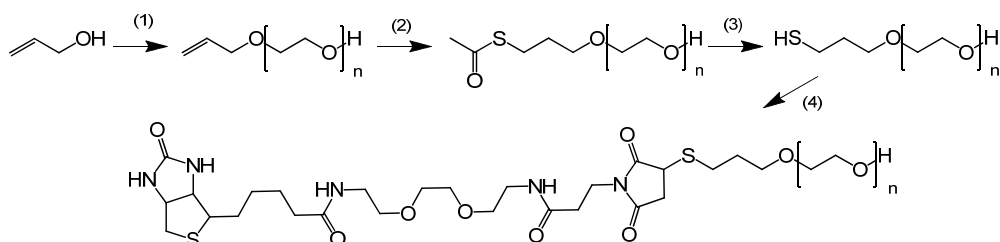
Figure 74: Synthetic pathway of PEO-biotin. (Reaction conditions: (1): THF, phosphazene base P$_4$-t-Bu, allyl alcohol, ethylene oxide, 45 °C, 2 days[84], (2): H$_2$O, thiolacetic acid, UV, (3): CHCl$_3$, NaOH in methanol, (4): NaBH$_4$, HCl, biotin-maleimide.)

Using an allyl alcohol/phosphazene base (P$_4$-t-Bu-base) initiator system, PEO is polymerized by anionic polymerization. The resulting polymer contains an allyl end-group. This group is transformed to a thiol end-group by thiol-ene functionalization with thiolacetic acid and successive hydrolysis of this group. The thiol end-group is used to end-functionalize the polymer with maleimide-biotin. In this way a biotin-end functionalized PEO was obtained (M$_n^{App}$ 6.1 kg/mol, n = 97, PDI^{App} 1.12, as determined by SEC in THF with PEG standards, Figure 75).
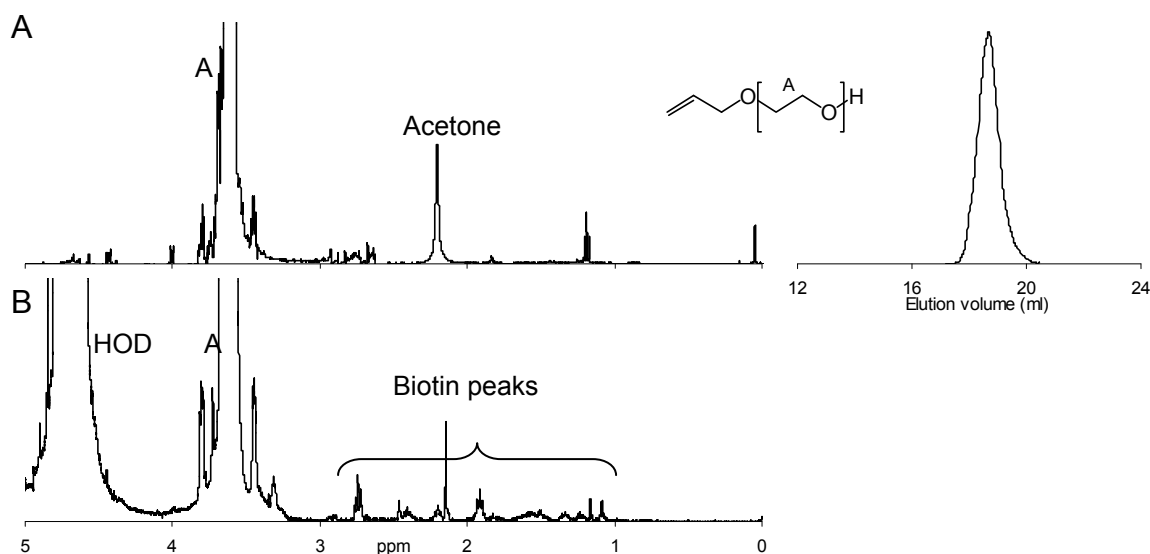
Figure 75: A) ^{1}H-NMR (CDCl$_3$) and SEC elugram (in THF) of allyl-PEO, as well as its chemical structure. B) ^{1}H-NMR of biotin end-functionalized PEO (D$_2$O).

The success of the thiolation was confirmed by elemental analysis. The molar S/C ratio that was found was $2.99 \cdot 10^{-3}$, which, within experimental error, represents full functionalization (if one were to determine the degree of polymerization from this a value of 84 is found). Though it is hard to quantify, several characteristic peaks that can be attributed to biotin are observed in the ^{1}H-NMR spectrum of the biotin end-functionalized PEO, which shows that functional groups were incorporated.
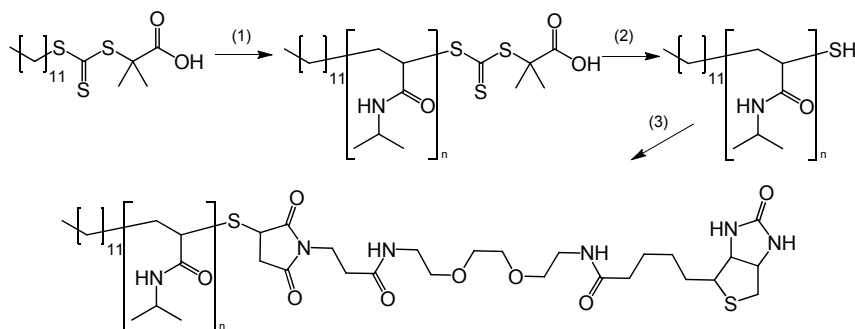
Figure 76: Synthetic pathway of PNIPAAm-biotin. (Reaction conditions: (1): DMP, NIPAAm, AIBN, DMF, 65 °C, 7 days, (2): H$_2$O, NaBH$_4$, (3): NaBH$_4$, HCl, biotin-maleimide.)

By RAFT PNIPAAm is polymerized, after which the trithiocarbonate residue is reduced to a thiol[67] which is used to end-functionalize the polymer with maleimide-biotin. In this way a biotin-end functionalized polymer was obtained (M$_n$^{App} 31.9 kg/mol, n = 300, PDI^{App} 1.21, as determined by SEC in NMP with PS standards, Figure 77).
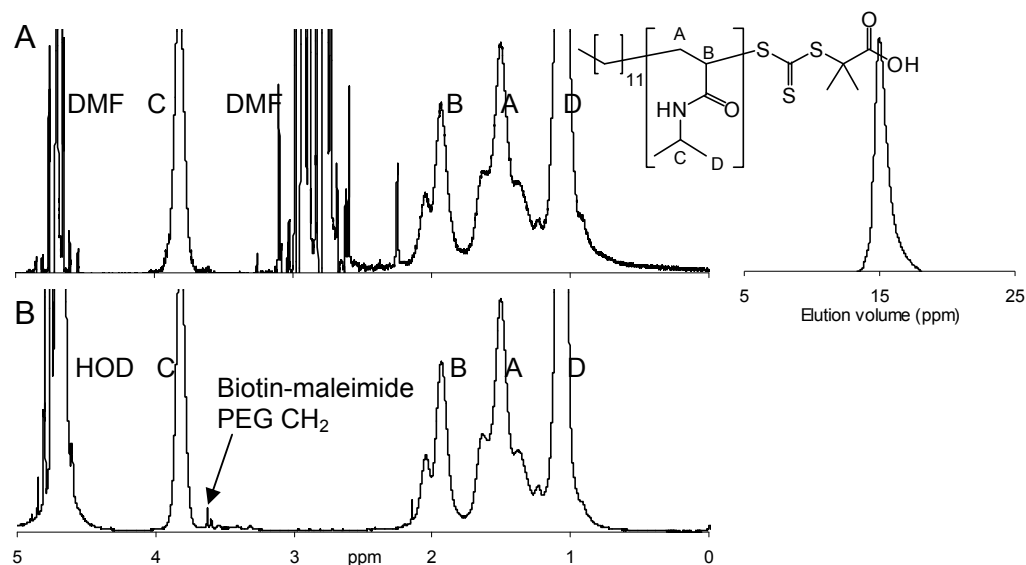
Figure 77: A) ¹H-NMR (CDCl₃) and SEC elugram (in NMP) of PNIPAAm, as well as its chemical structure. B) ¹H-NMR of biotin end-functionalized PNIPAAm (D₂O).

The success of the reduction of the CTA was evaluated using elemental analysis. The molar S/C ratio that was found before reduction was $2.21 \cdot 10^{-3}$. After reduction this ratio was $1.20 \cdot 10^{-3}$. That not even half of the sulfur atoms was removed might indicate an incomplete deprotection (the values imply a degree of reduction of 68 %). The polymer is used nevertheless for the functionalization with maleimide-biotin. The small number of biotin moieties per monomer unit makes a quantification of the degree of functionalization impossible, though the peak originating from the PEG spacer is observed.

It can be concluded that the synthesis and functionalization of the three-armed star polymer was successful, as was the synthesis of biotin-end functionalized PEO, though the exact degree of functionalization with biotin end-groups could not be determined. The reduction of the CTA end-groups of the PNIPAAm homopolymer was not quantitative, and in this case the number of end-groups could not be quantified either, though some biotin groups are present.

5.3 Polymer-protein complexes

5.3.1 Janus complexes

Using dynamic light scattering, the behavior of streptavidin with varying amounts of three-arm star polymers and homopolymers end-functionalized with biotin is investigated. In Table 5 the results are shown. Most experiments are done in a stepwise fashion, first adding one polymer to the streptavidin solution, and after characterization of the complexes adding a second polymer. Please note that all experiments, unless mentioned otherwise, are performed at a concentration of 0.1 g/l. This low concentration is chosen to prevent non-selective interactions as much as possible, since at high concentrations cross-linking and aggregation might occur much more readily.
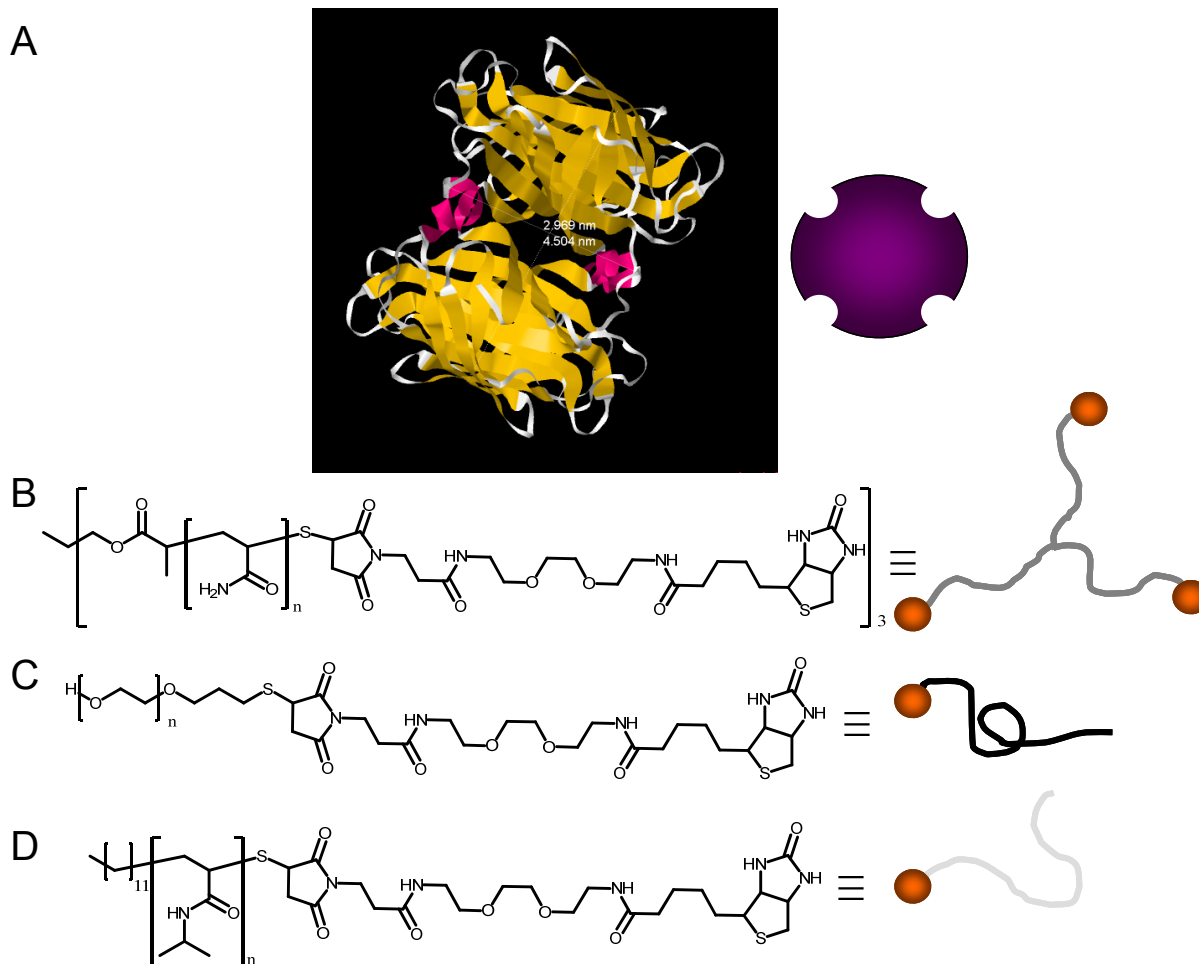
Figure 78: A: Crystal structure of streptavidin[85], B: three-arm polyacrylamide end-functionalized with biotin, C: poly(ethylene oxide) end-functionalized with biotin, D: poly(N-isopropylacrylamide) end-functionalized with biotin and the way they are schematically represented throughout this chapter.

From the crystal structure, shown in Figure 78, an average distance between the binding sites for biotin can be determined to be approximately 2.3 nm. One should distinguish between two kinds of binding site pairs, denoted as *cis* or *trans*. The *cis* pairs are closer to each other than the *trans* ones. For binding of all the biotin moieties of the three-armed star polymer, the arms should have a minimal length in the order of 6 nm (~ 20 repeat units). The three-arm star polymer synthesized in this work has a significantly higher molecular weight, so it should be able to reach all binding sites.

Table 5: Results from dynamic light scattering for polymer-protein conjugates (0.1 g/l in phosphate buffer pH 7.5).

Initial mixture	Second step	Norm Int	R_h cum (nm)	R_h contin (nm)
Streptavidin		7.7	2.54	2.69
s-PAAm		7.3	0.00	4.80
PEO		4.9	0.00	931.67
PNIPAAm		13.2	20.29	18.51
Strep + 1 eq s-PAAm		9.4	3.41	2.66
	+1 eq PEO	5.1	3.30	2.88
Strep + 1.5 eq s-PAAm		6.2	2.56	2.43
	+1 eq PEO	7.0	3.02	3.04
Strep + 3 eq s-PAAm		9.0	3.32	3.24
	+1 eq PEO	4.9	3.35	3.53
Strep + 1 eq PEO		7.4	2.56	2.42
	+1 eq sPAAm	7.1	2.52	2.55
Strep + 2 eq PEO		9.5	2.43	2.39
	+2/3 eq sPAAm	6.6	2.85	3.53
Strep + 3 eq PEO		6.5	2.53	2.77
	+1/3 eq sPAAm	9.4	2.96	3.07
Strep + 1 eq s-PAAm		6.5	3.04	2.67

Upon addition of up to one equivalent of three-armed poly acrylamide functionalized with biotin (s-PAAm-Biotin) to a streptavidin solution no significant change in the size of the particles is observed (R_h 2.69 → 2.66 nm). This can be explained by the fact that three of the four active sites of streptavidin are occupied with biotin-moieties. Therefore no cross-linking between streptavidin units takes place, which would be seen as an increase in the size of the particles.

That binding takes place at all is shown using size exclusion chromatography. Figure 79 shows the elution traces of streptavidin, s-PAAm-Biotin and PEO-Biotin, as well as the mixture of the three (1 eq s-PAAm-Biotin and 1 eq PEO-Biotin). The elution curve of the mixture is shifted compared to the one of streptavidin, indicating an increase in size (M_n^{App} 10.9 kg/mol → 13.5 kg/mol). The apparent polydispersity stays approximately the same (PDI^{App} 1.20). Since the elution traces overlap, a theoretical elution trace is calculated, based on the curves of the single components (also taking into account the relative amounts and refractive indices). If no binding would take place, the elution trace is expected to look like this calculated elution trace (a superposition of the single peaks). Since a significant shift between the theoretical curve and the curve of the actual mixture is observed, as well as a significant difference in polydispersity (calculated to be approximately 1.3 compared to 1.2 for the actual mixture) it can be concluded

that at least the s-PAAm-Biotin is bound to the streptavidin. The resolution of the technique unfortunately is not high enough to confirm the binding of PEO-Biotin.

The fact that in DLS no big change in size is observed, though binding takes place, indicates that there is no cross-linking between different streptavidin proteins. This strongly suggests that one s-PAAm-Biotin polymer binds to a single streptavidin (thereby blocking three of the four binding sites).
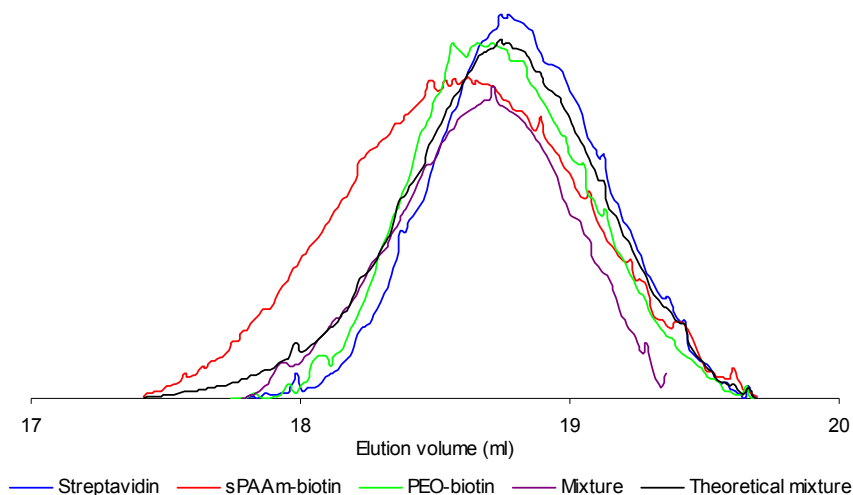
Figure 79: SEC (H$_2$O, 0.1 g/l) elution traces of the three single components (three armed star PAAm end-functionalized with biotin (s-PAAm-Biotin), PEO end-functionalized with biotin (PEO-Biotin) and streptavidin), a 1:1:1 mixture of these components and the elution trace which is expected when no biotin binding would take place (theoretical mixture).

Similarly, the selective binding of two biotin groups bound to one molecule has been described[86]. In this system one molecule (consisting of three arms, two of which were end-functionalized with biotin moieties and the third with a metal binding species) binds to two of the binding sites. The other two binding sites are used for the binding of a second molecule. Upon addition of metal ions, linear polymers could be made. This work already shows that two of the binding sites can be used to bind one molecule.

The work of Wilbur *et al.*[87] shows similar binding of three-armed, biotin end-functionalized molecules. They report the binding of two of the biotin groups to one protein, the other binding to a second protein, thereby cross-linking them. This work was performed with spacers between 2.5 and 5.5 nm, which are not long enough to wrap around the protein to reach the *trans* binding sites, thereby forcing cross-linking to take place. Longer arms, as used in this work, should be able to reach the *trans* binding sites.

This does not mean that no cross-linking of streptavidin might occur. Under the chosen experimental conditions these aggregates are not observed though. This indicates that at these

dilute conditions cross-linking is absent or the degree to which cross-linking takes place is extremely small.

Upon addition of PEO-Biotin the size of the aggregates increases slightly (2.66 → 2.88 nm). This change is within experimental error though. If the polymers are added in the reverse order the same behavior is observed. This indicates that a certain degree of flexibility remains, since when one equivalent of PEO-Biotin is added first, on average only one of the binding sites might be occupied, but also proteins without any or with more bound polymer chains are present in solution. Upon addition of s-PAAm-Biotin, some of the PEO-Biotin chains need to dissociate to allow for the complexation of the three-arm star polymer with a single streptavidin protein. That this happens indicates that the binding is still reversible, and rearrangements are still possible.

Scheme 6: Creation of protein-polymer aggregates with a phase separated (Janus) shell.
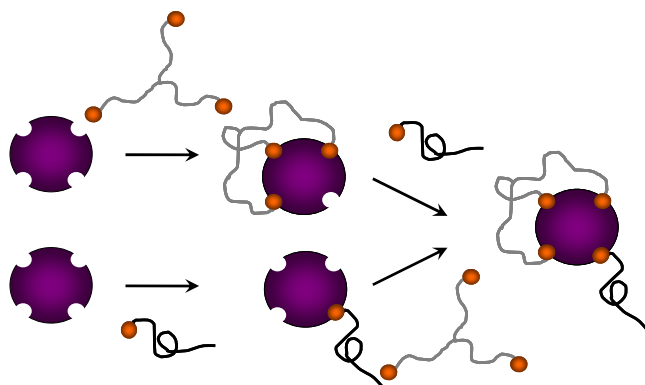
It must be noted that due to the binding of two different polymers to one streptavidin tetramer one forces the two polymers in a morphology where they are phase separated from each other, thereby creating a new type of Janus particles. This is not necessarily the case when using single chain polymers, since, like with normal polymer micelles, one would end up with a mixture of different populations. The use of three-arm star-polymers in dilute solutions is a way by which this problem can be circumvented and by which ideally only one population is obtained. This Janus character is difficult to prove since the concentration is rather low. Additionally the materials are so expensive that high concentrations, as e.g. needed for NOESY, cannot be used. Nor would such experiments yield reliable results, since at higher concentrations the structure of the aggregates might very well change through e.g. cross-linking. Other scattering methods than light scattering cannot be applied either, since the necessary measurement times would be extremely long.

This Janus-type aggregation is interesting since it opens a new way to make bioconjugates, e.g. of different proteins[88], in new, modular and selective ways. One can imagine e.g. functionalizing two different proteins, one with a biotin end-functionalized homopolymer and the other with a polymer bearing three-biotin groups. Upon addition of streptavidin these two

proteins would be joined together to form one conjugate of the two different proteins and streptavidin. Also the self-assembly of such Janus structures at surfaces could be extremely interesting.

5.3.2 Cross-linking

When more than one equivalent of s-PAAm-Biotin is added, cross-linking between streptavidin groups is clearly observed. With 1.5 eq of s-PAAm-Biotin to streptavidin tetramer no significant cross-linking is observed yet (R_h = 2.43 nm), but upon addition of PEO-Biotin it is (as a significant increase in size, from R_h = 2.43 to 3.04 nm), which can be explained by the replacement of some of the PAAm-Biotin groups by PEO-Biotin. When three equivalent of s-PAAm-Biotin is used, cross-linking is observed from the start, though the average size even increases upon addition of PEO-Biotin (from R_h = 3.24 to 3.53 nm), indicating that the degree of cross-linking increases even further.

Scheme 7: Controlled physical cross-linking of streptavidin.
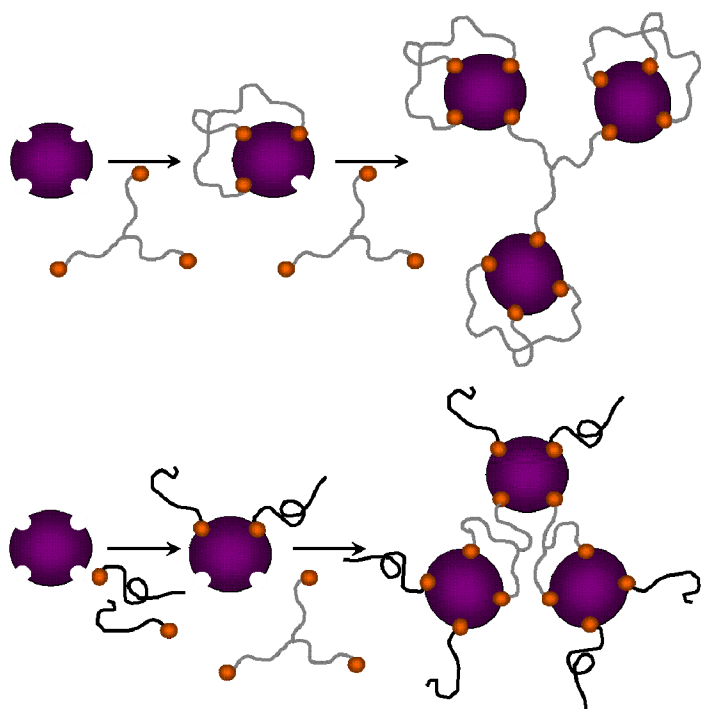
A similar effect is observed when first more than one equivalent of PEO-Biotin is added to the streptavidin, after which the appropriate amount of s-PAAm-Biotin is added to fill all remaining binding sites. Before the addition of s-PAAm-Biotin no cross-linking observed (R_h = 2.39 or 2.77 nm for two, respectively three equivalents of PEO-Biotin). The degree of cross-linking after the addition depends on the amount of s-PAAm-Biotin which is involved in the cross-linking. This is seen through the difference in size between the sample with 2 eq of PEO-Biotin and 2/3 eq of s-PAAm-Biotin (R_h = 3.53 nm), and the sample with 3 eq of PEO-Biotin

and 1/3 eq of s-PAAm-Biotin (R_h = 3.07 nm), showing that more cross-linking took place in the first sample, where more s-PAAm is present.

Using stimuli-responsive polymers one can also induce a kind of cross-linking between the proteins. To this end, PNIPAAm, a thermoresponsive polymer, end-functionalized with biotin, is used. Upon heating, the polymer collapses and becomes hydrophobic, inducing aggregation of the PNIPAAm chains (DLS data summarized in Figure 80).
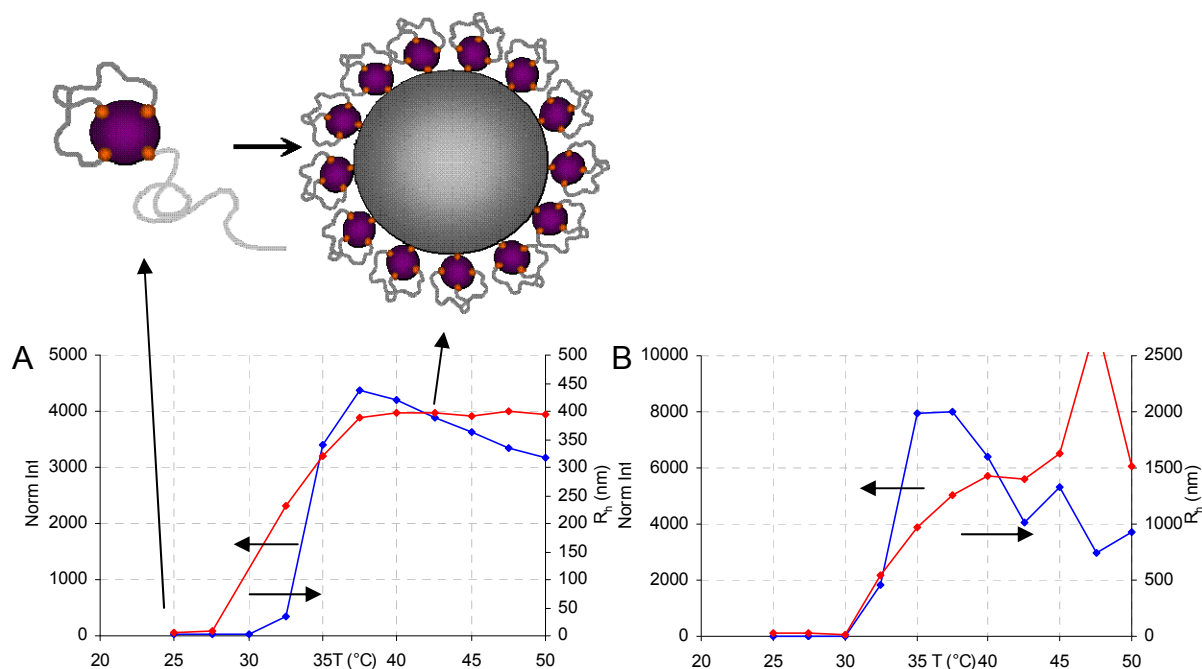
Figure 80: Temperature dependent DLS data of A) streptavidin with one equivalent of s-PAAm and one equivalent of PNIPAAm and a schematic representation of the collapse and aggregation of the PNIPAAm chains, and B) of PNIPAAm (0.1 g/l, phosphate buffer pH 7.5).

Aggregates with a constant size are formed, that are stabilized by streptavidin-PAAm conjugate groups. The aggregates that are formed are rather large, (R_h ~ 400 nm), but not as big as the particles formed from PNIPAAm homopolymer, where aggregates are observed with dimensions in excess of 1 μm.

5.4 Conclusion

In conclusion, the formation of Janus type protein-polymer conjugates, based on the binding of biotin-end functionalized three-arm polymer and biotin-end functionalized homopolymer to streptavidin is described. The same components can also be used for the controlled cross-linking of streptavidin, by choosing different ratios of the different materials. Using biotin end-functionalized PNIPAAm a thermoresponsiveness could be introduced.

Chapter 6: Summary and outlook

The creation of complex (polymer) structures has been one of the major research topics over the last couple of decades. By now an extremely large number of different synthetic approaches have been developed to prepare all kinds of different polymers. Using different polymerization techniques a large number of monomers can be polymerized in a controlled fashion, as well as in all kinds of combinations. Not only linear polymers but also hyperbranched and other topologies have been prepared in a controlled fashion. Now that these structures can be prepared, the study of their behavior becomes more and more important, the ultimate goal being the formation of structures that can be used to fulfill complex functions, e.g. in drug-delivery, as surfactants, etc..

This work deals with the creation of complex and stimuli-responsive systems, specifically the creation of Janus type architectures and cross-linked structures, using the self-assembly of block copolymers. Also the self-assembly of these structures into higher-order aggregates is investigated.

The formation of micelles in aqueous solution and their cross-linking by a side reaction of thiol-yne chemistry is presented e.g.. This cross-linking only takes place at higher concentrations of triple bonds as e.g. in the core of micelles. A variety of different thiols can be introduced while cross-linking the micelles at the same time. This yields an interesting system to study the influence of pH responsive groups in the core of the micelles on the entire structure, since acidic or basic moieties can easily be incorporated into the cores of the micelles. The charging of these groups leads to a swelling of the core and thereby a decrease in the local concentration of the corona forming block (PEtOx). This decrease in concentration yields a shift in the cloud point temperature to higher temperatures for this Type I thermoresponsive polymer. When the swelling of the core is prohibited, e.g. by the introduction of sufficient amounts of salt, this behavior disappears.

Similar structures can be prepared using C3Ms built through the interaction of weakly acidic and basic polymer blocks. The advantage of these structures is that two different stabilizing blocks can be incorporated, which allows for more diverse and complex structures and behavior

of the micelles. Examples are the formation of asymmetric (e.g. Janus micelles) structures using phase separating polymers, or the introduction of multiple different stimuli responsive, non-ionic polymers (as shown for systems with PEO and PDMAAm or PEO and PNIPAAm as non-ionic blocks). Since the cores of the micelles bear carboxylic acid and primary amine groups, they can easily be cross-linked. This can be performed either by selectively cross-linking one block copolymer (leaving the other block copolymer free to dissociate from and associate with the core cross-linked micelle) or by e.g. using NHS/EDC chemistry, thereby cross-linking both types of block copolymer with each other. The non-cross-linked structures are strongly responsive to pH and ionic strength. This responsiveness can partly be removed by the cross-linking procedure, but functional groups do remain. It could be shown that the cross-linked C3Ms show very similar behavior as the micelles cross-linked by thiol-yne chemistry, though they can be charged both positively and negatively, whereas the micelles cross-linked using thiol-yne chemistry can only be charged either positively or negatively. A change in cloud point temperature is only for PEtOx, not for PNIPAAm. This could be related to the different Types of thermoresponsive behavior. The cloud point temperature of PNIPAAm, a Type II thermoresponsive polymer, is nearly independent on concentration, whereas the cloud point temperature of PEtOx (Type I) is strongly dependent on the (local) concentration.

Core cross-linked Janus micelles with a PEO block could be shown to adsorb onto silica nanoparticles, and could be shown to stabilize them in solution upon acidification, which normally leads to precipitation of the silica. If one of the hemispheres of the Janus micelles is functionalized with thiol groups, it can be adsorbed onto gold nanoparticles.

Besides phase separation taking place by itself, it can also be induced by external stimuli, most easily temperature when a thermoresponsive polymer is present. Cross-linking of this phase separated situation can also yield asymmetric aggregates. Using this synthetic pathway also worm-like micelles can be obtained.

Finally, a new way to prepare asymmetric aggregates is presented, based on the streptavidin-biotin binding motive. This is achieved by using three out of the four binding sites of streptavidin for the binding of one three-arm star polymer, end-functionalized with biotin groups. A homopolymer with one biotin end-group can be used to occupy the last position. This binding of two different polymers makes it possible to create asymmetric complexes. This phase separation is theoretically independent of the kind of polymer since the structure of the protein is the driving force, not the intrinsic phase separation between polymers. Besides Janus structures also specific cross-linking can be achieved by using other mixing ratios.

Although a lot of work has already been done on these systems, there are always experiments which could or should still be done. To further investigate the structure of the aggregates,

specifically the structure of the C3JMs, SANS should be performed for example. SANS, specifically using contrast matching, yields a lot of information on the form and size of the aggregates, but also on where the different components are located in the micelles.

For the cross-linked C3Ms, one of the main challenges not addressed yet is the cross-linking using reversible cross-linking methods[89,90]. One of the easiest approaches is the functionalization of the polyionic blocks with a small number of thiol groups, which, after formation of C3Ms, can form disulfide bonds. Disulfide bonds are easily broken, e.g. by changes in the pH[91]. Other interesting approaches might be the use of ionic monomers which are labile towards e.g. irradiation with light.

Also the creation of linear higher-order aggregates instead of (more or less) spherical structures, as they are introduced in this work, would be very interesting. To accomplish the creation of linear higher-order aggregates of C5Ms different interactions need to be introduced in the different polymers constituting the micelles. These interactions should not take place between two identical units, so that one of the neutral blocks can be functionalized with one group and the other with the complementary unit. Through the addition of some complexation inhibitor during cross-linking, normal C5JMs would be formed, which upon removal of these inhibitors start complexing, forming linear (or, more likely, branched) structures. Examples of suitable complexation motives are the complexation of streptavidin with biotin or that of lectins with sugar groups. Hydrogen bonding interactions analogous to the base-pairing in DNA can also be considered.

The synthesis of non-spherical, phase separated structures using external stimuli can still be extended, e.g. by using other stimuli such as solvent quality. Also the influence of electric fields on the morphology of C3Ms, which was shown to yield elongated structures[92], might be worthwhile investigating. Though in this case no-phase separation is triggered it might yield access to more different morphologies.

For the Janus complexes formed from streptavidin with different biotin end-functionalized polymers it is worthwhile determining whether the presumed phase separation actually takes place. This could e.g. be done by Förster Resonance Energy Transfer (FRET), which could yield information about the distance between the two polymers, when a homopolymer is end-functionalized with both biotin and a fluorescent moiety, and the center of the three-arm star polymer is labeled with a complementary fluorescent label. Also the surface active behavior of the complexes should be investigated in more detail, since the introduction of different polymers makes the aggregates slightly amphiphilic and therefore surface active.

Appendix

A.1 References

[1] Hadjichristidis, N., Iatrou, H., Pitsikalis, M., Mays, J., *Prog Polym Sci*, **2006**, 31, 1068-1132.

[2] Riess, G., *Prog Polym Sci*, **2003**, 28, 1107-1170.

[3] Katsumoto, Y., Kubosaki, N., *Macromolecules*, **2008**, 41, 5955-5956.

[4] Rodríguez-Hernández, J., Chécot, F., Gnanou, Y., Lecommandoux, S., *Polym Sci*, **2005**, 30, 691-724.

[5] Matsen, M.W., Bates, F.S., *Macromolecules*, **1996**, 29, 1091-1098.

[6] Förster, S., Plantenberg, T., *Angew Chem Int Ed*, **2002**, 41, 688-714.

[7] Asayev, V., Tenhu, H., Winnik, F.M., *Adv Polym Sci*, **2010**, 1-61.

[8] Zhao, J., Hoogenboom, R., Van Assche, G., Van Mele, B., *Macromolecules*, **2010**, 43, 6853-6860.

[9] Kunz, W., Henle, J., Ninham, B.W., *Curr Opin Colloid Interface Sci*, **2004**, 9, 19–37.

[10] Zhang, Y., Cremer, P.S., *Curr Opin Chem Bio*, **2006**, 10, 658-663.

[11] López-León, T., Santander-Ortega, M.J., Ortega-Vinuesa, J.L., Bastos-González, D., *J Phys Chem C*, **2008**, 112, 16060-16069.

[12] Luo, C., Zuo, F., Ding, X., Zheng, Z., Cheng, X., Peng, Y., *J Appl Polym Sci*, **2008**, 107, 2118-2125; Luo, C., Zuo, F., Zheng, Z., Ding, X., Peng, Y., *J Macromol Sci A Pure Appl Chem*, **2008**, 45, 364-371.

[13] Sumaru, K., Kameda, M., Kanamori, T., Shinbo, T., *Macromolecules*, **2004**, 37, 4949-4955.

[14] Voets, I.K., Keizer, A. de, CohenStuart, M.A., *Adv Colloid Interface Sci*, **2009**, 300-318.

[15] Harada A., Kataoka, K., *Macromolecules*, **1995**, 28, 5294-5299.

[16] Hofs, B., Voets, I.K., Keizer, A. de, CohenStuart, M.A., *Phys Chem Chem Phys*, **2006**, 8, 4242-4251.

[17] Voets, I.K., Keizer, A. de, Waard, P. de, Frederik, P.M., Bomans, P.H.H., Schmalz, H., Walther, A., King, S.M., Leermakers, F.A.M., CohenStuart, M.A., *Angew Chem Int Ed*, **2006**, 45, 6673 -6676; Voets, I.K., Fokkink, R., De Keizer, A., May, R.P., CohenStuart, M.A., *Langmuir*, **2008**, 24, 12221-12227.

[18] Kataoka, K., Harada, A., Nagasaki, Y., *Adv Drug Del Rev*, **2001**, 47, 113-131.

[19] Oupický, D., Koňáka, Č., Ulbricha, K., Wolfert, M.A., Seymour, M.W., *J Controlled Release*, **2000**, 65, 149-171.

[20] Anraku, Y., Kishimura, A., Oba, M., Yamasaki, Y., Kataoka, K., *J Am Chem Soc*, **2010**, 132, 1631-1636; Kishimura, A., Koide, A., Osada, K., Yamasaki, Y., Kataoka, K., *Angew Chem Int Ed*, **2007**, 46, 6085-6088; Koide, A., Kishimura, A., Osada, K., Jang, W.D., Yamasaki, Y., Kataoka, K., *J Am Chem Soc*, **2006**, 128, 5988-5989.

[21] Becker, A.L., Johnston, A.P.R., Caruso, F., *Small*, **2010**, 6, 1836-1852.

[22] Cheng, L., Hou, G., Miao, J., Chen, D., Jiang, M., Zhu, L., *Macromolecules*, **2008**, 41, 8159-8166; Feng, X., Taton, D., Ibarboure, E., Chaikof, E.L., Gnanou, Y., *J Am Chem Soc*, **2008**, 103, 11662-11676; Saez, I.M., Goodbye, J.W., *Chem Eur J*, **2003**, 9, 4869-4877.

[23] Erhardt, R., Böker, A., Zettl, H., Kaya, H., Pyckhout-Hintzen, W., Krausch, G., Abetz, V., Müller, A.H.E., *Macromolecules*, **2001**, 34, 1069-1075; Erhardt, R., Zhang, M., Böker, A., Zettl, H., Abetz, C., Frederik, P., Krausch, G., Abetz, V., Müller, A.H.E., *J Am Chem Soc*, **2003**, 125, 3260-3267.

[24] Walther, A., André, X., Drechsler, M., Abetz, V., Müller, A.H.E., *J Am Chem Soc*, **2007**, 129, 6187-6198; Walther, A., Göldel, A., Müller, A.H.E., *Polymer*, **2008**, 49, 3217-3227.

[25] Bhaskar, S., Roh, K.-H., Jiang, X., Baker, G.L., Lahann, J., *Macromol Rapid Comm*, **2008**, 29, 1655-1660.

[26] Hong, L., Jiang, S., Granick, S., *Langmuir*, **2006**, 22, 9495-9499; Ling, X.Y., Phang, I.Y., Acikgoz, C., Yilmaz, M.D., Hempenius, M.A., Vancso, G.J., Huskens, J., *Angew Chem Int Ed*, **2009**, 48, 1-7; Nie, L., Liu, S., Shen, W., Chen, D., Jiang, M., *Angew Chem Int Ed*, **2007**, 46, 6321-6324; Paunov, V.N., Cayre, O.J., *Adv Mater*, **2004**, 16, 788-791.

[27] Dupont, J., Liu, G., *Soft Matter*, **2010**, 6, 3654-3661.

[28] Baskaran, D., Müller, A.H.E., *Prog Polym Sci*, **2007**, 32, 173-219.

[29] Penczek, S., Cypryk, M., Duda, A., Kubisa, P., Sömkowski, S., *Prog Polym Sci*, **2007**, 32, 247-282.

[30] Bywater, S., *Prog Polym Sci*, **1994**, 19, 287-316.

[31] Goethals, E.J., Du Prez, F., *Prog Polym Sci*, **2007**, 32, 220-246.

[32] Penczek, S., Cypryk, M., Duda, A., Kubisa, P., Sömkowski, S., *Prog Polym Sci*, **2007**, 32, 247-282.

[33] Chiefari, J., Chong, Y.K., Ercole, F., Krstina, J., Jeffery, J., Le, T.P.T., Mayadunne, R.T.A., Meijs, G.F., Moad, C.L., Moad, G., Rizzardo, E., Thang, S.H., *Macromolecules*, **1998**, 31, 5559-5562.

[34] Vana, P., Albertin, L., Barner, L., Davis, T.P., Barner-Kowollik, C., *J Pol Sci A Pol Chem*, **2002**, 40, 4032-4037.

[35] Moad, G., Rizzardo, E., Thang, S.H., *Polymer*, **2008**, 49, 1079-1131.

[36] Matzjaszewski, K., Xia, J., *Chem Rev*, **2001**, 101, 2921-2990.

[37] Hawker, C.J., Bosman, A.W., Harth, E., *Chem Rev*, **2001**, 101, 3661-3688.

[38] Rodríguez-Hernández, J., Chécot, F., Gnanou, Y., Lecommandoux, S., *Polym Sci*, **2005**, 30, 691-724; Bronich, T.K., Keifer, P.A., Shlyakhtenko, L.S., Kabanov, A.V., *J Am Chem Soc*, **2005**, 127, 8236-8237; Guo, A., Liu, G., Tao, J., *Macromolecules*, **1996**, 29, 2487-2493; Jiang, J., Qi, B., Lepage, M., Zhao, Y., *Macromolecules*, **2007**, 40, 790-792; Chan, Y., Wong, T., Byrne, F., Kavallaris, M., Bulmus, V., *Biomacromolecules*, **2008**, 9, 1826-1836; O'Reilly, R.K., Joralemon, M.J., Hawker, C.J., Wooley, K.L., *New J Chem*, **2007**, 31, 718-724; Saito, K., Ingalls, L.R., Lee, J., Warner, J.C., *Chem Comm*, **2007**, 2503-2505; Harada, A., Kataoka, K., *Prog Polym Sci*, **2006**, 31, 949-982; Xu, J., Liu, S., *Soft Matter*, **2008**, 4, 1745-1749; Hoogenboom, R., *Angew Chem Int Ed*, **2010**, 49, 3415-3417.

[39] Chi, Y., Scroggins, S.T., Fréchet, J.M.J., *J Am Chem Soc*, **2008**, 130, 6322-6323: Helms, B., Guillaudeu, S.J., Xie, Y., McMurdo, M., Hawker, C.J., Fréchet, J.M.J., *Angew Chem Int Ed*, **2005**, 44, 6384-6387; Rodionov, V., Gao, H., Scroggins, S., Unruh, D.A., Avestro, A.-J., Fréchet, J.M.J., *J Am Chem Soc*, **2010**, 132, 2570-2572.

[40] Chan, J.W., Hoyle, C.E., Lowe, A.B., *J Am Chem Soc*, **2009**, 131, 5751-5753; Yu, B., Chan, J.W., Hoyle, C.E., Lowe, A.B., *J Pol Sci A Pol Chem*, **2009**, 47, 3544-3557; Konkolewicz, D., Gray-Weale, A., Perrier, S., *J Am Chem Soc*, **2009**, 131, 18075-18077; Chen, G., Kumar, J., Gregory, A., Stenzel, M.H., *Chem Comm*, **2009**, 6291-6293; Benati, L., Montevecchi, P.C., Spagnolo, P., *J Chem Soc Perkin Trans*, **1991**, 1, 2103-2109; Melandri, D., Pier Carlo Montevecchi, P.C., Navacchia, M.L., *Tetrahedron*, **1999**, 55, 12227-12236.

[41] Fairbanks, B.D., Scott, T.F., Koxin, C.J., Anseth, K.S., Bowman, C.N., *Macromolecules*, **2009**, 42, 211-217.

[42] Gress, A., Völkel, A., Schlaad, H., *Macromolecules*, **2007**, 40, 7928-7933.

[43] Ten Brummelhuis, N., Diehl, C., Schlaad, H., *Macromolecules*, **2008**, 41, 9946-9947.

[44] De Geest, B.G., Van Camp, W., Du Prez, F., De Smedt, S.C., Demeester, J., Hennink, W.E., *Macromol Rapid Commun*, **2008**, 29, 1111-1118; Krieg, A., Becer, R., Hoogenboom, R., Schubert, U.S., *Macromol Symp*, **2009**, 275-276, 73-81; Semsirilar, M., Ladmiral, V., Perrier, S., *Macromolecules*, **2010**, 43, 1438-1443; Luxenhofer, R., Jordan, R., *Macromolecules*, **2006**, 39, 3509-3516.

[45] Fairbanks, B.D., Sims, E.A., Anseth, K.S., Bowman, C.N., *Macromolecules*, **2010**, 43, 4113-4119.

[46] Schilli, C.M., Zhang, M., Rizzardo, E., Thang, S.H., Chong, Y.K., Edwards, K., Karlsson, G., Müller, A.H.E., *Macromolecules*, **2004**, 37, 7861-7866.

[47] Yin, X., Hoffman, A.S., Stayton, P.S., *Biomacromolecules*, **2006**, 7, 1381-1385.

[48] Bontha, S., Kabanov, A.V., Bronich, T.K., *J Controlled Release*, **2006**, 114, 163-174; Yu, H., Grainger, D.W., *J Appl Pol Sci*, **1993**, 49, 1553-1563;

[49] Park, J.-S., Akiyama, Y., Yamasaki, Y., Kataoka, K., *Langmuir*, **2007**, 23, 138-146.

[50] Christova, D., Velichkova, R., Loos, W., Goethals, E.J., Du Prez, F., *Polymer*, **2003**, 44, 2255-2261.

[51] Park, J.S., Kataoka, K., *Macromolecules*, **2006**, 39, 6622-6630.

[52] Park, J.S., Kataoka, K., *Macromolecules*, **2007**, 40, 3599-3609.

[53] Huber, S., Jordan, R., *Colloid Polym Sci*, **2008**, 286, 395-402.

[54] Kishimura, A., Liamsuwan, S., Matsuda, H., Dong, W.-F., Osada, K., Yamasaki, Y., Kataoka, K., *Soft Matter*, **2009**, 5, 529-532.

[55] Bronich, T.K., Keifer, P.A., Shlyakhtenko, L.S., Kabanov, A.V., *J Am Chem Soc*, **2005**, 127, 8236-8237.

[56] Kim, J.O., Nukolova, N.V., Oberoi, H.S., Kabanov, A.V., Bronich, T.K., *Polym Sci Ser A*, **2009**, 51, 708-718.

[57] Walther, A., Drechsler, M., Rosenfeldt, S., Harnau, L., Ballauf, M., Abetz, V., Müller, A.H.E., *J Am Chem Soc*, **2009**, 131, 4720-4728; Walther, A., Barner-Kowollik, C., Müller, A.H.E., *Langmuir*, **2010**, 26, 12237-12246.

[58] Wang, J., Varshney, S.K., Jérôme, R., Teyssie, P., *J Polym Sci: Part A: Polym Chem*, **1992**, 30, 2251-2261.

[59] Taton, D., Wilczewska, A.-Z., Destarac, M., *Macromol Rapid Commun*, **2001**, 22, 1497-1503.

[60] Maki, Y., Mori, H., Endo, T., *Macromol Chem Phys*, **2007**, 208, 2589-2599.

[61] Briscoe, B., Luckham, P., Zhu, S., *Polymer*, **2000**, 41, 3851-3860.

[62] Tacx, J., Schoffeleers, H.M., Brands, A.G.M., Teuwen, L., *Polymer*, **2000**, 41, 947-957.

[63] Kawamura, A., Harada, A., Kono, K., Kataoka, K., *Bioconjugate Chem*, **2007**, 18, 1555-1559.

[64] Burgh, S. Van der, Keizer, A. de, CohenStuart, M.A., *Langmuir*, **2004**, 20, 1073-1084.

[65] Khousakoun, E., Gohy, J.-F., Jérôme, R., *Polymer*, **2004**, 45, 8303-8310.

[66] Kwon, I.C., Bae, Y.H., Kim, S.W., *Nature*, **1991**, 354, 291-293.

[67] Djerassi, C., Gorman, M., Markley, F.X., Oldenburg, E.B., *J Am Chem Soc*, **1955**, 77, 568-571.

[68] Lowe, A.B., Sumerlin, B.S., Donovan, M.S., McCormick, C.L., *J Am Chem Soc*, **2002**, 124, 11562-11563.

[69] Tsuboi, Y., Nishino, M., Sasaki, T., Kitamura, N., *J Phys Chem B*, **2005**, 109, 7033-7039.

[70] Schlaad, H., You, L., Sigel, R., Smarsly, B., Heydenreich, M., Mantione, A., Masic, A., *Chem Comm*, **2009**, 1478-1480.

[71] Voets, I.K., Moll, P.M., Aqil, A., Jérôme, C., Detrembleur, C., Waard, P. de, Keizer, A. de, CohenStuart, M.A., *J Phys Chem B*, **2008**, 112, 10833-10840.

[72] Zeeman, R., Dijkstra, P.J., Van Wachem, P.B., Van Luyn, M.J.A., Hendriks, M., Cahalan, P.T., Feijen, J., *Biomaterials*, **1999**, 20, 921-931.

[73] Li, Y., Bronich, T.K., Chelushkin, P.S., Kabanov, A.V., *Macromolecules*, **2008**, 41, 5863-5868.

[74] Erhardt, R., Böker, A., Zettl, H., Kaya, H., Pyckhout-Hintzen, W., Krausch, G., Abetz, V., Müller, A.H.E., Macromolecules, 2001, 34, 1069-1075; Erhardt, R., Zhang, M., Böker, A., Zettl, H., Abetz, C., Frederik, P., Krausch, G., Abetz, V., Müller, A.H.E., J Am Chem Soc, 2003, 125, 3260-3267; Fustin, C.-A., Abetz, V.,Gohy, J.-F., *Eur Phys J E*, **2005**, 16, 291-302.

[75] Cao, Z., Jin, Y., Zhang, B., Miao, Q., Ma, C., *Iranian Pol J*, **2010**, 19, 689-698.

[76] Rupprecht, H., Liebl, H., *Archiv Pharm*, **1974**, 307, 817-824; Malmsten, M., Linse, P., Cosgrove, T., *Macromolecules*, **1992**, 25, 2474-2481.

[77] Pfefferkorn, E., Tran, Q., Varoqui, R., *J Pol Sci Pol Chem Ed*, **1981**, 19, 27-34.

[78] Nirmalya K. Chaki, K. Vijayamohanan, *Biosensors Bioelectronics*, **2002**, 17, 1-12.

[79] Liu, C., Zhang, K., Chen, D., Jianga, M., Liu, S., *Chem Comm*, **2010**, 46, 6135-6137.

[80] Meeussen, F., Nies, E., Berghmans, H., Verbrugghe, S., Goethals, E., Du Prez, F., *Polymer*, **2000**, 41, 8597-8602.

[81] Li, Z., Xiong, D., Xu, B., Wu, C., An, Y., Ma, R., Shi, L., *Polymer*, **2009**, 50, 825-831.

[82] Bontempo, D., Maynard, H.D., *J Am Chem Soc*, **2005**, 127, 6508-6509; Bulmus, V., Ding, Z., Long, C.J., Stayton, P.S., Hoffman, A.S., *Bioconjugate Chem*, **2000**, 11, 78-83; Kulkarni, S., Schilli, C., Grin, B., Müller, A.H.E., Hoffman, A.S., Stayton, P.S., *Biomacromolecules*, **2006**, 7, 2736-2741; Ding, Z., Fong, R.B., Long, C.J., Stayton, P.S., Hoffman, A.S., *Nature*, **2001**, 411, 59-62.

[83] Shimoboji, T., Ding, Z.L., Stayton, P.S., Hoffman, A.S., *Bioconjugate Chem*, **2002**, 13, 915-919.

[84] Schlaad, H., Kukula, H., Rudloff, J., Below, I., *Macromolecules*, **2001**, 34, 4302-4304

[85] Hyre, D.E., Le Trong, I., Merritt, E.A., Eccleston, J.F., Green, N.M., Stenkamp, R.E., Stayton, P.S., *Protein Sci*, **2006**, 15, 459-467.

[86] Burazerovic, S., Gradinura, J., Pierron, J., Ward, T.R., *Angew Chem Int Ed*, **2007**, 46, 5510-5514.

[87] Wilbur, D.S., Pathare, P.M., Hamlin, D.K., Weerawarna, A., *Bioconjugate Chem*, **1997**, 8, 819-832.

[88] Roth, P.J., Jochum, F.D., Zentel, R., Theato, P., *Biomacromolecules*, **2010**, 11, 238-244; Heredia, K.L., Grover, G.N., Tao, L., Maynard, H.D., *Macromolecules*, **2009**, 42, 2360-2367.

[89] Chan, Y., Wong, T., Byrne, F., Kavallaris, M., Bulmus, V., *Biomacromolecules*, **2008**, 9, 1826-1836.

[90] Zhang, L., Bernard, J., Davis, T.P., Barner-Kowollik, C., Stenzel, M.H., *Macromol Rapid Commun*, **2008**, 29, 123-129.

[91] Kakizawa, Y., Harada, A., Kataoka, K., *J Am Chem Soc*, **1999**, 121, 11247-11248.

[92] Lee, S.J., Park, M.J., *Langmuir*, **2010**, 26, 17827-17830.

A.2 List of abbreviations

Chemicals and solvents

ACVA: 4,4'-azobis(4-cyanovaleric acid)

AIBN: azo-bis-(isobutyronitrile)

BDDGE: 1,4-butanedioldiglycidylether

BPATT: 3-benzylsulfanyl thiocarbonylsulfanyl propionic acid

$CDCl_3$: deuterated chloroform

$CHCl_3$: chloroform

D_2O: deuterium oxide

DMF: dimethylformamide

DMSO-d_6: deuterated dimethylsulfoxide

EDAC/EDC/EDC·HCl: 1-ethyl-3-(3-dimethyl-aminopropyl)carbodiimide (hydrochloric acid)

HCl: hydrochloric acid

KOH: potassium hydroxide

MeOH: methanol

Na_2SO_4: sodium sulfate

$NaBH_4$: sodium borohydride

$NaNO_3$: sodium nitrate

NaOH: sodium hydroxide

NaSCN: sodium thiocyanate

NHS: *N*-hydroxysuccinimide

NMP: *N*-methylpyrrolidone

TFA: trifluoric acid

THF: tetrahydrofuran

Polymers

P2MVP: poly(2-methyl vinylpyridinium iodide)

P2VP: poly(2-vinylpyridine)

PAA: polyacrylic acid

PAAm: poly(acrylamide)

PButenOx: poly[2-(3-butenyl)-2-oxazoline]

PButinOx: poly[2-(3-butinyl)-2-oxazoline]

PDMAAm: poly(dimethylacrylamide)

PEO: poly(ethylene oxide)

PEtOx: poly(2-ethyl-2-oxazoline)

PiPrOx: poly(2-isopropyl-2-oxazoline)

PMAA: polymethacrylic acid

PMMA: polymethylmethacrylate

PNIPAAm: poly(*N*-isopropylacrylamide)

PS: polystyrene

PSS·Na: polystyrene sulfonate sodium salt

PtBuMA: poly(*tert*-butyl methacrylate)

PVA: polyvinyl amine

PVAc: polyvinyl acetate

PVOH: polyvinylalcohol

PVPh: polyvinylphthalimide

s-PAAm: three-arm star poly(acrylamide)

Methods

^{13}C-NMR: carbon 13 nuclear magnetic resonance spectroscopy

^{1}H-NMR: proton nuclear magnetic resonance spectroscopy

CryoTEM: Cryogenic transmission electron microscopy

DLS: dynamic light scattering

NOESY: nuclear Overhauser effect spectroscopy

SAXS: small angel x-ray scattering

SANS: small angle neutron scattering

SEC: size exclusion chromatography

SERS: surface enhanced Raman spectroscopy

SLS: static light scattering

TEM: transmission electron microscopy

General

ATRP: atom transfer radical polymerization

C3Ms: complex coacervate core micelles

C3JMs: complex coacervate core Janus micelles

C5Ms: core cross-linked complex coacervate core micelles

C5JMs: core cross-linked complex coacervate core Janus micelles

CTA: chain transfer agent

eq: equivalent

f^+: fraction of groups which can be positively charged out of the total number of chargeable groups

LCST: lower critical solution temperature

MADIX: macromolecular design via interchange of xanthates

M_n: number average molecular weight

M_n^{App}: apparent number average molecular weight

n: degree of polymerization

N_{Agg}: number of aggregation

NOE: nuclear Overhauser effect

NMP: nitroxide mediated polymerization

PDI: polydispersity index

PDI^{App}: apparent polydispersity index

RAFT: reversible addition fragmentation chain transfer

R_g: radius of gyration

R_h: (apparent) hydrodynamic radius

R_h contin: hydrodynamic radius as determined by Contin analysis.

R_h cum: hydrodynamic radius as determined by cumulant analysis.

rt: room temperature

T_{cp}: cloud point temperature

UCST: upper critical solution temperature

wt: weight

A.3 General materials and methods

A.3.1 Chemicals

Unless noted otherwise the following chemicals were used as received.

Acetonitrile (Sigma-Aldrich Chromasolv®) and dichloromethane were dried over calcium hydride, distilled, and stored under argon atmosphere. Bidistilled water was used. THF (Sigma-Aldrich, 99.5 %) was freshly distilled from sodium. Methanol (Sigma-Aldrich, 99.5 %), ethanol (VWR, 99.9 %), diethyl ether (Sigma-Aldrich, 99.5 %), hexane (Merck, 96 %), ethyl acetate (VWR, 99.5 %), DMF (Sigma Aldrich, > 99.8 %, over molsieves), chloroform (Merck, 99.8 %), dioxane (Sigma-Aldrich, 99.5 %), acetone (J.T. Baker, 99.5 %), N,N-dimethylacetamide (Fluka, 99.5 %), isopropanol (Roth, HPLC-grade).

Methyl trifluoromethanesulfonate (methyl triflate, Aldrich, ≥ 98 %) was dried over calcium hydride, distilled, and stored under argon atmosphere. AIBN was recrystallized from methanol, 4,4'-azobis(4-cyanovaleiric acid) (Sigma-Aldrich, > 98 %) was recrystallized from methanol. Phosphazene base P_4-t-Bu (Sigma-Aldrich, ~ 1 M in hexane) was used as received.

2-ethyl-2-oxazoline (Aldrich, ≥ 99 %) was dried over calcium hydride, distilled, and stored under argon atmosphere N-vinylphthalimide (Alfa Aesar, 99 %, recrystallized from 5:1 diethyl ether hexane), N-isopropyl acrylamide (Acros, 99 %) was recrystallized from toluene/hexane. Dimethylacrylamide (TCl Europe, > 98 %), acrylic acid (Alfa Aesar, 99 %, stabilized), 2-vinyl pyridine (Sigma-Aldrich, 97 %) and vinyl acetate (Acros, > 99 %) were recondensed using a vacuum line just prior to polymerization. $Tert$-butyl methacrylate (Sigma-Aldrich, 98 %), ethylene oxide (Fluka, 99.8 %), acrylamide (Acros, 98.5 %).

Poly(2-ethyl-2-oxazoline) (Sigma-Aldrich, M_n ~ 50 kg/mol, PDI 3-4), PSS·Na (Acros, M_n 70 kg/mol), Streptavidin (Vector Laboratories, Catalog No. SA-5000),

N-hydoxysuccinimide (NHS, Merck, 99 %), EDC·HCl (Iris Biotech, 99.7 %), glutaraldehyde (Alfa Aesar, 50 % solution in water), 1,4-butanedioldiglycidylether (Alfa Aesar, 96 %), 3-mercaptopropionic acid (Aldrich, ≥ 99 %), methyl 3-mercaptoprionate (Aldrich, ≥ 98 %), 2-aminoethanethiol hydrochloride (Acros, 98 %), 2-aminoethanethiol HCl (Acros, 98 %), biotin-maleimide (maleimide-PEG₂-biotin, Thermo Scientific). iodomethane (Acros, 99 %), hydrazine (Alfa Aesar, > 99 %), TFA (Acros, 99.5 %), allyl alcohol (Merck, ≥ 99 %), thiolacetic acid (Fluka, ~ 97 %).

1 M hydrochloric acid solution (Merck, TitriPUR®), 1 M sodium hydroxide solution (Merck, TitriPUR®), sodium chloride (Acros, ≥ 99.5 %), sodium nitrate (Merck, 99.99 %), sodium sulfate (Sigma-Aldrich, ≥ 99.0 %), sodium thiocyanate (Aldrich, ≥ 99.99 %), sodium hydroxide (Sigma-Aldrich, ≥ 98 %), potassium hydroxide (Sigma-Aldrich, ≥ 86 %), monosodium phosphate (Sigma-Aldrich, > 99 %), disodium phosphate (Sigma-Aldrich, 99 %), sodium azide (Fluka, 99.5 %), sodium borohydride (Sigma-Aldrich, 99 %), sodium carbonate (Riedel-de Haën, 99.8 %), $MgSO_4$ (Fisher Scientific, 62 - 70 %, dried), calcium hydride (Acros, 93 %),

4-pentynoic acid (Acros, 98 %), 2-chloroethylamine hydrochloride (Aldrich, 99 %), *O*-ethyl xanthic acid potassium salt (Sigma-Aldrich, 96 %), methyl 2-bromopropionate (Sigma-Aldrich, 98 %), ethylene glycol (Sigma-Aldrich, 99.8 %, anhydrous), 2-bromopropionyl bromide (Sigma-Aldrich, 97 %), 1,1,1-tris(hydroxymethyl)ethane (Fluka, 98 %), naphthalene (Acros, 99 %), potassium (Sigma-Aldrich, 98 %, chunk in mineral oil), diphenylmethane (Alfa Aesar, > 99 %), *n*-BuLi (Acros, 1.0 M in hexane), pyridine (Acros, 99.5 %, extra dry).

A.3.2 Characterization methods

Elemental analysis

Elemental analysis (EA) was performed using a Vario EL Elemental Analyzer. The samples were analyzed for carbon, hydrogen and nitrogen content.

SEC DMSO

SEC using DMSO (with 0.5 g/l LiBr and BHT as internal standard) as eluent was performed at 70 °C with a flow of 1 ml/min. The used column set consists of two GRAL-LIN columns (highly cross-linked polyvinylalcohol, PSS-Polymer Standards Service Mainz) of 300×7.5 mm and a pre-column of 50×7.5 mm. Commercially available polymer standards were used for calibration.

SEC THF

SEC in THF with simultaneous UV and RI detection was performed at room temperature using THF as eluent with a flow of 1.0 ml/min. The used column-set consists of two 300×8 mm MY-SD*plus* columns (PSS-Polymer Standards Service Mainz) filled with round polystyrene particles with an average diameter of 5 μm and pore sizes of 10^3 and 10^5 Å respectively.

SEC NMP

SEC using NMP (1-methyl-2-pyrrolidone with 0.05 M LiBr and BSME as internal standard) as eluent was performed at 70 °C with a flow of 0.8 ml/min. The used column set consists of two GRAM-100/1000 (polyester without functional groups) columns with particle sizes of 7 μm (PSS-Polymer Standards Service Mainz) of 300×8 mm and a pre-column of 50×8 mm. Commercially available polymer standards were used for calibration.

SEC H₂O (neutral and anionic species)

SEC for non-charged and negatively charged polymers was measured using a 0.1 M $NaNO_3$ solution in water as eluent. The experiments are performed at room temperature with a flow of 1 ml/min. Two PSS-SUPREMA-30/3000Å columns (8×300 mm) with 10 μm particles, in combination with a precolumn were used. Commercially available polymer standards were used for calibration.

SEC H₂O (cationic species)

SEC for positively charged polymers was measured using an 0.2 M Na_2SO_4 solution in water with 1 % acetic acid as eluent was performed at room temperature with a flow of 1 ml/min. TSK-gel columns

(polyglycidyl methacrylate gel, TOSOH Bioscience) (precolumn and 6000, 5000, 3000 and 2000 Å, each 7.5×300 mm) were used. Commercially available polymer standards were used for calibration.

^{1}H- and ^{13}C-NMR

^{1}H-NMR and ^{13}C-NMR spectra were recorded at room temperature on a Bruker DPX-400 spectrometer operating at 400.1 MHz.

NOESY

2D-NOESY measurements were performed on a Varian VNMRS 600 spectrometer operating at 600 MHz.

Raman spectroscopy

For Raman spectroscopy, a 532 nm Nd:YAG laser (WITec, Ulm, Germany) beam was focused down to a micrometer size spot on the sample through a confocal Raman microscope (CRM300, WITec, Ulm, Germany) equipped with piezo-scanner (P-500, Physik Instrumente, Karlsruhe, Germany). The spectra were acquired using an air-cooled CCD detector (DU401-BV, Andor, Belfast, UK) behind a grating (600 g/mm) spectrograph (UHTS 300, WITec, Ulm, Germany). The ScanCtrlSpectroscopyPlus (version 2.02, Witec) was used for measurement setup and data processing.

SERS

SERS (Surface Enhanced Raman Spectroscopy) is measured in the same way as normal Raman spectroscopy, though an excess of colloidal gold ($R_h \sim 20$ nm) is added to the solution.

Cloud point measurements

Cloud point measurements were performed using a Tepper Trübungsphotometer. The temperature was varied at 1 °/min. The temperature at which a transmission of 80 % is reached is taken as the cloud point.

Light scattering

Dynamic light scattering (DLS) was measured using an ALV-7004 Multiple tau digital correlator equipped with CGS-3 Compact Goniometer system, 22 mW He-Ne laser (wavelength $\lambda = 632.8$ nm) and a pair of avalanche photodiodes operated in a pseudo-cross-correlation mode. Unless noted otherwise R_h means the hydrodynamic radius as determined by Contin analysis. Contin analyses were performed using AfterALV by Dullware.

Static light scattering (SLS) was performed using the same instrument, measuring DLS at angles ranging from 30 - 150 ° in steps of 10 °. The data is evaluated using a partial Zimm and partial Guinier analysis.

(Cryo)TEM

Transmission electron microscopy (TEM) was performed with a Zeiss EM 912 Omega microscope operating at 120 kV. The TEM samples were prepared by placing a drop of the solutions on a 200 mesh carbon-coated copper grid. The samples were left to dry overnight.

The samples for CryoTEM were prepared using a Vitrobot. A Jeol JEM-3200FSC Liquid Helium Cryo-TEM was used.

Zeta potential

The zeta potential of the (cross-linked) micelles was measured on a Malvern Instruments Zetasizer Nano-Z. A concentration of 10 g/l was used. The pH of the solutions was set to 3 or 11 for the non-cross-linked micelles, to 3 for the base cross-linked micelles and to 11 for the acid cross-linked micelles, the pH being chosen such that all incorporated moieties are charged.

Photoaddition

For photoaddition a 150 Watt TQ 150 (Heraeus) UV-lamp was used.

A.4 Appendix to Chapter 3

A.4.1 Synthesis

Monomer synthesis

2-(3-butinyl)-2-oxazoline was synthesized analogous to 2-(3-butenyl)-2-oxazoline[42], as described below.
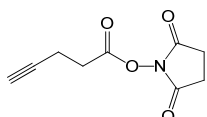
***N*-succinimidyl-4-pentynate.** 10 g of 4-pentynoic acid was dissolved in 200 ml of dry dichloromethane. Solutions of NHS (18.76 g in 130 ml dry dichloromethane) and EDAC (23.55 g in 60 ml dry dichloromethane) were added and the solution was stirred overnight. After removal of the solvent the crude product was dissolved in diethyl ether/water. The water phase was extracted with ether several times. The combined organic phases are dried over sodium sulfate after which the solvent is removed. Yield: 90 %

^{1}H-NMR: (400 MHz, DMSO-d$_6$): δ = 2.3-2.5 (m, 4 H, CH$_2$s side-chain), δ = 2.75 (s, 1 H, CH≡C), δ = 2.83 (s, 4 H, CH$_2$-NHS).
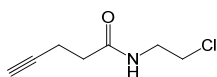
***N*-(2-chloroethyl)-4-pentynamide.** 21.32 g of 2-chloroethylamine hydrochloride and 7.36 g of NaOH are dissolved in 200 ml of water. A solution of 17.88 g *N*-succinimidyl-4-pentynate (0.092 mol) in 500 ml dichloromethane was added drop wise to the solution under vigorous stirring. The mixture is stirred overnight at room temperature. The phases are separated and the organic phase is washed twice with water, after which it is dried over sodium sulfate and the solvent is removed. Yield for this step: 85 %. Overall yield: 76 %.

^{1}H-NMR: (400 MHz, DMSO-d$_6$): δ = 2.1-2.4 (m, 4 H, CH$_2$s side-chain), δ = 2.75 (s, 1 H, CH≡C), δ = 3.38 (dt, 2 H, CH$_2$-N), δ = 3.59 (t, 2 H, CH$_2$-Cl), δ = 8.18 (s, 1H, NH).
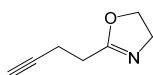
2-(3-butinyl)-2-oxazoline. 12.42 g (0.0779 mol) of *N*-(2-chloroethyl)-4-pentynamide was placed in a flame dried three-necked flask with a condenser connected to it under inert atmosphere. 50 ml of methanol is added to the flask, followed by 50 ml of a degassed 1.5 M potassium hydroxide solution in methanol. The solution is refluxed overnight and the precipitate is removed by filtration, after which the solvent is removed to yield a pink solid, which is further purified by recondensation at 90 °C on a vacuum line to afford a white solid. Yield: 37 % for this step. Overall yield: 28 %.

^{1}H-NMR (400 MHz, DMSO-d$_6$): δ = 2.14 (s, 4 H, CH$_2$s side-chain), δ = 3.06 (s, 1 H, CH≡C), δ = 3.43 (t, 2 H, CH$_2$-N), δ = 3.91 (t, 2 H, CH$_2$-O). ^{13}C-NMR (100 MHz, CDCl$_3$): δ = 15.4 (*C*-C≡C), δ = 27.3 (*C*-CNO), δ = 54.4 (C-N), δ = 67.5 (C-O), δ = 69.0 (C-C≡*C*), δ = 82.7 (C-*C*≡C), δ = 166.7 (*C*NO). M$_p$: 55 °C.

Micelle cross-linking

To a 1 wt % solution of PButinOx-*b*-PEtOx block copolymer in water, one equivalence to triple bonds (unless noted) of the appropriate thiol (either 3-mercaptopropionic acid, 2-aminoethanethiol hydrochloride or methyl 3-mercaptopropionate) was added. The solutions are degassed by two freeze thaw cycles and put under an argon atmosphere. The solutions are irradiated with UV-light for approximately 14 hours, after which an extra 5 equivalence of the corresponding thiol is added to the solution under argon overflow. After another 6 hours of UV-irradiation the excess thiol is removed by dialysis (MWCO 1000) against water or THF, depending on the solubility of the thiol. After three days of dialysis, during which the solvent is changed twice a day, the pure polymer micelles are obtained by freeze drying (from water directly or from dioxane when dialysis is performed using THF).

Synthesis PButenOx-*b*-PEtOx and PButenOx-*b*-PiPrOx

Block copolymers of 2-(3-butenyl)-2-oxazoline (ButenOx) and 2-ethyl-2-oxazoline (EtOx) or 2-isopropyl-2-oxazoline (iPrOx) were prepared by cationic ring opening polymerization. The monomers, acetonitrile (solvent) and methyl triflate (initiator) were dried over calcium hydride overnight. The components are recondensed under reduced pressure. Acetonitrile and the first monomer (30 wt %) are placed in a flame dried reactor. The appropriate amount of methyl triflate is added and the mixture is heated to 70 °C for several days. After approximately three days the second monomer is added together with enough acetonitrile to keep the concentration of monomer at 30 wt %. The reaction mixture is heated at 70 °C for another three weeks after which the polymerization is terminated by the addition of a 1:1 mixture of methanol and 1 M NaOH. The polymer is purified by dialysis against THF and is obtained by freeze drying from dioxane. ^{1}H-NMR spectra and SEC elugrams are shown in Figure 81 and Figure 82.
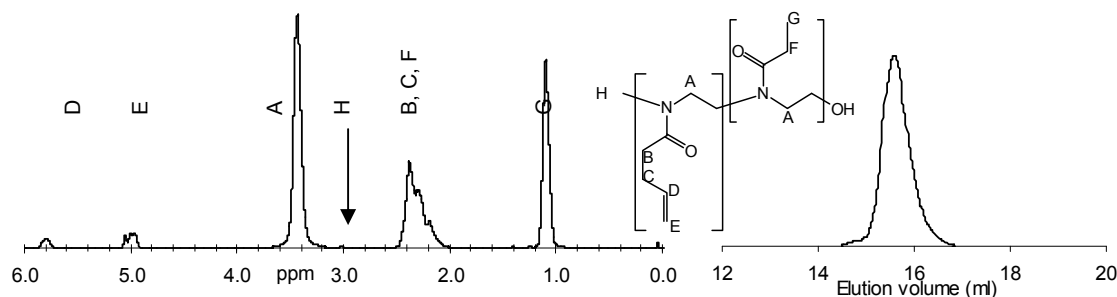
Figure 81: ^{1}H-NMR (CDCl$_3$) and SEC (in NMP) elugram of PButenOx$_{33}$-*b*-PEtOx$_{184}$.
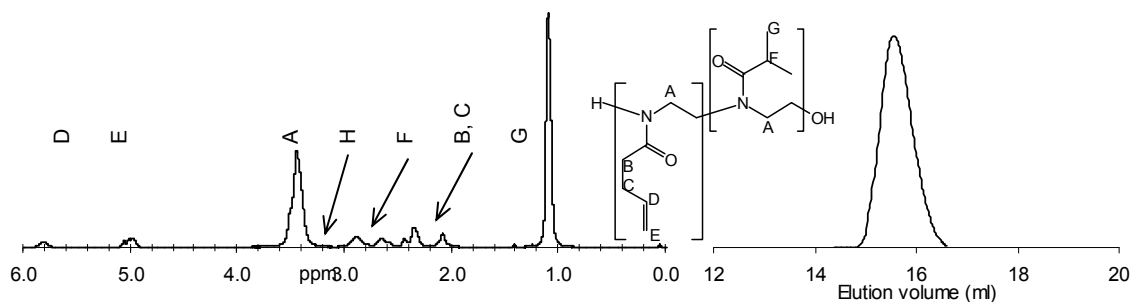
Figure 82: ^{1}H-NMR (CDCl$_3$) and SEC (in NMP) elugram of PButenOx$_{26}$-b-PiPrOx$_{140}$.

Block copolymers with narrow polydispersity indices (< 1.1, SEC in NMP) were obtained. The block lengths were determined by end-group analysis from ^{1}H-NMR, and were in relatively good agreement with the block lengths which were aimed for, yielding the following two polymers: PButenOx$_{33}$-b-PEtOx$_{184}$ and PButenOx$_{26}$-b-PiPrOx$_{140}$.

Cross-linking of PButenOx-b-PEtOx and PButenOx-b-PiPrOx micelles

To a 1 wt % solution of block copolymer in water up to 0.5 equivalence (to double bonds) of 1,3-propanedithiol is added. The solutions are degassed by two freeze thaw cycles and put under an argon atmosphere. The solutions are irradiated with UV-light for approximately 24 hours. If less than 0.5 equivalence of 1,3-propanedithiol was used, an excess of functional thiol (either 3-mercaptopropionic acid or 2-aminoethanethiol hydrochloride) was added to the mixture to functionalize remaining double bonds, after which the solution was once again irradiated with UV-light for 24 hours. The cross-linked micelles are purified by dialysis (MWCO 1000) against water. After 3 days of dialysis, during which the water is changed twice a day, the pure polymer micelles are obtained by freeze drying.

A.4.2 Sample preparation

Cloud point determinations were performed in a 1 g/l solution unless noted otherwise.

1 g/l samples for light scattering were prepared. The samples were subjected to a short centrifugation prior to filling the light scattering tubes in order to remove dust.

A.4.3 Characterization

Raman spectra
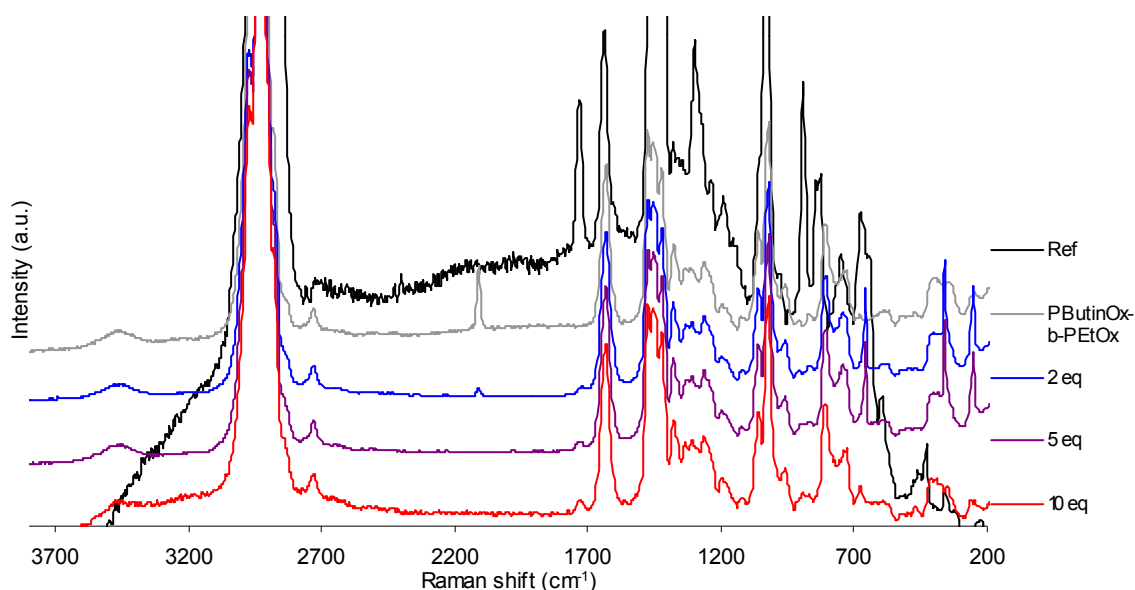
Figure 83: Raman spectroscopy data for PButenOx modified with methyl 3-mercaptopropionate[42], PButinOx-*b*-PEtOx and micelles cross-linked with respectively 2, 5 and 10 equivalences of methyl 3-mercaptopropionate.

A.4.4 Reference experiments

Cross-linking of PButenOx-*b*-PEtOx and PButenOx-*b*-PiPrOx

The micelles of PButenOx-*b*-PEtOx or PButenOx-*b*-PiPrOx are cross-linked by functionalizing them with a difunctional thiol (1,3-propanedithiol) in a 'thio-click' reaction[42], analogous to the vulcanization of rubbers. No more than one equivalent of thiol groups to double bonds is used to cross-link the micelles. If a smaller amount of cross-linker is used, double bonds remain after cross-linking which are available for functionalization with a functional thiol. The two routes are schematically shown in Scheme 8. To observe the effect of both cross-linking and the effect of pH responsive moieties in the core of the micelles PButenOx-*b*-PEtOx micelles are cross-linked using nearly all double bonds (0.95 equivalence of thiol groups to double bonds) in a first experiment.

Scheme 8: Cross-linking and functionalization of PButenOx polymers (R$_1$: another polymer chain, R$_2$: functional group).
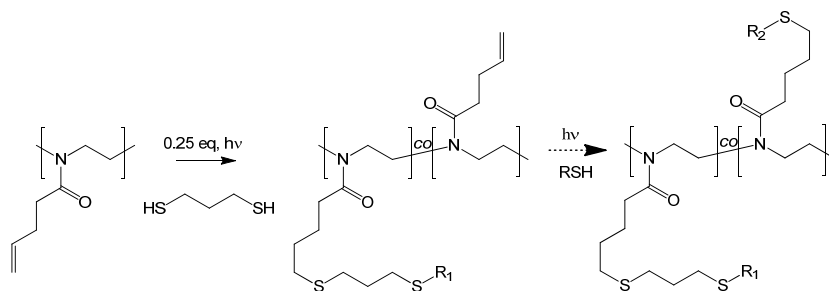
Cross-linking is shown using dynamic light scattering in THF. Far stronger scattering is observed for the cross-linked micelles than for the non-cross-linked micelles (Table 6), showing that the cross-linking was successful.

Table 6: Scattering intensity of plain polymer and cross-linked micelles with different functional groups incorporated in the core of the micelle in THF (1 g/l).

Polymer	Modification	Scatt int (kHz)
PButenOx-*b*-PEtOx	-	0.2
" "	CL dithiol	16.8
" "	CL and acid funct.	16.2
" "	CL and base funct.	27.2
PButenOx-*b*-PiPrOx	-	15.6
" "	CL dithiol	27.6

First of all the influence of the cross-linking process on the cloud point temperature of the micelles is investigated, both for PButenOx-*b*-PEtOx and PButenOx-*b*-PiPrOx (Figure 84). The cloud point temperature (which were measured at identical pH values) is lowered somewhat upon cross-linking, likely due to changes in either the density of the water soluble block near the core of the micelle.
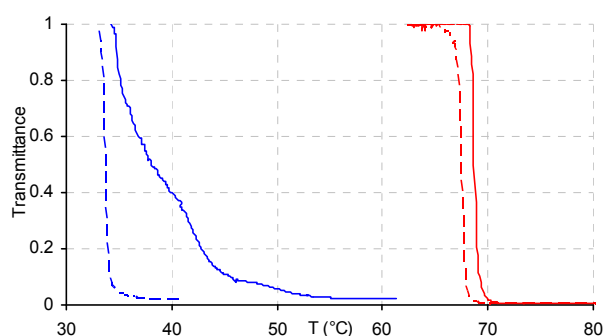
Figure 84: The effect of cross-linking on the cloud point temperature of oxazoline based micelles (1 g/l, pH 7). Red: PButenOx-*b*-PEtOx micelles. Blue: PButenOx-*b*-PiPrOx micelles. Solid lines: Normal micelles. Dashed lines: cross-linked micelles.

This method of core cross-linking also allows for the incorporation of functional groups if not all double bonds are used for cross-linking. To show this, 0.25 equivalence of dithiol (0.5 eq to double bonds) was used for the cross-linking of PButenOx-*b*-PEtOx micelles. An excess of a functional thiol is added after cross-linking (either 3-mercaptopropionic acid or 2-aminoethanethiol hydrochloric acid) and the mixture is once again irradiated with UV-light. The cross-linking is confirmed using light scattering

(Table 6). The influence of pH on the cloud point temperature is studied. As references, both normal polymer micelles and cross-linked, non-functionalized, micelles are used. The results are shown in Figure 85 and are summarized in Figure 86.
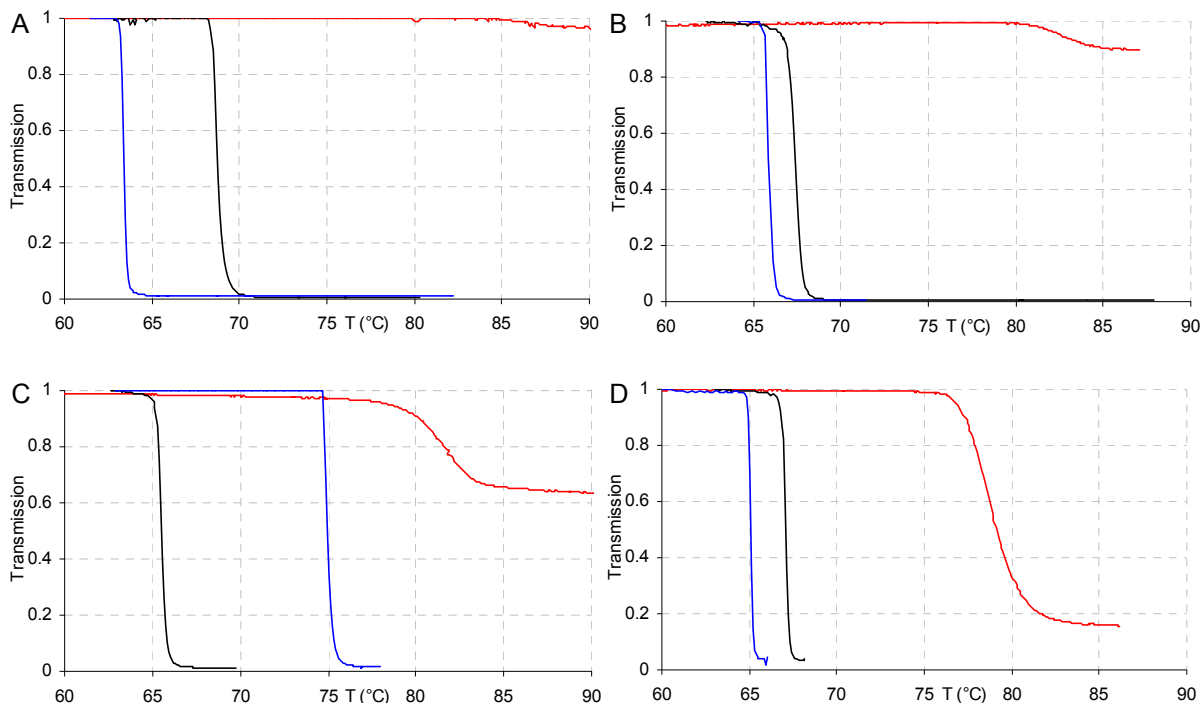
Figure 85: Cloud point determination at different pH values for A) PButenOx-*b*-PEtOx micelles, B) dithiol cross-linked micelles, C) dithiol cross-linked and acid functionalize micelles, D) dithiol cross-linked and base functionalized micelles (1 g/l, red: pH 3, black: pH 7, blue: pH 11).
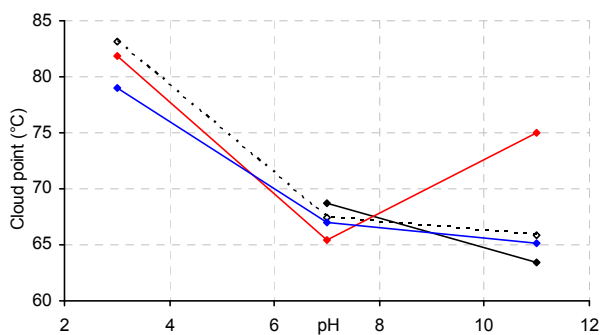
Figure 86: The cloud point temperatures of normal micelles, cross-linked micelles and cross-linked and functionalized polymers (1 g/l). Black solid lines: normal micelles, black dotted lines: dithiol cross-linked micelles, red: cross-linked, acid functionalized micelles, blue: cross-linked, base functionalized micelles.

These results show that a pH dependence of the cloud points exists even in the absence of functional groups (the normal micelles and cross-linked non-functionalized micelles), leading to higher cloud point temperatures at lower pH. As mentioned in Chapter 3, this seems to be an inherent property of poly(2-ethyl-2-oxazoline) since a commercial homopolymer shows the same behavior.
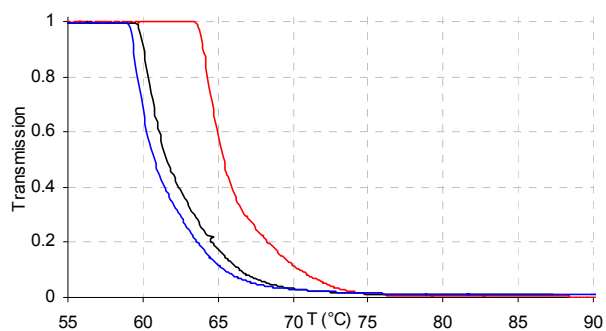
Figure 87: Cloud point determination at different pH values for PButinOx-*b*-PEtOx at 1 g/l (red: pH 3, black: pH 7, blue: pH 11).
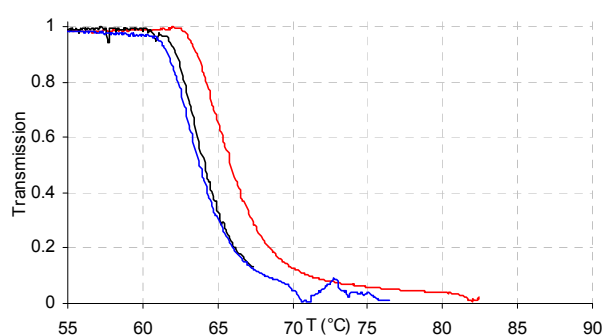
Figure 88: Cloud point determination at different pH values for a commercial PEtOx at 1 g/l (red: pH 3, black: pH 7, blue: pH 11).

Table 7: Overview of cloud point temperatures of PButinOx-b-PEtOx micelles cross-linked with mercaptopropionic acid in the presence of different salt, ionic strength and pH.

Salt	[Salt] (M)	pH	T_{cp} (°C)
-	-	3	61.7
-	-	7	72.7
-	-	11	77.6
Na$_2$SO$_4$	0.01	3	60.3
" "	0.01	7	61.0
" "	0.01	11	61.2
" "	0.1	3	48.0
" "	0.1	7	47.9
" "	0.1	11	47.8
NaNO$_3$	0.1	3	61.7
" "	0.1	7	62.7
" "	0.1	11	62.7
" "	1	3	51.4
" "	1	7	52.6
" "	1	11	52.6
NaSCN	0.01	3	65.1
" "	0.01	7	69.9
" "	0.01	11	70.7
" "	0.1	3	79.1
" "	0.1	7	81.2
" "	0.1	11	81.4

Appendix to Chapter 4

A.4.5 Synthesis

CTAs and initiators
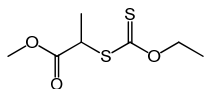
O-ethyl-S-(1-methoxycarbonyl) ethyldithiocarbonate[2]. 1.0 g (6.24 mmol) of O-ethyl xanthic acid potassium salt is dissolved in 12.5 ml ethanol and heated to 55 °C, after which 0.696 ml (6.24 mmol) of methyl 2-bromopropionate is added to the solution. A white precipitate is formed. The reaction mixture is stirred at 55 °C for approximately 6 hours, after which ~ 30 ml water is added. The mixture is extracted 4 times with diethyl ether. The organic phases are combined and dried over MgSO$_4$, which is removed by filtration. A yellowish oil is obtained after evaporation of the solvent. The product is purified by column chromatography using a 10:1 vol/vol mixture of hexane and ethyl acetate. Yield: 38 %

^{1}H-NMR (400 MHz, CDCl$_3$): δ = 1.39 (t, 3 H, CH$_3$-c), δ = 1.56 (d, 2 H, CH$_2$), δ = 3.74 (s, 3 H, CH$_3$-O), δ = 4.39 (q, 1 H, CH), δ = 4.62 (d, 3 H, CH$_3$-CH).
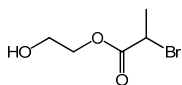
Hydroxyethyl 2-bromopropionate is synthesized as described by White et al.[3]. 200 ml ethylene glycol is placed in a flame dried flask under argon atmosphere. The ethylene glycol is cooled to 0 °C after which 10 ml (95.5 mmol) 2-bromopropionyl bromide is added drop wise. The mixture is stirred at 0 °C for 5 hours, after which the mixture is allowed to heat up to room temperature and is stirred overnight. The reaction is stopped by the addition of 100 ml water. The mixture is extracted three times with chloroform. The organic phases are combined and the solvent is removed. The crude product is purified by distillation under reduced pressure.

^{1}H-NMR (400 MHz, CDCl$_3$): δ = 1.80 (d, 3 H, CH$_3$), δ = 3.81 (t, 2 H, CH$_2$-O-C), δ = 4.26 (t, 2 H, CH$_2$-OH), δ = 4.39 (q, 1 H, CH-Br).
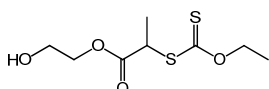
S-(1-Methyl-4-hydroxyethyl acetate) O-ethyl dithiocarbonate[2]. 2.568 g (13 mmol) hydroxyethyl 2-bromopropionate is dissolved in 50 ml ethanol. 2.08 g (13 mmol) of O-ethyl xanthic acid potassium salt is added and the mixture is heated to 60 °C for 2 days, after which 100 ml water is added and the mixture is extracted three times with diethyl ether. The organic phases are combined, dried and the solvent is

[2] Ladavière, C., Dörr, N., Claverie, J.P., *Macromolecules*, **2001**, 34, 5370-5372.

[3] White, M.A., Johnson, J.A., Koberstein, J.T., Turro, N.J., *J Am Chem Soc*, **2006**, 128, 11356-11357.

removed. The product is purified by column chromatography using a 7:3 mixture of hexane and ethyl acetate.

^{1}H-NMR (400 MHz, CDCl$_3$): δ = 1.37 (t, 3 H, CH$_3$-C-O), δ = 1.55 (d, 2 H, CH$_2$-O-C=S), δ = 2.30 (s, 1 H, OH), δ = 3.79 (t, 2 H, CH-OH), δ = 4.22 (t, 2H, CH$_2$-C-OH), δ = 4.37 (q, 1H, CH-S), δ = 4.60 (q, 2H, CH$_2$-O-C=S).

3-benzylsulfanyl thiocarbonylsulfanyl propionic acid (BPATT) was kindly provided by the group of A.H.E. Müller.
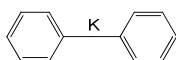
Diphenyl methyl potassium. Two Schlenk flasks are connected to each other using a frit. Into one of the flasks 1.0 g (7.8 mmol) of naphthalene is introduced, 1.976 g (11.8 mmol) of diphenylmethane is introduced into the other. The glassware is dried under vacuum, after which 0.48 g (12.3 mmol) of potassium is added to the naphthalene as well as 40 ml of THF (dried over Na/K alloy and freshly distilled). The mixture is stirred overnight, during which a dark green color evolved. The solution is poured through the frit (to remove remaining potassium) onto the diphenylmethane, after which a strong red/brown color evolved. This initiator for anionic polymerization is stored under argon. The concentration of the initiator is assumed to be set by the amount of naphthalene used.

Polymers
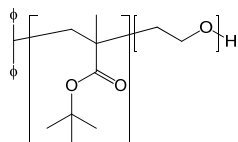
PtBuMA-*b*-PEO. The vacuum line is extensively flame dried under high vacuum. Approximately 500 ml dry (dried over Na/K alloy) THF is condensed directly into the reactor. *Tert*-butyl methacrylate is dried over calcium hydride for several hours, after which it is condensed into a graduated flask. Ethylene oxide is condensed onto calcium hydride, where it is dried for an hour, after which it is condensed onto a sodium mirror, where it is once again stirred for an hour. Eventually it is condensed into a graduated flask with a small amount of *n*-BuLi (dry). 7.87 ml of the prepared diphenyl methyl potassium solution is introduced into the reactor, which is thereafter cooled to - 80 °C. 10 ml *tert*-butyl methacrylate is condensed into the reactor and stirred for two hours, after which 30.5 ml of EO is condensed into the reactor, which is put under argon and is sealed. The reaction mixture is heated to 45 °C for three days, after which the reaction is stopped by the addition of a small amount of methanol. The polymer is purified by dialysis (THF, MWCO 1000).
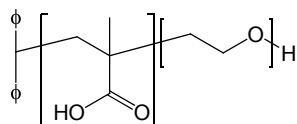
PMAA-*b*-PEO. 1.5565 g of PtBuMA-*b*-PEO is dissolved in 10 ml chloroform to which 10 ml TFA is added. The mixture is stirred overnight at room temperature. The solvents are removed and the product

is redissolved in THF, from which it is precipitated in acidified water with Na_2SO_4. The solids are collected by centrifugation. It is redissolved in dichloromethane and precipitated in ether. After drying the final product is obtained.
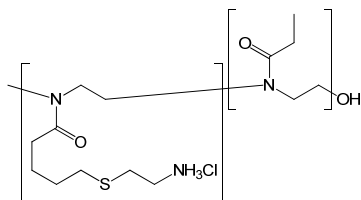
PButenOx-*b*-PEtOx mod base. The synthesis of the PButenOx-*b*-PEtOx block copolymer by ring opening cationic polymerization is described in the appendix to Chapter 3. Using thiol-click chemistry the PButenOx block of this polymer is modified with 2-aminoethanethiol HCl. This is done in the following way.

0.513 g of the precursor polymer is dissolved in 19 ml of water to which 0.843 g 2-aminoethanethiol HCl is added. The solution is degassed by two successive freeze-thaw cycles. The solution is placed near a UV-lamp and is irradiated for 24 hours, after which the product is purified by dialysis (H_2O, MWCO 1000).
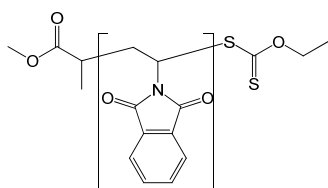
PVPh. 1.006 g of recrystallized *N*-vinylphthalimide, 11.9 mg of AIBN and 30 mg of *O*-ethyl-*S*-(1-methoxycarbonyl) ethyldithiocarbonate are dissolved in 3 ml dry DMF. The solution is degassed by two freeze-thaw cycles. The mixture is heated to 70 °C overnight. The polymer is precipitated from the reaction mixture into cold diethyl ether.
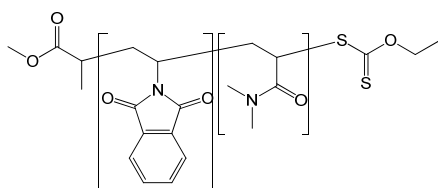
PVPh-*b*-PDMAAm. 60 mg of PVPh, 0.384 ml dimethyl acrylamide and 0.15 mg of AIBN are dissolved in 1.33 ml DMF. The reaction mixture is degassed by two freeze-thaw cycles. The mixture is heated to 65 °C for 6 days, after which the polymer is purified by dialysis (H_2O, MWCO 1000) and is obtained by freeze drying.
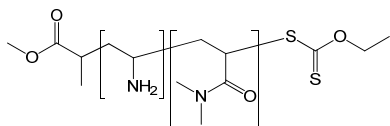
PVA-*b*-PDMAAm. 0.2116 g of PVPh-*b*-PDMAAm is dissolved in 1.41 ml of dioxane. 2.814 ml of methanol and 1.41 ml of hydrazine are added to the solution. The solution is refluxed overnight. The polymer is purified by dialysis (H$_2$O, MWCO 1000) and is obtained by freeze drying.
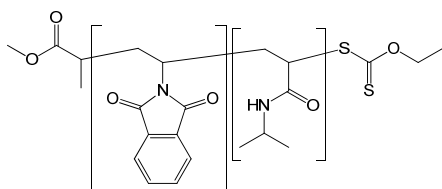
PVPh-*b*-PNIPAAm. 101.2 mg of PVPh, 0.717 g *N*-isopropyl acrylamide (recrystallized) and 0.26 mg of AIBN are dissolved in 2.45 ml DMF. The reaction mixture is degassed by two freeze-thaw cycles. The mixture is heated to 65 °C for 6 days, after which the polymer is purified by dialysis (H$_2$O, MWCO 1000) and is obtained by freeze drying.
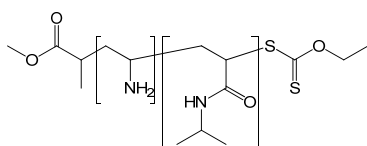
PVA-*b*-PNIPAAm. 0.411 g of PVPh-*b*-PDMAAm is dissolved in 2.73 ml of dioxane. 5.46 ml of methanol and 2.74 ml of hydrazine are added to the solution. The solution is refluxed overnight. The polymer is purified by dialysis (H$_2$O, MWCO 1000) and is obtained by freeze drying.
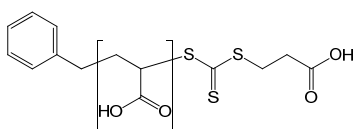
PAA (1). 47.6 mg (0.175 mmol) of BPATT, 0.489 ml (6.99 mmol) freshly distilled acrylic acid and 0.1 equivalent of 4,4'-azobis(4-cyanovaleric acid) (ACVA) relative to BPATT are dissolved in 2 ml of a 1:1 mixture of H$_2$O and acetone. The reaction mixture is degassed by two freeze-thaw cycles and is heated to 65 °C for 5 days. The polymer is purified by dialysis (H$_2$O, MWCO 1000) and is obtained by freeze drying.
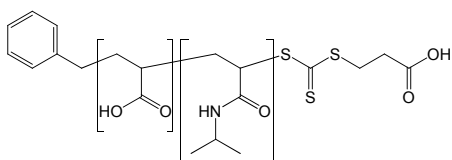
PAA-*b*-PNIPAAm. 60.7 mg of PAA (1), 0.677 g (400 eq) of recrystallized NIPAAm and 0.24 mg of recrystallized AIBN are dissolved in 2.21 ml DMF. The reaction mixture is degassed by two freeze-thaw cycles and is heated to 65 °C for 4 days. The polymer is purified by dialysis (H$_2$O, MWCO 1000) and is obtained by freeze drying.
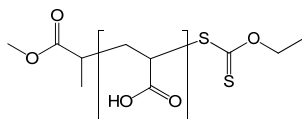
PAA (2). 58.9 mg (0.27 mmol) of *O*-ethyl-*S*-(1-methoxycarbonyl) ethyldithiocarbonate and 0.84 ml (10.8 mmol) of freshly distilled acrylic acid are dissolved in 1.79 ml of a 1:1 H_2O methanol mixture. 4.4 mg (0.027 mmol) of AIBN in a small amount of DMF is added to the solution. The reaction mixture is degassed by two freeze-thaw cycles and is heated to 65 °C for 6 days. The polymer is purified by dialysis (H_2O, MWCO 1000) and is obtained by freeze drying.
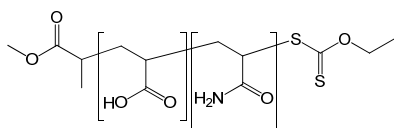
PAA-*b*-PAAm. 145 mg of PAA (2), 1.40 g of acrylamide, and 0.81 mg of AIBN are dissolved in a 4:1 mixture of isopropanol and water. The reaction mixture is degassed by two freeze-thaw cycles and is heated to 65 °C for 7 days. The polymer is purified by dialysis (H_2O, MWCO 1000) and is obtained by freeze drying from dioxane.
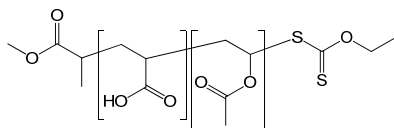
PAA-*b*-PVAc. 56.1 mg of PAA (2), 0.703 ml (400 eq) of freshly distilled VAc and 0.31 mg of AIBN are dissolved in 2.13 ml of DMF. The reaction mixture is degassed by two freeze-thaw cycles and is heated to 65 °C for 7 days. The polymer is purified by dialysis (THF, MWCO 1000) and is obtained by freeze drying from dioxane.
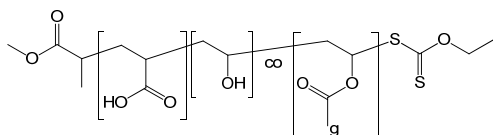
PAA-*b*-PVOH. 0.196 g of PAA-*b*-PVAc is dissolved in 20 ml of MeOH. 20 ml of a 20 g/l KOH solution in methanol is added and the reaction mixture is stirred for 24 hours, after which the solution is acidified with 1 M hydrochloric acid. The polymer is purified by dialysis (H_2O, MWCO 1000) and is obtained by freeze drying.
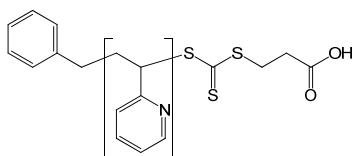
P2VP. 47 mg (0.17 mmol) of BPATT, 0.743 ml (6.9 mmol) of freshly distilled 2-vinylpyridine and 0.1 equivalent of AIBN relative to the amount of BPATT are dissolved in, 1.49 ml DMF. The reaction mixture is degassed by two freeze-thaw cycles and is heated to 65 °C for 5 days. The polymer is purified by dialysis (THF, MWCO 1000) and is obtained by freeze drying from dioxane.
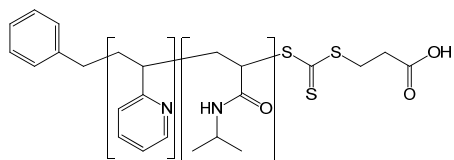
P2VP-*b*-PNIPAAm. 0.245 g of P2VP, 2.63 g (400 eq) of NIPAAm and 0.94 mg of AIBN are dissolved in 8.61 ml of DMF. The reaction mixture is degassed by two freeze-thaw cycles and is heated to 65 °C for 5 days. The polymer is purified by dialysis (H$_2$O, MWCO 1000) and is obtained by freeze drying.
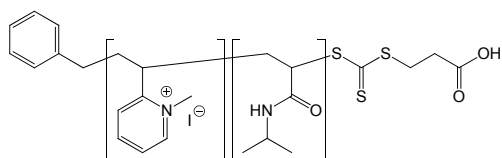
P2MVP-*b*-PNIPAAm. 0.175 g of P2VP-*b*-PNIPAAm is dissolved in 6.11 ml DMF, to which 0.216 ml of iodomethane is added. The mixture is heated to 60 °C under argon for 48 hours. The product is precipitated in diethyl ether and is successively washed extensively with diethyl ether.
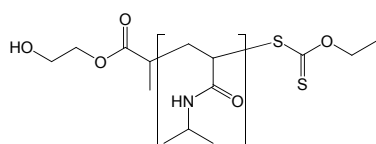
PNIPAAm. 40.8 mg of *S*-(1-methyl-4-hydroxyethyl acetate)*O*-ethyl dithiocarbonate, 7.75 g of recrystallized NIPAAm and 2.8 mg of recrystallized AIBN are dissolved in 31 ml dimethylacetamide. The reaction mixture is degassed by two freeze-thaw cycles and is heated to 65 °C for 5 days. The polymer is purified by dialysis (H$_2$O, MWCO 1000) and is obtained by freeze drying.
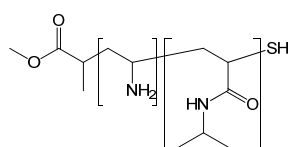
PVA-*b*-PNIPAAm-SH. PVA-*b*-PNIPAAm is dissolved in H$_2$O. The solution is degassed by flushing with argon. A large excess of sodium borohydride is added after which the solution is stirred for 24 hours. The solution is acidified with 1 M HCl solution. The polymer is purified by dialysis (H$_2$O, MWCO 1000) and is obtained by freeze drying.

C5Ms with PNIPAAm-SH. C5Ms prepared of PMAA-*b*-PEO/PVA-*b*-PNIPAAm are dissolved in H$_2$O. The solution is degassed by flushing with argon. A large excess of sodium borohydride is added after which the solution is stirred for 24 hours. The solution is acidified with 1 M HCl solution. The polymer is purified by dialysis (H$_2$O, MWCO 1000) and is obtained by freeze drying.

Sample preparation

Unless mentioned otherwise all solutions were prepared with a 1 mM NaNO$_3$ solution. All polymer solutions, again unless mentioned otherwise, were prepared at a concentration of 1 g/l and are filtered

using 0.45 μm syringe filters. The polymer solutions are mixed at the appropriate ratio. The pH of the solution is set using minimal amounts of 1 or 0.1 M HCl and NaOH solutions.

Ionic strength series are performed by adding different amounts of a concentrated salt solution (typically 2 M) to a C3M solution.

For NOESY and CryoTEM a 10 g/l solution with D_2O and 1 mM $NaNO_3$. The same solutions were used for CryoTEM. Similar solutions with normal water are used for SERS.

Cross linking of C3Ms

To a 1 g/l solution of C3Ms 0.5 equivalent to the number of acidic groups in the system of cross-linking agent (glutaraldehyde, BDDGE or a combination of NHS and EDC·HCl) is added, unless mentioned otherwise. NHS and EDC·HCl are used in equimolar ratio. The cross-linked micelles are purified by dialysis (H_2O, MWCO 1000) and successive freeze drying.

A.4.6 Data

Selected DLS data
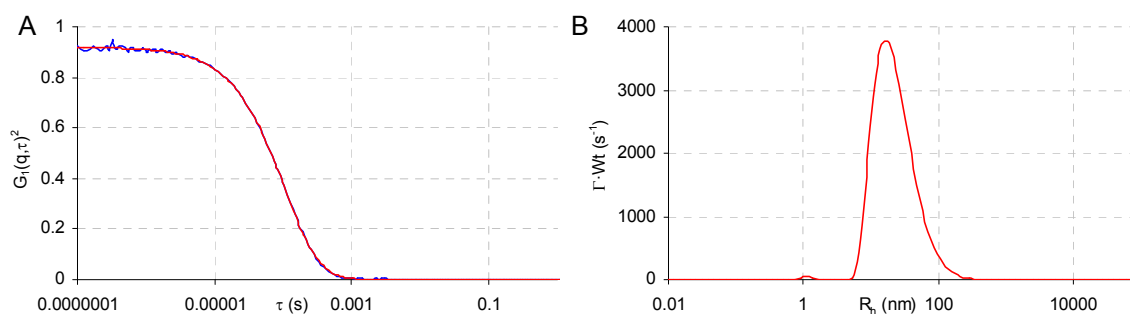
Figure 89: DLS data for C3Ms of PMAA-*b*-PEO and PVA-*b*-PDMAAm at pH 7, f^+ 0.7 (1 g/l, 1 mM $NaNO_3$). A) Correlation G_1 (blue: data, red: Contin fit) as a function of the correlation time τ, B) weighted size distribution.
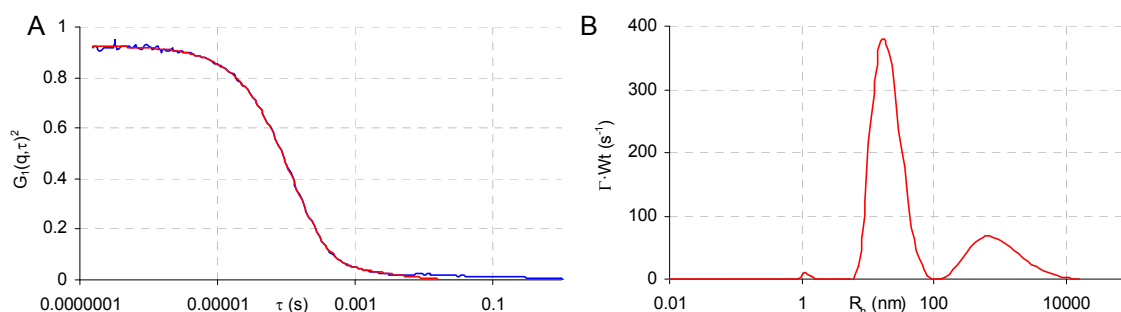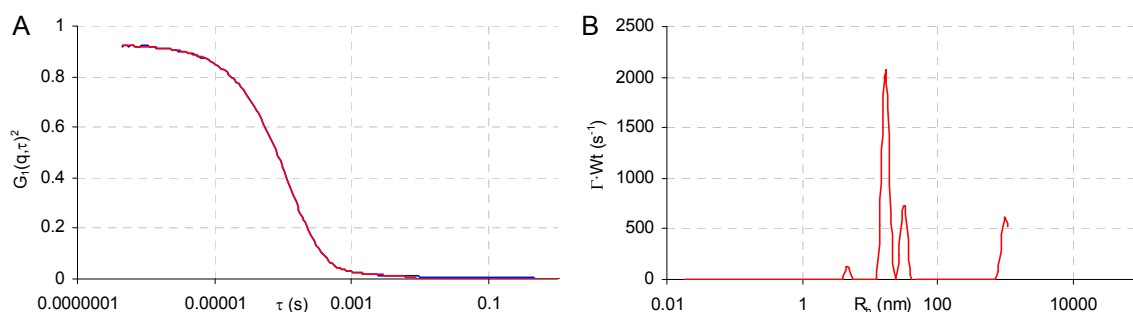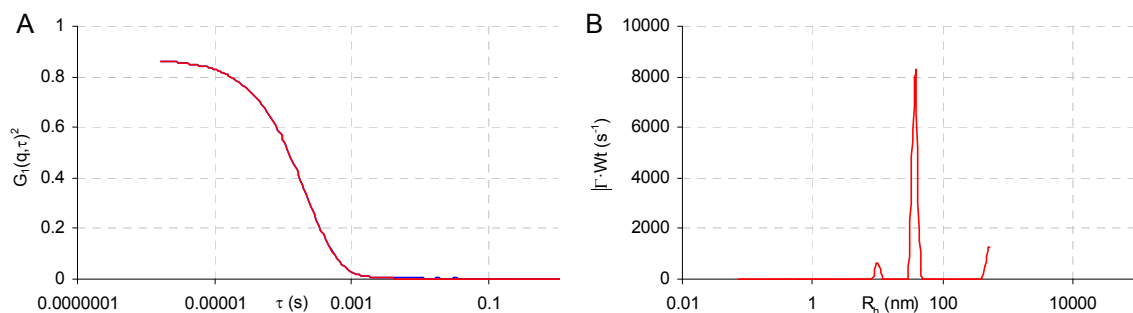

Figure 90: DLS data for C3Ms of PMAA-*b*-PEO and PVA-*b*-PDMAAm at pH 5.2, f^+ 0.5 (1 g/l, 1 mM $NaNO_3$). A) Correlation G_1 (blue: data, red: Contin fit) as a function of the correlation time τ, B) weighted size distribution.
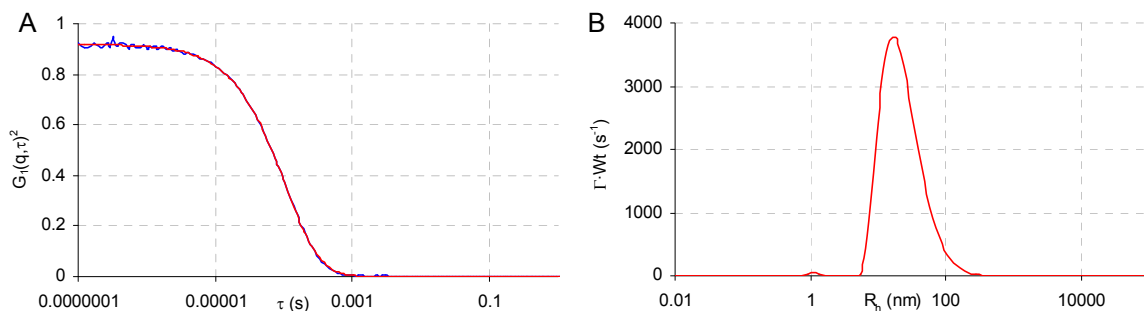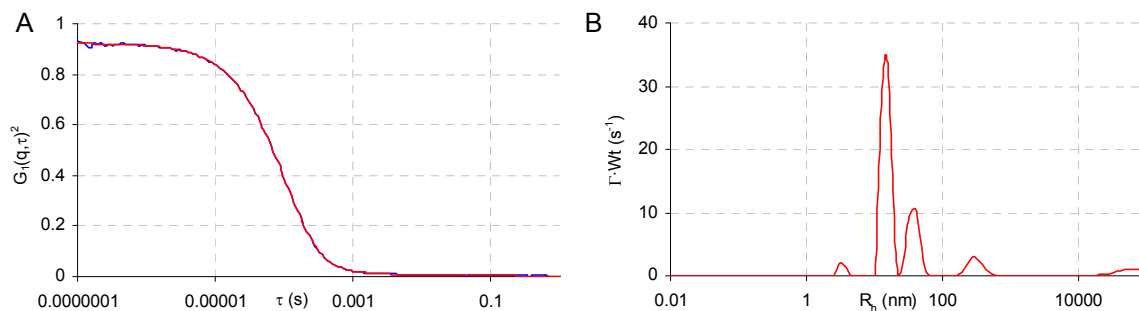
Figure 91: DLS data for C3Ms of PMAA-*b*-PEO and PVA-*b*-PNIPAAm at pH 7, f^+ 0.7 (1 g/l, 1 mM NaNO$_3$). A) Correlation G$_1$ (blue: data, red: Contin fit) as a function of the correlation time τ, B) weighted size distribution.
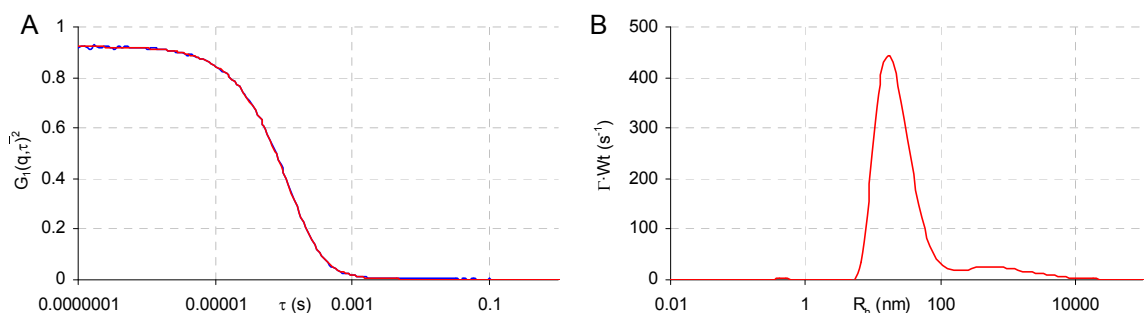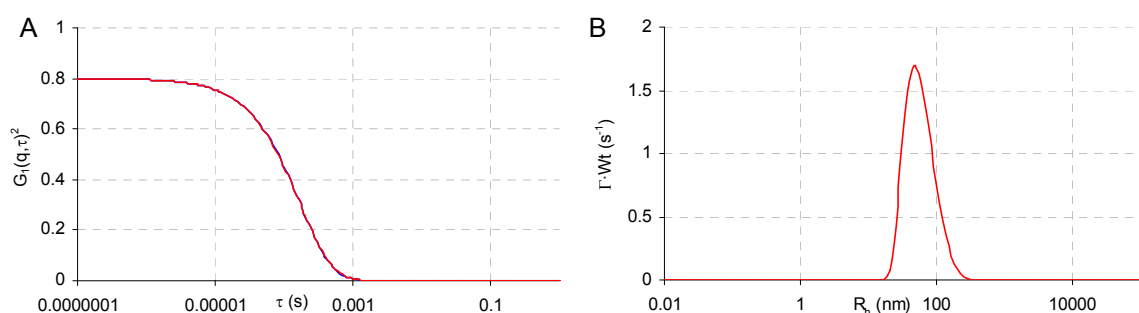

Figure 92: DLS data for C3Ms of PMAA-*b*-PEO and PVA-*b*-PDMAAm at pH 5, f^+ 0.5 (1 g/l, 1 mM NaNO$_3$). A) Correlation G$_1$ (blue: data, red: Contin fit) as a function of the correlation time τ, B) weighted size distribution.
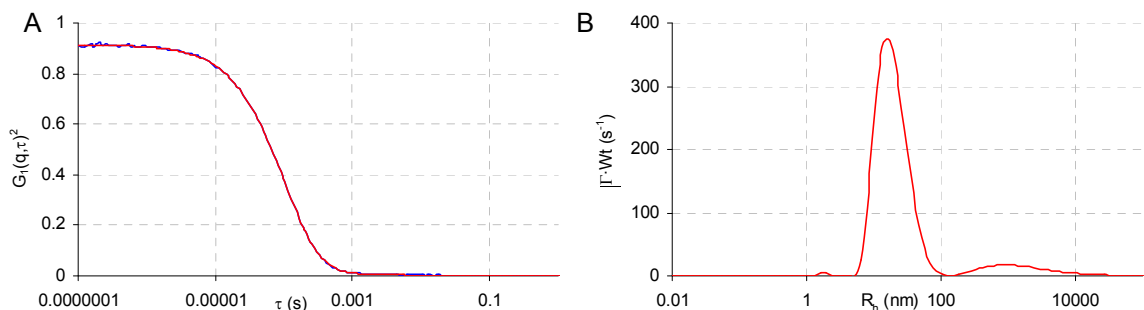
Figure 93: DLS data for C3Ms of PAA-*b*-PVOH and PVA-*b*-PNIPAAm at pH 5, f^+ 0.5 (1 g/l, 1 mM NaNO$_3$). A) Correlation G$_1$ (blue: data, red: Contin fit) as a function of the correlation time τ, B) weighted size distribution.
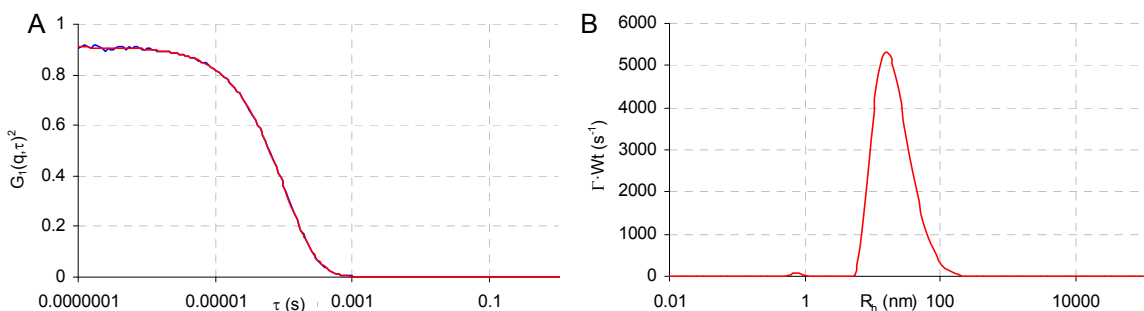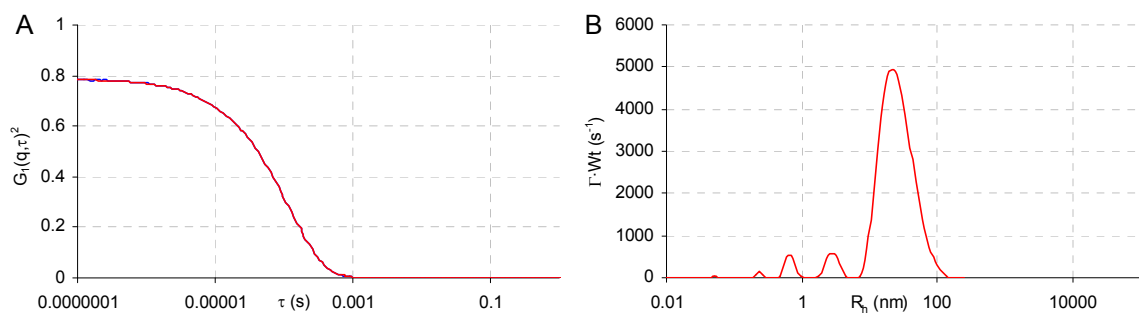

Figure 94: DLS data for C3Ms of PAA-*b*-PVOH and PVA-*b*-PNIPAAm at pH 7, f^+ 0.8 (1 g/l, 1 mM NaNO$_3$). A) Correlation G$_1$ (blue: data, red: Contin fit) as a function of the correlation time τ, B) weighted size distribution.
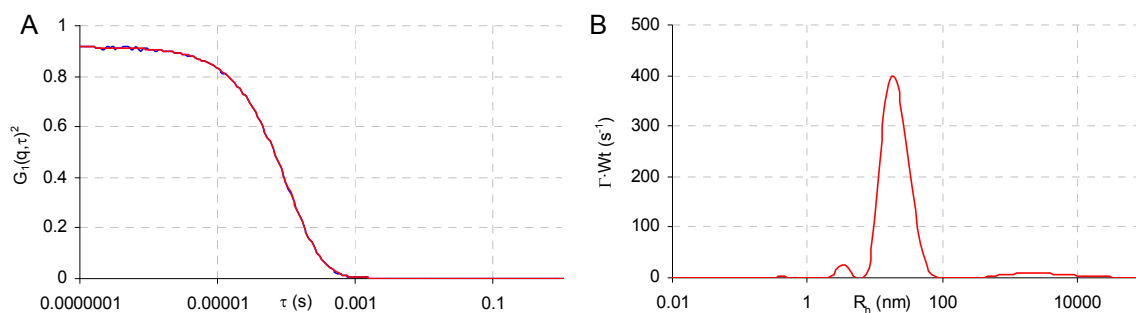
Figure 95: DLS data for C3Ms of PAA-*b*-PVOH and PVA-*b*-PNIPAAm at pH 6.4, f+ 0.8 (1 g/l, 1 mM NaNO₃). A) Correlation G_1 (blue: data, red: Contin fit) as a function of the correlation time τ, B) weighted size distribution.
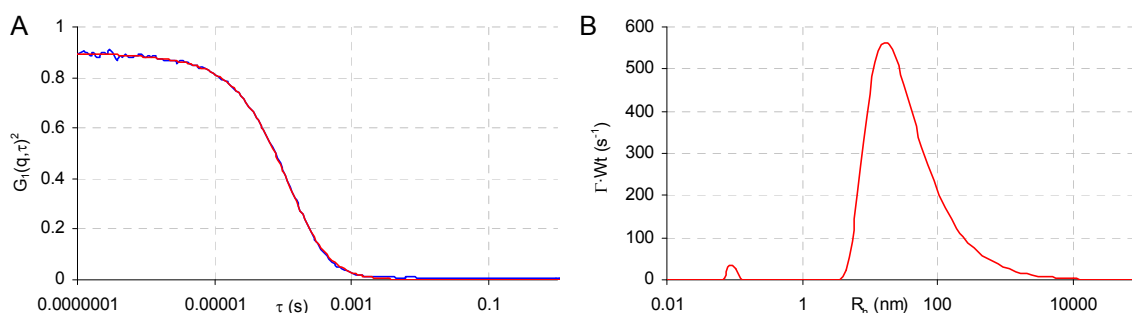
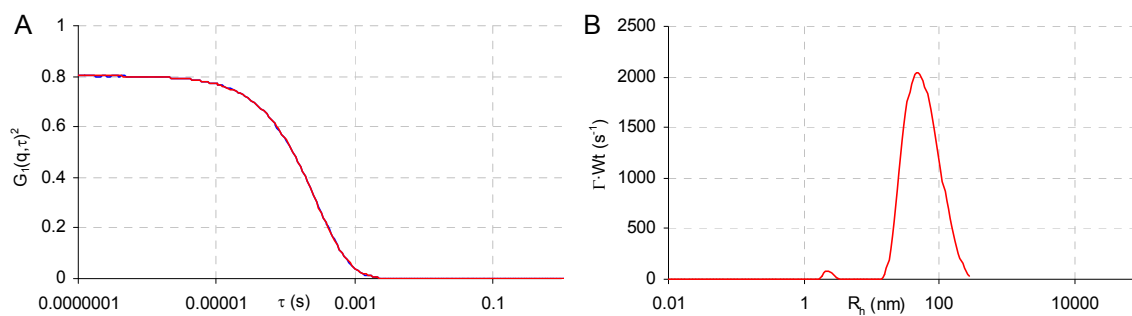**Figure 96:** DLS data for C5Ms of PMAA-*b*-PEO and PVA-*b*-PDMAAm cross-linked with BDDGE, at pH 5, 500 mM NaNO₃ (0.67 g/l). A) Correlation G_1 (blue: data, red: Contin fit) as a function of the correlation time τ, B) weighted size distribution.
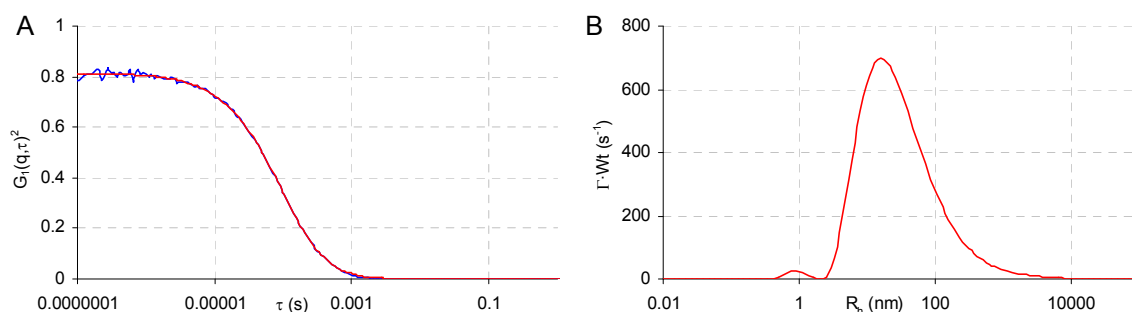
Figure 97: DLS data for C5Ms of PMAA-*b*-PEO and PVA-*b*-PDMAAm cross-linked with glutaraldehyde, at pH 5, 500 mM NaNO₃ (0.67 g/l). A) Correlation G_1 (blue: data, red: Contin fit) as a function of the correlation time τ, B) weighted size distribution.
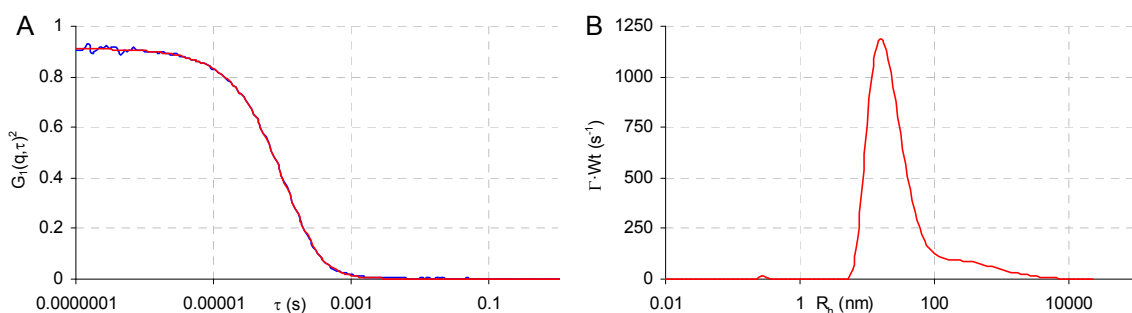
Figure 98: DLS data for C5Ms of PMAA-*b*-PEO and PVA-*b*-PDMAAm cross-linked with NHS and EDC, at pH 5, (1 g/l, 1 mM NaNO₃). A) Correlation G_1 (blue: data, red: Contin fit) as a function of the correlation time τ, B) weighted size distribution.
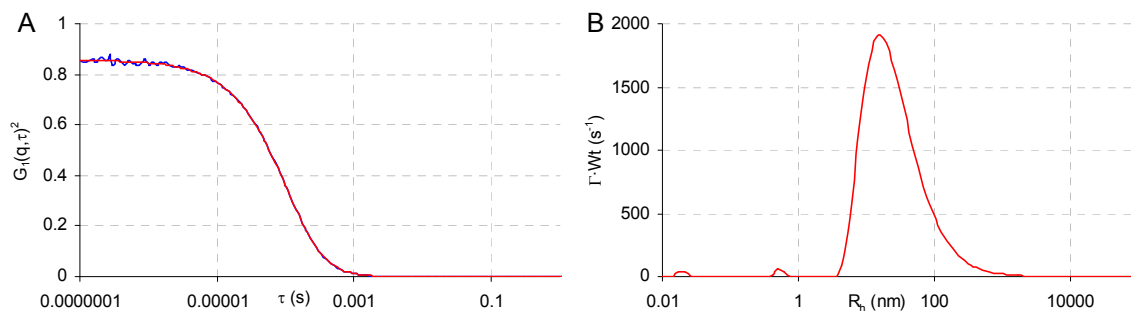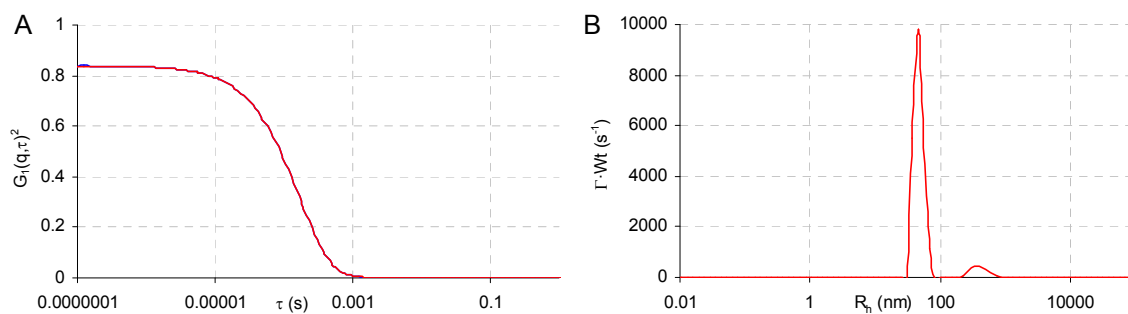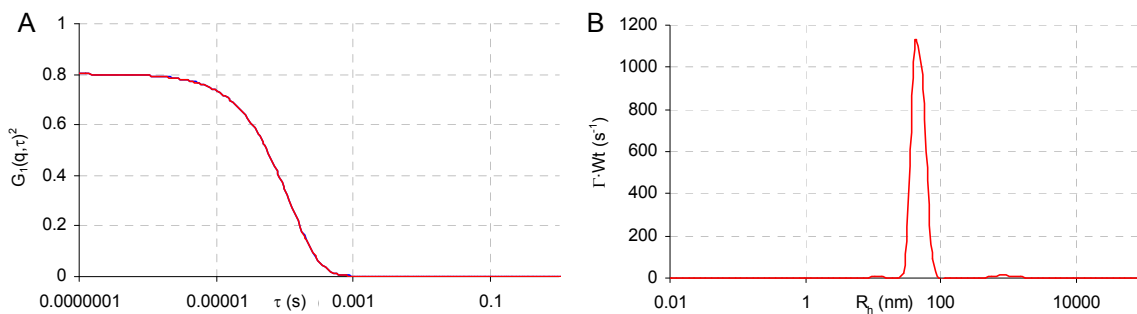
Figure 99: DLS data for C5Ms of PMAA-*b*-PEO and PVA-*b*-PDMAAm cross-linked with NHS and EDC, at pH 5, 500 mM NaNO$_3$ (0.67 g/l). A) Correlation G$_1$ (blue: data, red: Contin fit) as a function of the correlation time τ, B) weighted size distribution.
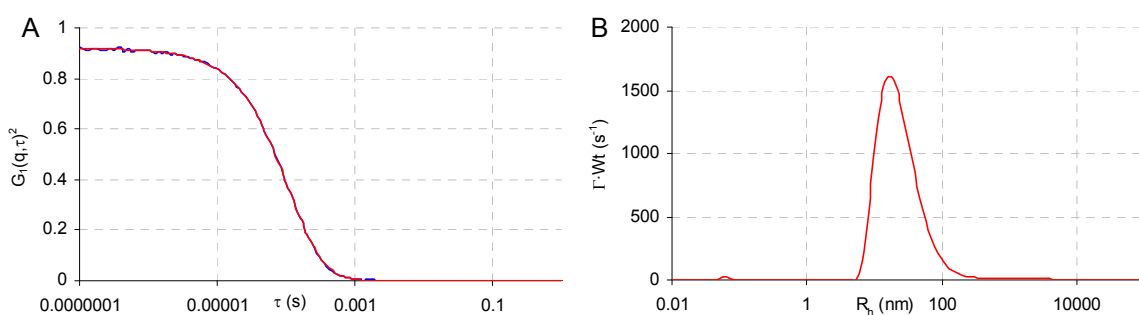
Figure 100: DLS data for C5Ms of PMAA-*b*-PEO and PVA-*b*-PNIPAAm cross-linked with NHS and EDC, at pH 5 (1 g/l, 1 mM NaNO$_3$). A) Correlation G$_1$ (blue: data, red: Contin fit) as a function of the correlation time τ, B) weighted size distribution.
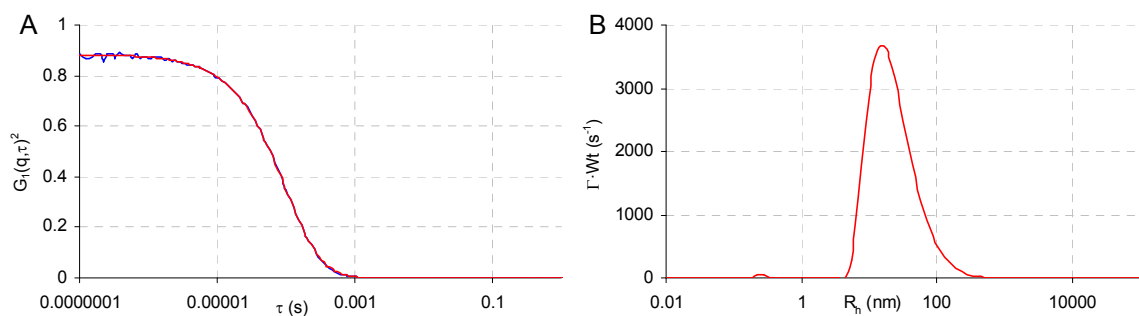
Figure 101: DLS data for C5Ms of PMAA-*b*-PEO and PVA-*b*-PNIPAAm cross-linked with NHS and EDC, at pH 5, 500 mM NaNO$_3$ (0.67 g/l). A) Correlation G$_1$ (blue: data, red: Contin fit) as a function of the correlation time τ, B) weighted size distribution.
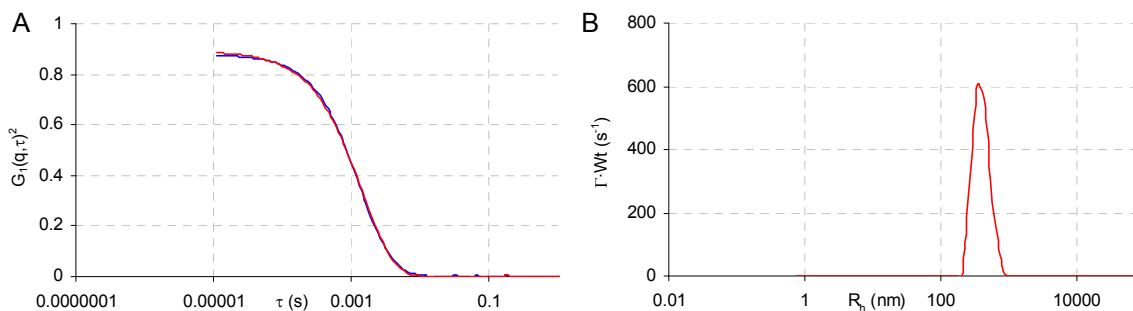
Figure 102: DLS data for C5Ms of PMAA-*b*-PEO and PVA-*b*-PNIPAAm cross-linked with NHS and EDC, at pH 5, 45°C (1 g/l, 1 mM NaNO₃). A) Correlation G_1 (blue: data, red: Contin fit) as a function of the correlation time τ, B) weighted size distribution.
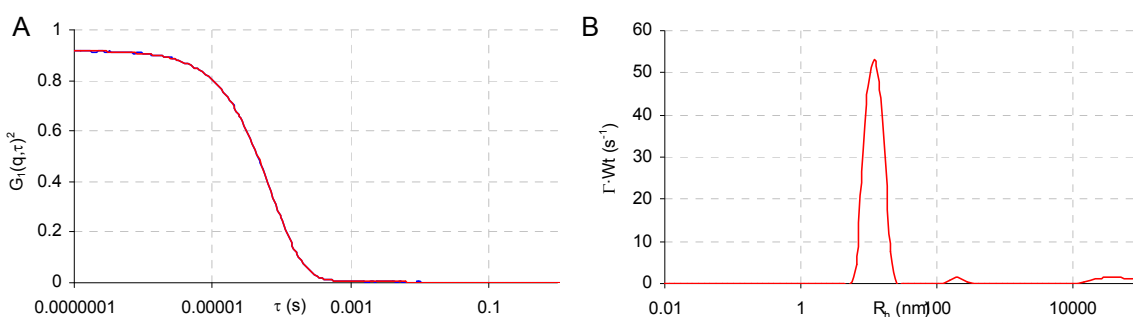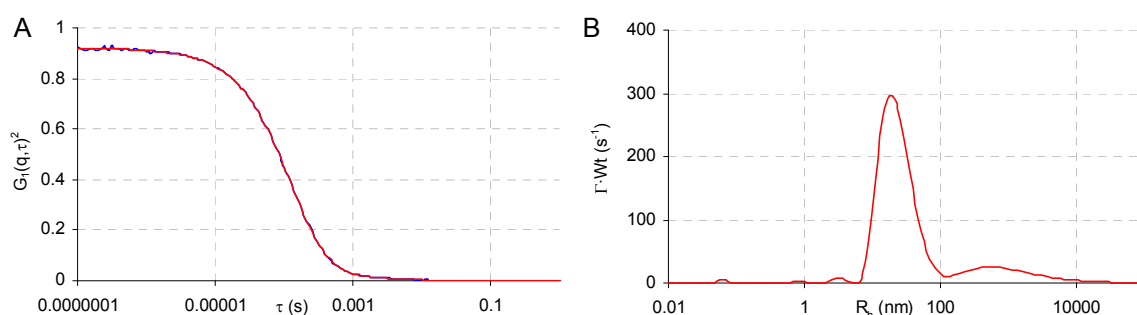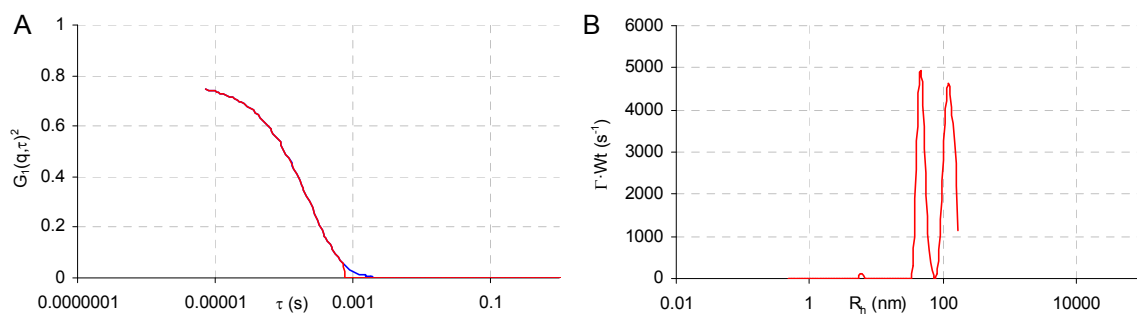

Figure 103: DLS data for Ludox HS-40 (1 g/l, pH 7). A) Correlation G_1 (blue: data, red: Contin fit) as a function of the correlation time τ, B) weighted size distribution.

Figure 104: DLS data for Ludox HS-40 with C5Ms of PMAA-*b*-PEO and PVA-*b*-PDMAAm cross-linked with NHS and EDC, at pH 7, 80 wt% C5Ms (1 g/l, 1 mM NaNO₃). A) Correlation G_1 (blue: data, red: Contin fit) as a function of the correlation time τ, B) weighted size distribution.


Figure 105: DLS data for Ludox HS-40 with C5Ms of PMAA-*b*-PEO and PVA-*b*-PDMAAm cross-linked with NHS and EDC, at pH 3, 80 wt% C5Ms (1 g/l, 1 mM NaNO₃). A) Correlation G_1 (blue: data, red: Contin fit) as a function of the correlation time τ, B) weighted size distribution.
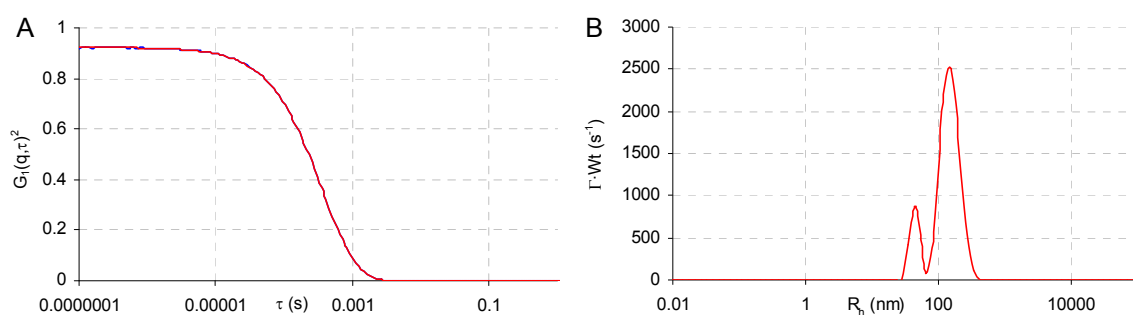
Figure 106: DLS data for Ludox HS-40 with C5Ms of PMAA-*b*-PEO and PVA-*b*-PNIPAAm cross-linked with NHS and EDC, at pH 7, 80 wt% C5Ms (1 g/l, 1 mM NaNO$_3$). A) Correlation G$_1$ (blue: data, red: Contin fit) as a function of the correlation time τ, B) weighted size distribution.


Figure 107: DLS data for Ludox HS-40 with C5Ms of PMAA-*b*-PEO and PVA-*b*-PNIPAAm cross-linked with NHS and EDC, at pH 7, 80 wt% C5Ms, 50°C (1 g/l, 1 mM NaNO$_3$). A) Correlation G$_1$ (blue: data, red: Contin fit) as a function of the correlation time τ, B) weighted size distribution.

Figure 108: DLS data for gold nanoparticles (as received, ~0.1 g/l). A) Correlation G$_1$ (blue: data, red: Contin fit) as a function of the correlation time τ, B) weighted size distribution.

Figure 109: DLS data for gold nanoparticles with C5Ms of PMAA-*b*-PEO and PVA-*b*-PNIPAAm cross-linked with NHS and EDC, of which the CTA end-groups were reduced to thiol groups, at pH 7, 33 wt% C5Ms (1 mM NaNO$_3$). A) Correlation G$_1$ (blue: data, red: Contin fit) as a function of the correlation time τ, B) weighted size distribution.
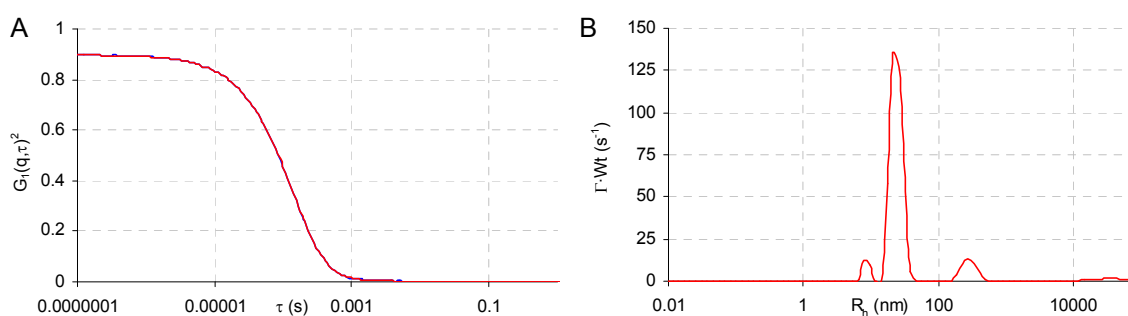
Figure 110: DLS data C3Ms of PAA-*b*-PNIPAAm and PButenOx-*b*-PEtOx at pH 7, f$^+$ 0.4 (1 g/l, 1 mM NaNO$_3$). A) Correlation G$_1$ (blue: data, red: Contin fit) as a function of the correlation time τ, B) weighted size distribution.

Figure 111: DLS data C3Ms of PAA-*b*-PNIPAAm and PButenOx-*b*-PEtOx at pH 7, f$^+$ 0.4, 50°C (1 g/l, 1 mM NaNO$_3$). A) Correlation G$_1$ (blue: data, red: Contin fit) as a function of the correlation time τ, B) weighted size distribution.

Figure 112: DLS data C3Ms of PAA-*b*-PNIPAAm and PButenOx-*b*-PEtOx at pH 7, f$^+$ 0.4, 70°C (1 g/l, 1 mM NaNO$_3$). A) Correlation G$_1$ (blue: data, red: Contin fit) as a function of the correlation time τ, B) weighted size distribution.

Figure 113: DLS data C5Ms of PAA-*b*-PNIPAAm and PButenOx-*b*-PEtOx cross-linked with NHS and EDC, at pH 7, 500 mM NaNO$_3$ (0.67 g/l). A) Correlation G$_1$ (blue: data, red: Contin fit) as a function of the correlation time τ, B) weighted size distribution.

Figure 114: DLS data C5Ms of PAA-*b*-PNIPAAm and PButenOx-*b*-PEtOx cross-linked with NHS and EDC, at pH 7, 50°C (1 g/l, 1 mM NaNO$_3$). A) Correlation G$_1$ (blue: data, red: Contin fit) as a function of the correlation time τ, B) weighted size distribution.
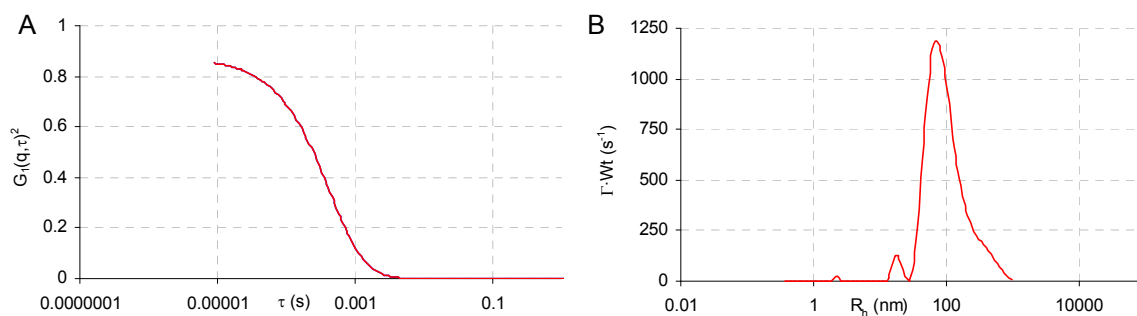
Figure 115: DLS data C5Ms of PAA-*b*-PNIPAAm and PButenOx-*b*-PEtOx cross-linked at 50°C with NHS and EDC, at pH 7, 500 mM $NaNO_3$ (0.67 g/l). A) Correlation G_1 (blue: data, red: Contin fit) as a function of the correlation time τ, B) weighted size distribution.

Figure 116: DLS data C5Ms of PAA-*b*-PNIPAAm and PButenOx-*b*-PEtOx cross-linked at 50°C with NHS and EDC, at pH 7, 50°C (1 g/l, 1 mM $NaNO_3$). A) Correlation G_1 (blue: data, red: Contin fit) as a function of the correlation time τ, B) weighted size distribution.

Selected SLS data
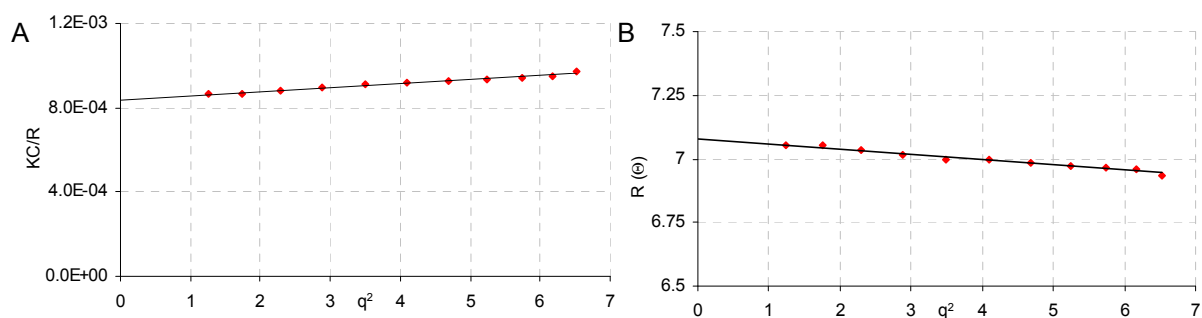
Figure 117: Partial Zimm (A) and Guinier (B)-plot of C3Ms of PMAA-*b*-PEO and PVA-*b*-PDMAAm (f+ 0.5, pH 5, 1 mM $NaNO_3$, 10 g/L).
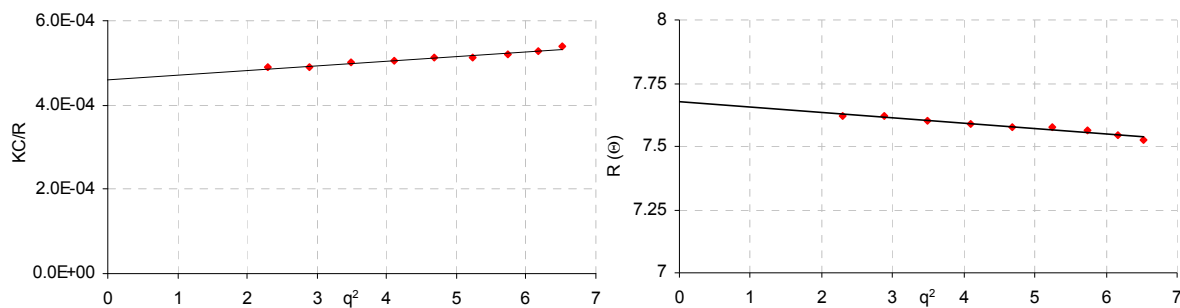
Figure 118: Partial Zimm (A) and Guinier (B)-plot of C3Ms of PMAA-*b*-PEO and PVA-*b*-PNIPAAm (f+ 0.4, pH 7, 1 mM NaNO₃, 10 g/L).
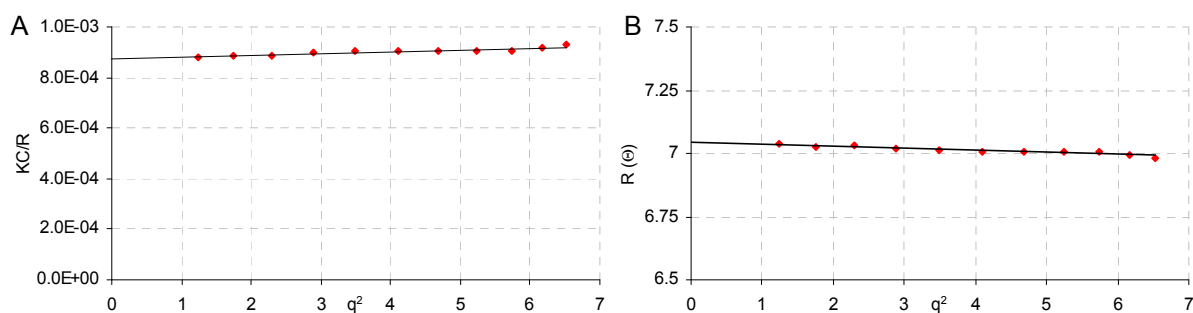
Figure 119: Partial Zimm (A) and Guinier (B)-plot of C3Ms of PAA-*b*-PNIPAAm and PButenOx-*b*-PEtOx (f+ 0.5, pH 5, 1 mM NaNO₃, 10 g/L).
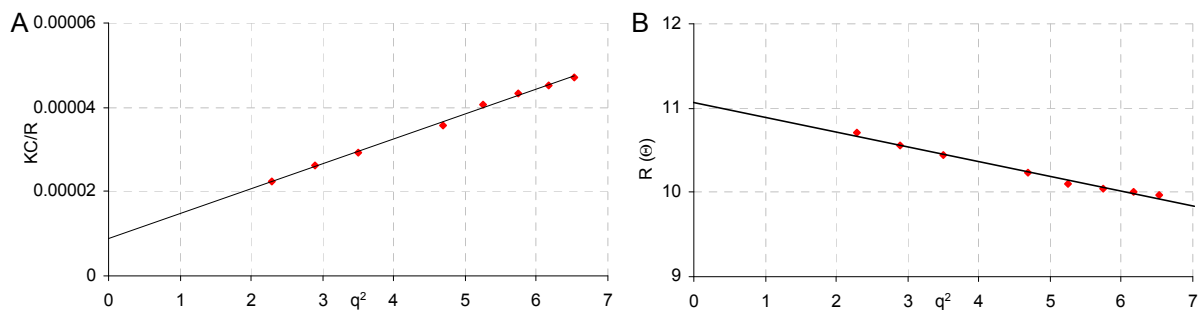
Figure 120: Partial Zimm (A) and Guinier (B)-plot of C5Ms of PAA-*b*-PNIPAAm and PButenOx-*b*-PEtOx cross-linked at 50°C with NHS and EDC (pH 7, 1 mM NaNO₃, 10 g/L).
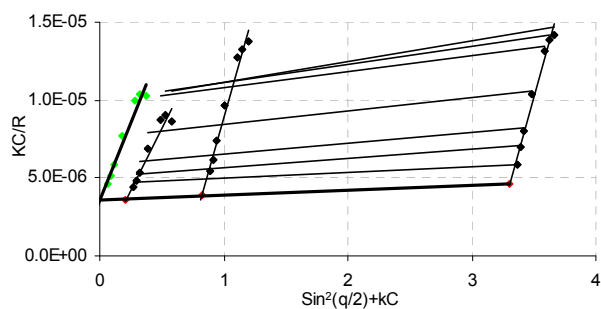
Figure 121: Full Zimm-plot of the larger fraction of aggregates of C5Ms of PAA-*b*-PNIPAAm and PButenOx-*b*-PEtOx cross-linked at 50°C with NHS and EDC (pH 7, 1 mM NaNO₃).

DLS data
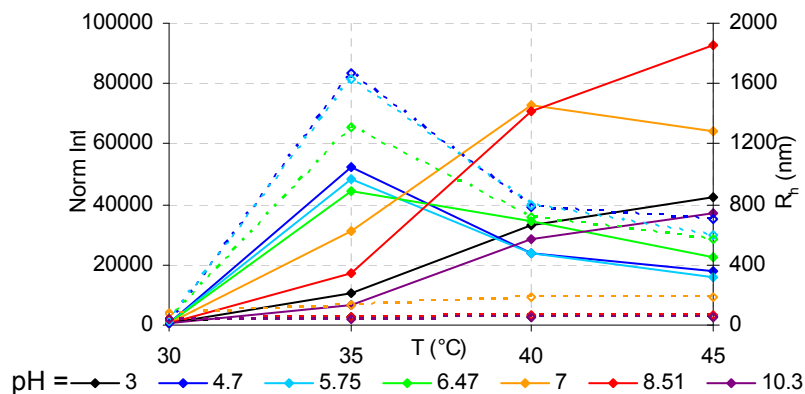
Figure 122: Temperature series at different pH values for PMAA-*b*-PEO/PVA-*b*-PNIPAAm C5Ms (1 g/l, 1 mM NaNO₃, solid lines: normalized scattering intensity, dashed lines: R_h cum.)
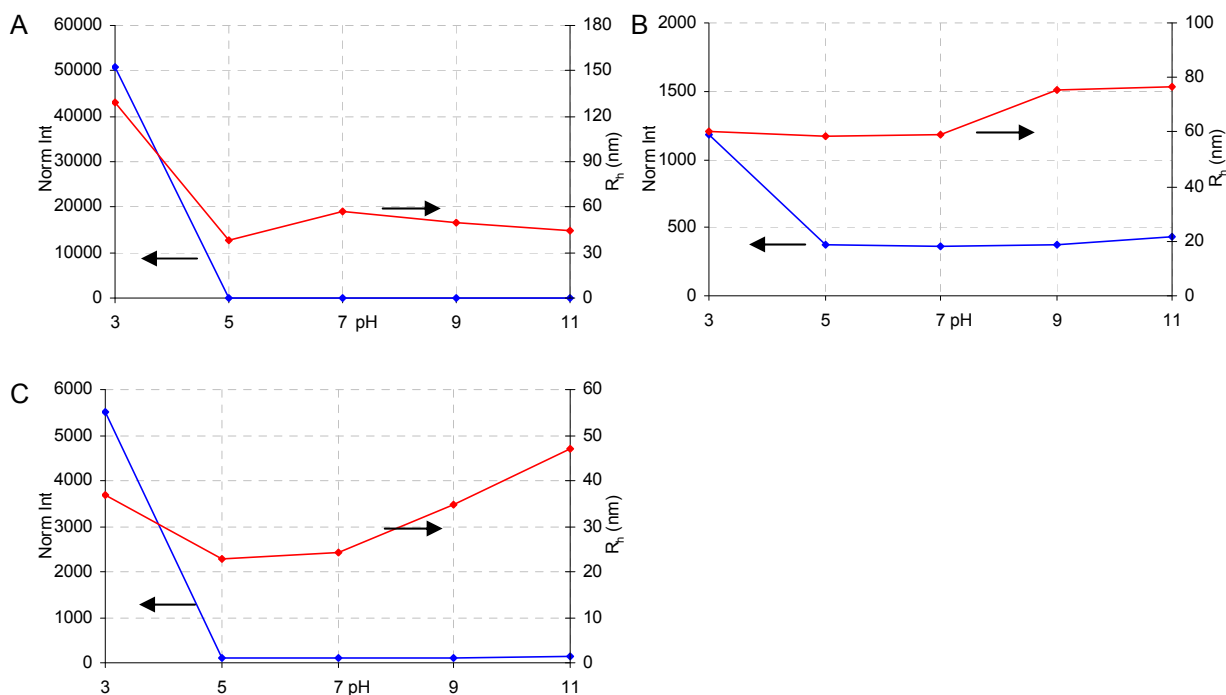
Figure 123: DLS data of pH series for PMAA-*b*-PEO (A), PAA-*b*-PDMAAm (B) and PAA-*b*-PNIPAAm (C) (1 g/l, 1 mM NaNO₃).
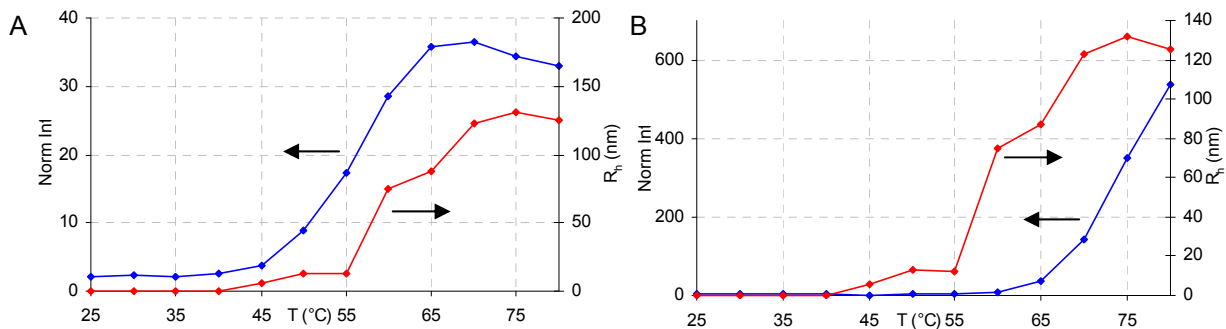
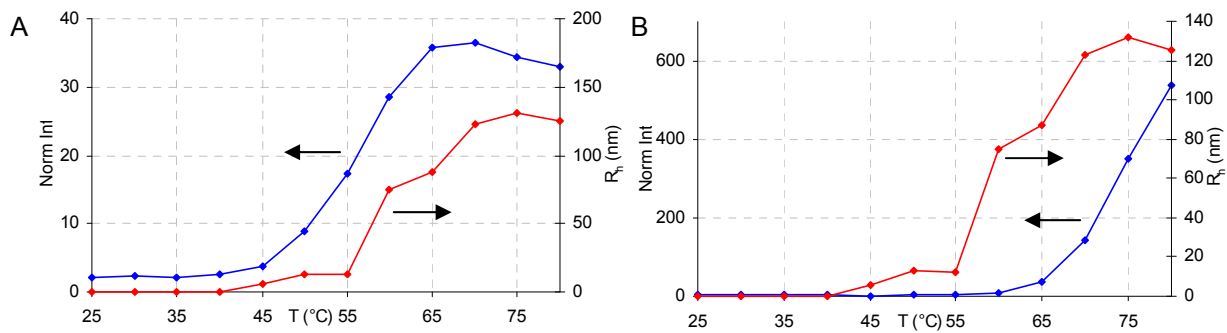**Figure 124:** Temperature series (0.5 g/l, 1 M Na₂SO₄) for (A) PDMAAm₃₃₁ and (B) PEO₅₀₅.

Raman spectroscopy
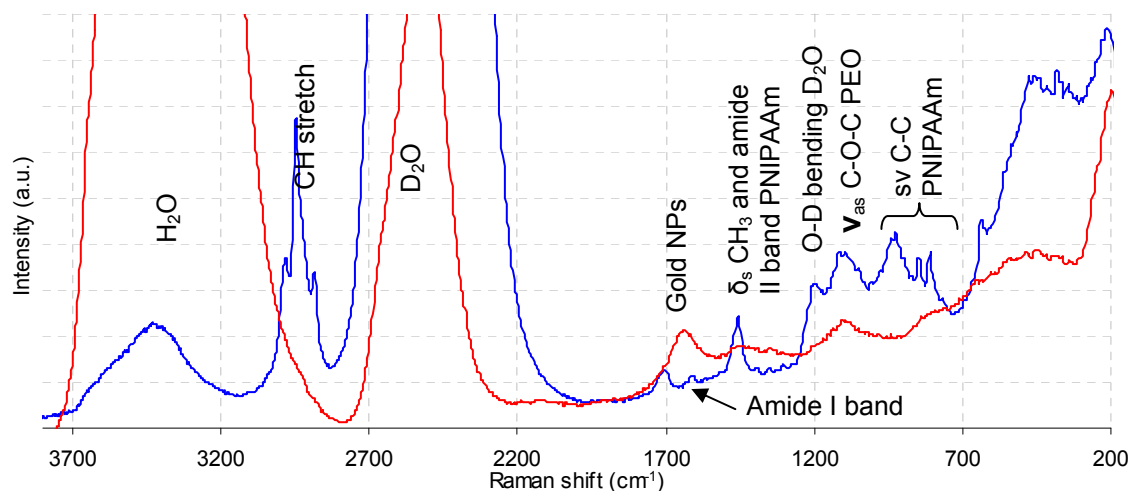
Figure 125: Raman spectra of C3Ms of PMAA-*b*-PEO/PVA-*b*-PNIPAAm (10 g/l in D$_2$O, blue) of which the PNIPAAm has a thiol end-group, and these C3Ms with gold nanoparticles (red, 1:1 mixture of C3M solution and gold nanoparticle solution; 0.1 g/l, R$_h$ ~ 20 nm).
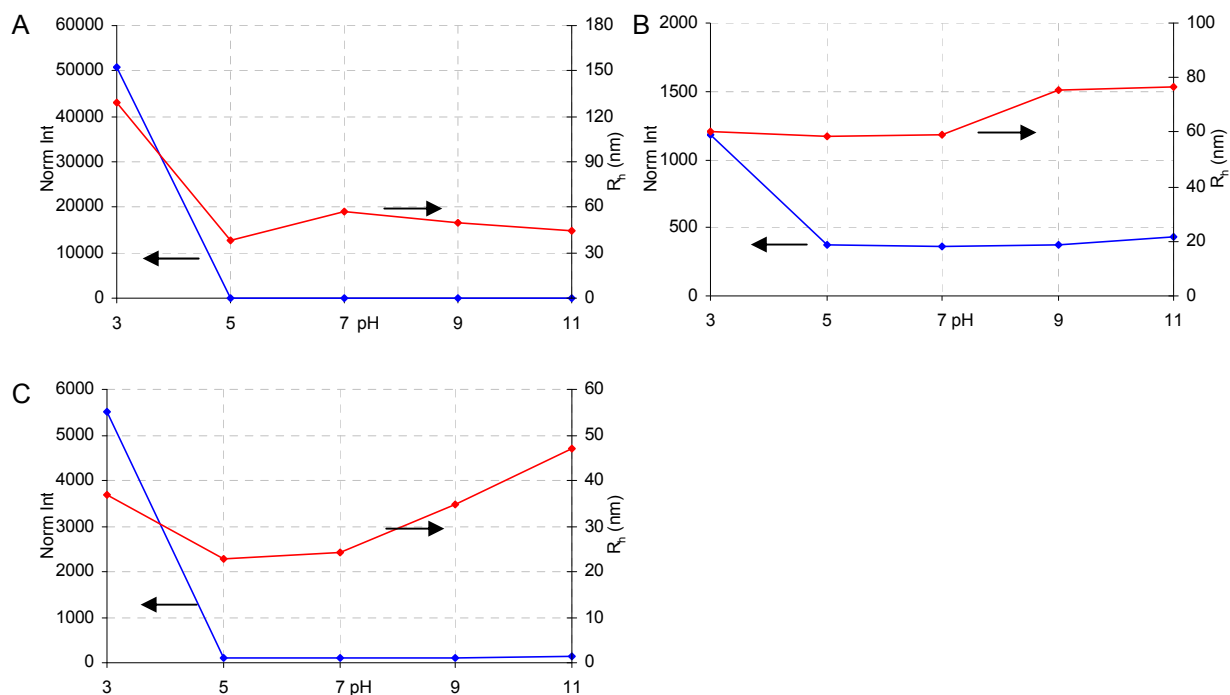
Figure 126: DLS data of pH series for PMAA-*b*-PEO (A), PAA-*b*-PDMAAm (B) and PAA-*b*-PNIPAAm (C) (1 g/l, 1 mM NaNO$_3$).

Figure 127: Temperature series (0.5 g/l, 1 M Na_2SO_4) for (A) $PDMAAm_{331}$ and (B) PEO_{505}.

A.5 Appendix to Chapter 5

A.5.1 Synthesis

Chain transfer agents
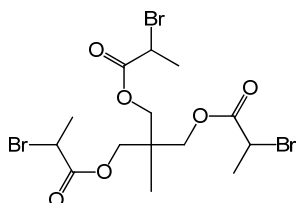
Trifunctional bromide precursor[4]: 7.2 g of 1,1,1-tris(hydroxymethyl)ethane is dissolved in 90 ml chloroform with 15 ml anhydrous pyridine. The solution is cooled to 0 °C, after which 58.28 g of 2-bromopropionyl bromide is added dropwise. The solution is stirred at room temperature for 4 hours, after which a 10 % HCl solution is added. The organic phase is washed three times with 5 wt % sodium carbonate solution. The organic phase is dried over sodium sulfate and after removal of the drying agent the solvent is removed.

^{1}H-NMR (400 MHz, CDCl$_3$): δ = 1.10 (s, 3 H, CH$_3$-core), δ = 1.81 (d, 9 H, CH$_3$-C-Br), δ = 4.13 (m, 6 H, CH$_2$-core), δ = 4.37 (q, 3 H, CH-Br).
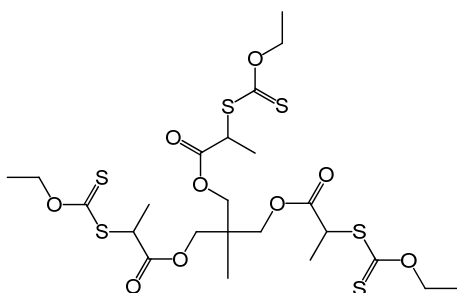
Trifunctional xanthate RAFT agent[4]: 7.97 g (15.2 mmol) of trifunctional bromide precursor is dissolved in 100 ml chloroform. 24.5 g (152 mmol) of *O*-ethyl xanthic acid potassium salt is added. The mixture is stirred at room temperature for 2 days. The mixture is filtrated and the solids are washed with chloroform. The liquid fractions are concentrated and the product is purified by column chromatography using a 7:3 hexane ethyl acetate mixture as the eluent.
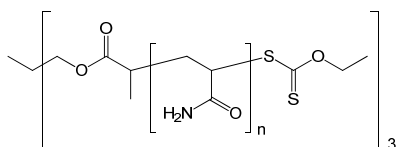
^{1}H-NMR (400 MHz, CDCl$_3$): δ = 0.83 (s, 3 H, CH$_3$-core), δ = 1.42 (t, 9 H, CH$_3$-C-O), δ = 1.56 (d, 9 H, CH$_3$-C-S), δ = 4.07 (m, 6 H, CH$_2$-core), δ = 4.40 (q, 3 H, CH-S), δ = 4.63 (q, 6 H, CH$_2$-O-C(=S)).

---

[4] Bernard, J., Favier, A., Zhang, L., Nilasaroya, A., Davis, T.P., Barner-Kowollik, C., Stenzel, M.H., *Macromolecules*, **2005**, 38, 5475-5484.
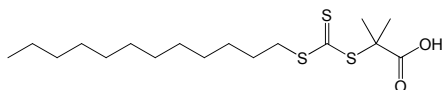
**2-dodecylsulfanylthiocarbonylsulfanyl-2-methyl propionic acid (DMP)** was kindly provided by the group of A.H.E. Müller.

Polymer synthesis

s-PAAm. 0.145 g trifunctional CTA, 4.765 g acrylamide and 11.8 mg of recrystallized AIBN are dissolved in 14.5 ml *N,N*-dimethylacetamide. The reaction mixture is degassed by three freeze-thaw cycles and is heated to 70 °C for 24 hours. The polymer is purified by dialysis (H$_2$O, MWCO 1000) and is obtained by freeze drying.
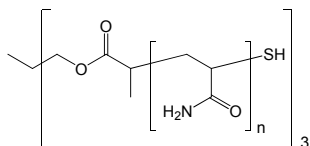
s-PAAm-SH. 0.7 g of s-PAAm is dissolved in 40 ml H$_2$O. The solution is degassed by flushing with argon. A large excess of sodium borohydride is added after which the solution is stirred for 24 hours. The solution is acidified with 1 M HCl solution. The polymer is purified by dialysis (H$_2$O, MWCO 1000) and is obtained by freeze drying.
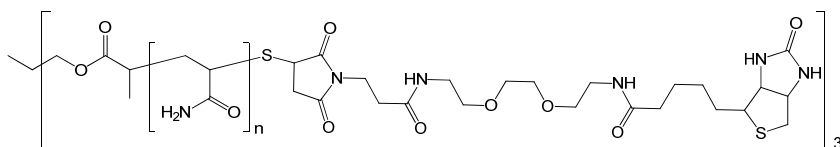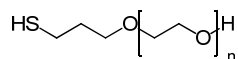

s-PAAm-biotin. To 7.24 ml of a 10 g/l solution of s-PAAm-SH 17 μl of a 1 M sodium borohydride solution is added to reduce any disulfide bonds. The mixture is stirred for an hour, after which it is neutralized with a 1 M HCl solution. 2.25 ml of a 10 g/l solution of biotin-maleimide (5 eq) is added and the mixture is stirred for two days, after which the polymer is purified by dialysis (H$_2$O, MWCO 1000) and is obtained by freeze drying.
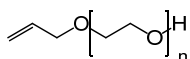

Allyl-PEO. The vacuum line is extensively flame dried under high vacuum. Approximately 150 ml dry (dried over Na/K alloy) THF is condensed directly into the reactor. Ethylene oxide is condensed onto calcium hydride, where it is dried for an hour, after which it is condensed onto a sodium mirror, where it is once again stirred for an hour. Eventually it is condensed into a graduated flask with a small amount of *n*-BuLi (dry). 0.228 g allyl alcohol and 0.92 ml (~1 M in hexane) phosphazene base P$_4$-*t*-Bu are added to the reactor, which is cooled to ~ - 80 °C. 23 ml of ethylene oxide is condensed into the reactor and stirred at 45 °C for 2 days. The reaction is stopped by adding a small amount of methanol to the solution. The

solvent is removed and the crude product is redissolved in chloroform. The phosphazene base is removed by stirring this solution over ion exchange resin (Dowex® 50WX4-100), filtering the dispersion and repeating this three times. The solution is concentrated and the polymer is precipitated in diethyl ether. The polymer is obtained after filtration and drying.


PEO-SH. 5.24 g of allyl-PEO and 1.68 ml of thiolacetic acid are dissolved in 50 ml water. The solution is degassed by flushing with argon. The solution is subjected to UV-irradiation for 30 hours. The solvent and most of the excess thiolacetic acid are removed under reduced pressure. The polymer is dissolved in chloroform, to which a 0.5 M sodium hydroxide solution in methanol is added. The mixture is stirred for 2 days. The polymer is purified by dialysis (H_2O, MWCO 1000) and is obtained by freeze drying.
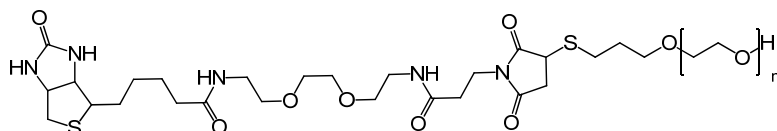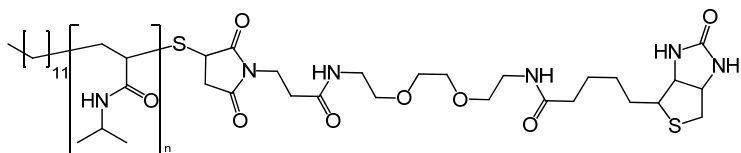

PEO-biotin. To 2.64 ml of a 10 g/l solution of PEO-SH 12 μl of a 1 M sodium borohydride solution is added to reduce any disulfide bonds. The mixture is stirred for an hour, after which it is neutralized with a 1 M HCl solution. 1.61 ml of a 10 g/l solution of biotin-maleimide (5 eq) is added and the mixture is stirred for two days, after which the polymer is purified by dialysis (H_2O, MWCO 1000) and is obtained by freeze drying.
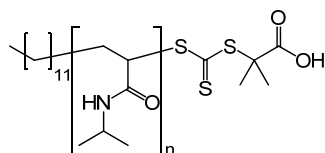
PNIPAAm. 49.3 mg of DMP (0.135 mmol), 6.11 g (54.1 mmol) of recrystallized NIPAAm and 0.1 equivalent of recrystallized AIBN (relative to the amount of DMP) are dissolved in 11.7 ml DMF. The reaction mixture is degassed by two freeze-thaw cycles and is heated to 65 °C for 7 days. The polymer is purified by dialysis (H_2O, MWCO 1000) and is obtained by freeze drying.
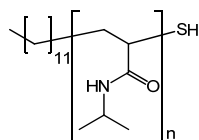
PNIPAAm-SH. The reduction of the CTA end-group is performed in the same fashion as described for the s-PAAm-SH polymer.

PNIPAAm-biotin. To 6.40 ml of a 10 g/l solution of PNIPAAm-SH 3.7 µl of a 1 M sodium borohydride solution is added to reduce any disulfide bonds. The mixture is stirred for an hour, after which it is neutralized with a 1 M HCl solution. 0.976 ml of a 10 g/l solution of biotin-maleimide (10 eq) is added and the mixture is stirred for two days, after which the polymer is purified by dialysis (H₂O, MWCO 1000) and is obtained by freeze drying.

A.5.2 Sample preparation

All experiments were performed using the following buffer: 10 mM phosphate buffer pH 7.5 with 0.15 M NaCl and 0.1 % sodium azide. The solutions of the components were prepared separately and were filtered using a 0.45 µm syringe filter before use. All DLS experiments were performed at a concentration of 0.1 g/l. SEC was performed at the same concentration.
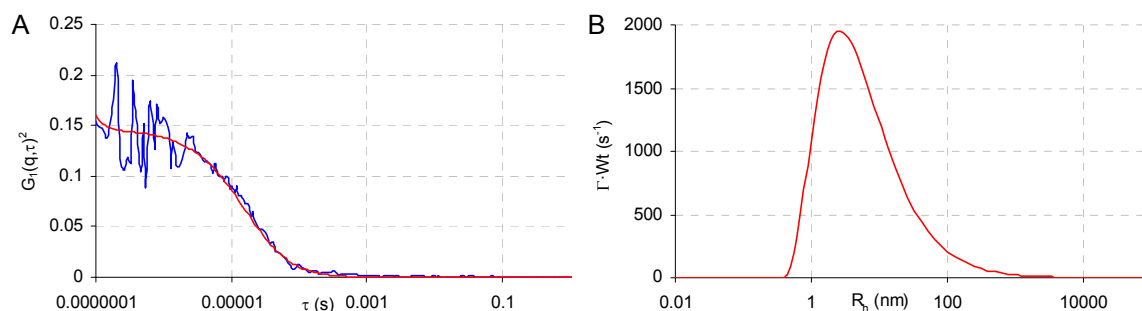
A.5.3 Selected DLS data

Figure 128: DLS data for a mixture of streptavidin with 1 eq of s-PAAm-Biotin and 1 eq of PEO-Biotin (0.1 g/l in phosphate buffer pH 7.5). A) Correlation G_1 (blue: data, red: Contin fit) as a function of the correlation time τ, B) weighted size distribution.
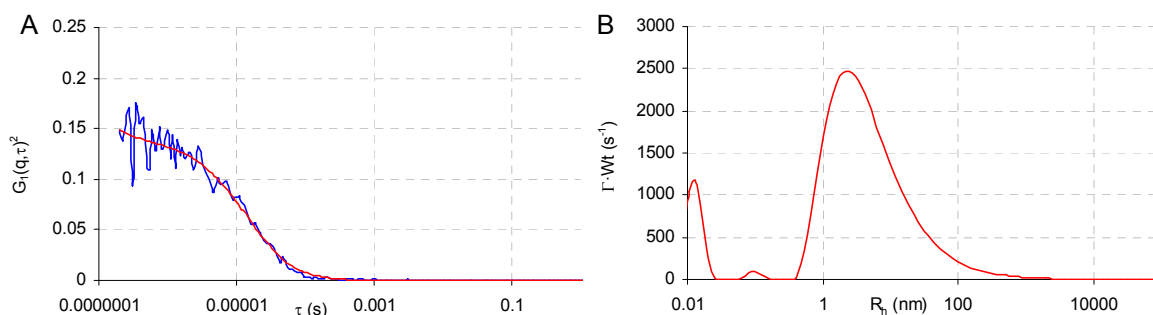

Figure 129: DLS data for a mixture of streptavidin with 1 eq of PEO-Biotin and 1 eq of s-PAAm-Biotin (0.1 g/l in phosphate buffer pH 7.5). A) Correlation G_1 (blue: data, red: Contin fit) as a function of the correlation time τ, B) weighted size distribution.
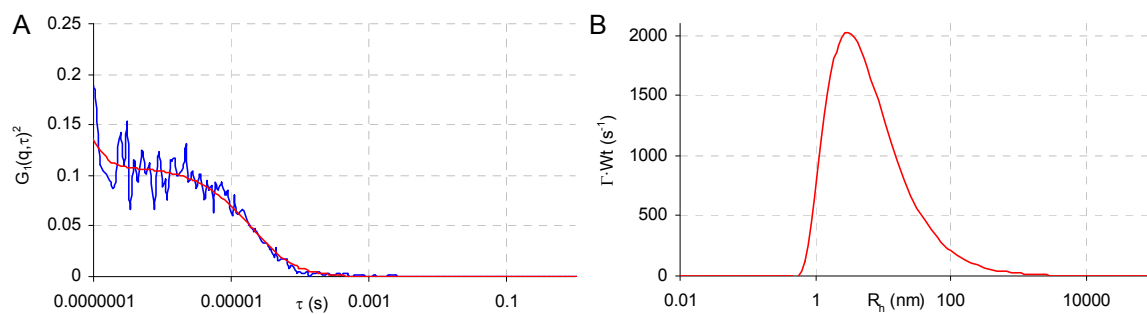
Figure 130: DLS data for a mixture of streptavidin with 3 eq of s-PAAm-Biotin and 1 eq of PEO-Biotin (0.1 g/l in phosphate buffer pH 7.5). A) Correlation G_1 (blue: data, red: Contin fit) as a function of the correlation time τ, B) weighted size distribution.

A.6 Acknowledgements

Firstly I would like to thank Dr. habil. P.D. Helmut Schlaad for both the daily supervision when needed, and the freedom to 'fool-around' and develop some of my own ideas.

Secondly I would like to thank Prof. Dr. Markus Antonietti for the opportunity to work in the Colloids department, in which it has been a great opportunity and pleasure to work, and his support.

The present work would not have been possible without the help of many people whose help in the lab and with numerous analytical techniques was extremely useful:

Jessica Brandt (synthesis of ButinOx), Peter Cernoch (DLS), Marlies Gräwert (GPC), Martin Hoffmann (DDLS), Admir Masic and Gabi Wienskol (Raman spectroscopy), Olaf Niemeyer (NMR and NOESY), Sylvia Pirok (elemental analysis), Prof. Dr. Janne Ruokolainen (CryoTEM), Irina Shekova (titrations), Dr. Jens Weber (SAXS), Dr. Jiayin Yuan (TEM), Heidemarie Zastrow (zeta potential measurements).

A special thank you goes to Ines Below-Lutz, Jessica Brandt, Marlies Gräwert and Katharina Otte for their never relenting help, always taking the time to help even when busy themselves.

The 'Schlaad girls' I would like to thank for the great working atmosphere and helpful discussions: Dr. Peter Cernoch, Dr. Christina Diehl, Dr. Florian Hermes, Clara Valverde-Serrano, Dr. Annabelle Bertin, Ina Dambowsky, Joshua Robinson, Dr. Jing Sun, Dr. Hua Zou.

Andreas Verch, Christine Lausser, Raffael Gentsch, Tim Fellinger, Jens Paraknowitsch, Johannes Schmidt, Miriam Unterlaß, Jens Weber, Nancy Weber, Jiayin Yuan, and numerous others I would like to thank for the great atmosphere in the office, department, labs and the institute in general.

A special thanks goes to Chez Briel and its regulars for the possibility to relax a bit among likeminded people every now and then.

Last, but most certainly not least, I would like to thank Katharina, my family and friends for their support.

Erklärung

Die vorliegende Arbeit habe ich, Niels ten Brummelhuis, selbst verfasst und keine anderen als die von mir angegebenen Quellen und Hilfsmittel verwendet.

Ferner erkläre ich, dass ich nicht versucht habe, anderweitig mit oder ohne Erfolg eine Dissertation einzureichen oder mich der Doktorprüfung zu unterziehen.

Potsdam-Golm, im Januar 2011